



UNIVERSITY OF IOANNINA
SCHOOL OF SCIENCES
DEPARTMENT OF CHEMISTRY

**Development of New Methods for the Extraction and Passive
Recovery of Organic and Inorganic Micropollutants using
Hybrid Micro/Nano-sorbent Materials**

Gouma Vasiliki

Chemist

M. Sc. Chemistry

Philosophy of Doctorate

Ioannina 2025



UNIVERSITY OF IOANNINA
SCHOOL OF SCIENCES
DEPARTMENT OF CHEMISTRY

**Development of New Methods for the Extraction and Passive
Recovery of Organic and Inorganic Micropollutants using
Hybrid Micro/Nano-sorbent Materials**

Gouma Vasiliki

Chemist

M. Sc. Chemistry

Philosophy of Doctorate

Ioannina 2025

«The approval of the doctoral thesis by the Department of Chemistry of the School of Sciences, University of Ioannina does not indicate acceptance of the author's opinions Law 5342/32, article 202, paragraph 2»

Appointment of a Three-member Advisory Committee by the G.S.E.S.: 1032/12.02.2021

Members of the Three-member Advisory Committee:

Supervisor:

Giokas Dimosthenis, Professor

Members:

Vlessidis Athanasios, Professor

Tsogas Georgios, Assistant Professor

Date of topic definition: 22/4/2021

Topic: "Development of New Methods for the Extraction and Passive Recovery of Organic and Inorganic Micropollutants using Hybrid Micro/Nano-sorbent Materials"

APPOINTMENT OF A SEVEN-MEMBER EXAMINATION COMMITTEE by the Assembly.: 1126/06-09-2024

1. Giokas Dimosthenis, Professor, University of Ioannina, Department of Chemistry, Supervisor.
2. Vlessidis Athanasios, Professor, University of Ioannina, Department of Chemistry, Member of the Three-member Advisory Committee.
3. Tsogas Georgios, Assistant Professor, University of Ioannina, Department of Chemistry, Member of the Three-member Advisory Committee.
4. Manos Emmanuel, Professor, University of Ioannina, Department of Chemistry, Member.
5. Stalikas Konstantinos, Professor, University of Ioannina, Department of Chemistry, Member.
6. Plakatouras Ioannis, Professor, University of Ioannina, Department of Chemistry, Member.
7. Hela Dimitra, Professor, University of Ioannina, Department of Chemistry, Member.

Approval of Doctoral Thesis with Grade: Excellent (10)

The Chair of the Department of Chemistry

Hela Dimitra, Professor

The Secretary of the Department

Toutounzoglou Xanthi

to my family...

I Acknowledgements

This doctoral thesis was conducted in the Research Laboratory of Analytical Chemistry, at the Department of Chemistry, University of Ioannina, under the supervision of Professor Dimosthenis Giokas. His unwavering support and decisive contributions at every stage of the research were invaluable. I am deeply grateful for his scientific advice, supervision, and close guidance, all of which were instrumental in the successful completion of this thesis.

I would like to express my deep gratitude to the members of my Advisory Committee, Professor Athanasios Vlessidis and Assistant Professor Georgios Tsogas, for their invaluable suggestions and constructive feedback throughout this thesis. Additionally, I am especially thankful to Professor Emmanuel Manos for his expert advice on the synthetic processes and his assistance with the FE-SEM, BET, EDS, and p-XRD characterizations of the materials. My thanks also extend to the other members of my examination committee, particularly Professor Konstantinos Stalikas, for his significant contributions to the zeta potential measurements, as well as Professor Ioannis Plakatouras and Professor Dimitra Chela and I would also like to thank them for their suggestions and advice regarding the editing of the final text of the PhD Thesis.

I would also like to extend my heartfelt thanks to my colleagues and friends in the Analytical Chemistry Laboratory, particularly the postgraduate students Ilias Moisiadis, Christina Matiaki, and Toti Efthymia, for their exceptional collaboration, the wonderful atmosphere, and their unwavering moral support throughout my doctoral thesis. My deep gratitude also goes to the colleagues and friends I made in the Inorganic Chemistry Laboratory, especially Dr. Anastasia Pournara, PhD candidates Dimitris Evangelou, Nikolas Anastasiadis, Vasiliki Karagianni, Eleni

ACKNOWLEDGEMENTS

Makri, and postgraduate student Yiannis Gikas, for their invaluable assistance, cooperation, and steadfast support whenever needed during the course of my research.

Finally, my deepest thanks belong to my family, who have supported me unwaveringly over the years. I dedicate this thesis to them with all my love.

Vasiliki G. Gouma

Ioannina, February 2025

II Abstract

The presence of pollutants—including organic and inorganic compounds, oxyanions, and various bio-organisms—in aquatic and terrestrial systems poses significant risks to environmental health, human well-being, and food chains. This underscores the urgent need for innovative and effective purification technologies for environmental remediation. This study introduces fabric phase sorptive extraction (FPSE) as a novel, eco-friendly sample preparation technique that addresses many limitations of traditional methods. FPSE offers multiple advantages: it is easy to use, minimizes solvent consumption, supports a diverse range of sorbents, and provides a high surface area for efficient analyte interaction. FPSE is also stable across a broad pH spectrum, enhances analyte diffusion through magnetic stirring, facilitates rapid back-extraction with minimal solvent, reduces sample preparation steps to minimize errors, and can detect analytes at trace levels (ng/L).

In the present study we introduce the use of MOFs immobilized on cotton fabrics as a sorbent phase for the fabric phase sorptive extraction and passive sampling of non-polar organic compounds from water samples. A water-stable, Zr^{4+} -based MOF (UiO-66(Zr)- NH_2) was irreversibly immobilized on polydopamine decorated cotton through a step-wise synthetic procedure that maximized the amount of MOF immobilized on the fabric surface. In this manner it was possible to combine the permeability and the large contact surface area of the host cotton substrate with the high specific surface area and sorption capacity of the MOF. The MOF@cotton composite was used as a new sorbent phase for the fabric phase sorptive extraction of UV filters, as model organic compounds, not only under static (i.e. stirring assisted) but also in dynamic, flow-through extraction mode (i.e. as a solid phase extraction sorbent phase), producing satisfactory analytical results in terms of linearity of calibration curves (10-250 $\mu\text{g L}^{-1}$), precision (<11%),

ABSTRACT

detection limits $<10 \mu\text{g L}^{-1}$ (using a single wavelength UV detector) and recoveries (86 - 119%) from various natural water samples. As a passive sampling sorbent phase, the MOF@cotton composite could linearly accumulate UV filters over time period of 35 days with sampling rates from $0.026\text{-}0.352 \text{ L d}^{-1}$, which are comparable to other passive sampling sorbent phases.

The Zr^{4+} -based MOF ($\text{UiO-66}(\text{Zr})\text{-NH}_3^+$ or MOR-1) was also tested as a novel material for the remediation of contaminated soils by *in-situ* extraction of soil contaminants on retrievable sorbents. The remediation process is based on adding cotton fabric sheets decorated with metal-organic frameworks in a contaminated soil matrix, followed by mixing to sorb the contaminants. The MOF-modified cotton fabric is then easily recovered to extract the contaminants from the soil. The remediation efficiency was optimized regarding the fabric surface area per soil mass, the soil moisture capacity, and the remediation time, yielding satisfactory removal efficiencies (43-90%) for most compounds in 60 days. Notably, the sorbent could be reused up to 5 times after eluting the organic compounds and exhibited good stability in aqueous and acidic media, enabling its safe disposal. The method offers a practical solution for in-situ soil remediation and paves the way for future applications, exploring bulk-supported nanosorbent materials.

Additionally in this work, aiming to address the lack of passive sampling sorbent phases for nanoparticle species, we designed a new sorbent phase consisting of a novel Zr-MOF material with thiophene functional groups called MOR-3 and immobilized it onto a bulk support comprised of cotton fabrics. The MOR-3@cotton composite was used as a new sorbent phase for the fabric phase sorptive extraction of AuNPs, as model nanoparticle species, not only under static (i.e. stirring assisted) but also in dynamic, flow-through extraction mode (i.e. as a solid phase extraction sorbent phase), producing satisfactory analytical results in terms of linearity of calibration curves in the range of $0.2\text{-}20 \text{ nM}$ of 4 nm PVP@AuNPs (or to $0.05\text{-}8.0 \mu\text{g Au /mL}$) at pH 3, precision

ABSTRACT

(<9%) and detection limits of 0.18 nM (0.045 $\mu\text{g Au /mL}$). Recovery experiments in environmental water samples of different matrix complexities (i.e. river water, lake water and seawater) were also examined and the results show that the method effectively extracts both AuNPs and Au ions with recoveries ranging from 80.8% to 115%. As a passive sampling sorbent phase, the MOR-3@fabric composite could linearly accumulate AuNPs over time period of 110 days, which is significantly higher than most passive samples used for inorganic ions and good sampling rate ($R_s=2.1 \text{ mL/h}$), which is comparable to those obtained with commercial passive samplers for metal.

III Table of contents

I	Thanks.....	i
II	Abstract.....	iii
III	Table of contents.....	vi
1	Introduction.....	1
1.1	Introduction to Advanced Porous Materials	2
1.2	Metal Organic Frameworks, MOFs.....	6
1.3	MOF features.....	7
1.4	Structural characteristics	9
1.4.1	Primary units (Connectors & Linkers)	9
1.4.2	Coordination bonds	13
1.4.3	Shaping the Structure and Properties of MOFs.....	14
1.5	Synthetic strategies for MOFs	18
1.5.1	Classical methods	19
1.5.2	Hydrothermal/solvothermal method	22
1.5.3	Mechanochemical method.....	27
1.5.4	Microwave-assisted method.....	29
1.5.5	Sonochemical method	32
1.5.6	Electrochemical method.....	35
1.5.7	Prefunctionalization	39
1.5.8	Post-synthetic modification	41
1.6	Fundamentals of MOF stability.....	47
1.6.1	Stability in water	47
1.6.2	Stability to Acids/Bases	49
1.6.3	Stability in the presence of coordination anions.....	54
1.6.4	Mechanical stability	54
1.7	MOF applications.....	55
1.7.1	Gas storage and separation	55
1.7.1.1	Gas storage	56
1.7.1.2	Gas separation.....	57
1.7.2	Sensing applications	59
1.7.3	Catalytic applications	61

TABLE OF CONTENTS

1.7.4	MOFs in biomedical applications	63
1.7.5	MOFs in analytical sample preparation	65
1.7.5.1	Solid-phase extraction (SPE)	67
1.7.5.2	Dispersive solid-phase extraction (d-SPE)	69
1.7.5.3	Magnetic solid-phase extraction (MSPE)	71
1.7.5.4	Solid-phase microextraction (SPME)	73
1.8	MOFs in environmental remediation	77
1.8.1	MOFs as adsorbents for water purification	83
1.8.1.1	Removal of organic pollutants	83
1.8.1.1.1	Removal of dyes	83
1.8.1.1.2	Removal of agriculture-related pollutants	86
1.8.1.1.3	Removal of pharmaceuticals and personal care products (PPCPs)	90
1.8.1.2	Removal of inorganic pollutants	95
1.8.1.2.1	Removal of heavy metal cations	95
1.8.1.2.1.1	Lead (Pb)	95
1.8.1.2.1.2	Mercury (Hg)	97
1.8.1.2.1.3	Cadmium (Cd)	100
1.8.1.2.2	Removal of oxyanions	101
1.8.1.2.2.1	Arsenic (As)	101
1.8.1.2.2.2	Chromium (Cr)	104
1.8.1.2.2.3	Selenate and selenite	106
1.8.1.2.3	Removal of halide ions	107
1.8.1.2.3.1	Fluoride	107
1.8.1.2.4	Removal of radioactive substances	108
1.8.1.2.4.1	Uranium (^{235}U)	109
1.8.1.2.4.2	Barium (^{133}Ba)	109
1.8.1.2.4.3	Cobalt (^{60}Co)	110
1.8.1.2.5	Removal of precious metals	111
1.8.1.2.5.1	Gold (Au)	112
1.8.1.2.5.2	Silver (Ag)	113
1.8.1.2.5.3	Palladium (Pd)	113
1.8.2	MOFs as adsorbents for soil remediation	116
1.9	Fabric phase sorptive extraction	118

TABLE OF CONTENTS

1.9.1	FPSE approaches	126
1.9.1.1	Stir-FPSE	126
1.9.1.2	Stir-bar FPSE	127
1.9.1.3	Magnet integrated (MI) FPSE	128
1.9.1.4	Dynamic FPSE (DFPSE)	129
1.9.1.5	Injection fabric disk sorptive extraction (FI-FDSE)	130
1.10	Purpose of the study	132
2	Experimental Part	133
2.1	Fabric phase sorptive extraction and passive sampling of ultraviolet filters from natural waters using a zirconium metal organic framework-cotton composite	133
2.1.1	Introduction	133
2.1.2	Experimental	135
2.1.2.1	Chemicals and Materials	135
2.1.2.2	Instrumentation	136
2.1.2.3	Synthesis of MOR-1@cotton fabric	137
2.1.2.4	Experimental procedure of static FSPE	138
2.1.2.5	Experimental procedure of dynamic FPSE	139
2.1.2.6	Calibration of MOR-1@cotton fabrics for passive sampling	139
2.1.2.7	Real samples	140
2.1.3	Results and Discussion	141
2.1.3.1	Preparation and Characterization of MOR-1@cotton fabrics	141
		144
2.1.3.2	Optimization of FSPE experimental conditions	146
2.1.3.2.1	Effect of MOR-1 amount and dimensions of the fabric phase	147
2.1.3.2.2	Optimization of sample pH and ionic strength during extraction	149
2.1.3.2.3	Extraction time	150
2.1.3.2.4	Optimization of desorption conditions	151
2.1.3.2.5	Sample volume	153
2.1.3.2.6	Reusability of the fabric	155
2.1.3.2.7	Analytical figures of merit	155
2.1.3.2.8	Method application in real samples	158
2.1.3.2.9	Method application to passive sampling of UV filters in natural waters	160
2.1.4	Conclusions	161

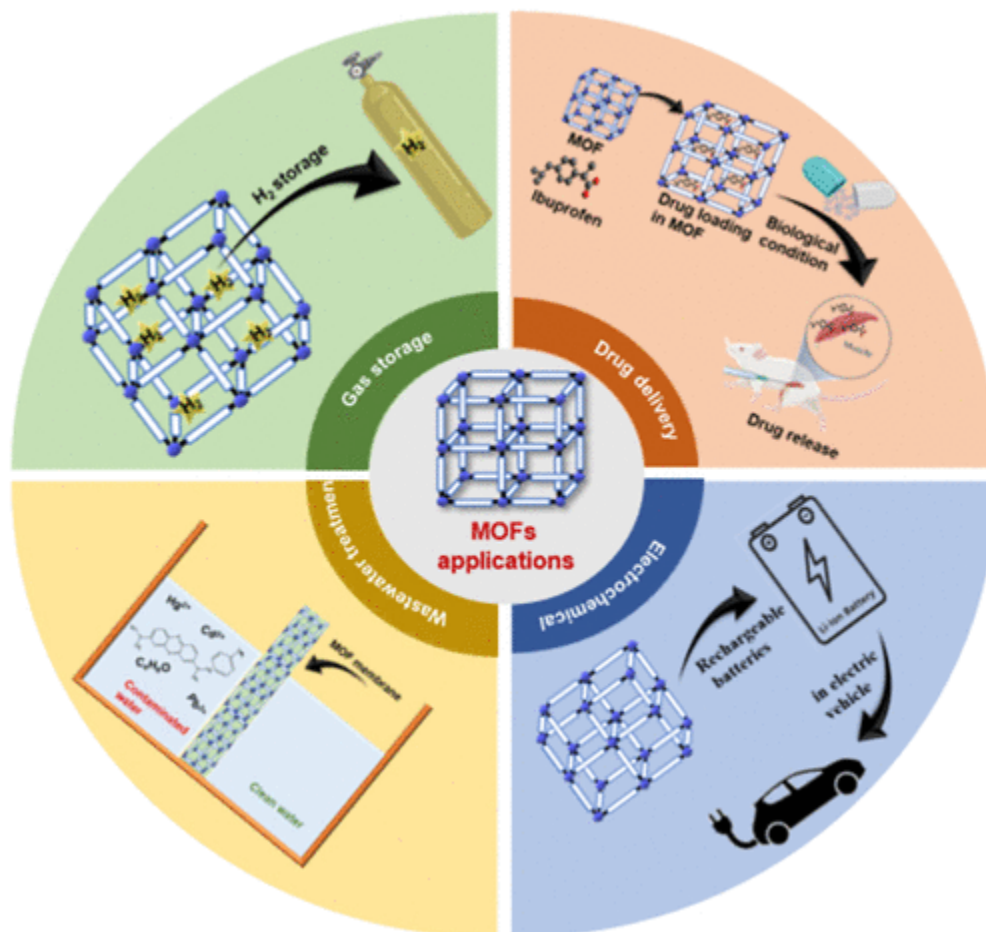
2.2 In-situ, extractive remediation of soil using retrievable bulk-supported nanosorbents composed of metal-organic framework-decorated cotton fabrics	163
2.2.1 Introduction	163
2.2.2 Experimental	165
2.2.2.1 Chemicals and Materials	165
2.2.2.2 Instrumentation	166
2.2.2.3 Synthesis of MOR-1@cotton fabrics	167
2.2.2.4 Batch sorption studies of UV filters on MOR-1@cotton fabric	167
2.2.2.5 Preparation of the contaminated soil	167
2.2.2.6 Soil remediation studies with MOR-1@PDA-cotton fabrics	168
2.2.2.7 Extraction of residual UV filters from soil	168
2.2.3 Results and Discussion	169
2.2.3.1 Characterization of MOR-1@cotton fabrics	169
2.2.3.2 UV filter sorption on MOR-1@PDA-cotton fabric	171
2.2.3.3 Remediation of soil with MOR-1@PDA-cotton fabrics	177
2.2.3.4 Regeneration and stability of MOR-1@PDA-cotton fabric	180
2.2.4 Conclusions	182
2.3 Extraction and passive sampling of gold nanoparticles and gold ions using a Zr (IV) MOF-cotton composite with thiophene functional groups	183
2.3.1 Introduction	183
2.3.2 Experimental procedure	185
2.3.2.1 Chemical and Materials	185
2.3.2.2 Instrumentation	186
2.3.2.3 Synthesis of 2-((thiophene-2-ylmethyl) amino) terephthalate (TATP2)	187
2.3.2.4 Fabrication of MOR-3@cotton fabric	187
2.3.2.5 Synthesis of AuNPs	188
2.3.2.5.1 Citrate capped AuNPs (CA@AuNPs) with different size distributions	188
2.3.2.5.2 CA@AuNPs 4nm in diameter	188
2.3.2.5.3 CA@AuNPs 7nm in diameter	188
2.3.2.5.4 CA@AuNPs 15nm in diameter	189
2.3.2.5.5 CA@AuNPs 25nm in diameter	189
2.3.2.5.6 CA@AuNPs 40, 60 and 80nm in diameter	189
2.3.2.6 AuNPs with different coatings	189

TABLE OF CONTENTS

2.3.2.6.1	PVP ₁₀ coated AuNPs (PVP ₁₀ @AuNPs).....	190
2.3.2.6.2	Cysteine coated AuNPs (Cys@AuNPs)	190
2.3.2.6.3	Glycine coated AuNPs (Gly@AuNPs)	190
2.3.2.6.4	CTAB coated AuNPs (CTAB@AuNPs).....	190
2.3.2.7	Batch sorption studies	191
2.3.2.8	Calibration of MOR-3@cotton fabric as passive sampling receiving phase ..	192
2.3.2.9	Extraction and determination of AuNPs in water samples based on fabric phase sorptive extraction.....	193
2.3.2.10	Application of MOR-3@cotton as solid phase extraction disks.....	193
2.3.2.11	Real samples	194
2.3.3	Results and discussion	194
2.3.3.1	Characterization of MOR-3@cotton fabrics	194
2.3.3.2	Effect of pH on sorption	202
2.3.3.3	Investigation of the sorption kinetics	203
2.3.3.4	Sorption isotherms.....	205
2.3.3.5	Sorption of AuNPs of various sizes and surface coatings.....	209
2.3.3.6	Optimization of desorption conditions.....	210
2.3.3.7	Application of MOR-3@fabric	212
2.3.3.7.1	Evaluation of MOR-3@cotton fabrics as passive sampling receiving phase	212
2.3.3.7.2	Application of MOR-3@fabric for the fabric phase sorptive extraction of AuNPs	215
2.3.3.7.3	Application of MOR-3@fabric for the solid phase extraction of AuNPs	217
2.3.4	Conclusions	218
3	REFERENCES	220

TABLE OF CONTENTS

1 Introduction



1.1 Introduction to Advanced Porous Materials

The escalating risk to humanity posed by water pollution is attributed to the widespread presence of pollutants in water sources. Extensive endeavors have been undertaken to address this issue by employing various methods to separate and purify contaminated water. **Conventional water purification** methods, such as boiling, sedimentation and distillation, are convenient but limited, due to the limited uptake capacity or selectivity, prompting increased interest in **chemical** and **biological processes** as alternatives to efficiently oxidize contaminants not easily eliminated by traditional means. Despite the considerable interest in biological cleaning techniques such as activated sludge, aerated lagoons, trickling filters, and rotating biological contactors, these endeavors to tackle water pollution have proven inadequate in effectively mitigating the growing risks associated with persistent contaminants like heavy metals and trace organic contaminants (TrOCs), posing a significant threat to public health[1].

In addition to the mentioned strategies, **sorption** is regarded as the most effective method for efficiently removing trace contaminants from water sources thanks to its notable efficiency, cost-effectiveness, environmental friendliness, minimal generation of harmful byproducts, simple design, scalability, exceptional adsorptive capacity, and the presence of diverse adsorbents that are easily recoverable[2], [3], [4]. Moreover, the sorption technique offers a means of eliminating both dissolved and undissolved organic, inorganic, and biological impurities from water, catering to various needs such as domestic and industrial applications. With the increasing demand for enhanced water quality, there is a call for more advanced sorbents with superior properties to meet the progressively stringent water standards[5], [6].

INTRODUCTION

Porous materials are one of the materials that find extensive application across diverse domains thanks to their expansive specific surface area and efficient facilitation of ion and electron diffusion within their pores. Determining an effective sorbent plays a pivotal role in ensuring the feasibility of implementing this process. Despite their significance, inorganic porous materials like zeolites, silica, and other metal oxides typically possess an ordered network structure or crystalline nature, which grants them higher thermostability. However, this characteristic makes them suffer from structural modifications and functional adjustments. On the other hand, organic porous solids like activated carbon or graphene generally exhibit an amorphous nature, resulting in poor thermal stability[7]. These challenges impose significant restrictions on their broader application. Table 1.1 offers a concise overview of the benefits and drawbacks of these advanced materials.

Table 1.1 *The benefits and drawbacks of various advanced materials in analytical sample preparation.* Retrieved from Ref [6].

Advanced materials	Advantages	Disadvantages
Metal/Metal-Oxide Nanoparticles	<ul style="list-style-type: none"> • High specific surface area • High adsorption capacity • High mechanical, thermal & pH stability • Low-temperature Modifiability 	<ul style="list-style-type: none"> • Decreasing efficiency after a few cycles
Magnetic Nanoparticles	<ul style="list-style-type: none"> • Magnetic separation • Ease of preparation • Low cost • Controllable rebinding process • Chemical stability • Reuse of magnetic nanoparticles • Low consumption of organic solvents 	<ul style="list-style-type: none"> • Disruption of surfactant aggregates during analyte elution • Instability and vulnerability to aggregation • Propensity to form a cluster • Fast oxidation under air • Potential toxicity • Lack target selectivity
Layered Double Hydroxides	<ul style="list-style-type: none"> • Ion exchange property • High adsorption capacity • High surface area, • Chemical stability and great surface modification • Controlled particle size • Excellent biocompatibility • Flexibility in interlayer spaces 	<ul style="list-style-type: none"> • Complex synthesis • Limited capacity for large molecules • Limited selectivity • Lack of commercial availability • Limited reusability
Nanofibers	<ul style="list-style-type: none"> • Lower consumption of organic solvent • Higher precision • Improved repeatability • Large surface area • High reaction ability 	<ul style="list-style-type: none"> • Low rate of the adsorption/desorption kinetic procedure • Exceeding the pressure limits of the system

	<ul style="list-style-type: none"> • Facile task-specific functionalization with copolymers or composites • Easy combination with peptides, antibodies, or DNA with a good biocompatibility • High active surface and surface to volume ratio • Better stability in high-pressure system • Great porosity • Particular chemical, mechanical, physical performance • Ease of production 	<ul style="list-style-type: none"> • Leakage from the home-made columns • Incompatibility of extraction and separation dimensions • Flow inconsistency • Pump pressurization • Surface roughness
Quantum Dots	<ul style="list-style-type: none"> • Minuscule size • Vast surface area • Straightforward synthetic processes • Ecologically benign nature • Chemical resistance • Low toxicity • Higher moisture dispersibility • Abundance of –OH, –C=O, and –COOH functional groups on their surface • High water solubility • Environmental friendliness • Negligible toxicity • High photostability • Excellent photocatalytic activities of CQDs • Quicker mass transfer • Larger sample capacity • Better sensitivity and selectivity 	<ul style="list-style-type: none"> • Mostly complex • Time-consuming to prepare • Limited types are used as sorbent materials • Vague separation mechanism of these sorbents
Ionic Liquids	<ul style="list-style-type: none"> • Structural tuneability • High thermal, chemical, and electrochemical stability • Negligible vapor pressure • Recyclability 	<ul style="list-style-type: none"> • High synthesis cost • High viscosity (negative for mass transference and electrospray ionization processes) • Lack of volatility (would dirty the GC system and could even
Carbon-Based Nanomaterials	<ul style="list-style-type: none"> • Structural diversity (0D to 3D structures) • Reasonable surface area • Chemical stability • Low toxicity • Commercial availability 	<ul style="list-style-type: none"> • Low density • Strong electrostatic repulsion in water (difficult for their separation by centrifugation)
Conductive Polymers	<ul style="list-style-type: none"> • Tuneable electrical property • Optical and high mechanical properties • Easy synthesis and effortless fabrication • High environmental stability • Reversible redox activity • Thermal resilience • Specific doping capabilities for property modification • High reusability and life time 	<ul style="list-style-type: none"> • Limited application in their pristine form • Potential toxicity concerns • Lack of commercial availability • Challenges in regeneration and reusability • Limited applicability to non-Polar compounds • High cost
Covalent Organic Frameworks	<ul style="list-style-type: none"> • High yields • Pore porosity • High crystallinity • High surface area • Customizable pore sizes and shapes • High stability in the vast majority of solvents • High thermal and physical stability under harsh condition • High adsorption capacity • Fast mass transferability 	<ul style="list-style-type: none"> • High backpressure by directly packing SPE columns • Agglomeration of micron size of COF particles • Lower surface area
Metal-Organic Frameworks	<ul style="list-style-type: none"> • High surface area • Recyclability • High stability • Low cost of certain reactants 	<ul style="list-style-type: none"> • Sensitive to humidity

	<ul style="list-style-type: none"> • Highly tuneable structures • High adsorption capacity 	
Polyoxometalates	<ul style="list-style-type: none"> • High crystallinity • Thermal and chemical stability • Desirable interactions with analytes • Tunability of the active sites 	<ul style="list-style-type: none"> • High solubility • Low surface area • Sensitivity to reaction conditions
Molecularly Imprinted Materials	<ul style="list-style-type: none"> • High selectivity • High chemical, thermal, mechanical stability • pH stability • High reusability • Absorption capacity 	<ul style="list-style-type: none"> • Poor water compatibility • Incomplete removal of template molecules in their structure
Restricted Access Materials	<ul style="list-style-type: none"> • Possible determination of analytes from biological matrix in the presence of macromolecules such as proteins 	<ul style="list-style-type: none"> • Poor selectivity • Limited range of pH • High additional time and costs • High pressure when a protein sample is flown through the RACNTs packed column
MXenes	<ul style="list-style-type: none"> • Tunable surface functionality • Excellent mechanical properties • High electrical conductivity • Large surface areas • High hydrophilicity • Good flexibility 	<ul style="list-style-type: none"> • The usage of highly toxic fluorine-based etching agents • Long-time ultrasound in etching process • Low environmental compatibility • Lateral size and number of layers not adjustable
Immunosorbent materials	<ul style="list-style-type: none"> • High selectivity and sensitivity • High extraction efficiency • Safe and eco-friendly • Simultaneous analysis without complicated sample pre-treatment • Easy to perform with a simple procedure 	<ul style="list-style-type: none"> • Antibody preparation is costly and labour-intensive. • Instability of antibody • Sophisticated methods and high-cost culture media are essential. • Antibodies (a protein) must be transported and stored under refrigeration.
Aptamers	<ul style="list-style-type: none"> • Exceptional molecular recognition abilities • Remarkable stability • Versatility in being immobilized on diverse support materials • Tolerant of variations in temperature and pH • Without aggregation • Less expensive against the antibody • Without viral and bacterial contamination • Aptamers can be produced by the in vitro SELEX method against nearly all targets. • Extraction and detection of small molecules 	<ul style="list-style-type: none"> • SELEX technologies that are time-consuming and labour-intensive • Reduce the extraction recovery in biological matrix • Quick degradation in biological media • It is also possible for aptamers to interact with the incorrect target in vivo extraction
Natural materials	<ul style="list-style-type: none"> • Low toxicity • Biodegradability • Easy accessibility from renewable sources • Suitable functional groups on their surfaces 	<ul style="list-style-type: none"> • Low sorption capacities and are mostly hydrophilic • Need to modification with another sorbents

To overcome the limitations mentioned above and provide improved versatility across different applications, a recent class of **advanced porous materials (APMs)**, notably **metal–organic frameworks (MOFs)** and **covalent organic polymers (COPs)**, has emerged [5], [8]. MOFs characterized by frameworks constructed through coordination bonds in a predictable manner. This

construction results in a crystalline network that enables versatile manipulation of functional units and precise control over pores, significantly expanding the application of MOFs in different areas of research, especially adsorption removal, separation and purification have been proven[2], [9], [10], [11]. The COPs category encompasses amorphous porous organic polymers (POPs) and their crystalline counterparts, covalent organic frameworks (COFs)[1]. Crystalline COFs differ from MOFs as they are synthesized using purely organic monomers through stronger covalent bonds into elongated structures with periodic skeletons and ordered nanopores, offering the advantage of easily customizable building blocks and pore surfaces[12], [13]. Additionally, porous materials with purely organic backbones, lacking long-range order, are typically referred to as amorphous POPs[14]. These materials exhibit promising capabilities for enhanced segregation of contaminants in relation to traditional porous materials regarding uptake capacity and selectivity. Also, they possess advantages like a large surface area and versatile functionality, making them ideal platforms for crafting innovative adsorbents.

1.2 Metal Organic Frameworks, MOFs

Metal-organic frameworks (MOFs) have recently gained attention due to their effectiveness in removing toxic pollutants from the environment while simultaneously generating fewer secondary wastes and consuming less energy compared to alternative treatment methods. As a very important subclass of coordination polymers, MOFs are high crystalline porous materials consisting of inorganic metal-containing nodes (usually referred as Secondary Building Units, SBUs, or Molecular Building Blocks, MBBs) connected with bridged organic ligands through coordination bonds and other weak chemical bonds, to construct a 3D arrangement (Figure 1.2) [3], [5], [15], [16].

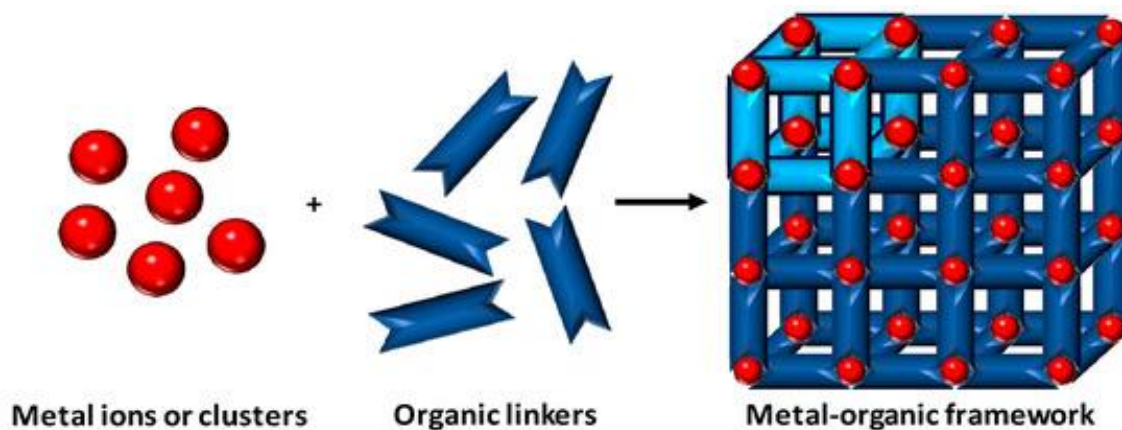


Figure 1.2 Scheme for the preparation of a MOF. Various metal ions or clusters are combined with organic linkers in a suitable solvent. Coordination polymerization occurs between the components, leading to the construction of a 3D arrangement with potential empty spaces[17].

This architecture has led to the creation of diverse structures assembled from multitude molecular building blocks that exhibit distinct interactions. The unique coordination structural units formed by the binding among the metal ion and the organic ligand have attracted significant interest due to their ability to regulate topology across both microporous and mesoporous domains[4], [5].

1.3 MOF features

Among other applications, MOF materials have attracted significant attention as exceptional adsorbents for removing emerging contaminants, distinguishing themselves from other porous materials. MOFs exhibit remarkable features including **large BET** (Brunauer–Emmett–Teller) **surface area** exceeding 10,000 m²/g, exceptionally **high porosity**, with some reaching up to 90% free volume, **adjustable pore structure** and **controllable pore size distribution**[3], [4], [10]. MOFs are classified based on the sizes of their cavities or pores: nanoporous materials have pores

INTRODUCTION

smaller than 20 Å in diameter, mesoporous materials range from 20 to 500 Å, and macroporous materials exceed 500 Å. Most mesoporous and macroporous MOFs typically exhibit an amorphous structure. The pore size can be accurately controlled by changing the length and functionalization of organic linkers incorporated into the polymer structures[4]. Enlarging pore size remains a challenge due to interpenetration, which impedes the creation of unoccupied space within the network. This interpenetration is facilitated by organic ligands featuring aromatic rings that promote π - π interactions. To achieve highly porous MOFs, strategies include using polycarboxylate and rigid alkyne ligands, along with SBUs (Secondary Building Units) of significant dimensions that dictate pore size[18]. The inclusion of bridging organic ligands leads to a variety of topologies and potential properties in metal-organic coordination networks[19]. Moreover, MOFs feature **low skeleton density, high crystallinity, open metal sites, precisely managed surface chemistry, robust host-guest interactions, excellent stability, and flexibility**[3], [5], [20].

MOFs as adsorbent materials unlock opportunities for designing innovative materials with tailored properties offering significant advantages as adsorbents: 1) Their high specific surface area and porous structure enable numerous adsorption sites within the framework, allowing for efficient adsorption or degradation of pollutants compared to other porous materials. 2) Their exceptional suitability for shaping into various morphologies such as pellets, membranes, and monoliths, etc. 3) The straightforward synthesis method of MOFs allowing for large-scale preparation and 4) the outstanding stability under complex conditions[3], [5]. As a result, the landscape of MOFs and related structures has witnessed a transformative evolution in recent years, offering significant prospects for effectively removing pollutants from aqueous solutions.

1.4 Structural characteristics

As mentioned before, MOFs are created by combining metal ions or clusters with organic ligands, which are referred to as primary units, building units, or building blocks. These are linked via strong coordination bonds to form well defined frameworks. Choosing these building blocks for a MOF is an important process. While the type and amount of monomers impact its processability, physical and optical characteristics, the interconnection of building units within the structure determines the MOF's properties. Thus, the careful selection of these primary units not only affects the structure's stability but also controls the functional features of the material. These properties may encompass magnetic exchange, acentricity for non-linear optical (NLO) applications, or the creation of expansive channels facilitating molecular passage. Additionally, incorporating chiral centers or reactive sites into an open framework is actively pursued to create functional materials. Consequently, MOF synthesis involves not only selecting and preparing desired components but also considering how they will link together in the final solid product[21].

1.4.1 Primary units (Connectors & Linkers)

Initially, the network's topology is influenced by the inherent structural characteristics of the **organic linkers** and the **selection of the metal ion**, including its oxidation state. Alongside these key components, there are supplementary components like blocking ligands, counter anions, and nonbonding guests or template molecules, which contribute to the **overall** complexity and functionality of the resulting polymer (Figure 1.4.1.a)[22].

Metal ions serve as connectors in network formation, based on their size, hardness/softness, ligand-field stabilization energy, and coordination geometries. A broad spectrum of metal atoms,

INTRODUCTION

such as transition metal ions particularly those from the first row, lanthanide ions, and alkaline earth metals have been thoroughly investigated, due to their capacity to exhibit a broad range of coordination numbers, geometries, and oxidation states. This characteristic provides a plethora of synthetic and structural possibilities, contributing to increased diversity in materials[18]. Based on the specific metal and its oxidation state, coordination numbers can vary from 2 to 7, resulting in a diverse array of geometries. These geometries can encompass various shapes such as linear, angular, tetrahedral, octahedral, prismatic, etc. (refer to Figure 1.4.1.a)[16], [22].

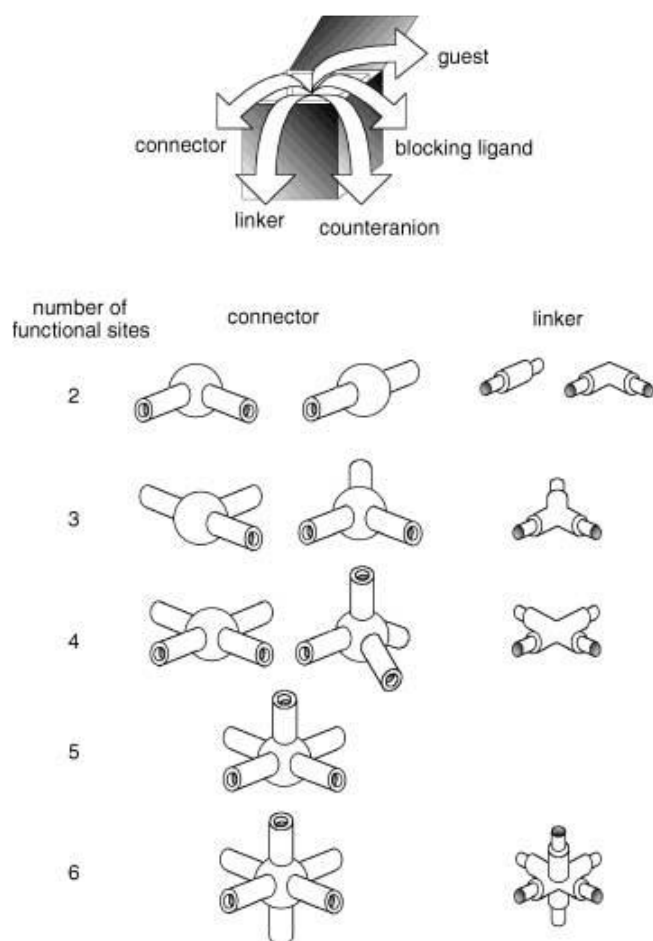


Figure 1.4.1.a Diagram depicting the components of coordination polymers and their different coordination geometries[22].

The incorporation of metals into MOFs significantly impacts their adsorption capacity, primarily owing to the presence of their partial positive charge or the availability of specific sites. Initially, single metal ions were employed in constructing coordination networks. However, the utilization of small metal clusters has emerged as advantageous, as it facilitates the creation of frameworks that retain porosity even after the removal of guest molecules. Specifically, metal ions have the capability to coordinate with carboxylates or other ultimate groups/atoms of linkers, resulting in the formation of metal clusters or secondary building units (SBUs). Typically, these clusters form in situ during MOF synthesis under specific reaction conditions and can be classified based on the number of metal ions they contain in one-metal, two-metals, three-metals, four-metals and six-metals SBUs. Additionally, SBUs offer an opportunity to construct and employ non-interpenetrating, intricately connected networks with enhanced framework stability and porosity[7]. Consequently, these SBUs, characterized by specific extension points, well defined coordination geometries and diverse topologies, can be further interconnected by a large assortment of organic linkers via robust coordination bonds. This process leads to the creation of numerous MOFs[23], [24].

Organic ligands, also referred to as linkers, act as connectors between metal ions, effectively forming connections in the process. These ligand molecules need to possess multiple donor atoms, typically nitrogen (N), oxygen (O), or sulfur (S) donors, to facilitate the formation of expansive networks[16]. Depending on the number of donor atoms they contain, these bridging ligands are classified as di-, tri-, or tetratopic. Ligand molecules can vary in their electrical charges, with the majority being either neutral or negatively charged. The presence of these bridging ligands is crucial for controlling the steric consequences during assembly, with rigid bridging ligands being

INTRODUCTION

particularly significant for this purpose. The diverse array of organic constituents provides the basis for a wide range of structural topologies. Importantly, the organic components of coordination polymers can be precisely adjusted and modified through synthetic organic chemistry to achieve the desired linker geometry. This ability to adjust the organic elements enhances the flexibility and customization potential of the coordination networks[25]. Considerable efforts are dedicated to synthesizing novel ligand systems. Common ligands in property-focused studies of metal coordination polymers are illustrated in Figure 1.4.1.b, with nitrogen and oxygen-donor ligands frequently featured in their construction[26].

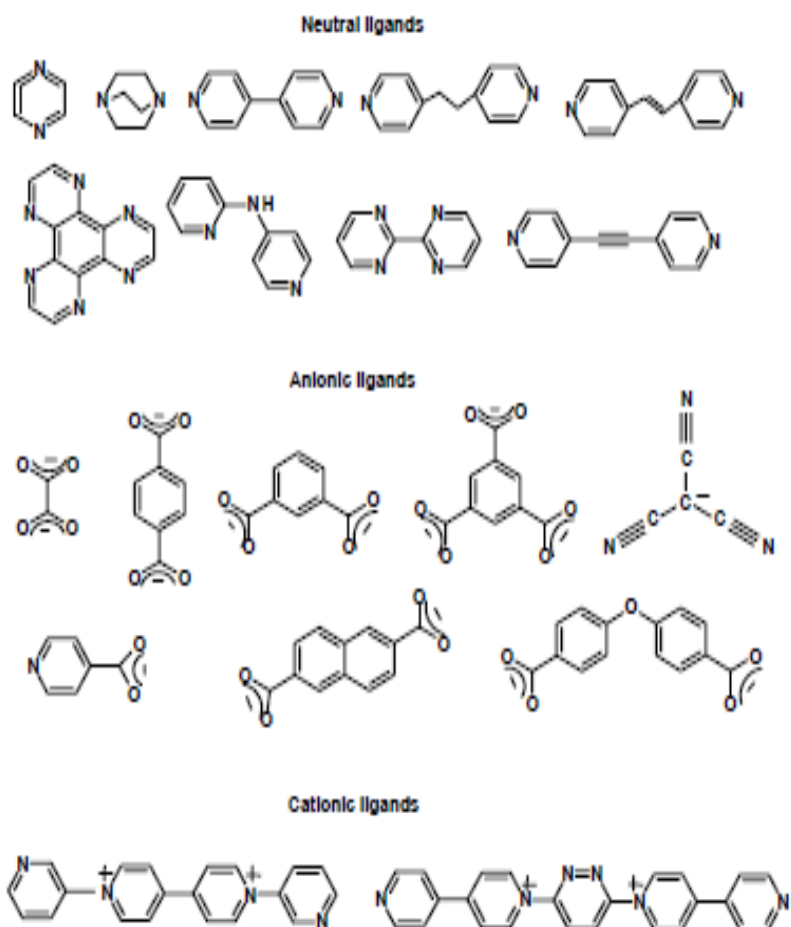


Figure 1.4.1.b Examples of organic linkers used metal-organic frameworks exhibiting different geometries and charges[16].

Generally, MOFs commonly utilize two primary types of linkers: i) Carboxylates, recognized for their hard donor characteristics, are often categorized as di-, tri-, and tetra-topic variants. Examples include 1,4-benzene dicarboxylate (terephthalic acid) found in UiO-66 and MIL-101, and 1,3,5-benzene tricarboxylate (trimesic acid) in MIL-100 and HKUST-1, among others. ii) N-donors, characterized as neutral soft ligands, encompass imidazoles or functionalized imidazoles observed in the ZIF-n series. Furthermore, organic linkers demonstrate strong electrostatic interactions, stemming from their predominantly aromatic structure and the characteristics of their functional groups[23].

Concerning primary units, when neutral ligands are present, **counter ions** become integrated into the structure. They possess the ability to impact the environment surrounding metal ions by adjusting their coordination. Additionally, counter ions play a role in shaping the overall structure, participating in weak interactions, or occupying void spaces within the solid state. Moreover, the incorporation of **solvent molecules** into the crystalline structure through co-crystallization expands the range of potential weak interactions. These solvent molecules can also function as guest molecules within the empty spaces of the network[16].

1.4.2 Coordination bonds

The intricate three-dimensional framework of MOFs emerges from the robust coordination bonds forged among metal ions and organic ligands. These bonds are formed when the ligand, functioning as a Lewis base, donates a lone pair of electrons to the metal cation, which acts as a

Lewis acid. Within this structure, cavities and inner surfaces accommodate counterions, guest molecules, or solvate molecules. Although hydrogen bonds, metal-metal bonds, and π - π interactions may also play a role in reinforcing the stability of MOFs, coordination bonds are notably stronger and form more resilient networks[18]. Also, aromatic interactions manifest in face-to-face configurations (with or without offset) and edge-to-face arrangements (C-H... π). These interactions result from the cumulative effect of various factors (electrostatic forces, van der Waals interactions, repulsion, etc.), and aromatic rings are stacked to minimize repulsion components and maximize attraction[16], [19].

1.4.3 Shaping the Structure and Properties of MOFs

The building blocks themselves can demonstrate a wide range of geometries and coordination numbers. The building units mentioned above can be arranged in countless combinations, providing a modular toolkit for synthesizing an extensive variety of coordination networks. The ultimate structural outcome heavily relies on the rigidity or non-rigidity of the bridging ligand, highlighting its pivotal role in determining the overall architecture[16].

Enhancing the pore dimensions and surface area of MOFs, transitioning from micro to mesoporous dimensions, poses a significant challenge for materials chemists. To address this challenge, researchers have proposed employing the iso-reticular principle and secondary building units (SBUs) chemistry. By incorporating SBUs with rigid and directional properties, it becomes possible to alter the geometry of specific MOFs into infinite nets, thereby controlling their porosity and pore volume. Additionally, this can be achieved by adjusting factors such as the functional groups on the organic ligand, allowing for precise tuning of pore size, prediction of topology or

INTRODUCTION

structure, and the creation of distinct classes of porous materials. However, elongating the organic linker is essential for producing porous MOFs, albeit it may compromise their thermal stability and kinetic robustness. Moreover, elongating the organic linker and expanding the pore size might lead to interpenetrated networks and decreased crystal stabilities. Nevertheless, efforts to develop highly porous MOFs involve strategies like elongating the ligand chain while avoiding interpenetration. Leveraging this capability to regulate pore size and structural chemistry has led to the development of MOFs featuring adjustable pore size, remarkable thermal stability (surpassing 500°C), and exceptionally high porosity (ranging from 500 to 10,000 m²/g). Four MOFs, named MOF-180, -200, -205, and -210, have been created using the Zn₄O(CO₂)₆ unit combined with one or two organic linkers (Figure 1.4.3)[27]. These MOFs exhibit exceptional porosity and gas uptake capacities, with MOF-200, -205, and -210 having BET surface areas of 4530, 4460, and 6240 m² g⁻¹, respectively. Ligands possessing rigid and stable frameworks prove particularly beneficial for enhancing the porosity and thermal resilience of MOFs[7].

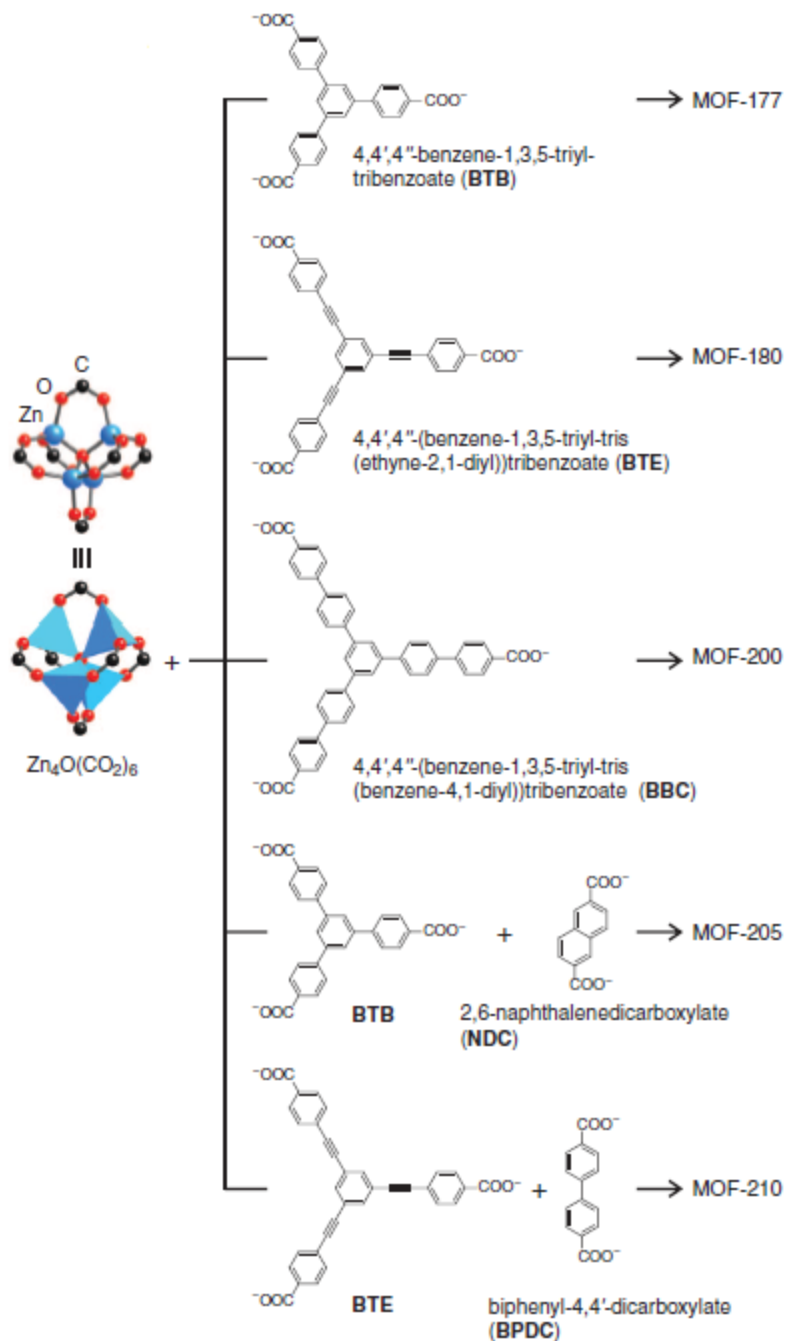


Figure 1.4.3 The $\text{Zn}_4\text{O}(\text{CO}_2)_6$ unit is connected with organic linkers to form ultra-high porous MOFs[27].

While MOFs were initially conceived as consisting of rigid, aromatic linkers acting as supports and metal clusters as nodes, numerous MOFs have been observed to exhibit **flexibility** when

INTRODUCTION

subjected to external stimuli such as pressure, temperature, and light. Designing MOFs with expansion and contraction capabilities, known as "breathing", can affect their properties, particularly in gas adsorption and separation applications, which are absent in rigid frameworks. These specific MOFs feature flexible frameworks without rigidity, often referred to as soft porous crystals, flexible MOFs, sponge-like MOFs, among others. Their ordered crystal structure enables transformations through phase changes or gate openings. This inherent flexibility is often evident during the adsorption-desorption process, stemming from the interplay between adsorbate molecules and the surface of the pores. A significant factor influencing the contraction or expansion of MOFs is their structural makeup, which encompasses the metal ion or cluster, also known as SBUs and the organic linker. Additionally, the interconnection of these components, known as "topology," holds considerable importance. These factors significantly influence the flexibility within MOF structures by affecting the type and strength of framework bonds, as well as the characteristics of the pore environment[28].

Not all Secondary Building Units (SBUs) allow for the dynamic movement, such as expansion or contraction, of the framework. There are some specific empirical principles regarding the conditions under which this phenomenon occurs. For instance, it is suggested that inorganic SBUs should exhibit a mirror plane with carboxylates symmetrically arranged around it, as demonstrated in structures like MIL-88 (Fe, Cr)[29]. Another criterion entails that the fraction of C/M (where C represents the quantity of carbon atoms of the carboxylates around the cluster and M signifies the quantity of metal atoms within the cluster) must surpass 2 to enable the SBU to undergo dynamic breathing[28]. These two principles have been demonstrated to hold true for several well-known flexible MOFs, including $[\text{Zn}_2(\text{bdc})_2(\text{dabco})]_n$ (where bdc = 1,4-benzenedicarboxylate and dabco = 1,4-diazabicyclo[2.2.2]-octane), and the previously mentioned MIL-88 (Fe, Cr)[29], [30].

Also, flexible linkers influence the MOF properties, either by elucidating the mechanisms through which flexible linkers induce breathing in MOFs or by analyzing the effects of different functional groups within the linker that facilitate expansion/contraction in MOFs. An empirical guideline regarding the impact of linkers on breathing was proposed by Férey, suggesting that carboxylate ligands that are di-topic, linking two metal clusters or SBUs, offer advantages in the design of flexible MOFs[31]. In contrast, carboxylate linkers that are tri- or tetra-topic restrict the structural flexibility of MOFs[31]. Organic linkers capable of rotation due to the presence of internal flexible bonds (or flexible metal-linker bonding) can promote framework flexibility. This rotation enables pore expansion, leading to unexpected adsorption of larger guest molecules. An example illustrating linker rotation in flexible MOFs is observed in $[\text{Cd}_2(\text{pzdc})_2(\text{BHE-bpb})]_n$ (where pzdc = 2,3-pyrazinedicarboxylate and BHE-bpb = 2,5-bis(2-hydroxyethoxy)-1,4-bis(4-pyridyl)benzene). Here, cadmium metal centers are interconnected with the dicarboxylate linker (pzdc) to form layers of $[\text{Cd}_2(\text{pzdc})_2]_n$. These layers are then joined by a pillaring BHE-bpb linker to create a three-dimensional framework. The pillaring linker features an -OH group capable of interacting with other -OH groups from adjacent pillars, potentially leading to pore blockage. However, the adsorption of polar guest molecules like water prompts the rotation of the linker, consequently opening the pore[28], [32].

1.5 Synthetic strategies for MOFs

When fabricating composite materials based on MOFs, it's crucial to address not only the challenge of forming dense polycrystalline layers on the substrates but also to ensure the stability of the MOF materials[5]. MOFs have been fabricated using diverse methods, each influenced by different

INTRODUCTION

energy sources, which significantly impact the final particle sizes and size distributions, including classical methods, solvothermal/hydrothermal, microwave-assisted, sonochemical, mechanochemical, electrochemical, etc. Additionally, MOF structures can be adjusted by varying the solvent, changing the metal precursors, and altering the organic ligands[33]. Traditionally, MOF materials have been synthesized through hydrothermal or solvothermal processes, employing water or organic solvents as carriers, with reaction temperatures ranging from 37 to 200°C and reaction durations spanning from several hours to a few days. Also, solvothermal and classical methods are typically employed for the formation of single crystals suitable for structural determination. Smaller particle sizes with higher surface area benefit from expeditious synthetic techniques like microwave and sonochemical approaches. Moreover, alternative synthesis techniques such as solvent-free methods (e.g., the mechanochemical method) have gained rapid traction. These solvent-free methods not only circumvent the need for solvents but also mitigate pollution and impurities in the crystals. Additionally, electrochemical methods are commonly utilized for continuous synthesis protocols[23]. As evidenced by records from the Cambridge Crystallographic Data Centre, there are currently over 90,000 reported MOFs[7].

1.5.1 Classical methods

In **classical methodologies**, MOFs are crafted at temperatures below 100°C, typically by allowing the slow evaporation of a solution containing the initial components (Figure 1.5.1.a) or assisted by the slow diffusion of reactants (Figure 1.5.1.b)[34]. These processes could also, occur at ambient temperature and require no external energy.

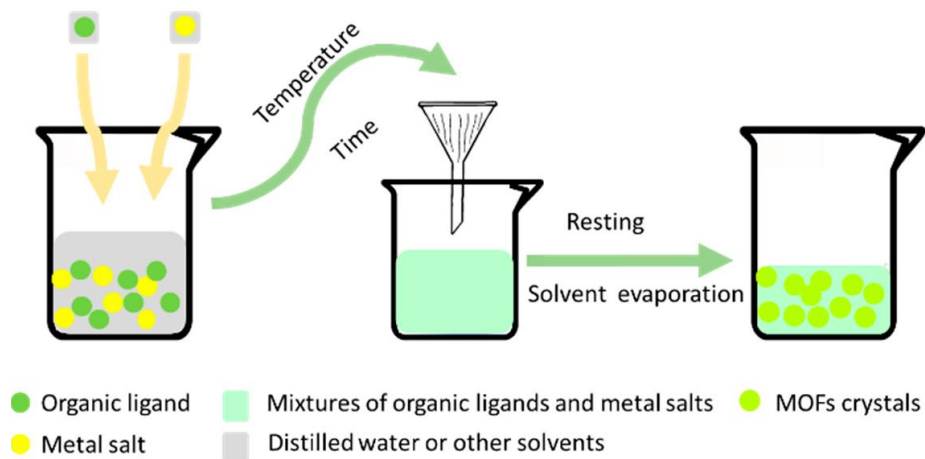


Figure 1.5.1.a Illustration outlining the synthesis of MOFs via the slow evaporation method[34].

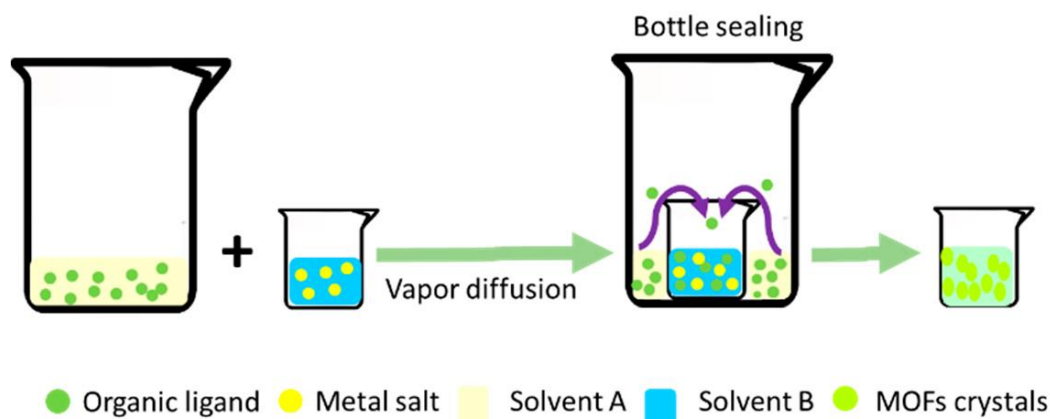


Figure 1.5.1.b Illustration outlining the synthesis of MOFs via the gas phase diffusion method[34].

The **slow evaporation** approach entails blending metal elements, organic ligands, along with other necessary materials in a specialized solvent at precise proportions. This mixture undergoes stirring for a predetermined period at a fixed temperature and left to slowly evaporate, prompting crystal formation upon reaching a critical concentration threshold, thereby facilitating nucleation and

INTRODUCTION

crystal expansion[34]. Frequently, mixtures of solvents with low boiling points are utilized to enhance the efficiency of this process. Table 1.5.1 summarizes some of the MOFs synthesized via the slow evaporation method[35]. The **diffusion** method for synthesizing MOFs primarily involves three approaches: gel diffusion, liquid phase diffusion, and gas phase diffusion. Gel diffusion involves blending materials like organic ligands dispersed in a gel substance with a solution of center metal ions, resulting in MOF crystal growth through these two different types of groups in gel. Liquid phase diffusion, on the other hand, dissolves center metal ions and organic ligands in an incompatible solvent, prompting a reaction upon contact and subsequent MOF crystal formation. Gas phase diffusion employs an organic volatile ligand solution as a solvent, facilitating MOF generation through the reaction between organic ligands and center metal ion solutions. Although these methods typically operate under mild conditions, they often require significant time investment. The diffusion method is particularly employed when the products exhibit low solubility[18], [23], [34].

Table 1.5.1 MOFs synthesized using the slow evaporation approach.

MOFs	Precursors		Solvents	Reference
	Organic ligand	Metal salt		
HKUST-1	1,3,5 Benzene Tricarboxylic acid	Cu(NO ₃) ₂ ·3H ₂ O	DMSO	[36]
MOF-177	Benzenetribenzoic acid	Zn(OAc) ₂ ·2H ₂ O	DEF	[37]
Ni-MOF	1,3,5 Benzene Tricarboxylic acid	Ni(NO ₃) ₂ ·6H ₂ O	NaOH, H ₂ O, CH ₃ CN	[38]
Cd-MOF	1,3-bis(4-pyridyl)propane, 2,6-pyridine dicarboxylic acid	Cd(NO ₃) ₂ ·4H ₂ O	H ₂ O, EtOH, NaOH	[39]
Ag-MOF	(1S)-1-(5-tetrazolyl) ethylamine	AgCl	MeOH, NH ₃ ·H ₂ O	[40]
Cu-MOF	Benzene 1,2,4,5-tetrasulfonic acid	Cu ₂ (OH) ₂ (CO ₃)	H ₂ O	[41]
Co-MOF	2,6-pyridine dicarboxylic acid	CoCl ₂ ·6H ₂ O	H ₂ O, C ₅ H ₅ N	[42]

DMSO= Dimethyl Sulfoxide, DEF= N,N-diethylformamide.

1.5.2 Hydrothermal/solvothermal method

The primary method used to create MOFs typically involves **hydrothermal/solvothermal synthesis**. This approach, which has been utilized for many years, is renowned for its ability to produce high-quality porous materials like zeolites, metal oxides (MOs), and MOFs. Hydrothermal synthesis takes place in the presence of water, serving as a protic solvent. Conversely, solvothermal synthesis utilizes organic solvents, which may be either protic or aprotic. In both techniques, the metal ion precursor and the organic ligand are dissolved together in the presence of an appropriate solvent and stirred within a polytetrafluoroethylene (PTFE) liner. This mixture undergoes a reaction inside a high-pressure autoclave, under controlled conditions of temperature, pressure, and duration. After the reaction, the resulting products are cooled to room temperature, thoroughly rinsed with an appropriate solvent, and subsequently vacuum drying to obtain high purity MOFs (Figure 1.5.2)[43].

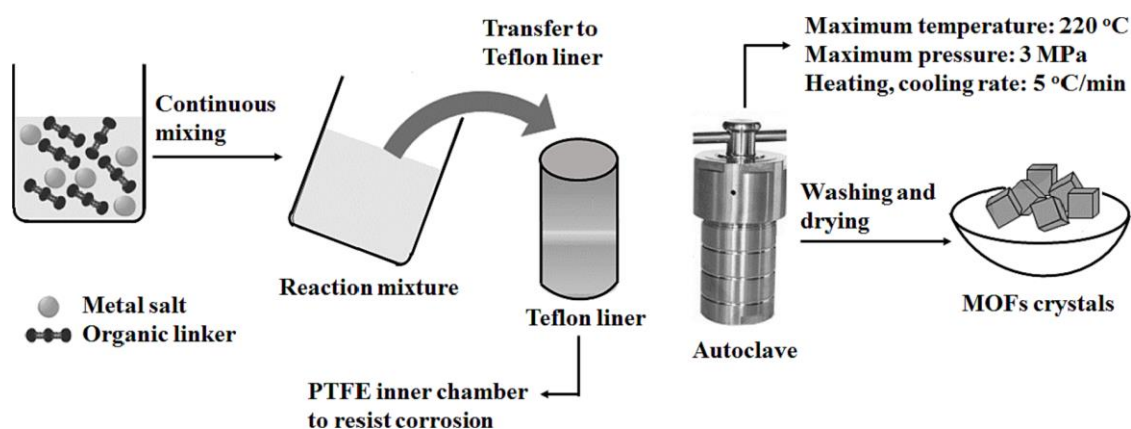


Figure 1.5.2 Illustrative depiction of the solvothermal process for MOFs[43].

Factors such as reaction conditions (volume, concentration, temperature, duration) and cooling rate can significantly impact synthesis. More specifically, temperature influences the shape and structure of crystals, whereas extended reaction durations might result in the collapse of the ultimate product. The rate at which cooling occurs should be deliberately slow as it directly impacts crystallization. In this process, solvents with elevated boiling points are typically preferred. Solvents employed are predominantly highly polar, and include water, ethanol, methanol, acetic acid, dimethyl sulfoxide, N,N-dimethylformamide, acetonitrile, and acetone[18], [23], [33]. Additionally, the careful selection and inclusion of chemical regulators (e.g. high molecular weight compounds, modulated ligands, etc.) play a crucial role in controlling crystallite sizes and influencing nucleation sites. Recent advancements in this field have enabled the creation of various porous composite materials with stable chemical properties by strategically choosing modifier with diverse characteristics[44]. This synthesis method is commonly applied to produce different MOFs, including those from the UiO-n, MIL-n, and MOF-n series[5]. Table 1.5.2.a provides a comprehensive overview of the precursors, conditions, and characteristics of select MOFs synthesized via the hydrothermal/solvothermal method in the literature[43].

Table 1.5.2.a MOFs synthesized using the hydrothermal/solvothermal approach.

MOFs	Precursors		Solvent	Reaction conditions	Remark	Reference
	Organic ligand	Metal salt				
MIL-47	Terephthalic acid	V ₂ O ₅	DMF	180 °C, 20 h	Chemically and thermally stable	[45]
UiO-66	Terephthalic acid	Co ₃ O ₄	DMF	120 °C, 24 h	Enhanced charge separation and visible light absorption	[46]
SIMOF-4	2,3-dihydroxyterephthalic acid	Ca(NO ₃) ₂ ·4H ₂ O	Ethanol/water	120 °C, 72 h	MOFs with excellent electrochemical	[47]

INTRODUCTION

					properties	
Cu-HKUST-1	Trimesic acid	$\text{Cu}(\text{NO}_3)_2 \cdot 3\text{H}_2\text{O}$	Ethanol/ water	120 °C, 24 h	High purity MOFs with high specific surface area and good crystallinity. Water unstable MOFs at elevated temperatures.	[48]
Cd/Zr-MOF	Terephthalic acid	CdCl_2	DMF	120 °C, 2 h	Bimetallic MOFs with high photocatalytic activity	[49]
Zr-PCN-111	4,4'-(buta-1,3-diyne-1,4-diyl)dibenzoate	ZrCl_4	DMF, CF_3COOH H	120 °C, 3-5 d	High volumetric surface area MOFs. Air and moisture sensitive. Useful in gas sorption applications	[50]
Bi-MOF	Trimesic acid	$\text{Bi}(\text{NO}_3)_3 \cdot 5\text{H}_2\text{O}$	DMF	120 °C, 24 h	MOFs were spindle-shaped and dominated by micropores	[51]
Ni/Mn-MOF	Trimesic acid	$\text{Ni}(\text{CH}_3\text{COO})_2 \cdot 4\text{H}_2\text{O}$ $\text{Mn}(\text{CH}_3\text{COO})_2 \cdot 4\text{H}_2\text{O}$	Ethanol/ water	150 °C, 15 h	Bimetallic MOFs with excellent electrochemical properties	[52]
Mg-MOF-74	2,5-dihydroxyterephthalic acid	$\text{Mg}(\text{CH}_3\text{COO})_2 \cdot 4\text{H}_2\text{O}$	DMF, Ethanol, water	125°C, 6h	MOF with the highest CO_2 adsorption capacity of any porous material	[53]
La-MOF	5-(4-(tetrazol-5-yl)phenyl)-isophthalic acid	$\text{La}(\text{NO}_3)_3 \cdot 6\text{H}_2\text{O}$	DMF	90 °C, 72 h	MOF with improved sensitivity for sensing amino acids and antibiotics	[54]
Eu-MOF	9,9-dimethylfluorene-2,7-dicarboxylic acid	$\text{Eu}(\text{NO}_3)_3 \cdot 6\text{H}_2\text{O}$	$\text{CH}_3\text{CH}_2\text{OH}$, DMF, Water	120 °C, 3d	MOF with improved sensitivity for sensing Fe(III) and picric acid	[55]
Typ-MOF	Terpyridine	$\text{Ni}(\text{NO}_3)_2 \cdot 6\text{H}_2\text{O}$	Ethanol/ water	160 °C, 120 h	MOF with multiple binding sites for the adsorption of caffeine from solution	[56]

DMF= N,N-dimethylformamide

INTRODUCTION

Ionic liquids (ILs) represent a novel category of environmentally friendly solvents with broad applications across various fields. **Ionothermal synthesis** utilizes ILs as both solvents and templates to guide the formation of solid structures and can be viewed as a subtype of the hydrothermal/solvothermal technique. Initially, precursor compounds required for MOF synthesis, typically an inorganic metal salt and an organic acid, are dissolved in the IL. Subsequently, the mixture undergoes prolonged heating in an autoclave. Upon synthesis completion, the mixture is cooled to ambient temperature, facilitating the isolation of the crystalline product[57]. Ionic liquids are considered eco-friendly substances compared to traditional organic solvents due to their attributes such as low volatility, significant affinity for organic reagents, increased heat resilience, and lack of flammability. These qualities render them excellent candidates for generating MOFs and other material types like zeolites and chalcogenides. Moreover, ionic liquids provide both anions and cations that can serve as counterions or patterns for MOFs, thus, they have attracted significant attention as substitutes for MOF synthesis. Ionic liquids, derived from a spectrum of 1-alkyl-3-methylimidazolium-X compounds (alkyl = ethyl to amyl and X = halide ions), form the basis for crafting diverse types of MOFs with varying metals and organic linkers, detailed in Table 1.5.2.b[35]. Furthermore, ILs can be reclaimed and reused, rendering them highly effective solvents for achieving successful MOF preparation[5], [18].

Table 1.5.2.b MOFs synthesized using the ionothermal approach.

MOFs	Precursors		Ionic liquid	Reference
	Organic ligand	Metal salt		
Co-MOF	1,4 Benzene Dicarboxylic acid	Co (NO ₃) ₂ ·6H ₂ O	1-Ethyl-3-methylimidazolium chloride	[58]

Zn-MOF	1,3,5 Benzene Tricarboxylic acid	Zn (NO ₃) ₂ ·6H ₂ O	1-Ethyl-3- methylimidazolium bromide	[59]
Mn-MOF	1,3,5 Benzene Tricarboxylic acid	Mn (OAc) ₂	propyl -3- methylimidazolium-iodine	[60]
Cd-MOF	1,4 Benzene Dicarboxylic acid	Cd (NO ₃) ₂ ·4H ₂ O	1-butyl-3- methylimidazolium bromide	[61]
Zn-MOF	1,4 Benzene Dicarboxylic acid	Zn (NO ₃) ₂ ·6H ₂ O	1-butyl-3- methylimidazolium bromide	[62]
Zn-MOF	1,4 Benzene Dicarboxylic acid	Zn (NO ₃) ₂ ·6H ₂ O	1-Amyl-3- methylimidazolium Iodine	[62]
Mg-MOF	4,40-Oxybis (benzoic acid)	Mg (NO ₃) ₂ ·6H ₂ O,	1-butyl-2,3- dimethylimidazolium- Bromide	[63]
In-MOF	1,4-diazabicyclo [2.2.2]octane	In (NO ₃) ₃ ·6H ₂ O	1-Ethyl-3- methylimidazolium ethylsulfate	[64]
Cu-MOF	2,6 bis(pyrazol-3-yl) pyridine	Cu (NO ₃) ₂ ·3H ₂ O	1-butyl-3- methylimidazolium- tetrafluoroborate	[65]
Ni-MOF	1,3,5- benzenetricarboxylic acid	Ni (OAc) ₂ ·4H ₂ O	1-butyl 3- methylimidazolium- bromide	[66]
Eu-MOF	1,4 Benzene Dicarboxylic acid	EuCl ₃ ·6H ₂ O	1-ethyl-3- methylimidazolium bromide	[67]

Nonetheless, these solvents exhibit considerable dynamic viscosity, hindering solute diffusion within the solution and complicating stirring and filtration processes. Additionally, many of these solvents lack a well-defined melting point and may inadvertently crystallize during synthesis. This approach typically involves two synthesis stages: initially synthesizing ILs, followed by MOF synthesis, thereby escalating synthesis costs. Lastly, extracting the final structure from any remaining IL residues poses a significant challenge in ionothermal synthesis[35].

1.5.3 Mechanochemical method

As research advances, there is a notable trend in MOF synthesis towards adopting solvent-free conditions. **Mechanochemical (MC) synthesis** involves inducing chemical reactivity through mechanical force, which can be achieved by manually grinding solid reactants (using a mortar and pestle) or automatically (using electric ball mills), often with minimal or no solvent usage (Figure 1.5.3).

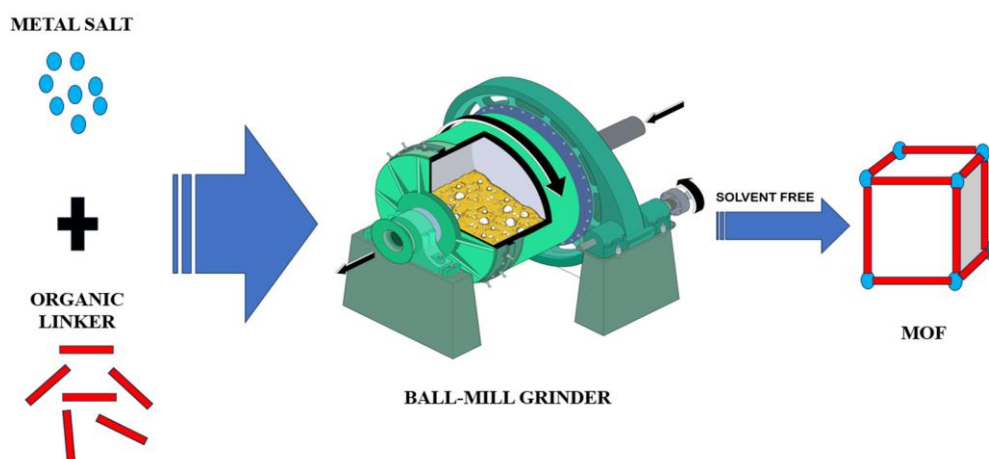


Figure 1.5.3 Illustrative depiction of mechanochemical synthesis of MOFs[68].

Initially, mechanical force breaks down the material's structure into a fine powder, increasing its specific surface area and crystallinity. Subsequent aggregation of particles occurs due to Van der Waals forces. Eventually, as particle agglomeration occurs, the material begins to crystallize and undergo mechanochemical reactions. If solvents are utilized, they typically act as catalysts, enhancing reactant mobility and speeding up reactions. Importantly, unlike other methods, mechanochemical synthesis doesn't necessitate initiators, catalysts, or thermal reactions. The material is obtained solely through grinding. Consequently, MC synthesis is valued for its

INTRODUCTION

environmental friendliness and cost-effectiveness due to its simplicity, mild temperature and pressure conditions, cleanliness, and energy-efficient synthesis. It also eliminates the need for bulk solvents and offers faster reaction times (usually minutes to hours)[5], [23]. Table 1.5.3 provides a comprehensive overview of the precursors, conditions, and characteristics of select MOFs synthesized using the mechanochemical approach according to the literature[43]. The primary drawback of this approach is the challenge in isolating amorphous products[18].

Table 1.5.3 MOFs synthesized using the mechanochemical approach.

MOFs	Precursors		Solvent	Reaction conditions	Remark	Reference
	Organic ligand	Metal salt				
ZIF-62	Imidazole	ZnO	SF	G, 30 min	Mixed metal MOFs via mechanochemical synthesis	[69]
Zn-MOF-74	2,5-dihydroxyterephthalic acid	ZnO	H ₂ O	G, 70min	Highly crystalline MOFs with a high surface area	[70]
Ni-Uio-66	Terephthalic acid	Ni(NO ₃) ₂ ·6H ₂ O	SF	BL, 10 min, 350 rpm	Highly catalytic nickel-modified MOFs for hydrogenation reactions	[71]
ZIF-8	2-methylimidazole	ZnO	SF	BL, 12 h	Well-dispersed MOFs	[72]
MOF-74	2,5-Dihydroxyterephthalic acid	Mg(NO ₃) ₂ ·6H ₂ O	SF	G, 5 min	Highly crystalline MOFs with a high surface area	[73]
Ni-MOF	benzene-1,3,5-tricarboxylic acid	Ni (OAc) ₂ ·4H ₂ O	SF	BL, 10Hz, 1min	Ultrafast synthesis of high crystallinity by ball milling	[74]
ZIF-8, ZIF-67	2-methylimidazole	Zn(CH ₃ COO) ₂ ·2H ₂ O, Co (CH ₃ COO) ₂ ·2H ₂ O	SF	BL, 2 h	Water-stable MOFs	[75]
MOF-74	2,5-dihydroxyterephthalic acid	ZnO	DMF	G, 70 min	Highly porous and crystalline mechanochemically synthesized MOFs	[76]
In-OF-1	3,3',5,5'-biphenyltetracarboxylic acid	In (OAc) ₃ ·6H ₂ O	CH ₃ CN	BL, 40Hz, 20min	Water stable MOF with high CO ₂ adsorption capacity, as well as high CO ₂ /CH ₄ and	[77]

					CO ₂ /N ₂ adsorption selectivities.	
ZIF-8	2-methylimidazole	Zn(OH) ₂	SF	G, 1 h	Fast synthesis of MOFs via manual grinding	[78]
ZIF-8	2-methylimidazole	ZnCO ₃	SF	BL, 1 h, 300 rpm	High surface area MOFs	[79]
Fe-MOF	1,3,5 benzenetricarboxylic acid	Fe (NO ₃) ₃ ·9H ₂ O	TMAOH	BL, 1 h	High crystalline MOF with good thermal stability, high surface area and pore volume	[80]

SF = solvent-free, BL = ball milling, G = grinding, TMAOH = tetramethyl ammonium hydroxide.

1.5.4 Microwave-assisted method

Researchers have proposed various conventional heating methods such as electric heating, sand baths, oil baths, and jacket heating for material synthesis. However, these approaches are time-intensive and demand a considerable amount of energy. In recent times, **microwave heating** has emerged as an alternative to conventional methods, presenting a highly favorable, straightforward, cost-efficient and environmentally friendly approach to synthesizing MOFs. Microwaves, falling between radio waves and infrared waves on the electromagnetic spectrum with frequencies ranging from 0.3 to 300 GHz. Microwave-facilitated synthesis of MOFs relies on the synergy between mobile charges (dipoles) of molecules within the polar solution and microwave radiation (Figure 1.5.4)[81].

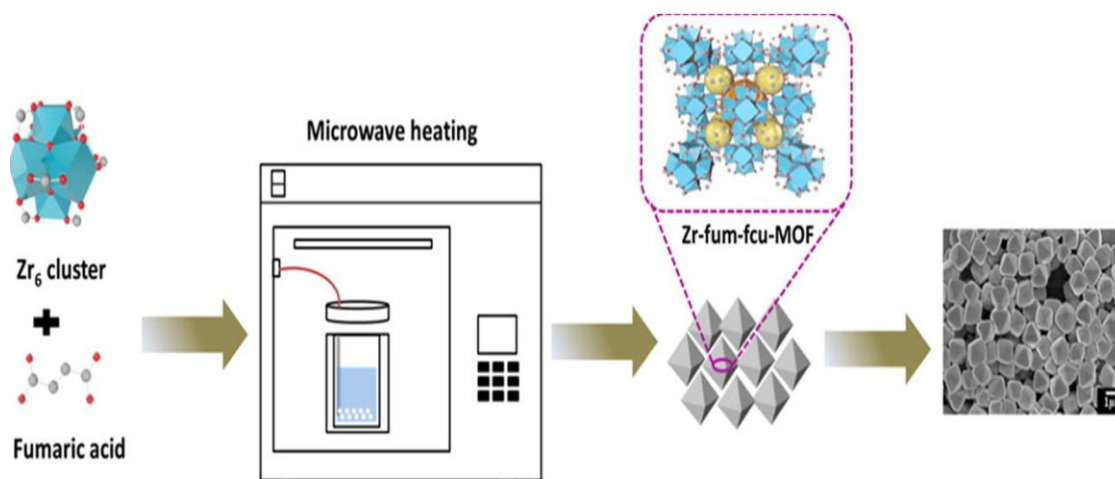


Figure 1.5.4 Schematic description of preparation of Zr-fum-fcu-MOF via microwave-assisted heating method[81].

These mobile charges typically include polar solvents, metal ions, and deprotonated organic ligands present in the solution. Diverging from conventional heating methods, microwave energy serves as the heat source. This method facilitates rapid and consistent heating within materials, significantly reducing synthesis times from hours to seconds and improving the product yield. Factors such as reaction duration and precursor concentration significantly influence both the yield and crystalline quality of the resulting product. In addition to yielding higher quantities and expediting reactions, this approach minimizes the production of undesired byproducts. However, challenges persist, notably in ensuring consistent results, often attributed to differences in microwave apparatus, leading to inconsistencies across different setups [5], [23], [33]. Table 1.5.4 presents a comprehensive summary of the precursors, conditions, and attributes of various MOFs synthesized using microwave methodology[43].

Table 1.5.4 MOFs synthesized using the microwave method.

MOFs	Precursors		Solvent	Reaction conditions	Remark	Reference
	Organic ligand	Metal salt				
Zr-UiO-66, Hf-UiO-66	Terephthalic acid	ZrCl ₄ , HfCl ₄	DMF	110 °C, 3 min	Highly homogeneous nano-sized MOFs with excellent removal capacity for curcumin	[82]
UTSA-16	Citric acid	Zn(CH ₃ COO) ₂ ·2H ₂ O	Ethanol/water	90 °C, 4 h	Highly stable and selective MOFs with excellent CO ₂ capture capabilities	[83]
Cu-HKUST-1	1,3,5 benzene tricarboxylic acid	Cu(NO ₃) ₂ ·3H ₂ O	Ethanol/water	120–170 °C, 10–60 min	MOF with large surface area, high pore volume, high chemical stability, high Lewis acidity and lability of coordinated water molecules. Suitable for adsorption, gas storage applications and catalysis.	[84]
Ni-MOF-74	DHBDC	Ni(NO ₃) ₂ ·6H ₂ O	DMSO, DMF	100 °C, 40 min	Hierarchical MOFs with tunable porosity	[85]
Fe-MIL-100	2, 5-diaminoterephthalic acid	FeCl ₃ ·6H ₂ O	DMF, ethanol, water, HCl	100–180 °C, 5–30 min	MOF with potential for relevant industrial and societal applications (i.e., catalysis, drug delivery, gas sorption).	[86]
MIL-53(Al)	p-phthalic acid	AlCl ₃ ·6H ₂ O	DMF	220 °C, 2 min	Size-controlled MOFs were synthesized in minutes with excellent capability for furfural separation	[87]
Ni₄Co₄Fe₂-MOF	Terephthalic acid	NiCl ₂ ·6H ₂ O, CoCl ₂ ·6H ₂ O, FeCl ₃ ·6H ₂ O	DMF, ethanol, water	40 °C, 30 min	Ultra-thin trimetallic MOFs with excellent electrochemical applications	[88]

Zr-MOF	Formic acid	ZrOCl ₂ ·8H ₂ O	DMF	100 °C, 1 h	Octahedral Zr-MOFs for gas separation applications	[81]
UiO-66	Terephthalic acid	ZrCl ₄	DMF	120 °C, 30 min	Rapidly synthesized Zr-MOF for sensing applications	[89]
Zr-UiO-67	4,4'-biphenyldicarboxylic acid	ZrCl ₄	DMF, benzoic acid, HCl	120 °C, 2.5 h	Thermally stable up to 450 °C and chemically stable in various organic solvents	[90]
MIL-88B	Terephthalic acid	FeCl ₃ ·6H ₂ O, NiCl ₂ ·6H ₂ O	DMF	100 °C, 1 h	Spindle-shaped microporous MOFs with excellent photocatalytic properties	[91]
Cd/Zr-MOF	Terephthalic acid	ZrCl ₄ , CdCl ₂	DMF	120 °C, 30 min	Bimetallic MOFs with high photocatalytic activity	[49]

1.5.5 Sonochemical method

Recently, there has been a noticeable emphasis on exploring **sonochemical methods** for producing various types of MOFs. This technique, employing ultrasound frequencies ranging from 20 kHz to 10 MHz, offers a straightforward and eco-friendly means of producing MOF materials. Utilizing high-energy ultrasound (US), this process induces mechanical vibrations, leading to cyclic fluctuations of high and low-pressure zones within solvents, which in turn prompts bubble formation. These bubbles undergo expansion and collapse, known as acoustic cavitation, generating localized high temperatures (ranging from 5000 to 25,000 K), pressures (~1000 bar), and rapid heating and cooling rates, termed hot spots. Hot spots play a critical role in swiftly releasing energy and expediting the ultrasound-assisted synthesis process (Figure 1.5.5).

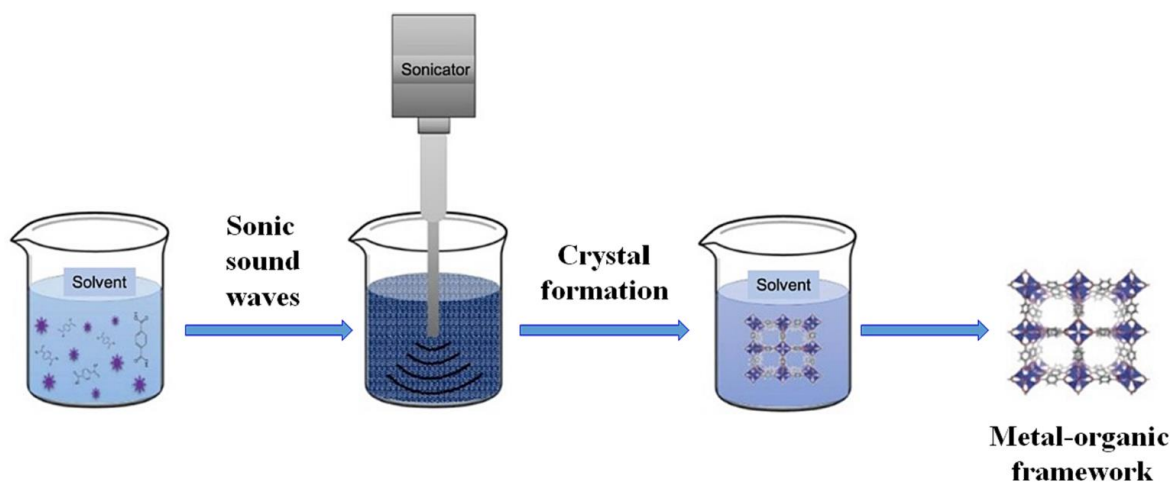


Figure 1.5.5 Schematic description of sonochemical synthesis of MOFs[43].

Significant performance enhancements have frequently been documented through the integration of the sonochemical method. The efficiency of the process and structural properties of synthesized materials are significantly affected by parameters such as ultrasonication duration, frequency, temperature and reactant concentration. Ultrasound intensity, specifically, has been observed to affect the arrangement of linkages within the framework[18], [23], [33]. Sonochemical synthesis offers several advantages over conventional methods, including uniform nucleation, significantly shorter crystallization times, small-particle MOFs with improved surface areas under exceptionally gentle reaction conditions. Table 1.5.5 provides an overview of several MOFs synthesized using the sonochemical approach[43].

Table 1.5.5 MOFs synthesized using the sonochemical method.

MOFs	Precursors		Solvent	Reaction conditions	Remark	Reference
	Organic ligand	Metal salt				

INTRODUCTION

U-CDMOF	Cyclodextrin	KOH	Methanol	20 kHz, 540 W, 10 min, 60 °C	Ultra-fast synthesis of CD-MOF for caffeic acid loading	[92]
Ce-UiO-66	1,4-benzenedicarboxylate	(NH ₄) ₂ Ce (NO ₃) ₆	Water, DMF	30 min, 50 °C, 35 kHz	MOF with uniform and small particles, water stable and a promising feature for CO ₂ sorption	[93]
TMU-34	H2DPT	Zn(CH ₃ COO) ₂ ·2H ₂ O	DMF	40 kHz, 150 W, 160 min, 120 °C	Plate-like MOFs for sensing applications	[94]
Ag-MOF	p-hydroxybenzoic acid	AgNO ₃	Methanol	60 W, 60 min, 70 °C	Silver-based MOF with excellent catalytic capability for the degradation of herbicides	[95]
Mg-MOF-74	2,5-dihydroxyterephthalic acid	Mg(NO ₃) ₂ ·6H ₂ O	DMF, NMP, Ethanol, Water	20 kHz, 150–500 W	High quality crystals and open metal sites showed both high CO ₂ and water vapor sorption capacities. Efficient separation of CO ₂ from N ₂ .	[96]
MOF-525	Tetrakis (4-carboxyphenyl) porphyrin	ZrCl ₄ ·8H ₂ O	DMF	20 kHz, 200 W, 2.5 h, 80 °C	Cubic-shaped MOF with high surface area and pore volume	[97]
MOF-545	Tetrakis (4-carboxyphenyl) porphyrin	ZrCl ₄ ·8H ₂ O	DMF	20 kHz, 300 W, 30 min, 80 °C	Needle-shaped MOF with high surface area and pore volume	[97]
TMU-42	1,4-bis(4-pyridyl)-3,4-diaza-1,3-butadiene	Zn(CH ₃ COO) ₂ ·2H ₂ O	DMF	5 min, RT	Rod-shaped MOF with excellent catalytic activity	[98]
Cu-HKUST-1	1,3,5 benzene tricarboxylic acid	Cu(CO ₂ CH ₃) ₂ ·xH ₂ O	DMF, Ethanol, Water	5–60 min, 40 kHz, 60 W	Nano-sized 3D MOF, high efficient and environmental friendly	[99]

Co-MOF	Trimesic acid	$\text{Co}(\text{CH}_3\text{CO}_2)_2 \cdot 4\text{H}_2\text{O}$	Deionized water	40 kHz, 300 W, 30 min, RT	Low-cost Co-MOFs with high Congo red dye removal efficiency	[100]
Zn/Co-ZIFs	2-methylimidazole	$\text{Zn}(\text{NO}_3)_2 \cdot 6\text{H}_2\text{O}$, Co $(\text{NO}_3)_2 \cdot 6\text{H}_2\text{O}$	Methanol	16 min, RT	Highly catalytic and chemically stable ZIF	[101]

RT = room temperature, NMP= N-Methyl-2-pyrrolidone.

1.5.6 Electrochemical method

The **electrochemical (EC)** approach shows significant potential for producing MOFs on a large scale rapidly and with minimal environmental harm. EC synthesis is divided into two primary types: anodic deposition and cathodic deposition. In anodic deposition, a metal plate serves as the anodic electrode, immersed in a saturated solution including the organic linker and an electrolyte. Upon applying a particular voltage, corrosion happens at the anode, causing the metal (M) in the electrode to oxidize into M^{n+} ions in the solution surrounding the electrode's surface. These oxidized metal ions swiftly undergo a reaction with the dissolved linker, resulting in the creation of MOF forming a dual layer around the electrode. Figure 1.5.6.a shows the anodic deposition of

HKUST-1 on a thin Cu mesh[102]. To hinder the reduction of M^{n+} ions on the electrode surface, protic solvents or sacrificial compounds like acrylonitrile, acrylic, or maleic esters are employed.

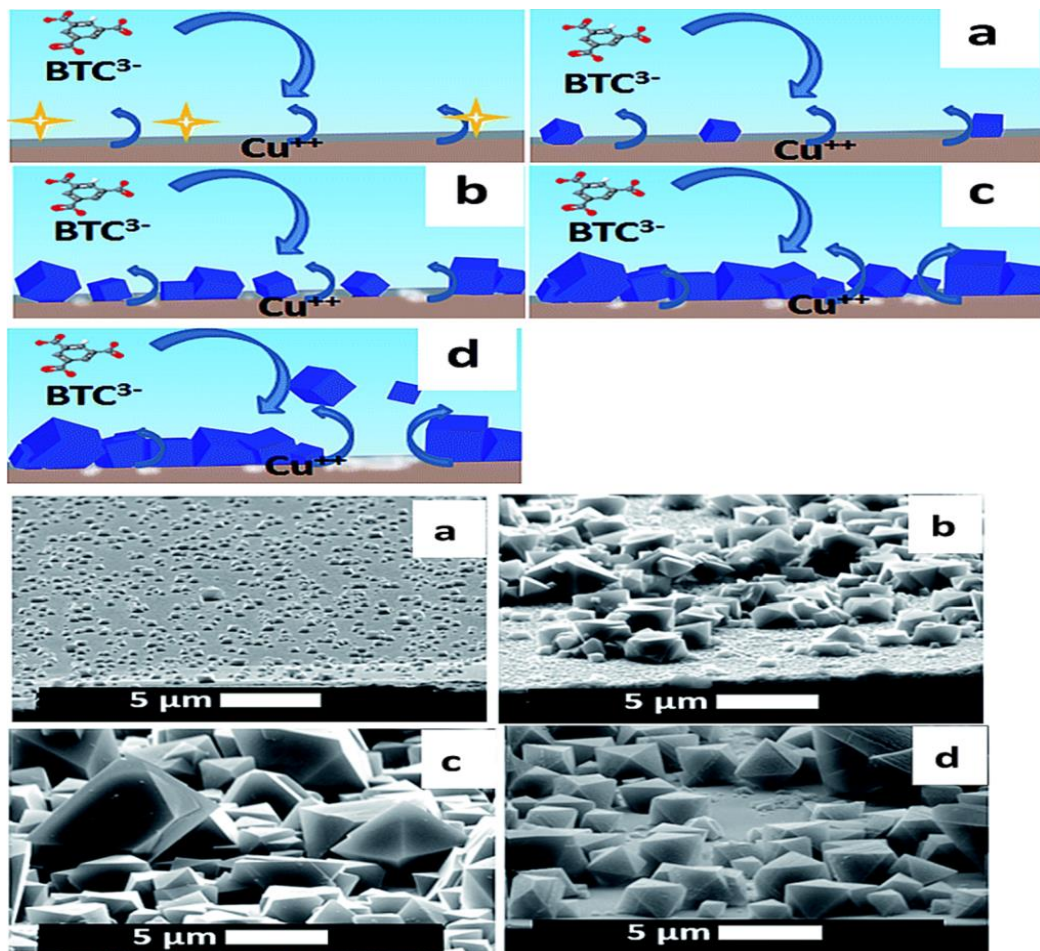


Figure 1.5.6.a Mechanism of anodic deposition of MOFs[102].

Cathodic deposition involves a solution of organic linker, metal ions, a pro-base (e.g. NO_3^- , Et_3NH^+ , H_2O etc.) and an appropriate electrolyte with a cathodic electrode. The necessity of pro-base is to deprotonate the organic ligand in the bulk reaction medium. At an optimal electrical potential, the electrochemical reduction of pro-base yields to produce a base, elevating the pH locally around the electrode surface. This pH modulation induces the deprotonation of ligands,

INTRODUCTION

facilitating their coordination with metal ions and subsequently initiating the precipitation of MOF crystals. Figure 1.5.6.b presents a simple cathodic electrochemical synthesis of MOFs[103].

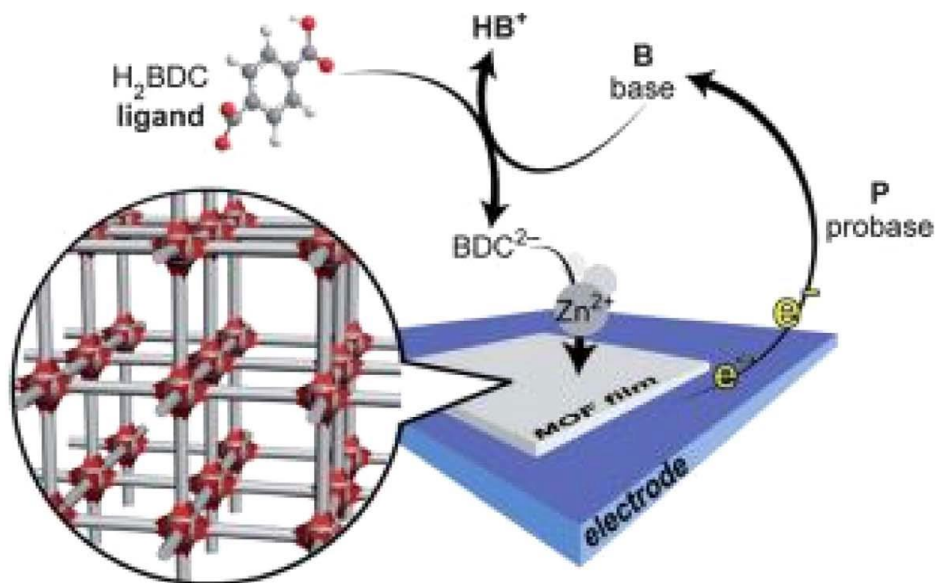


Figure 1.5.6.b Schematic representation for the cathodic electrochemical deposition of MOFs which involves the reduction of a probase (P), the generation of base (B), the deprotonation of organic ligand (H_2BDC) and MOF crystallization by the coordination between BDC^{2-} and metal ions (Zn^{2+})[103].

The characteristics of MOFs produced through electrochemical methods are shaped by a range of factors. These encompass voltage, current, electrode spacing, duration of the electrochemical procedure, the specific solvents employed in the electrolyte, the interplay between the linker and electrolyte/electrode, and the concentration of the electrolyte. In comparison to traditional methods, the electrochemical approach offers several advantages, such as gentle reaction conditions (including rapid reaction times, ambient pressures, and temperatures), consistent reaction environments, straightforward execution, precise regulation of applied voltage at the electrode, and the potential for large-scale MOF production. Nevertheless, achieving precise

control over parameters like layer thickness, particle size, and MOF structure during electrochemical synthesis remains a challenge[23], [33]. Furthermore, overcoming the solubility constraints of organic ligands can present a notable hurdle, particularly when dealing with ligands that exhibit reduced solubility. Table 1.5.6 summarizes several MOFs synthesized using the electrochemical approach[43].

Table 1.5.6 MOFs synthesized using the electrochemical approach.

MOFs	Precursors		Electrolyte	Synthesis conditions	Reference
	Organic ligand	Metal salt			
MOF-199	Trimesic acid	Copper plate	MTBS	1.3 A, 12-19 V, 150 min, cathode	[104]
MOF-199	Trimesic acid	Copper plate	MTBS	45.58 mA, 5 V, 30 min, 50 °C, anode	[105]
Ni-BTC-MOF	1,3,5 benzene tricarboxylic acid	Ni plate	TBATFB	15 V, 90 min, anode, Drying: 1) RT, 24 h, and 2) in an oven at 100 °C, 12 h. Activation: 200 °C, 2 hours.	[106]
Zn-BPDC	2,2' -bipyridine5,5' - dicarboxylic acid	Zinc foil	-	0.75 V, 30 min, 50 °C, anode	[107]
Zn-MOF-5	1,4- benzenedicarboxylate	Zn (NO ₃) ₂ ·6H ₂ O	Bmim-Cl	0.025 A/cm ² , 120 min, 80 °C, anode	[108]
Co-MOF	Trimesic acid	Coated cobalt	Triethylamine hydrochloride	2.5 V, 15 min, cathode	[109]
Zr-MOF	Tetrakis(4- carboxyphenyl)porphyrin	Zirconium plate	HNO ₃	30 mA, 5 V, 120 min, 110 °C, anode	[110]
Zr-UiO-66	1,4- benzenedicarboxylate	Pt and Al electrode, ZrCl ₄	TBAB	6 V, 5 h, cathode	[111]
Cu-MOF	Disodium 5,50 - bitetrazole-1-ide	Pencil graphite electrode	Triethylamine hydrochloride	30 mA, 1.4 V, 60 min, 110 °C, cathode	[112]
Ti-MIL-100	1,4- benzenedicarboxylate	Ni foam, TiCl ₄	TBAPF ₆	-1.2 V, 240 min, cathode, 120°C, 18h, N ₂	[113]
NENU-3	1,3,5 benzene tricarboxylic acid	Cu plate	PTA	2 V, 240 min, anode	[114]

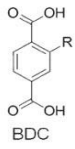
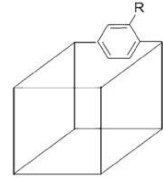
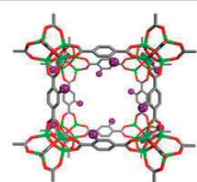
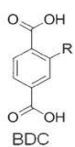
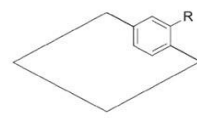
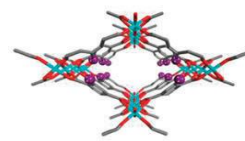
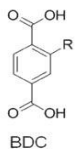
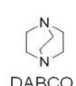
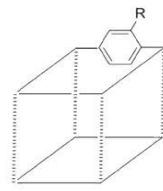
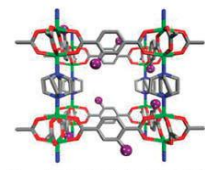
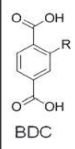
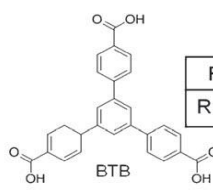
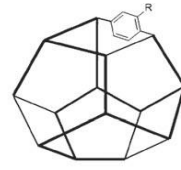
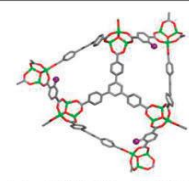
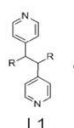
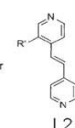
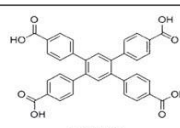
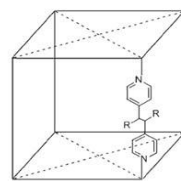

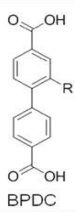
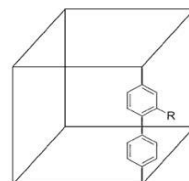
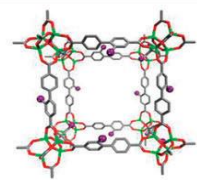
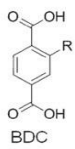
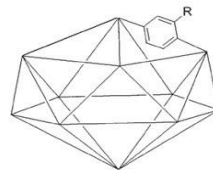

RT= room temperature, MTBS = methyltributylammonium methyl sulfate, TBATFB= Tetrabutylammonium tetrafluoroborate, Bmim-Cl: Butyl-3-methylimidazolium chloride, TBAB= Tetrabutylammonium bromide, MTBS= methyltributylammonium methyl sulfate, TBAPF6= Tetrabutylammonium hexafluorophosphate.

1.5.7 Prefunctionalization

Research on MOFs has focused heavily on their **functionalization** and **modification**, recognizing the pivotal roles of metal ions and organic ligands in determining framework structure, pore characteristics, and chemical behavior. The choice of building blocks, both metallic and organic, significantly influences the framework's capability for substance absorption and guest molecule interactions, impacting its utility in storage, catalysis, and separations. There's a notable trend towards enhancing MOFs by customizing their pore functionalities, typically achieved through “**prefunctionalization**”, the addition of specific substituents to organic ligands prior to solvothermal synthesis. This strategy has enabled the integration of specific groups including –Br, –NH₂, –CH₃, among others, along the cavity passages of MOFs. These functional groups have been successfully integrated into a diverse array of MOF products, exemplified by prominent instances such as ZIFs and the MIL-53(Fe) series (Table 1.5.7). While direct solvothermal synthesis has yielded a diverse array of functionalized MOFs, the scope of functional groups within their pores remains somewhat constrained. This limitation primarily stems from the challenge of compatibility or stability of certain functional groups under the high temperatures and pressures necessary for solvothermal MOF synthesis, crucial for achieving the desired crystalline phases[115].

INTRODUCTION

Table 1.5.7 Organic ligands (linkers, left), scaffold representation (middle), and lattice structure (from X-ray data, right) of several MOFs[115].

<div></div> <div><table><tr><td>R = H</td><td>IRMOF-1</td></tr><tr><td>R = NH₂</td><td>IRMOF-3</td></tr></table></div> <div>BDC</div>	R = H	IRMOF-1	R = NH ₂	IRMOF-3	<div></div>	<div></div> <div>Zn₄O(R-BDC)₃</div>
R = H	IRMOF-1					
R = NH ₂	IRMOF-3					
<div></div> <div><table><tr><td>R = H</td><td>MIL-53</td></tr><tr><td>R = NH₂</td><td>MIL-53-NH₂</td></tr></table></div> <div>BDC</div>	R = H	MIL-53	R = NH ₂	MIL-53-NH ₂	<div></div>	<div></div> <div>Al(OH)(R-BDC)</div>
R = H	MIL-53					
R = NH ₂	MIL-53-NH ₂					
<div></div> <div><div></div>DABCO</div> <div><table><tr><td>R = H</td><td>DMOF-1</td></tr><tr><td>R = NH₂</td><td>DMOF-1-NH₂</td></tr></table></div> <div>BDC</div>	R = H	DMOF-1	R = NH ₂	DMOF-1-NH ₂	<div></div>	<div></div> <div>Zn₂(R-BDC)(DABCO)</div>
R = H	DMOF-1					
R = NH ₂	DMOF-1-NH ₂					
<div></div> <div></div> <div><table><tr><td>R = H</td><td>UMCM-1</td></tr><tr><td>R = NH₂</td><td>UMCM-1-NH₂</td></tr></table></div> <div>BDC</div>	R = H	UMCM-1	R = NH ₂	UMCM-1-NH ₂	<div></div>	<div></div> <div>Zn₄O(BTB)_{4/3}(R-BDC)</div>
R = H	UMCM-1					
R = NH ₂	UMCM-1-NH ₂					
<div><div></div><div>or</div><div></div><div></div><div>TCPB</div><div><table><tr><td>R = OH</td><td>DO-MOF</td></tr><tr><td>R' = C≡C-TMS</td><td>TO-MOF</td></tr></table></div></div>	R = OH	DO-MOF	R' = C≡C-TMS	TO-MOF	<div></div>	<div></div> <div>Zn₂(L_n)(TCPB)</div>
R = OH	DO-MOF					
R' = C≡C-TMS	TO-MOF					
<div></div> <div><table><tr><td>R = H</td><td>IRMOF-9*</td></tr><tr><td colspan="2">* See main text for more details</td></tr></table></div> <div>BPDC</div>	R = H	IRMOF-9*	* See main text for more details		<div></div>	<div></div> <div>Zn₄O(R-BPDC)₃</div>
R = H	IRMOF-9*					
* See main text for more details						
<div></div> <div><table><tr><td>R = H</td><td>MIL-101</td></tr><tr><td>R = NH₂</td><td>MIL-101-NH₂</td></tr></table></div> <div>BDC</div>	R = H	MIL-101	R = NH ₂	MIL-101-NH ₂	<div></div>	<div></div> <div>M₃O(H₂O)₂X(R-BDC)₃ M/X = Cr/F or Fe/Cl</div>
R = H	MIL-101					
R = NH ₂	MIL-101-NH ₂					

1.5.8 Post-synthetic modification

Another versatile and practical approach to obtain functionalized MOFs involves **post-synthetic modification (PSM)**, which refers to chemically modifying a framework after the formation of the solid lattice. This approach offers distinct advantages over prefunctionalization by providing greater control over the types and quantities of functional groups integrated into the framework, while maintaining the framework's durability and preserving their topological integrity [5], [115]. The primary strategies of PSM to functionalize MOFs comprise **covalent** and **coordinate covalent modifications**, as depicted in Figure 1.5.8.

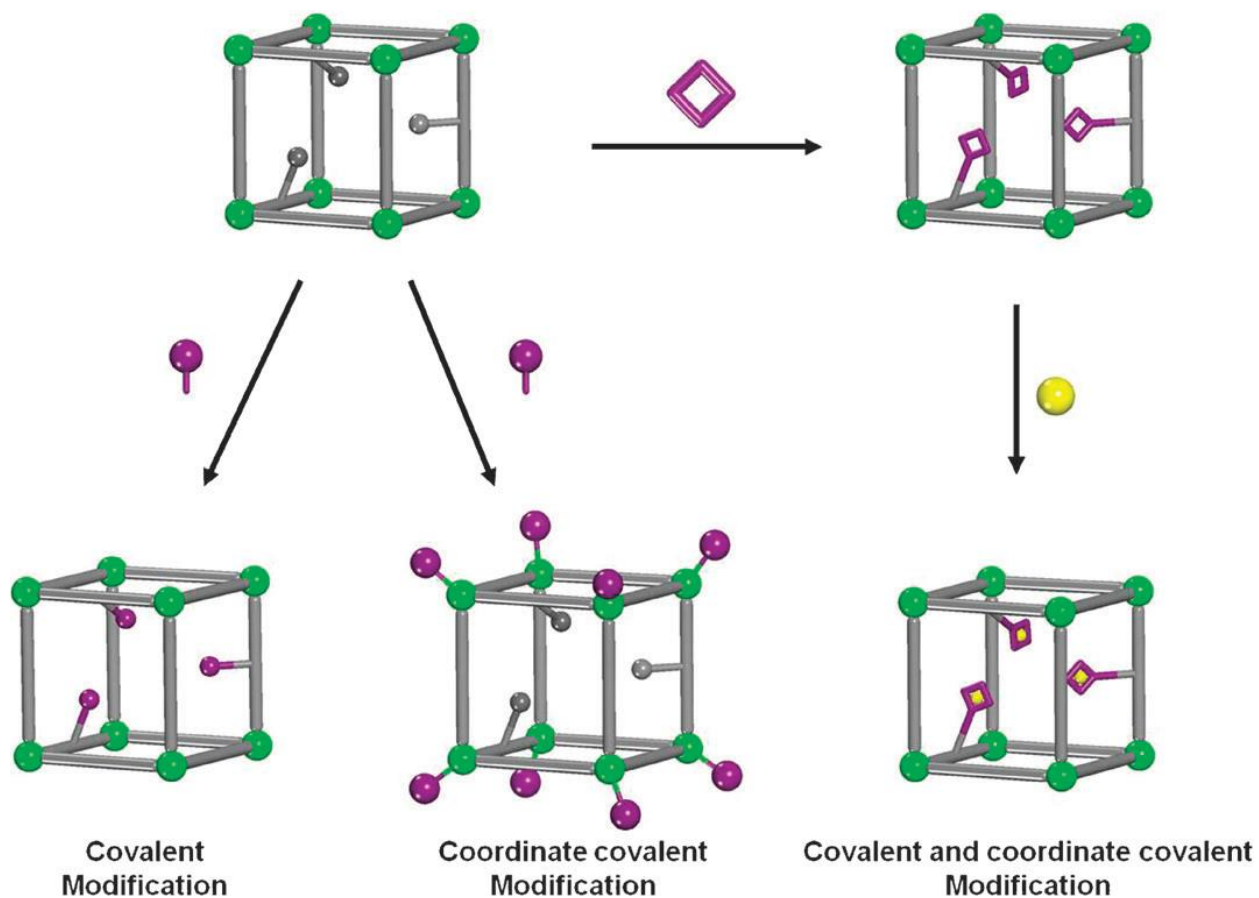


Figure 1.5.8 *Depiction of covalent modification (left), coordinate covalent modification (middle), and a combination of PSM strategies (right) for modifying MOFs[115].*

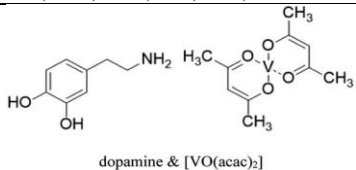
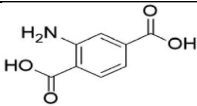
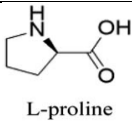
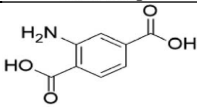
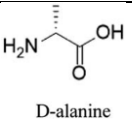
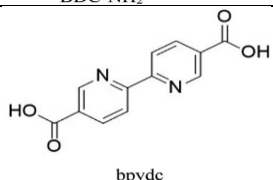
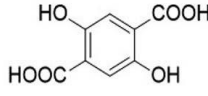
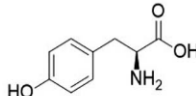
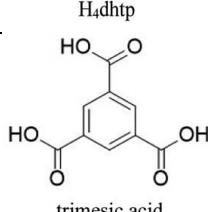
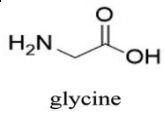
Covalent modification refers to the chemical alteration of the organic ligand within the MOF structure. In contrast, coordinate covalent modification entails adjusting the coordination environment of the SBUs enclosed to the framework while preserving the overall SBU or framework topology. There are two principal methods for coordinating covalent modification. The first principle occurs when unsaturated metal sites are present in the SBUs of the frameworks. In this scenario, coordinating ligands such as alkylamines or pyridines can be added to the framework to interact with these metal nodes (Figure 1.5.8). The second principle arises when the organic linker of the MOF contains metal-binding groups, such as $-OH$, that are not essential to the framework structure. In this instance, the organic linker can undergo metalation using the PSM[18], [115].

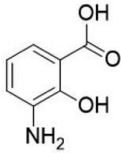
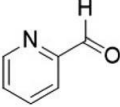
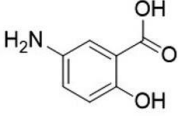
The activated sites within MOFs for post-synthetic modification (PSM) encompass amino ($-NH_2$), sulfonyl ($-SO_3H$), hydroxyl ($-OH$), carbonyl ($C=O$) groups, and metal ions. Notably, the amino group emerges as the primary locus for reactions, driving over 90% of PSM reactions in MOFs. Modifying agents in PSM range from amino acids to anhydrides, aldehydes, and metal ions. Table 1.5.8.a summarizes the activated PSM sites and functional groups crucial in the post-synthetic modification landscape of MOFs[116]. However, not all MOFs are inherently equipped with unsaturated metal sites or metal-binding groups. To overcome this limitation, a proposed solution involves integrating both covalent and coordinate covalent modifications (Figure 1.5.8). This approach extends the organic linker of the framework with a ligand, and then metallizing it.

INTRODUCTION

Specifically, this approach enables the introduction of various combinations of chelators (e.g., –OH, –COOH) and metal ions into the framework.

Table 1.5.8.a MOFs functionalized using the post-synthesis modification.

Parent MOFs	Activated PSM sites	Functional groups	Post-synthetic MOFs	References
Mn ^{III} SO-MOF	Mn ³⁺	Cr ²⁺ , Co ²⁺ , Mn ²⁺ , Ni ²⁺ , Cu ²⁺ , Zn ²⁺	M ^{II} SO-MOF	[117]
MIL-101(Cr)	Unsaturated chromium(III) centers	 dopamine & [VO(acac) ₂]	V(dop)-MIL-101(Cr)	[118]
(In) MIL-68-NH ₂	 BDC-NH ₂	 L-proline	(In) MIL-68-NH-(L)-Pro	[119]
(In) MIL-68-NH ₂	 BDC-NH ₂	 D-alanine	(In) MIL-68-NH-(D)-Ala	[119]
MOF-253	 bpydc	Pt ²⁺	MOF-253-Pt	[120]
Co-MOF-74	 H ₄ dhtp	 L-tyrosine	Co-MOF-74-L-Tyr	[121]
HKUST-1	 trimesic acid	 glycine	Gly@Cu MOF	[122]

DEMOF-I	 3-aminosalicylic acid	 2-pyridine aldehyde & Pd ²⁺	I-3-pSAx-Pdy I-5-pSAx-Pdy	[123]
	 5-aminosalicylic acid			

In essence, each synthesis approach for MOFs exhibits unique attributes, benefits, and limitations. The resulting MOFs' properties are tied to the conditions inherent in these diverse methods. Table 1.5.8.b gathers various synthesis pathways for MOFs, elucidating their advantages and disadvantages.

Table 1.5.8.b A summary of some main synthetic approaches used for MOFs synthesis (Retrieved from Ref.[34], [43], [115], [124]).

Method	Characteristics	Approx. reaction time	Temperature	Advantage	Disadvantage
Classical Method	MOF crystallization occurs typically by allowing the slow evaporation of a solution containing the initial components or assisted by the slow diffusion of reactants	Extended reaction times	< 100°C	Typically operates under mild conditions; Might does not require any external energy	Time consuming; Typically, MOFs with low purity are obtained, prompting the filtration of the reaction mixture and subsequent collection of the reaction product for further solvent evaporation
Solvothermal/Hydrothermal Method	MOF crystallization in a closed vessel at a temperature above the boiling point of the solvent and under autogenous high pressure	24 – 96 h	50 – 180°C	High yields; Good crystallinity; High porosity; Simple crystals; Basic equipment; Pure products; Easy to control the reaction conditions	Time-consuming; Requires special equipment such as autoclaves or sealed containers; Multistep process; High energy requirement; Large amount of solvent is needed
Ionothermal Method	Crystallization process based on ionic liquids	2 – 48 h	25 – 100°C	Almost zero vapor pressure; Solvating properties; High thermal stability.	Residues of ionic liquids
Mechanochemical Method	A solvent-free synthesis technique based on ball milling or manual grinding	30 – 180 min	RT	One step synthesis; Ambient synthesis; Green method; Minimal generation of postreaction waste; High yields; Solvent-free MOFs synthesis; Cost-effective	Limited to specific MOFs; MOFs with poor crystallinity; Requires special mills and grinders; There is potential for the introduction of impurities during milling; Difficult to control the reaction conditions
Microwave-assisted Method	The reaction by the molecular excitation resulting from the microwave electromagnetic radiation	5 min – 4 h	30 – 150°C	Reduced reaction time; High synthesis efficiency; Controllable particle size; Narrow particle size distribution; Pure and crystalline products; Low energy requirement; Minimal postreaction waste generation and side products	Low productivity; High equipment costs; Difficult to manipulate the reaction conditions; The reaction conditions are often not reproducible

Sonochemical Method	A synthesis technique using ultrasonic radiation (20 kHz – 10 MHz)	30 – 120 min	25 – 50°C	Effective particle size reduction; Concentrated suspensions; Short reaction times; Environmentally friendly; Low energy requirement; Highly homogeneous crystalline products	Restricted temperature range; Might lead to the poor crystallinity
Electrochemical Method	Crystallization and generation of metal ions using electrical energy	10 – 60 min	RT	Appropriate for scale-up; Continuous process; MOFs with high solids content can be produced; Fast reaction process; Mild reaction conditions	Requires special apparatus; Continuous electrical contact between the power source and electrode is needed to guarantee continued MOFs formation; The solubility of the inert organic linkers could be a limitation; Low throughput; Poorly understood mechanism of cathodic reactions
Post-synthesis Modification	Chemical modification of the framework after the solid lattice formation. The primary strategies of PSM to functionalize MOFs comprise covalent and coordinate covalent modifications	Few minutes to several days	Ambient or elevated temperatures, depending on the specific reaction conditions and the nature of the modification being performed	Precisely tailor the pores of the MOF in order to improve host-guest interactions; Greater control over the types and quantities of functional groups integrated into the framework, without compromising the overall stability of the framework; Creates functionally diverse frameworks while preserves their topological integrity	Not all MOFs inherently feature unsaturated metal sites at the SBUs or metal-binding groups within their organic linkers; Time consuming depending on factors such as the complexity of the modification, the reactivity of the reagents involved, and the desired extent of the modification

1.6 Fundamentals of MOF stability

Early MOFs were commonly synthesized using divalent metals such as Cu^{2+} and Zn^{2+} , which endowed them with remarkable porosity and broad application potential. However, the instability of M(II) carboxylate bonds rendered these MOFs vulnerable to degradation in aqueous environments or humid air, significantly diminishing their practical utility. For example, MOF-5, constructed from Zn^{2+} , represented a significant breakthrough in MOF research, yet its structure is prone to collapse and gradual decomposition upon exposure to atmospheric moisture. The relatively weak metal coordination bonds in many MOF materials lead to poor stability, and high sensitivity to water. This poses a challenge as industrial processes, including material preparation, storage, and transportation, often involve exposure to gaseous or liquid water. Consequently, the instability of many MOFs in air, water, and acidic or basic solutions severely limits their commercial applications and prevents large-scale production[125].

In recent years, researchers have increasingly prioritized the durability of MOFs. They are exploring the stability of MOFs under various conditions, investigating the causes and pathways of their decomposition, and aiming to design more stable framework structures. This research is crucial for enhancing the practical applications and commercial viability of MOF materials.

1.6.1 Stability in water

The degradation mechanism of MOFs in humid conditions involves a series of reactions where the metal-coordinated linkers are replaced by water molecules or hydroxide ions. Consequently, a direct approach to hinder this process is by enhancing the durability of the bonds between the organic ligands and the inorganic nodes. Following the HSAB theory, the association of hard Lewis

INTRODUCTION

acids with hard Lewis bases or soft Lewis acids with soft Lewis bases tend to be more robust compared to interactions between hard acids and soft bases or soft acids and hard bases. Therefore, a strategy for constructing stable MOFs involves using carboxylate-based ligands with high-valent metal ions, recognized as hard Lewis bases and hard Lewis acids, respectively, or azolate-based ligands with low-valency transition metal ions, recognized as soft Lewis bases and soft Lewis acids, respectively. By following this approach, numerous MOFs with outstanding stability have been successfully synthesized[11].

According to the above interpretation, carboxylate MOFs containing M^{3+} (Al^{3+} , Cr^{3+}) or M^{4+} (Zr^{4+} , Hf^{4+}) ions tend to exhibit greater chemical stability compared to those incorporating M^{2+} metal ions (e.g., Zn^{2+} , Co^{2+} , Ni^{2+})[24]. Notably, **Zirconium-based MOFs** have garnered considerable interest due to the variable and high oxidation state of Zr(IV) in comparison to other metal-based MOFs. Zirconium is abundantly available in nature and is ubiquitous in biological systems. Its widespread availability and low toxicity render zirconium metal ions favorable for the advancement and application of Zr-MOFs. The strong affinity between Zr(IV) and carboxylate oxygen atoms is likely due to high charge density, bond polarization, and adherence to HSAB principle. Specifically, Zr(IV) and carboxyls are categorized as hard acid and base, respectively, thereby forming exceptionally stable bonds (Figure 1.6.1.a, b)[7].

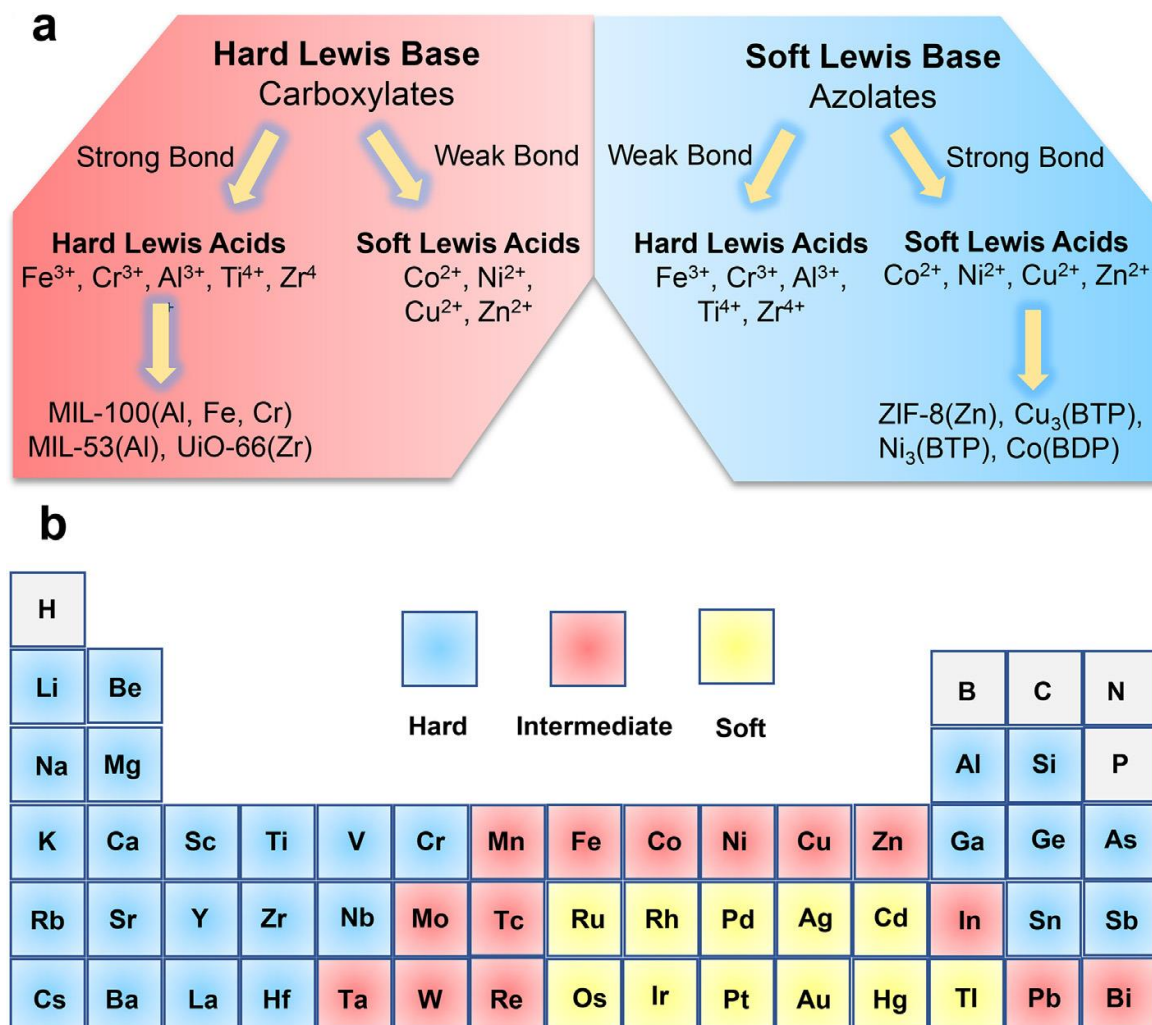


Figure 1.6.1 a) Strategies to construct stable MOFs guided by HSAB theory, b) Divide metals in the periodic table into soft acids (yellow), intermediate soft/hard acids (red), and hard acids (blue)[125].

1.6.2 Stability to Acids/Bases

Compared to moisture, acidic or alkaline environments pose significantly greater risks to MOFs. Consequently, constructing steady MOFs with strong endurance to proton and hydroxide ions proves to be exceptionally challenging. Moreover, different MOFs exhibit varying degrees of

INTRODUCTION

stability when exposed to acidic and alkaline environments. Under acidic conditions, despite the strong coordination bonds between soft acids and soft bases, the relatively high pK_a values of soft bases, like, azoles imply a robust affinity between azolate groups and protons (Figure 1.6.2)[126]. Therefore, this increased affinity makes the system susceptible to degradation in acidic solutions. However, MOFs featuring hard acids and hard bases exhibit remarkable stability in acidic conditions due to the combination of low pK_a values of hard bases, like, carboxylic acids and robust coordination bonds. An equivalent interpretation can also shed light on the stability of MOFs in alkaline solutions. Given the strong attraction between hard acids and OH⁻ ions, MOFs composed of hard acids and hard bases are prone to degradation in basic solutions. On the other hand, soft acids create strong bonds with soft bases and show similarly low affinity to OH⁻ ions, resulting in MOFs with exceptional stability in basic solutions[11]. Table 1.6.2 summarizes various pH-stable MOFs reported in the literature.

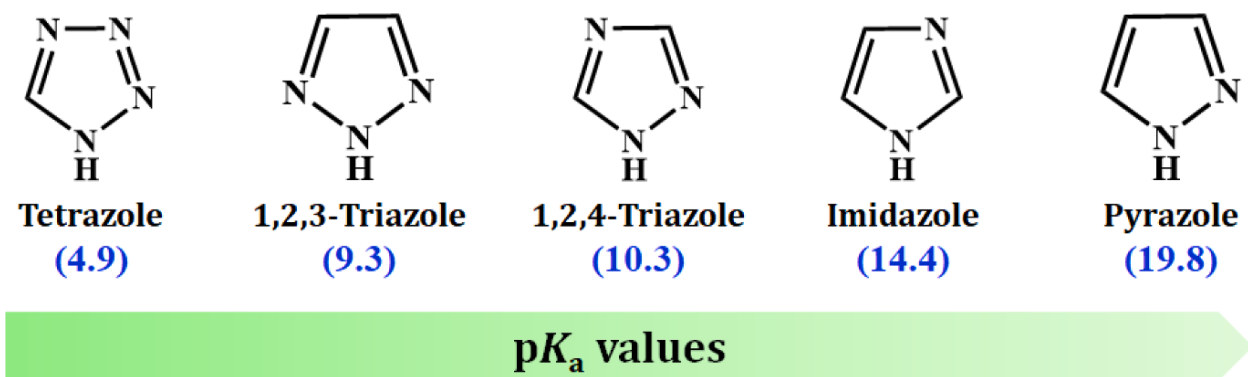


Figure 1.6.2. pK_a values of azolate-based ligands and the corresponding bond strengths with soft acid metal centers (listed in ascending order)[126].

Table 1.6.2 Comparison table of developed pH-stable MOFs (considered up to July 2022).

MOFs	Molecular formula	pH stability range	Duration	BET surface area (m ² /g)	Key reasons behind pH stability	Employed applications	References
BUT-14	Zr ₆ O ₄ (OH) ₈ (H ₂ O) ₄ (L ¹) ₂	1–10	48 h	1595	Due to the presence of ample Zr–O coordination along with high connectivity of metal center	Selective detection of Fe ³⁺ ion	[127]
BUT-66	Zr ₆ (μ ₃ -O) ₄ (μ ₃ -OH) ₄ (BDB) ₆	3–10	1 month	1096	Due to the presence of 2-fold interpenetrated framework, high connectivity around metal centre along with stronger Zr–O coordination	Adsorption of Volatile organic compounds (VOCs)	[128]
NU-1000	-	pH = 1.5–3.5, 0.1 M HCl, 1 mM NaOH	-	-	Due to strong ample Zr–O coordination along with rigid ligand employment	Potential insulin carrier for oral delivery	[129], [130]
SNNU-51	{[Co ₃ (μ ₃ -OH)][Co(PDC) ₂] ₃ (TPP) ₃ } _n	3–11	24 h	1170	Due to the presence of stronger metal–N coordination along with high connectivity of the metal centre	Efficient separation of CH ₄ /CO ₂ along with other C ₂ s hydrocarbons and acts as an electrochemical pseudocapacitor	[131]
USTC-8(In)	-	2–11	12 h	1139	Because of stable In-oxo clusters formation	Photocatalyst in Hydrogen Production	[132]
UiO-66 (Zr)	-	0–12	2 months	-	Due to the presence of strong Zr–O coordination and high connectivity of the metal centre	-	[133]
UiO-66-N = Nind	-	1–12	-	811	Due to the presence of strong Zr–O coordination and formation of an extended delocalized system of the postsynthetically modified	Used as a fluorescent pH sensor	[134]

					framework		
Zr-UiO-66-O^{Ph}-NO₂	[Zr ₆ O ₄ (OH) ₄ (BDC-C ₆ H ₄ NO ₃) ₆] ·6H ₂ O·7DMF	1 M HCl, AcOH, pH = 8–10	24–48 h	1040	Because of the strong electrostatic interaction between metal nodes and carboxylate linker owing to the high charge density of metal ions	Detection of H ₂ S both in the aqueous medium and vapour phase	[135]
CSMCRI-9	[Cd _{1.5} (TCA)(bpg) _{0.5} (H ₂ O)]·3DMA·2H ₂ O	4–10	12 h	469	Due to the formation of 2-fold interpenetrated framework along with presence of ample $\pi\cdots\pi$ and C–H $\cdots\pi$ stacking interactions between the aromatic rings of the ligand and the linker	Detection of organocontaminants in water and catalyses CO ₂ cycloaddition reaction	[136]
ZZU-281	[Mn ₃ (μ_3 -OH) ₂ (TTPE)(H ₂ O) ₄]·2H ₂ O	3–10	1 week	-	Due to the presence of strong metal-N coordination	Catalysis in ozone decomposition	[137]
FJI-H14	[Cu(BTTA)H ₂ O] _n ·6nH ₂ O	2–12	24 h	904	Due to the presence of unique paddle-wheel structure along with strong metal-N coordination	CO ₂ capture and conversion into cyclic carbonates	[138]
MIL-100(Fe)	-	1–10	7 days	1598	Due to the strong interaction between metal and O of carboxylate ligand having high charge density of metal ions	Acts as stationary phase in HPLC for both NP and RP	[139]
Al-MOF-1	[Al(OH)(PATP)]·solvent	2–12	-	38	Due to the presence of bulky hydrophobic -NH-CH ₂ -py groups	As(V) sorption and selective detection of Cr(VI)	[140]
Eu-TPTC	{[Eu(TPTC) _{0.5} (DMF) ₂ (NO ₃)]·2H ₂ O} _n	3–9	4 h	-	Due to the presence of dinuclear [M ₂ (COO) ₄] clusters and hydrophobicity of phenyl groups of the ligands	Adsorption and photocatalytic degradation of organic dye	[141]
Eu-BDC - CH = CH₂	[(Me ₂ NH ₂) ₂][Eu ₆ (μ_3 -OH) ₈ (BDC - CH = CH ₂) ₆ (H ₂ O) ₆]	2–11	2 days	-	Due to the presence of strong Eu–O interaction and the hydrophobicity of the linker	Detection of H ₂ S in the biological system	[142]
Zn-DDB	[Zn ₃ (DDB)(DPE)]·H ₂ O	2–12	24 h	-	Due to the presence of six-nuclear	Detection of toxic heavy metal cations, oxyanions	[143]

INTRODUCTION

					clusters and the intramolecular hydrogen bonds	and organochlorine pesticides in water	
Eu(SIP)	Eu(SIP)(H ₂ O) ₄	1–12	24 h	-	Due to the presence of strong Eu-O coordination and the hydrophobicity of employed ligand	Detection of tryptophan in human serum, urine and lake water	[144]
AUBM-1(In)	-	1–12	3 days	310	Due to the presence of strong In–O coordination	Removal of arsenic in water	[145]
Cd-pbdc	[Cd ₂ (pbdc)(H ₂ O) ₃]	4–10	24 h	-	Due to the strong interaction of the PO ₃ group with metal cluster	Detection of Cu ²⁺ , Al ³⁺ , and Fe ³⁺ ions in water	[146]
Zn-AIA	{[Zn(4,4-AP)(5-AIA)].(DMF) _{0.5} } _n	4–11	-	173	Due to the presence of strong ample metal–N coordination along with the free azo group in the framework	Detection of Hg(II) ion	[147]
UPC-98	Zn ₄ (BTB-NH ₂) ₃ ·xSolvent	4–9	-	980.3	Due to the presence of 2-fold interpenetrated framework, hydrophobic effect of rigid ligand along with strong Zn–O coordination	Separation of light hydrocarbon	[148]
ROD-Zn1	{[Zn ₂ (bcob)(OH)(H ₂ O)].DMA} _n	1–3 and 11–13	24 h	-	Due to the presence of oxygen atom on the ether bond located in the channel (prevent the attack of H ⁺ /OH [–] , restricted the dissociation of coordination bond) along with rod shaped SBUs	Detection and removal of antibiotics from water	[149]
NNU-1	[PMo ₈ ^V Mo ₄ ^{VI} O ₃₇ (OH) ₃ Zn ₄] [TPT] ₅ ·2TPT·2H ₂ O	1–11	24 h	-	Due to the presence of strong Zn–N coordination along with stabilizing effect of polyoxometalates unit	Used as anode material for lithium-ion batteries	[150]

1.6.3 Stability in the presence of coordination anions

Besides proton and hydroxide ions, numerous other coordinating anions, including F^- , CO_3^{2-} , and PO_4^{3-} , may affect the stability of MOFs. Regrettably, these species are commonly present in reactions, often serving as crucial reactants or operating alongside their corresponding acids to maintain the solution's pH. Consequently, it is imperative to investigate the resilience of MOFs in aqueous solutions containing these coordinating anions. Since all the previously mentioned coordinating anions share the classification of being hard Lewis bases, they exhibit a strong affinity for high-valency metal ions, as evidenced by their strong binding affinities with Zr^{4+} , Fe^{3+} , and Al^{3+} . Consequently, in MOFs composed of high-valency metal ions, the carboxylate ligands can be easily displaced by the aforementioned anions, which act as competing species present in the solution. To address this limitation, it has been proposed to construct MOFs using soft metal ions and azolate-based ligands. In doing so, the strong coordination bonds between metal ions and ligands are maintained, while reducing the interaction between the metal ions in the framework and the coordinating anions in the solution[11].

1.6.4 Mechanical stability

As it mentioned before, MOFs are notable porous materials with a wide spectrum of pore shapes and sizes and diverse chemical properties. Similar to other materials, MOFs must meet stability requirements to be suitable for most practical applications. The use of MOFs often involves repeated cycles of temperature and pressure changes, making mechanical stability critically important. Mechanical stability in porous materials measures their ability to maintain pore size

and structure under mechanical stress. The vulnerability of MOF pore structures to vacuum conditions or external pressures can occasionally result in phase alterations or the partial collapse of pores. The mechanical properties of materials can vary significantly with changes in atomic composition and crystal structure[151]. Since mechanical stiffness, or modulus of elasticity, typically scales quadratically with density, mechanical stability is particularly crucial for low-density materials like MOFs. However, it is important to recognize that there is no single method for testing the stability of MOFs, as different standards are needed for various operating environments[11].

1.7 MOF applications

The broad spectrum of structures, morphology, and specific surface area sizes, coupled with the adaptability to customize these attributes, presents a vast opportunity for leveraging these materials across a multitude of applications. Extensive studies on various MOFs have unveiled their outstanding performance in gas storage and separation, catalysis, drug storage and delivery, substance detection, as well as the adsorption of harmful compounds in both gaseous and aqueous environments[3], [4], [15], [152]. The sorption properties of MOFs have provided the springboard for vast applications in the fields of environmental remediation as well as analytical sample preparation.

1.7.1 Gas storage and separation

INTRODUCTION

Due to their outstanding properties, MOFs have attracted considerable interest, particularly for their applications in gas storage and separation. With record-breaking BET surface areas, these materials offer extensive porosity and ample space for accommodating gas molecules. Moreover, their adjustable pore sizes and active sites on the pore surfaces allow for precise regulation of sieving effects, enabling selective interactions with gas molecules[152].

1.7.1.1 Gas storage

The capability of MOFs for gas storage was quickly recognized following the discovery of their permanent porosity. Hydrogen (H₂) emerges as the prospective fuel for the future owing to its convenient preparation and environmentally-friendly combustion, producing only water as a byproduct. However, thorough investigation is crucial to improve the storage and transportation of H₂. Initially, hydrides seemed like a viable storage solution, but their high density led to a low H₂ storage capacity by weight, making them unattractive for industrial use. MOFs offer a solution to these limitations and regarded as exceptionally promising materials for H₂ storage, due to their incredibly low density (<1 g/cm³), expansive internal surface area and spacious pores. Numerous research studies have confirmed the efficacy of MOFs with enduring porosity for storing H₂. MOF-5 was introduced as the first MOF for H₂ storage[153], [154]. Notably, MOFs currently hold the record for the highest total H₂ gravimetric uptake, reaching 17.6 wt% at 80 bar and 77 K for MOF-210[155]. This exceeds the performance of carbon-based adsorbents such as COFs and zeolites, positioning MOFs on par with other favorable H₂ storage materials like metal hydrides[152]. Notable MOFs, including MOF-5, MOF-177, and UiO-66, have demonstrated H₂ uptake of 5 wt % (77 K, 90 bar), 7.5 wt % (77 K, 80 bar), and 4.2 wt % (77 K, 60 bar) respectively[156], [157], [158].

INTRODUCTION

A substitute high-density fuel option alongside hydrogen and gasoline, comes in the form of natural gas, particularly methane (CH_4), and has garnered notable attention. Remarkable strides have been taken in recent decades in the realm of MOFs for CH_4 storage. Similar to hydrogen adsorption, the total gravimetric CH_4 uptake capacity commonly aligns with the pore volume and surface area of MOFs. The calculated total uptake capacities for MOF-177, MOF-200, and MOF-210 are notably high, reaching 345 mg g^{-1} , 446 mg g^{-1} , and 476 mg g^{-1} , respectively, under conditions of 80 bar and 298 K. These values far exceed those of any other MOF studied. It has been proven that, when one of these MOFs fills a container, it can hold at least double the amount of methane compared to an empty vessel at room temperature and pressures up to 80 bar[18].

1.7.1.2 Gas separation

Moreover, recent studies underscore notable advancements in the design and synthesis of MOF materials, particularly tailored for a wide range of gas separation applications alongside their role in gas storage[159], [160]. These advancements have facilitated the accomplishment of significant and complex separations, such as CO_2 capture and separation, light hydrocarbon separation, O_2/N_2 separation, CO/N_2 separation, among others, leveraging the emerging capabilities of MOFs as adsorbent materials[152].

Pure oxygen (O_2) has attracted considerable interest due to its capacity to improve the effectiveness of various chemical processes, including natural gas combustion, sewage treatment, and welding. Recent studies have highlighted the effectiveness of Cr-HKUST-1 and MOF-74 series in efficiently separating O_2/N_2 [161], [162]. These studies have revealed a remarkable selectivity factor for O_2/N_2 , reaching 22, which exceeds that of cobalt(II) complexes attached to a silica substrate

INTRODUCTION

(approximately 4), while, it does not achieve the selectivity of 60 as seen in advanced ionic liquids membranes[163], [164].

CO₂ stands as the primary greenhouse gas, causing global warming and water acidification. The primary industrial approach to mitigate these emissions involves employing liquid amine-based absorbents to chemically capture CO₂ from flue gas at relative ambient temperatures[165]. However, this process is hindered by challenges such as solvent corrosiveness, equipment fouling, and significant energy expenses for solvent regeneration[166]. Porous MOFs have been extensively studied as adsorbents for CO₂ capture in recent decades. These studies have delved into strategies aimed at boosting CO₂ uptake and separation capabilities within MOFs, including the incorporation of functional sites and meticulous adjustment of pore sizes and shapes. Noteworthy examples include SIFSIX-3-Zn, which stands out with the highest reported CO₂/N₂ selectivity among all known MOFs (1700)[167]. These breakthroughs underscore the potential of MOFs to outperform traditional methods in the realm of CO₂ capture and mitigation.

Additionally, separating light hydrocarbons (C₁–C₃) into individual components is a critical industrial process, given their vital roles as both energy resources and essential raw materials in the petrochemical industry. The demand for these highly pure individual components is significant across various applications, driving extensive exploration of numerous MOF materials for these essential separations[168]. Ethylene (C₂H₄) and propylene (C₃H₆) serve as essential materials in polymer production. The efficacy of Fe-MOF-74 in achieving purity levels ranging from 99% to 99.5% when separating hydrocarbon mixtures into distinct components has demonstrated[169], [170]. Notably, Fe-MOF-74 demonstrates outstanding adsorption selectivity (14) for C₃H₆/C₃H₈ separation among MOF materials, surpassing even the remarkable zeolite NaX[170]. Additionally, a hydroxyl-functionalized Al-MOF called NOTT-300, renowned for its remarkable selectivity

towards unsaturated hydrocarbons was investigated [171]. NOTT-300 demonstrates unparalleled selectivity of 48.7 for C_2H_4/C_2H_6 separation, outperforming both the innovative porous aromatic framework (PAF-1- SO_3Ag , 26.9) and zeolites (NaEST-10 (13) and NaX (8))[172].

Heavier hydrocarbon isomeric compounds spanning from C_6 to C_{10} play a pivotal role as industrial feedstock chemicals. A groundbreaking advancement in this realm was achieved with the utilization of a gas chromatography (GC) column filled with discrete crystals of MOF-508, marking the inaugural instance of separating aliphatic isomers using this method[173]. Additionally, MAF-6 has identified as a promising candidate for GC separation, especially notable for its efficacy in separating C_6 – C_{10} linear alkanes and C_6 alkane isomers [174].

1.7.2 Sensing applications

Numerous luminescent MOF compounds and/films have been meticulously engineered to deliver tailored signal responses. MOFs stand out as promising sensing materials, thanks to their remarkable attributes. Their expansive surface area greatly heightens detection sensitivity, due to their unique building attributes like open metal sites (OMSs) and their customizable pore sizes facilitate well-defined host-guest interactions. Adjusting the dimensions of pores within MOFs facilitates selective adsorption and unloading of certain guest substrates contingent on size-specific recognition, accommodating a range from small molecules to biomolecules. Notably, guest molecules can trigger visible changes, such as shifts in emission spectra, alterations in emitted colors, and fluctuations in fluorescence intensity, through dynamic processes like 'turn-on' and 'turn-off' [18]. Furthermore, the immobilization of functional sites such as OMSs or Lewis

INTRODUCTION

acidic/basic sites acts as precise binding locations, triggering coordinated or hydrogen bonding interactions with specific analytes, thus boosting sensitivity[152], [175].

The microporous MOF, $\text{Zn}_2(\text{bpdc})_2(\text{bpee})$, was crafted to detect trace explosives with a focus on **size-selective recognition**[176]. This MOF exhibited a swift reduction in fluorescence, with over 80% quenching observed within 10 seconds upon exposure to counterparts of explosive molecules like DNT and DMNB, driven by a redox-quenching mechanism. The increased sensitivity and significant quenching effects were attributed to the confinement of analytes within the MOF's pores, which intensified the interaction of explosives with the framework[176].

Considering the favorable interaction between analytes and **open metal sites** (OMSs), exploiting OMSs for achieving highly selective sensing has gained significant attention. As notable example, Eu-MOF, with its open Eu^{3+} sites, demonstrated selective sensing capabilities for solvent molecules[177]. The selective changes in luminescence towards various solvents were driven by the unique binding interactions between the open Eu^{3+} sites and guest molecules. In another study, the alkene unit within ASMOF-5 was described for the selective bind and colorimetric detection of noble-metal species[178]. Specifically, at concentrations as low as parts per million (ppm), the color of ASMOF-5 crystals shifts from light yellow to orange-red upon exposure to Pd^{2+} ions in solution. It is noteworthy that the yellow color of ASMOF-5 crystals remains unchanged in the presence of other metal ions, highlighting its exceptional selectivity as a colorimetric sensor specifically designed for detecting Pd^{2+} species.

In an innovative study, a water-stable MOF, PCN-225, has been meticulously engineered for targeted signal response purposes, notably in pH sensing applications. This remarkable material demonstrates exceptional chemical stability across a broad pH spectrum from 1 to 11 in aqueous environments. Leveraging its extensive pH stability and incorporating a fluorescent porphyrin dye,

PCN-225 exhibits fluorescence that varies with pH. The fluorescence intensity of PCN-225 correlates closely with changes in pH, with the most sensitive response observed within the pH range of 7 to 10. The pH-sensitive fluorescence of PCN-225 predominantly results from the protonation or deprotonation of its porphyrin core[179].

1.7.3 Catalytic applications

MOFs have become indispensable tools in heterogeneous catalysis for fine chemical production, a cornerstone of the chemical industry. Their effectiveness in this field stems from the range of their advantageous properties. Notably, their robustness enables catalytic operations even under extreme conditions, while they may host catalytically active sites within their metal centers, organic ligands, and framework pores. Specifically, MOFs showcase impressive versatility by acting as Lewis acids through their metal ions or metal clusters, while the integrated organic ligands, crucially fine-tuning both catalytic reactivity and selectivity. The intricate network of pores and channels within MOFs contributes to precise catalytic selectivity, making them ideal frameworks for accommodating components carrying oxygen or noble metals, essential for catalytic activity[18].

Metal ions such as Cu^{2+} , Zn^{2+} , and lanthanides within the framework typically bind with solvent molecules, allowing for easy substitution by substrates without compromising the framework's structural stability. These metal centers, boasting vacant coordination sites, can serve as catalysts, particularly as Lewis acids, facilitating a variety of chemical transformations[152]. In light of their impressive thermal and chemical stability, MOFs featuring Zr_6 or Hf_6 nodes have emerged as highly promising materials, suitable for catalytic applications. These frameworks employ Lewis-

INTRODUCTION

acidic Zr^{4+} or Hf^{4+} ions as active sites, showcasing their versatility in heterogeneous catalysis. Notably, a milestone study introduced Hf-NU-1000, showcasing its remarkable efficacy in CO_2 fixation under ambient conditions, achieving a 100% yield[180]. Subsequent investigations revealed NU-1000's exceptional ability to deactivate nerve agent simulants like DMNP and lethal chemical warfare agents like GB and GD[181]. The exceptional catalytic performance of NU-1000 is attributed to the presence of Lewis-acidic Zr^{4+} ions, which play a pivotal role in facilitating crucial weak intermolecular interactions with DMNP and GD[152].

In the last decade, there has been a growing emphasis on utilizing catalytically active **organic ligands** to construct MOF materials for heterogeneous catalysis. Since the inception of the first homochiral zinc MOF in 2000, which demonstrated the organic components' ability within its pores to catalyze organic transformations, extensive efforts have been directed toward advancing MOF materials containing these catalytically active organic ligands[182]. A 2D homochiral MOF occurred through the reaction of a multitopic chiral ligand, with CuCl_2 , demonstrates catalytic activity in promoting the 1,2-addition of Grignard reagent to a variety of ketones (aldehydes), achieving exceptional enantiomeric excess (ee) values of up to 99%. Specific tests demonstrated the crucial role of the organic functionality within the framework in facilitating the reaction, emphasizing that the metal centers does not exhibit catalytic activity[183].

The **natural porosity** of MOF materials facilitates the encapsulation of catalytically active guests within their voids, making MOFs an excellent choice for embedding catalytic centers. Recent years have a surge in studies have been observed exploring the utilization of MOFs to host various catalytically active guest molecules, including porphyrins, enzymes, and metal nanoparticles, among others, for heterogeneous catalysis. To achieve this, innovative methodologies such as templating effects, single-molecule traps (SMTs), dissociative linker exchange, and

hydrophilicity-directed approaches have been developed and utilized to enable the encapsulation of large catalytically active guest molecules within the pores of MOF materials[152]. Recently, a series of robust MOFs featuring meticulously designed ultra-large mesoporous cages, acting as SMTs for enzyme encapsulation, have been developed[184]. Among these, PCN-333(Al) stands out with its remarkably spacious 5.5 nm cage, boasting one of the largest void volumes ($3.84 \text{ cm}^3 \text{ g}^{-1}$) and exceptional pH stability from 3 to 9 in aqueous solutions among all known MOFs. By utilizing the high concentration of mesoporous cages as SMTs, PCN-333(Al) has encapsulated three enzymes with exceptionally high loadings, showing minimal leaching during catalysis and recycling, and demonstrating sustained or enhanced catalytic activities compared to their free counterparts, even under challenging conditions[184].

1.7.4 MOFs in biomedical applications

MOFs and their derivatives are increasingly recognized for their outstanding physicochemical properties, making them promising candidates as carriers for drugs, bioimaging agents, and therapeutic applications. Traditional drug carriers like liposomes, and micelles frequently struggle with low drug loading capacities and rapid release. In contrast, porous MOFs provide high drug loading potential, making them highly suitable for delivery applications. Effective drug carriers must have high drug loading capacity, controlled drug release, regulated matrix degradation, and low toxicity. Drugs can be incorporated into MOFs through various methods: non-covalent encapsulation via physisorption, post-synthetic modification of the organic ligands and by using drugs as organic ligands during MOF synthesis[18].

INTRODUCTION

MIL-100 and MIL-101, incorporating trimetallic nodes with BTC or BDC, were the first MOFs introduced for use in drug delivery systems. These MOFs exhibited a remarkable ability to absorb significant amounts of ibuprofen, achieving up to 1.4 g g^{-1} of MIL-101. Under physiological conditions, ibuprofen was fully released within three days from MIL-100 and within six days from MIL-101[185].

Recent advancements in anticancer therapy focus on generating hydroxyl radicals ($\bullet\text{OH}$) from H_2O_2 , catalyzed by Fe^{3+} ions as well as Mn^{2+} , Cu^+ , and Cr^{4+} through the Fenton reaction. Unregulated tumor growth and metabolic dysfunction generate reactive oxygen species (ROS) including O_2^- , H_2O_2 , $\bullet\text{OH}$, and ClO^- . Hydroxyl radicals are especially effective at damaging tumor cells, more so than other ROS. Modern anticancer therapies, including photodynamic therapy (PDT), sonodynamic therapy (SDT), and chemodynamic therapy (CDT), build on these findings. Over the past decade, MOFs have been utilized in PDT, SDT, and CDT applications[186]. The drug delivery system Fe-MIL-53-NH₂-FA-5-FAM/5-FU, centered around the Fe-MIL-53-NH₂ MOF, exhibits a high loading capacity for the anticancer drug 5-fluorouracil (5-FU) (Figure 1.7.4). This system, combined with the fluorescence imaging agent 5-carboxyfluorescein (5-FAM) and folic acid (FA), offering enhanced toxicity to cancer cells due to targeted 5-FU release and acting as a potential magnetic resonance imaging (MRI) contrast agent[187].

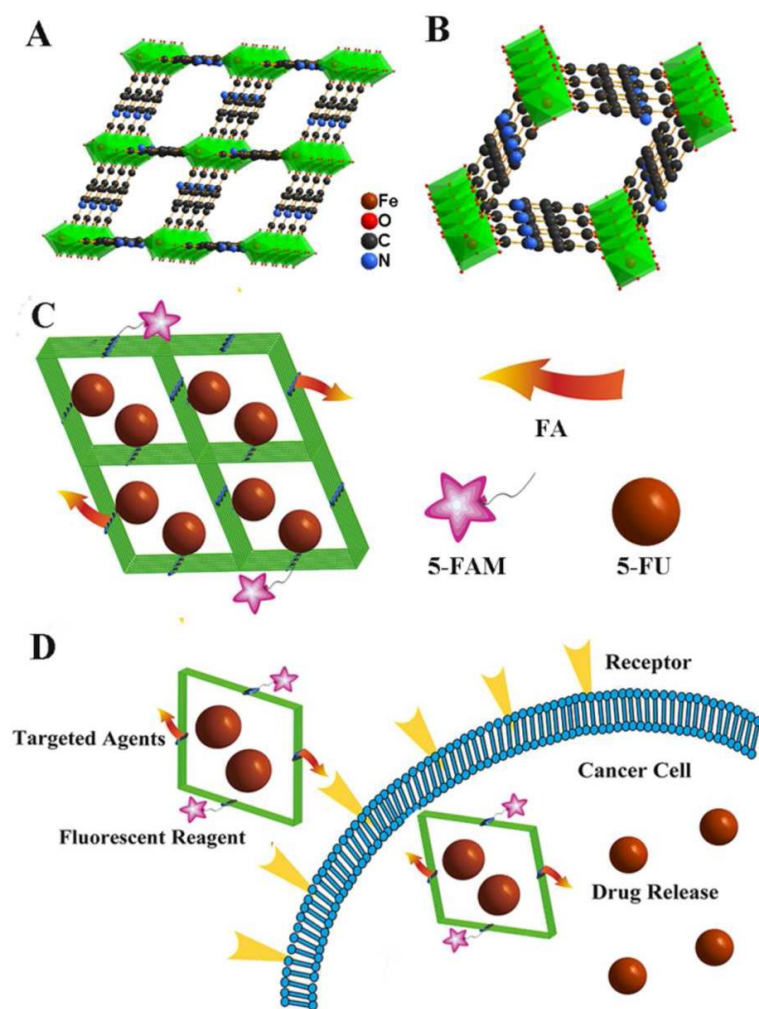


Figure 1.7.4 2D plane view of Fe-MIL-53-NH₂ (A,B), Diagrammatic depiction of the drug delivery system Fe-MIL-53-NH₂-FA-5-FAM/5-FU (C), and schematic illustrations of Fe-MIL-53-NH₂-FA-5-FAM/5-FU for targeting drug delivery (D)[187].

1.7.5 MOFs in analytical sample preparation

Sample preparation is a critical yet frequently undervalued step in chemical analysis[188]. Its role becomes increasingly essential when working with trace levels of target analytes in complex matrices, such as environmental, pharmaceutical, food, and biological samples. Without proper

INTRODUCTION

preparation, these samples are generally unsuitable for direct injection into analytical instruments. There are three main reasons why direct injection into analytical instruments is often impractical. First, the matrix components can negatively affect the instrument's performance or interfere with the detection of target analytes. Second, the concentration of analytes in the sample matrix may be too low for the instrument to detect. Third, the sample matrix might be incompatible with the instrument, leading to further complications. Thus, the main purpose of sample preparation is to extract and concentrate target analytes from diverse sample matrices into a new solvent or solvent system. This process also aims to reduce matrix interference, ensuring that a cleaner analyte solution can be fed into the analytical instrument for precise separation, identification, and quantification.

The distinctive properties of MOFs provide numerous adsorption active sites for capturing organic pollutants, large molecules, and heavy metals in various sample types, such as food, environmental, and biological samples[3]. This advantage is attributed to their customizable pore size distribution and expansive surface areas[4]. As a result, MOFs or composite materials containing MOFs have emerged as innovative sorbents in sample preparation methodologies. The adsorption mechanism involves several mechanisms, including hydrophobicity and dipole–dipole interactions, the formation of hydrogen bonds or π -stacking interactions between the functional groups of the sorbent and the organic linkers of the analyte. To date, a diverse array of MOFs or MOF-based composite materials has been applied across different extraction methods, including solid-phase extraction (SPE), dispersive solid-phase extraction (dSPE), magnetic solid-phase extraction (MSPE), and solid-phase microextraction (SPME)[23].

1.7.5.1 Solid-phase extraction (SPE)

MOFs and MOF-based composites excel as sorbents in SPE due to their unique structures, characterized by high surface areas and nanoscale pore sizes. These properties facilitate complete adsorption of target analytes in a single cycle, thereby greatly accelerating the process[23], [189], [190].

A Cu-based MOF polymer using isonicotinic acid as the linker was applied in SPE to capture trace amounts of polycyclic aromatic hydrocarbons (PAHs) from certified reference materials and water samples. Specifically, the pre-column packed with this sorbent phase was exceptionally suited for the SPE method. The diffusion of PAH molecules into the MOF network was significantly influenced by its porosity characteristics, enabling a throughput of 3 samples per hour under optimized conditions, with detection limits ranging between 2 and 14 ng L⁻¹[191].

In another study a water-resistant MOF, UiO-66(Zr), was utilized, among others, as sorbent for detecting four androgens and progestogens in aqueous samples[192]. This study highlighted UiO-66(Zr) as a superior sorbent for this purpose, leveraging its exceptional properties. Furthermore, micro-solid-phase extraction demonstrates remarkable selectivity, sensitivity, and precision in detecting testosterone (T), progesterone (P), testosterone propionate (TP), and medroxyprogesterone acetate (MPA) in natural water matrices simultaneously. The limits of detection (LODs) and limits of quantification (LOQs) were achieved between the values 2-10ng L⁻¹ and 7.0 -20 ng L⁻¹, respectively. Acceptable recoveries ranging from 80.5% to 102.4% were attained with a relative standard deviation (RSD) of less than 10.0%[192]. Additionally, UiO-67 was packed into empty cartridges to extract phenoxyacetic acid herbicides (PAAs) from vegetable samples. PAAs, a type of plant growth regulator, pose a risk of agricultural product contamination through excessive use and residue accumulation, particularly in vegetables, potentially leading to

INTRODUCTION

health hazards for humans and animals. UiO-67, a zirconium-based MOF characterized by a biphenyl skeleton and numerous Zr-O bonds in its SBUs, stands out among others for its high surface area, thermal stability, and ability to effectively capture PAAs through pi-pi or hydrophobic interactions, as well as Zr-O-H⁺ bonds[193].

In-syringe Solid Phase Extraction (SPE) represents an innovative form of sample pretreatment technology rooted in SPE principles. This technique involves constructing a device by packing sorbent material into the nozzle of a disposable syringe, with filters or cotton wool secured on either side of the sorbent. During the extraction process, the sample solution and eluent are iteratively drawn and pushed through the sorbent by manipulating the syringe plunger, typically for multiple cycles. This approach facilitates the execution of extraction steps including loading, washing, and elution[194].

MIL-101 was utilized as a sorbent to detect trace amounts of PAHs in natural aqueous samples using in-syringe SPE (Figure 1.7.5.1). Due to MIL-101's exceptional adsorption capacity, it achieved full adsorption of the target analytes in just one cycle, significantly reducing sampling time. Additionally, the stability of analytes on the sorbent was approximately 7 days, indicating the potential for on-site sampling of degradable materials in remote areas. With optimized conditions, the detection limit ranged from 0.20 to 1.9 ng L⁻¹, yielding good recoveries between 84.4% and 104.5% with an RSD % of 9.7%. This approach offers benefits including straightforward assembly, user-friendly operation, cost-effectiveness, and portability[195].



Figure 1.7.5.1 Diagram outlining the preparation process for the MIL-101-based in-syringe solid-phase extraction (SPE) device and its practical use in on-site sampling[195].

1.7.5.2 Dispersive solid-phase extraction (d-SPE)

Among the numerous pretreatment techniques available, considerable focus has been directed towards dispersed Solid Phase Extraction (dSPE) due to its simplicity, rapidity, and efficacy. Given the pivotal role of the sorbent in this method, utilizing advanced SPE sorbents enhances the performance and efficiency of the extraction process. Unlike SPE, dSPE disperses the solid sorbent into the sample matrix containing the target analyte. In this configuration, sorbent particles can interact more closely with analytes within a shorter period, thereby significantly enhancing extraction efficiency (Figure 1.7.5.2.).

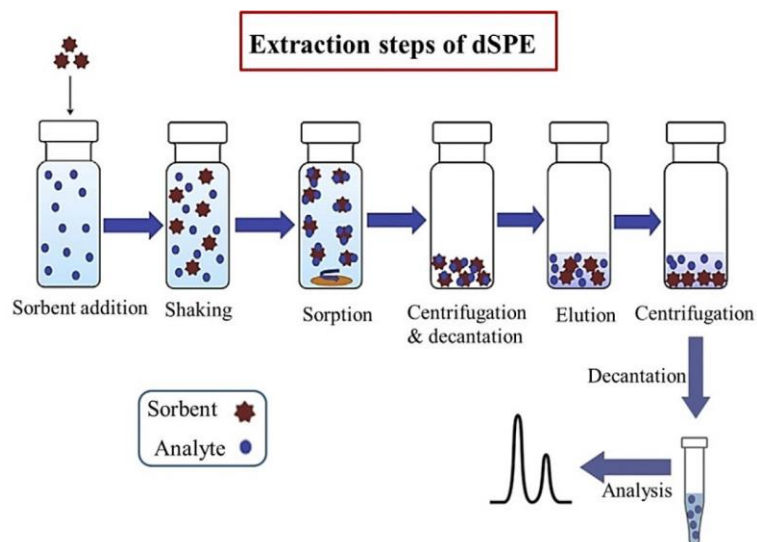


Figure 1.7.5.2: A diagram outlining the steps involved in dSPE extraction[196].

This approach effectively mitigates several drawbacks associated with traditional SPE methods, such as potential leakage of nano-sorbent particles from cartridges or the risk of high-pressure buildup within the SPE system. A wide array of materials can be employed as sorbents in dSPE, ranging from graphene and layered double hydroxides to molecularly imprinted polymers (MIPs), heteropolyacids, and conductive polymers. Nonetheless, the ongoing challenge lies in identifying dependable sorbents with ample capacity, as some choices may yield subpar recoveries or lack recyclability. Water-stable MOFs have recently gained attention as highly promising sorbents for dSPE applications in various fields related to sorption[23], [196].

As an illustration, UiO-66 was formulated and utilized as a sorbent to extract organophosphorus pesticides (OPPs) from edible vegetable oils. In this procedure, the pesticides are directly captured by UiO-66 through size exclusion interactions and extracted through ultrasonication elution. The method demonstrated limits of detection (LOD) ranging from 0.16 to 1.56 ng g⁻¹, with pesticide recovery rates falling between 81.1% and 113.5%. It has been shown that the highly porous

INTRODUCTION

structure of UiO-66, characterized by uniform micropores measuring 0.7 and 0.9 nm, effectively blocks larger compounds within the oil matrix while allowing relatively small OPPs (molecules smaller than 0.9 nm) to permeate, demonstrating a beneficial matrix suppression effect. Additionally, the robust structure of UiO-66, facilitates easy recycling and reusability for at least 10 cycles, thereby reducing the overall method costs[197].

The efficacy of MIL-101(Fe) and amino-functionalized MIL-101(Fe) was explored in extracting compounds from the bisphenol family (BP) in environmental waters using the dSPE, as a sample preparation method. NH₂-MIL-101(Fe) exhibited exceptional efficiency in concentrating and detecting trace-level BPs, comparing with MIL-101(Fe), achieving recoveries between 90.8% and 117.8% with detection limits ranging from 0.016 to 0.131 $\mu\text{g L}^{-1}$. This performance was attributed to the hydrogen bonding interactions between the N–H group of NH₂-MIL-101(Fe) and the OH group of the target analytes[198].

1.7.5.3 Magnetic solid-phase extraction (MSPE)

Magnetic Solid-Phase Extraction (MSPE) operates by dispersing a magnetic sorbent into the solution containing the target analytes and then employing an external magnetic field for separation. Notably, unlike traditional dSPE methods, there's no need for centrifugation or filtration of the sample, making this approach simpler and faster, without requiring expensive equipment or large eluent volumes. Moreover, it presents advantages such as effective dispersion of the adsorbent in large sample volumes, quicker extraction times, cost efficiency, environmental compatibility, and addresses issues like high back pressure or blockages in the packed bed during SPE. Various magnetic sorbents are used in MSPE spanning from bare magnetic nanoparticles

INTRODUCTION

(MNPs) to composite or hybrid materials incorporating MNPs with silica, polymers, carbon nanostructures, and MOFs[199], [200]. The integration of MOFs onto magnetic particles not only amplifies the surface area of the magnetic sorbent but also introduces novel functionalities based on the selected inorganic units and organic linkers employed in MOF construction. The variety of options allows for extensive utilization of MOFs as MSPE sorbents[23].

Fe₃O₄/MOF/L-cysteine was utilized as a sorbent for detecting Cd²⁺ in wastewater samples using MSPE (Figure 1.7.5.3). Consequently, Fe₃O₄/MOF/L-cysteine emerges as an effective sorbent for eliminating heavy metals such as Cd²⁺, Zn²⁺, Fe³⁺, Cu²⁺, Hg²⁺, and Pb²⁺ from water solutions owing to its diverse functional groups. However, the efficiency of the sorbent in removing Cd²⁺ exceeds that for other heavy metals. This is due to the diverse coordination interactions between different heavy metal ions and the -SH group in l-cysteine, as well as the physical adsorption affected by the size of the metal ion. The maximum adsorption capacity was determined to be 248.24 mg g⁻¹ with a LOD of approximately 10.6 ng mL⁻¹[201].

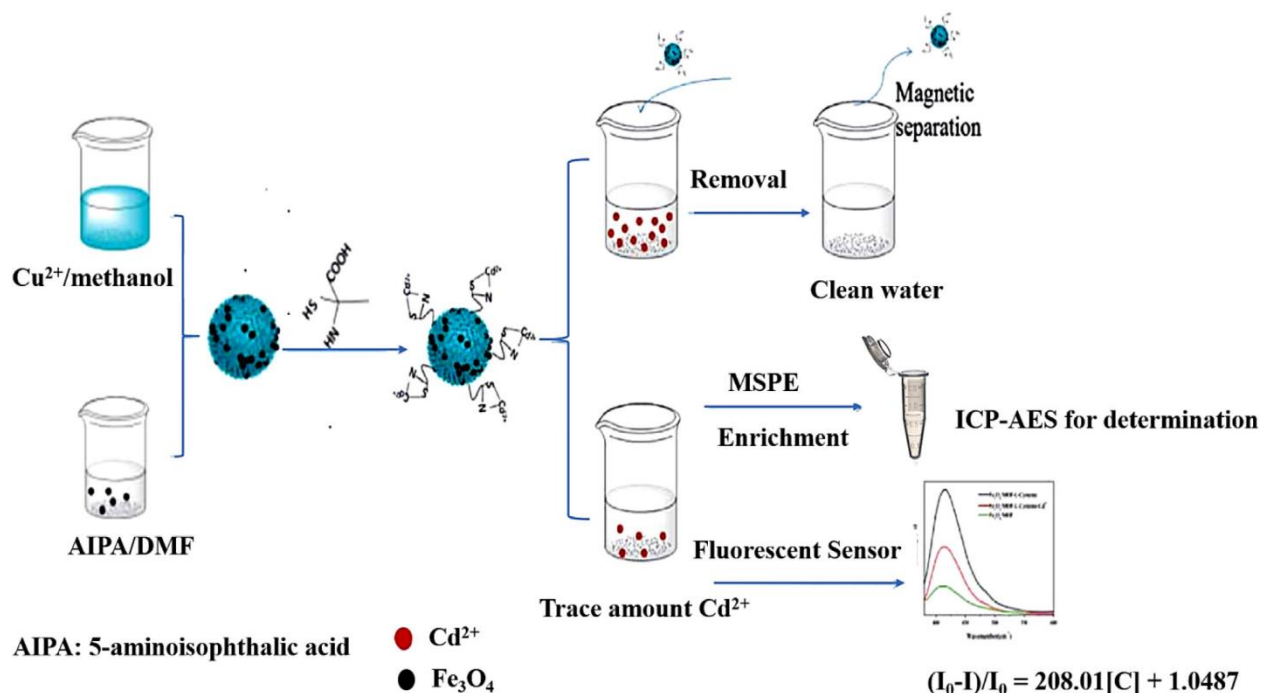


Figure 1.7.5.3 Diagram depicting the synthesis of Fe₃O₄/MOF/L-cysteine for Cd(II) removal[201].

1.7.5.4 Solid-phase microextraction (SPME)

SPME is recognized for its sensitivity, affordability, ease of use, and quick sample preparation. It combines sampling, analyte isolation, and concentration into a single step, making it efficient. Additionally, it's environmentally friendly since it requires minimal sample or solvent. This streamlined process not only reduces analysis errors, time, and costs but also holds particular importance in minimizing preparation steps, especially when dealing with trace or even ultra-trace samples from complex matrices[202]. In SPME, analytes adhere to a thin layer of sorbent material (typically ranging from 7 to 100 μm) applied onto a supporting substrate, such as stainless steel or glass fibers. Various commercial sorbents are utilized for SPME, including polydimethylsiloxane

INTRODUCTION

(PDMS), polyacrylate (PA), divinylbenzene (DVB), polyethyleneglycol (PEG), among others[203]. However, due to the limited range of commercially available SPME fiber coatings, there is a growing interest in exploring newer alternatives such as MOFs and MOF-based composites. The utilization of MOFs as SPME coatings began around 2009 with the introduction of in situ hydrothermal growth of thin MOF-199 films on etched stainless-steel wire for the extraction of benzene homologues[204]. To date, several sorptive microextraction methods have been studied, categorized by their alignment with the geometry of the extraction phase. These include techniques conforming to batch equilibrium microextraction (such as fiber SPME, stir-bar sorptive extraction, and thin-film extraction), as well as those adhering to flow-through equilibrium microextraction (such as in-tube SPME, syringe SPME, and in-tip SPME) (Figure1.7.5.4) [205].

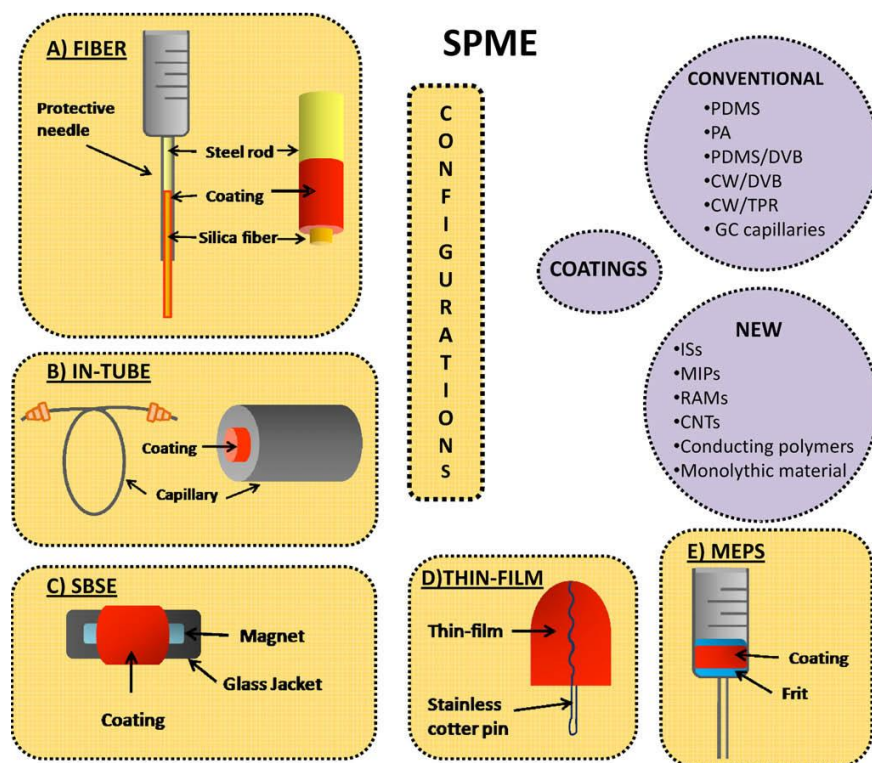


Figure 1.7.5.4 Sorptive-microextraction modes according to the geometry of the extraction phase and the coatings employed. Extraction phases: CNT, Carbon nanotube; IS; Immunosorbent; MEPS, Microextraction in packed syringe; MIP, Molecularly imprinted polymer; RAM, Restricted access material; SBSE: Stir-bar sorptive extraction. Coatings: CW/DVB, Carbowax/divinylbenzene; CW/TPR, Carbowax/template resin; PA, Polyacrylate; PDMS, Polydimethylsiloxane; PDMS/DVB, Polydimethylsiloxane/divinylbenzene[205].

In the **SPME fiber method**, either fused silica (FS) or metal wires serve as substrates, which are then coated with a sorbent, such as a MOF. Incorporating a MOF as both the coating and sorbent phase enhances the material's porosity, as well as its thermal and chemical stability. Yu et al. achieved a pioneering breakthrough by utilizing covalent bonding to coat a MOF onto fused silica for the first time. They initially functionalized the fused silica with 3-aminopropyltriethoxysilane before applying a layer of ZIF-90. This enhanced fiber exhibits significant improvements in

INTRODUCTION

extraction efficiency, showcasing substantial linearity, satisfactory reproducibility, and longevity in extracting and evaluating polar endocrine disruptors[206].

Capillary microextraction (CME) operates as an **in-tube SPME method** with a specialized operational setup, renowned for its swiftness, cost-effectiveness, and minimal analyte consumption, coupled with high selectivity. Here, analytes are extracted and preconcentrated by an adsorbent either coated onto the inner surface of the capillary column or packed as a monolith. This versatile technique finds utility in separating a wide array of polar and non-polar substances across diverse fields including environmental, biological, food, and medical applications. Its notable advantages include automation and online coupling capabilities[207]. A hybrid MOF-polymer (MIL-101(Cr)- poly(EMDA-BMA)) was synthesized for in-SPME of penicillin. The method exhibited a recovery rate ranging from 63% to 96.2%, attributed to the high sensitivity resulting from the sorbent's large surface area, along with high reproducibility and minimal solvent consumption[208].

Stir-bar sorptive extraction, boasts numerous advantages, including excellent sensitivity, satisfactory reproducibility, high recovery rates, and minimal organic solvent consumption. A method involving covalent modification was developed to immobilize MIL-68 onto a chemically resistant PEEK jacket (poly(ether ether ketone)) for detecting paraben analogs in cosmetics and rabbit plasma. It has been demonstrated that the exceptional sensitivity (with an LOD around 1 pg mL⁻¹) and method robustness were credited to the covalent modification process[209].

To enhance sensitivity and extraction efficiency, a novel variant of SPME known as **thin-film microextraction** (TFME) was introduced. TFME utilizes flake-like films with a large surface area-to-volume ratio as extraction phases for capturing analytes. This innovative approach not only enhances extraction capacity but also accelerates equilibrium times. With these advantageous

features, TFME has found utility in analyzing a diverse range of compounds[210]. Compared to conventional SPME, TFME offers superior extraction capacity due to its unique geometry. Moreover, the use of a thin sorbent layer results in expedited equilibrium times compared to traditional SPME techniques[210]. In alternative investigations, a 3D hierarchical ZIF-67 film was synthesized as a robust sorbent for caffeine detection in water and urine samples. Upon optimization, the linear range spanned from 1 to 200 $\mu\text{g L}^{-1}$ with an r^2 value exceeding 0.9915. The LODs were determined to be 0.33 and 0.38 $\mu\text{g L}^{-1}$ for water and urine, respectively. Enrichment factors ranged from 173 to 198, with absolute recoveries falling between 57.1% and 65.3%, and relative standard deviations (RSD) in the range of 4.9% to 6.1%[211].

1.8 MOFs in environmental remediation

Over the past five decades, human civilization has undergone rapid urbanization, industrialization, and motorization, leading to the release of numerous harmful pollutants. Toxic materials from human activities, industrial waste, oil spills, resource mining, nuclear waste leakage, along with natural resource depletion, are a significant global threat to human survival, adversely affecting our environment, health, and food chains. Pollution in soil, water, and air endangers all living beings. As a result, there is an increasing emphasis on tackling these challenges to create a less polluted environment[212], [213]. Major pollutants in aquatic and terrestrial systems include organic substances (pesticides, detergents, biomaterials, and pharmaceuticals), inorganic substances (heavy metals, oxyanions, etc.), and bio-organisms.

The presence of heavy metals in the environment can stem from both natural (geogenic or lithogenic) and anthropogenic sources. Natural sources include the weathering of metal-rich rocks

INTRODUCTION

and volcanic activity, while anthropogenic sources encompass mining, industrial processes, and agricultural practices[214]. Additionally, emissions introduce heavy metals into the atmosphere, where they deposit onto land through dry and wet processes. Specifically, persistent heavy metal cations (Hg^{2+} , Pb^{2+} , Cu^{2+} , Cd^{2+} , Zn^{2+} , Cr^{3+} , Ni^{2+} , $\text{Fe}^{2+}/\text{Fe}^{3+}$ etc.), which are defined by densities and atomic numbers exceeding 5 and 20 g/cm³, respectively, and oxyanions (CrO_4^{2-} , $\text{Cr}_2\text{O}_7^{2-}$, AsO_4^{3-} , SeO_3^{2-} , SeO_4^{2-} , etc.), as well as halide ions and radioactive substances are commonly found in industrial effluents and wastewater[215], [216], [217], [218], [219]. In both aquatic and terrestrial settings, heavy metal pollution, presents a critical concern due to its high-water solubility, nonbiodegradability, and toxic effects. These pollutants can permeate food chains, leading to prolonged bioaccumulation in living organisms. Additionally, the leakage of heavy metals into water bodies poses serious threats to human health and the ecosystem. Ensuring human safety and environmental security requires the effective removal of these toxic and carcinogenic substances from wastewater[43], [212]. Table 1.8.a shows some harmful inorganic contaminants in drinking water and their potential health effects, according to the U.S. Environmental Protection Agency (the U.S. EPA)[220].

Table 1.8.a Overview of inorganic contaminants in drinking water. Retrieved from Ref [221].

Contaminant	MCL (mg L ⁻¹)	Potential Health Effects from Long-Term Exposure Above the MCL (unless specified as short-term)	Sources of Contaminant in Drinking Water
Arsenic	0.01	Skin damage or problems with circulatory systems, and may increase the risk of getting cancer	Erosion of natural deposits; runoff from orchards, runoff from glass and electronics production wastes
Selenium	0.05	Hair or fingernail loss; numbness in fingers or toes; circulatory problems	Discharge from petroleum refineries; erosion of natural deposits; discharge from mines

INTRODUCTION

Barium	2	Increase in blood pressure	Discharge of drilling wastes; discharge from metal refineries; erosion of natural deposits
Cadmium	0.005	Kidney damage	Corrosion of galvanized pipes; erosion of natural deposits; discharge from metal refineries; runoff from waste batteries and paints
Chromium (total)	0.1	Allergic dermatitis	Discharge from steel and pulp mills; erosion of natural deposits
Copper	1.3	Short term exposure: gastrointestinal distress	Corrosion of household plumbing systems; erosion of natural deposits
Cyanide (as free cyanide)	0.2	Nerve damage or thyroid problems	Discharge from steel/metal factories; discharge from plastic and fertilizer factories
Lead	0.015	Infants and children: delays in physical or mental development; children could show slight deficits in attention span and learning abilities Adults: Kidney problems; high blood pressure	Corrosion of household plumbing systems; erosion of natural deposits
Mercury (inorganic)	0.002	Kidney damage	Erosion of natural deposits; discharge from refineries and factories; runoff from landfills and croplands
Nitrite (measured as nitrogen)	1	Infants below the age of six months who drink water containing nitrite in excess of the MCL could become seriously ill and, if untreated, may die. Symptoms include shortness of breath and blue-baby syndrome	Runoff from fertilizer use; leaking from septic tanks, sewage; erosion of natural deposits
Nitrate (measured as nitrogen)	10	Infants below the age of six months who drink water containing nitrate in excess of the MCL could become seriously ill and, if untreated, may die. Symptoms include shortness of breath and blue-baby syndrome	Runoff from fertilizer use; leaking from septic tanks, sewage; erosion of natural deposits
Fluoride	4	Bone disease (pain and tenderness of the bones); children may get mottled teeth	Water additive which promotes strong teeth; erosion of natural deposits; discharge from fertilizer and aluminum factories
Thallium	0.002	Hair loss; changes in blood; kidney, intestine, or liver problems	Leaching from ore-processing sites; discharge from electronics, glass, and drug factories

MCL: maximum contaminant level

INTRODUCTION

Additionally, environmental pollution is becoming a growing issue due to new human-made pollutants. A major concern is the rise of emerging organic contaminants (EOCs), which refers to both newly created compounds and those recently identified as environmental contaminants. EOCs, which contaminate water resources, encompass a wide variety of compounds. These include pharmaceuticals and personal care products (PPCPs), pesticides, veterinary medications, industrial chemicals and byproducts, food additives, and engineered nanomaterials[222]. Consequently, any contaminant or excessive material released into our environment can result in direct or indirect environmental impacts. As a result, contaminants at micro to nanogram per liter levels, derived from common products like PPCPs, may pose toxicity or carcinogenic risks[213], [223]. Table 1.8.b shows some harmful organic contaminants in drinking water and their potential health effects, according to the U.S. Environmental Protection Agency (the U.S. EPA)[220]. Therefore, once harmful substances are detected in our environment, remediation is essential. While the notion of completely eliminating pollutants to achieve a pollution-free world is idealistic, the emphasis should be on designing and employing sustainable technologies to minimize pollution. Thus, there is a critical need to develop efficient, eco-friendly remediation processes capable of removing contaminants at variable concentration levels[213].

Table 1.8.b Overview of organic contaminants in drinking water. Retrieved from Ref [221].

Contaminant	MCL (mg L ⁻¹)	Potential Health Effects from Long-Term Exposure Above the MCL (unless specified as short-term)	Sources of Contaminant in Drinking Water
Atrazine	0.003	Cardiovascular system or reproductive problems	Runoff from herbicide used on row crops
Benzene	0.005	Anemia; decrease in blood platelets; increased risk of cancer	Discharge from factories; leaching from gas storage tanks and landfills

INTRODUCTION

Benzo(a)pyrene (PAHs)	0.0002	Reproductive difficulties; increased risk of cancer	Leaching from linings of water storage tanks and distribution lines
Chlorobenzene	0.1	Liver or kidney problems	Discharge from chemical and agricultural chemical factories
Dalapon	0.2	Minor kidney changes	Runoff from herbicide used on rights of way
Dichloromethane	0.005	Liver problems; increased risk of cancer	Discharge from drug and chemical factories
Dioxin (2,3,7,8-TCDD)	0.00000003	Reproductive difficulties; increased risk of cancer	Emissions from waste incineration and other combustion; discharge from chemical factories
Endothall	0.1	Stomach and intestinal problems	Runoff from herbicide use
Epichlorohydrin	TT	Increased cancer risk, and over a long period of time, stomach problems	Discharge from industrial chemical factories; an impurity of some water treatment chemicals
Ethylbenzene	0.7	Liver or kidneys problems	Discharge from petroleum refineries
Hexachlorobenzene	0.001	Liver or kidney problems; reproductive difficulties; increased risk of cancer	Discharge from metal refineries and agricultural chemical factories
Polychlorinated biphenyls (PCBs)	0.0005	Skin changes; thymus gland problems; immune deficiencies; reproductive or nervous system difficulties; increased risk of cancer	Runoff from landfills; discharge of waste chemicals
Tetrachloroethylene	0.005	Liver problems; increased risk of cancer	Discharge from factories and dry cleaners

TT: Treatment Technique. Each water system must certify, in writing, to the state (using third-party or manufacturer's certification) that when acrylamide and epichlorohydrin are used to treat water, the combination (or product) of dose and monomer level does not exceed the levels specified, as follows: Acrylamide = 0.05% dosed at 1 mg/L (or equivalent), Epichlorohydrin = 0.01% dosed at 20 mg/L (or equivalent)

Currently, prominent techniques for environmental remediation involve, filtration, coagulation, sedimentation, adsorption, membrane separation, catalysis, electrochemical degradation, enzymatic biodegradation, chemical oxidation, etc.[224], [225], [226], [227], [228], [229]. Among these methods, adsorption is particularly promising due to its low operating costs, high removal efficiency, and minimal production of secondary toxic pollutants. Additionally, under specific conditions, adsorption allows for the recovery of contaminants, further demonstrating its substantial potential. The increasing emphasis on adsorption has led to significant advancements in porous materials, including zeolites, clays, activated carbons (AC), alumino-phosphates and silicate mesoporous materials, among others[230], [231], [232], [233]. Despite their widespread

INTRODUCTION

use in environmental remediation, these porous adsorbents often suffer from drawbacks such as limited surface area, lack of customizability, slow adsorption kinetics, limited reusability, thermal and chemical instability, and low adsorption capacity, resulting in poor performance[212], [234]. On the other hand, two-dimensional adsorbents such as carbon nanotubes (CNTs) have surpassed traditional sorbents by offering rapid equilibrium rates, structural integrity, and high adsorption capacity[235]. However, the environmental toxicity of CNTs presents a drawback, negatively affecting water and soil quality[236]. Consequently, there is a pronounced demand for advanced alternatives that can effectively adsorb pollutants while mitigating the limitations associated with conventional adsorbents.

MOFs have been explored as versatile tools for environmental remediation, capable of eliminating harmful gases, capturing heavy metal ions, and removing organic pollutants[237], [238], [239]. Despite the existence of over 75,000 reported MOFs, only a few dozen have been evaluated for their effectiveness in capturing or separating pollutants from water, air, and soil. This limited testing is largely due to their instability under harsh conditions, where MOF structures can collapse in acidic environments or during regeneration processes. The efficiency of MOFs in environmental remediation hinges on four key factors: stability, adsorption capacity, interaction ability, and regenerative capability. Stability is especially critical in environmental remediation processes. The adsorption capacity is influenced by the functionalities or active sites of the MOFs, which enable interactions with the target chemicals. Additionally, the regenerative ability of MOFs determines their reusability for future purification cycles. Given these characteristics, MOFs have become one of the most extensively researched materials of the 21st century[234]. Lastly, integrating MOFs with other nanomaterials can greatly broaden their applications in water treatment and soil amendment. For instance, integrating magnetic MWCNT with ZIF-8 enhances the adsorption of

organophosphates (OPs) by boosting water and mechanical stability[240]. Similarly, coupling UiO-66 with monoliths like poly(N-vinylcarbazole-co-divinylbenzene (poly(NVC/DVB)) amplifies fungicide adsorption through π - π interactions between the fungicides and the aromatic rings of the ligands[241].

1.8.1 MOFs as adsorbents for water purification

1.8.1.1 Removal of organic pollutants

1.8.1.1.1 Removal of dyes

Dyes alter the color of a substrate through processes that can change the structure of the colored substance. They are composing a type of organic pollutant that visibly contaminates water, indicated by water coloration[234]. According to statistics, industries produce over 100,000 types of dyes, with an annual production of 70,000 metric tons. Dyes can be classified as ionic or non-ionic. Ionic dyes include cationic dyes, which have positively charged ions in aqueous solutions, and anionic dyes, which have negatively charged ions. Cationic dyes include malachite green, methylene blue, and rhodamine B, while anionic dyes include acid, reactive, and direct dyes. Vat dyes and disperse dyes are non-ionic dyes[242]. Dyes can originate from natural or synthetic sources. Figure 1.8.1.1.1 illustrates the classification of dyes according to their production sources. Natural dyes, known for being eco-friendly, are mainly utilized in the food industry due to their high cost, which limits their application in other sectors. The textile industry generates substantial volumes of wastewater with elevated concentrations of dyes as part of its manufacturing processes. Due to their high water solubility, traditional methods for removing dyes are frequently ineffective[243]. Dyes as water contaminants pose significant health risks, including allergies,

blindness, chemosis, and vertigo. They also contribute to environmental issues such as increased chemical oxygen demand, reduced dissolved oxygen levels, and inhibited microbial growth.

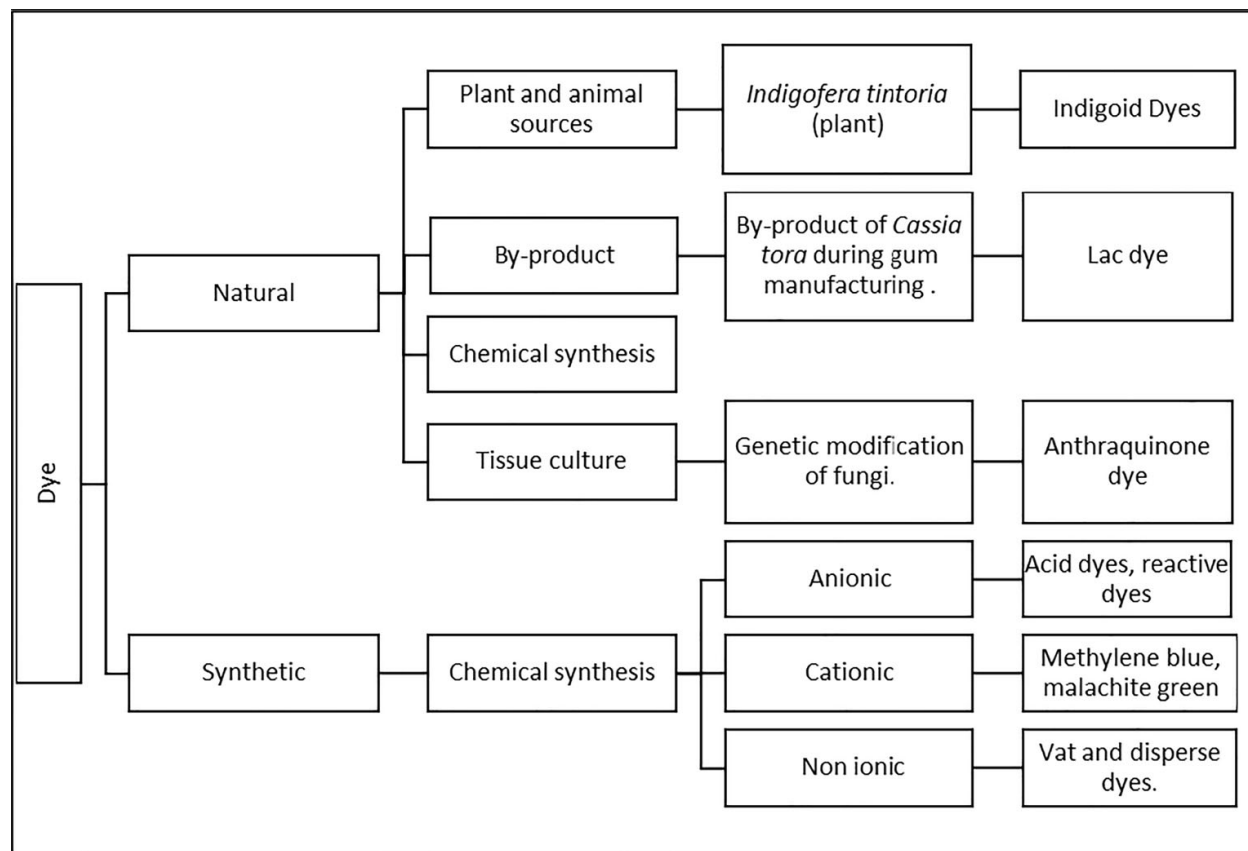


Figure 1.8.1.1.1 Classification of dye based on sources with examples[242].

The adsorption process for removing methylene blue (MB) and methyl orange (MO), using the MOF NH₂-MIL-101(Al) was examined. NH₂-MIL-101(Al) demonstrated a higher selectivity for MB. The adsorption of MB was spontaneous, with a maximum capacity of 762 ± 12 mg/g_{MOF} at 30°C. This capacity exceeds that observed for MB on other MOFs and the majority of other materials. The maximum adsorption capacity of MO by NH₂-MIL-101(Al) reached 188 ± 9 mg/g_{MOF}. This implies that the strong electrostatic interaction between the MOF's amino groups

and the cationic dye MB significantly enhanced its adsorption capacity. However, its regenerative ability was found to be lacking[244].

In another study, malachite green was effectively removed from solution using a ZnO/POA-MOF, named PAZ@ZIF-8. PAZ@ZIF-8 achieved a removal efficiency of approximately 96%, significantly higher than ZIF-8 and POA/ZnO, which had removal efficiencies of 34% and 61%, respectively. PAZ@ZIF-8 exhibits a maximum adsorption capacity for malachite green of 613 mg/g_{MOF}. Moreover, after three cycles, PAZ@ZIF-8 maintained about 90% dye removal efficiency, demonstrating excellent reusability of the adsorbent[245]. The findings from several studies on dye removal using MOFs and other adsorbents, as documented in the literature, are summarized in Table 1.8.1.1.1.

Table 1.8.1.1.1 Overview of Dye Capture Utilizing Specific MOFs.

MOFs	Dye	Adsorption capacity (mg/g)	Time to reach Equilibrium (min)	Reusability (cycles)	References
PAZ@ZIF-8	Malachite green	613	60	3	[245]
Fe-MOF	Rhodamine B	90% (removal efficiency)	90	4	[246]
Ni (II)-doped MIL-101(Cr)	Congo red(CR) and methyl Orange(MO)	1607.4 (CR) and 651.2 (MO)	80	4	[247]
{[Zn (1,3-BDC) L] \cdot H ₂ O} _n	Amido black 10B(AB), methyl orange(MO), and direct red 80(DR)	2402.82 (AB), 744 (MO), and 1496.34 (DR)	30	5	[248]
ZIF-67@Fe ₃ O ₄ @ESM	Basic red 18	250.81	NA	5	[249]
Ni-MOF-199	Methylene blue	765	240	-	[250]
ZIF-67	Active red X-3B	100% (removal efficiency)	-	-	[251]

Other adsorbents					
Orange peels activated carbon	Malachite	28.5	-	-	[252]
GO-HAp	Congo red(CR), Trypan blue(TB)	48.50 (CR), 41.00 (TB)	30 (CR), 45 (TB)	4 (CR), 4 (TB)	[253]
GO-activated carbon	Methylene blue	147.00	-	5	[254]
Rice husk activated carbon	Rhodamine B	478.50	300	-	[255]
Activated carbon aerogel	Methylene blue	416.67	370	3	[256]

1.8.1.1.2 Removal of agriculture-related pollutants

Pesticides are crucial for sustainable agriculture, as they help reduce crop losses from pests, weeds and diseases and increase yields. They can be categorized based on their (i) chemical structures, (ii) target organisms, and (iii) modes of action[257]. By their chemical compositions, **organophosphates** are among the most frequently employed classes of pesticides. They encompass compounds featuring a central phosphate atom, such as diazinon, chlorpyrifos, malathion, fenitrothion, and the herbicide glyphosate[258], [259], [260]. Usually, organophosphorus pesticides are employed to manage insects, combat plant diseases, and mitigate grass damage. Other notable groups include **chlorophenoxy herbicides** like 2,4-dichlorophenoxyacetic acid (2,4-D) and 2-methyl-4-chlorophenoxyacetic acid (MCPA), **carbamates** derived from carbamic acid, **pyrethroids** which are similar in structure to naturally occurring pyrethrins, and **neonicotinoids** that resemble nicotine in structure[261], [262], [263], [264]. When pesticides are classified based on the pests they target, they are categorized into **fungicides**, **insecticides**, **herbicides**, and **rodenticides**. Triazole and imidazole family compounds, such as epoxiconazole, are common antifungal agents used in fungicides[265]. In the

INTRODUCTION

case of insecticides, which are designed to eliminate insects, dichlorodiphenyltrichloroethane (DDT) was once prominently used until its significant environmental and health risks led to its replacement by chlorpyrifos. Herbicides, which account for 50% of total pesticide use, include glyphosate, a widely utilized agent for controlling broadleaf weeds[266], [267].

Despite controlling harmful effects on agricultural production, excessive pesticide use leads to the long-term accumulation of organic agrochemicals such as herbicides, insecticides, and fungicides. Indeed, only 1% of pesticides effectively reach their intended targets, while the remaining 99% are dispersed into soil and water bodies through processes like surface runoff, erosion, spray-drift, and leaching (Figure 1.8.1.1.2). The accumulation of these persistent organic pollutants causes significant environmental and health issues, as outlined in Table 1.8.b[221]. Unfortunately, the toxicity associated with these compounds has prompted regulatory measures in numerous countries, emphasizing the critical importance of detecting and removing them. Adsorption stands out for its simplicity and cost-effectiveness, providing a straightforward and effective solution for pesticide extraction[43], [257], [268].

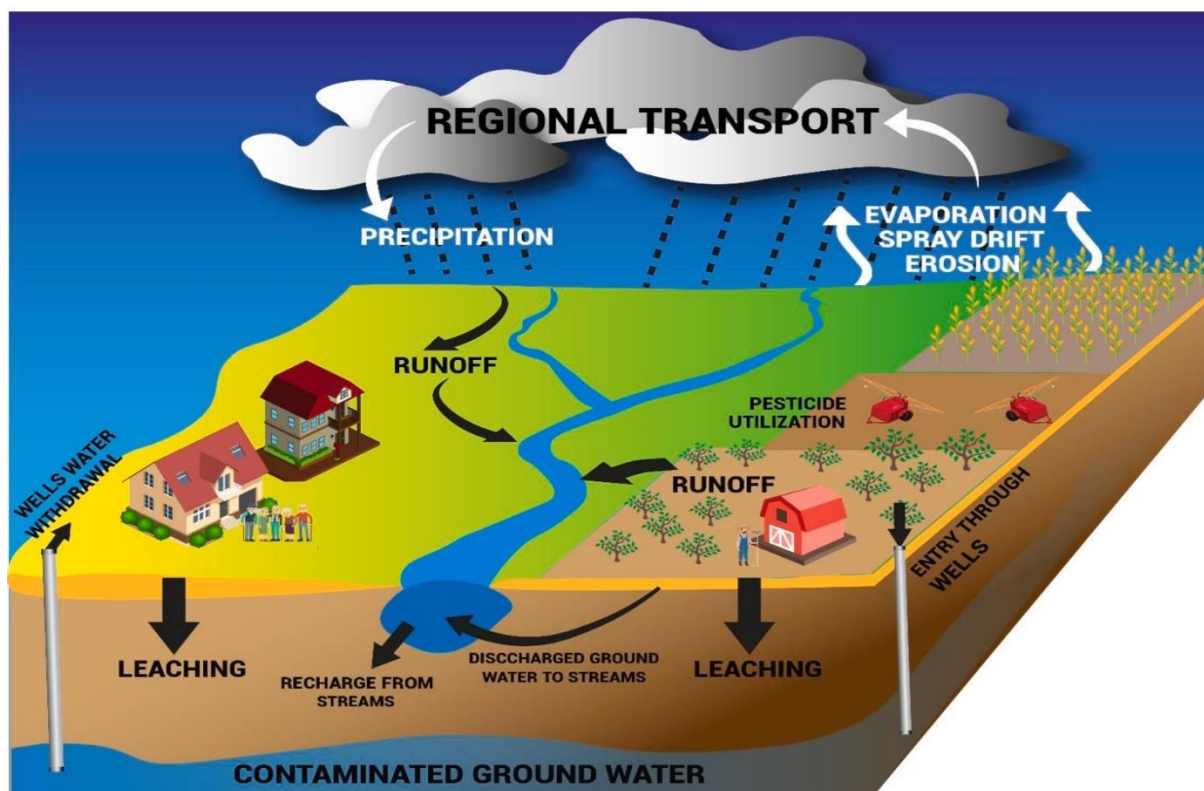


Figure 1.8.1.1.2 Pesticides transfer routes to surface and ground water[269].

Due to their unique attributes, MOFs have been introduced as novel adsorbents with superior performance for pesticide remediation. Various MOFs, including, MIL-53(Cr), UiO-66(Zr), UiO-67(Zr), ZIF-8(Zn), and Cu-BTC have been successfully employed as adsorbents for pesticide removal. Among them, MIL-53(Cr) was the first to be explored for the elimination of 2,4-dichlorophenoxyacetic acid (2,4-D)[270]. MIL-53(Cr) adsorbed 2,4-D rapidly within one hour and showed a significantly greater adsorption capacity compared to conventional adsorbents like activated carbon (AC) or USY zeolite. Moreover, MIL-53(Cr) exhibited highly effective adsorption of 2,4-D, particularly at low concentrations in the solution. Similarly, the adsorption efficiency of MOF-235(Fe) for removing bentazon, clopyralid, and isoproturon from water, comparing it with activated carbon (AC) and zeolite, was investigated[271]. Results showed that

INTRODUCTION

MOF-235(Fe) had superior kinetics and capacity. Despite its high performance, MOF-235(Fe) faced challenges with reusability due to its instability in water.

Additionally, Zr-based MOFs have been extensively studied for the adsorptive removal of pesticides. For example, UiO-66(Zr) was investigated for the removal of methylchlorophenoxypropionic acid (MCP) from water[272]. The findings revealed that the kinetic constant and adsorption capacity of UiO-66(Zr) were approximately 30 and 7.5 times greater, respectively, than those of activated carbon (AC), especially at a low MCP concentration of 1 mg/L. Table 1.8.1.1.2 summarizes the findings from various studies on pesticide removal using MOFs and their derivatives, as documented in the literature.

Table 1.8.1.1.2 Summary of pesticides adsorption over MOFs and their derivatives.

Adsorbent	Adsorbate	Conditions	Max. capacity, Q_0 (mg g ⁻¹)	References
MIL-53(Cr)	2, 4 dichlorophenoxyacetic acid	Conc.: 100 mg L ⁻¹ , Time: 12 h, pH: 2.8	556	[273]
MIL-101(Cr)	Diazinon	Conc.: 150 mg L ⁻¹ , Time: 3 min, pH: -	260	[274]
UiO-66(Zr)	Methylchlorophenoxypropionic acid	Conc.: 150 mg L ⁻¹ , Time: 12 h, pH: - 4.5	-	[275]
UiO-66(Zr)	Glyphosate	Conc.: 150 mg L ⁻¹ , Time: 300 min, pH: -4	357	[276]
UiO-67(Zr)	Dichlorvos Metrifonate	Conc.: 200 mg L ⁻¹ , Time: 210 min., pH: 2–4	571	[277]
NU-1000(Zr)	Atrazine	Conc.: 10 mg L ⁻¹ , Time: 120 min., pH: -	36	[278]
Cotton@UiO-66(Zr)	Dicamba 4-chlorophenoxyacetic acid 2,4-dichlorophenoxyacetic acid and 2-(2,4 dichlorophenoxy) propionic acid	Conc.: -, Time: 18 min, pH: 3	-	[279]
M- MOF	Neonicotinoid insecticides (thiamethoxam, imidacloprid, acetamiprid, nitenpyram, dinotefuran, clothianidin, and thiacloprid)	Conc.: 50 mg L ⁻¹ , Time: 100 min, pH: -	-	[280]

GO/UiO-67(Zr)	Glyphosate	Conc.: 1000 mg L ⁻¹ , Time: 10 h, pH: 4	483	[281]
ILCS/U-X	2,4-dichlorophenoxyacetic acid	Conc.: 500 mg L ⁻¹ , Time: 60 min, pH: 2.5	893	[282]
β-CD MOF-NPC	Metolachlor	Conc.: 50 mg L ⁻¹ , Time: 450 min, pH: 2	343	[283]
	Alachlor		291	
	Acetochlor		261	
	Pretilachlor		312	
Magnetic porous carbon	Atrazine	Conc.: -, Time: 20 min, pH: 7.04	21	[284]

1.8.1.1.3 Removal of pharmaceuticals and personal care products (PPCPs)

Pharmaceuticals and personal care products (PPCP), both synthetic and natural, are chemicals used to treat and prevent diseases. PPCPs encompass a wide array of medications, both prescribed and over-the-counter, typically categorized by their therapeutic function, along with the active and inactive ingredients in personal care products. This class of pollutants comprises a diverse range of substances, including antibiotics, painkillers, antiseptics, antiepileptics, hormones, stimulants, plasticizers, antifungal agents, anticancer drugs, sunscreens, cosmetics, shampoos, soaps, deodorants, toothpastes, etc. Increased usage has inevitably led to their detection in the environment, specifically in aquatic settings, including surface water, groundwater, drinking water and in the effluents of wastewater treatment plants (WWTPs) worldwide, and even at low concentrations, they pose significant risks to ecosystems and human health[3], [285].

Global research is focused on understanding the fate and transport of PPCPs in wastewater treatment processes. PPCPs enter the environment through several pathways. The predominant routes encompass pharmaceuticals consumed in healthcare facilities, human usage and excretion through urine and feces, and finally the improper disposal into wastewater systems. Subsequently, wastewater is treated at wastewater treatment plants (WWTPs), where PPCPs are subsequently

INTRODUCTION

released into water bodies through effluents. During treatment at WWTPs, PPCPs can undergo sorption, transferring some pollutants to sewage sludge. This sludge may then be incinerated, landfilled, or used as fertilizer on agricultural lands. In the latter two scenarios, the residual compounds in the sludge can be introduced into the aquatic environment. Additionally, veterinary medicines contribute to environmental contamination directly through application to pets, livestock, and aquaculture, and indirectly through the use of livestock manure as fertilizer, which results in agricultural runoff. Figure 1.8.1.1.3 depicts the diverse origins of pharmaceutically active compounds and their pathways into our water supplies[286].

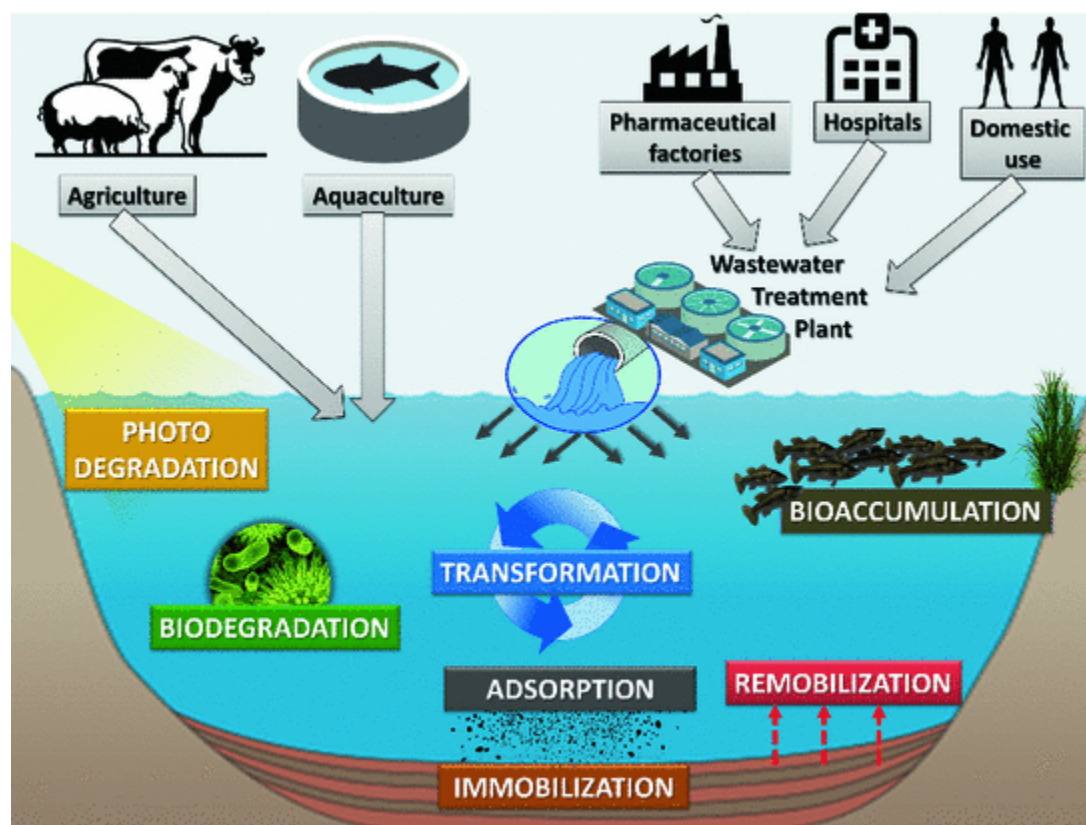


Figure 1.8.1.1.3 Sources and fate of pharmaceuticals and personal care products (PPCPs) in the aquatic environment[287].

INTRODUCTION

The uncontrolled transport of PPCPs in the environment, has raised concerns among stakeholders, including drinking-water regulators, governments, water suppliers, and the public[288]. Effectively removing PPCPs from aquatic systems presents a significant challenge due to their unique physicochemical properties and low concentrations. Adsorption has been reported to be effective in removing pharmaceuticals, outperforming conventional treatment methods[286], [289], [290], [291], [292], [293], [294]. Various MOFs, including MIL-100, MOF-5, MOF-505, HKUST-1, and UiO-66, have been utilized to remove PPCPs from wastewater[3], [222], [295]. UiO-66 and its functionalized derivatives, UiO-66s (specifically UiO-66 with SO₃H/NH₂ groups), were used to demonstrate the first application of MOFs for removing diclofenac sodium (DCF), a non-steroidal anti-inflammatory drug[296]. When comparing DCF adsorption across different adsorbents, UiO-66 and UiO-66s exhibited significantly superior performance over activated carbon (AC) in both kinetics and capacity. The pseudo-second-order rate constant for UiO-66 was 0.014, and its maximum adsorption capacity was 189 mg/g, which were 3.5 and 2.5 times higher, respectively, than those of AC.

In another study, researchers examined the removal of chloramphenicol from wastewater using PCN-222[297]. Chloramphenicol, an antibiotic, can cause severe side effects such as fatal bone marrow depression and aplastic anemia when present in drinking water. The study's findings indicated that PCN-222 outperformed other MOF and non-MOF adsorbents in terms of adsorption capacity and rates. Specifically, PCN-222 exhibited a high adsorption capacity of 370 mg/g and reached adsorption equilibrium quickly. Remarkably, it could remove about 99% of chloramphenicol from water at low concentrations.

Additionally, an innovative study describes the removal of tetracycline hydrochloride from wastewater using a MOF-derived magnetic porous carbon composite was explored[298]. The

results revealed that the MOF-derived α -Fe/Fe₃C composite is a highly effective adsorbent for this application, exhibiting outstanding reusability, with less than a 10% reduction in adsorption capacity after five consecutive adsorption-desorption cycles. Table 1.8.1.1.3 compiles the results from various studies on PPCPs removal utilizing MOFs and their derivatives, as reported in the literature.

Table 1.8.1.1.3 Summary of PPCPs adsorption over MOFs and their derivatives.

Adsorbent	Adsorbate	Adsorbate usage	Conditions	Max. capacity, Q ₀ (mg g ⁻¹)	References
MIL-101	Naproxen	A nonsteroidal antiinflammatory drug (NSAID) that is widely used for the reduction of pain, fever, inflammation and stiffness	Conc.: 10-15 mg L ⁻¹ , Time: 12h, pH: 4.5, T= 25 °C, 100 g adsorbent/L	132	[299]
	Clofibric acid	A bioactive metabolite of various lipid regulating pro-drugs		312	
MIL-53(Al)	Dimetridazole	A nitroimidazole antibiotic, that is widely used to treat infections caused by anaerobic and protozoan bacteria in humans and animals.	Time: 48h, pH: 6.4, T= 29.85 °C, 1 g adsorbent/L	467.3	[300]
Methanol activated HKUST-1	Sulfachloropyridazine	A sulfonamide antibiotic usually used in human medicine as well as cattle farming, either to treat bacterial infections and/or as a feed stock additives and husbandry because of its low cost and broad-spectrum antimicrobial activity.	Conc.: 20-100 mg L ⁻¹ , Time: 2h, pH: 7.5, T= 25 °C, 0.1 g adsorbent/L	384	[301]
Chloroform activated UiO-66			Conc.: 5-100 mg L ⁻¹ , Time: 2h, pH: 5.5, T= 25 °C, 250rpm, 0.1 g adsorbent/L	417	[302]
PPI@ SB-15/ZIF-8	Penicillin G	An antibiotic that is utilized for	Conc.: 20-200 mg L ⁻¹ , Time:	400	[303]

		treating different infectious diseases. Penicillin G has water solubility property, and its action mechanism is destroying the cell wall of bacteria through prevention of peptidoglycan generation.	90min, pH: 3, T= 25 °C, 100rpm, 0.03 g adsorbent		
UiO-66-NH ₂	Diclofenac	A common non-steroidal anti-inflammatory agent for treating various kinds of inflammatory disorders.	Conc.: 40-600 mg L ⁻¹ , Time: 24h, pH: 5.6, T= 25 °C, 3 mg adsorbent/15 ml	555	[304]
Ag@ZIF-67	Minocycline	Antibiotic that extensively used to cure animals and humans of bacterial infections	Conc.: 200mg L ⁻¹ , Time: 360min, pH: 8, T= 40°C, 0.02 g adsorbent	938.4	[305]
[Cu(BTTA)]n.2DMF	Diclofenac sodium	A nonsteroidal anti-inflammatory drug (NSAID) works by reducing substances in the body that cause pain and inflammation.	Conc.: 100-1200mg L ⁻¹ , Time: 450min, pH: 6.5, T= 20°C, 10 mg adsorbent	650	[306]
Fe ₃ O ₄ @COFs	Triclosan	Representative chlorinated antibacterial agents in PPCPs	Time: 20min, pH: 7, T= 25°C, C _{NaCl} =0.4mg/l	82.3~95.4%	[307]
	Triclocarban		0.8mg adsorbent	92.9~109.5%	
Other adsorbents					
Attapulgate/carbon (APT/C) composite	Tetracycline	An oral antibiotic in the tetracyclines family of medications, used to treat a number of infections, including acne, cholera, brucellosis, plague, malaria, and syphilis.	Conc.: 600mg L ⁻¹ , Time: 2-3h, pH: 4, T= 25°C, 20 mg adsorbent	297.90	[308]
Magnetic orange peel adsorbent	Sulfamethoxazole	A sulfonamide antibiotic, widely used in both human and veterinary medicine to prevent and treat disease and to support livestock growth	Conc.: 200mg L ⁻¹ , Time: 24h, 150rpm pH: 4, T= 25°C, 10 mg adsorbent/10ml	120	[308]
Hydrogel	Ciprofloxacin	Veterinary antibiotics (VAs)	Conc.: 10mg L ⁻¹ , Time: 660min.	106.04	[309]

	are used to prevent diseases and promote growth in animals.	pH: 7, T= 25°C, 1g adsorbent/L
Enrofloxacin		Conc.: 10mg L ⁻¹ , Time: 660min, pH: 7, T= 25°C, 1.5 g adsorbent/L
		100.43

1.8.1.2 Removal of inorganic pollutants

1.8.1.2.1 Removal of heavy metal cations

1.8.1.2.1.1 Lead (Pb)

Lead, a soft and malleable heavy metal, exists as Pb²⁺ ions and is classified as a non-essential trace element for biological systems. The World Health Organization (WHO) identifies it as one of the most toxic contaminants in wastewater[221], [310]. The daily maximum permissible limit for lead is 0.015 mg/L. Lead is non-biodegradable, with a biological half-life ranging from 10 to 35 years, leading to potentially fatal accumulation in the human body. Lead is often present in wastewater or effluents from lead mining, electronics manufacturing, urban runoff, and battery recycling plants. Known as a cumulative poison, lead can enter the body through water or food, causing a wide range of health problems[214]. Lead in solution disrupts calcium function and protein interactions[311]. Additionally, it severely affects almost all major organ systems, causing conditions such as anemia, heart disease, renal dysfunction, cancer, permanent brain damage, and can even result in death[312]. Therefore, removing lead from water sources is critical to ensure safe drinking water, and various metal-organic frameworks (MOFs) have been developed for this purpose.

INTRODUCTION

TMU-5, with its azine-functionalized pores, has demonstrated an impressive lead adsorption efficiency of 251 mg/g. Equilibrium was reached within minutes. However, the adsorption capacity decreased with lower pH levels, likely due to sorbent protonation. To optimize the process, the pH was maintained at 10[313]. In another study, the manganese-based MOF, MnO₂-MOF, synthesized by oxidizing MnSO₄ with KMnO₄, has demonstrated exceptional lead adsorption capacity of 917 mg/g, achieving equilibrium within 1 hour. Additionally, the solution's initial pH of 6 decreased to 5 during the process, likely due to proton release during adsorption[314].

In line with the recent trend of post-synthetic modification, UiO-66-NH₂ was treated with resorcylic aldehyde to target the removal of Pb²⁺ ions from wastewater[315]. The maximum adsorption capacity of resorcylic aldehyde-functionalized UiO-66-NH₂ (UiO-66-RSA) for Pb²⁺ ions reached 189.8 mg/g at pH 4, surpassing that of unmodified UiO-66-NH₂ (166.74 mg/g)[316]. Furthermore, the incorporation of resorcylic aldehyde into UiO-66-NH₂ significantly increased the lead ion removal rate from 29.8% to 78.9% and enhanced selectivity for lead ions over other metal ions. These results indicate that the nature and amount of functional groups are more critical than the porous structure of MOFs in the selective adsorption of lead ions. Regenerating UiO-66-RSA using thiourea/HNO₃ resulted in a slight decrease in the removal rate (<4%) after five consecutive adsorption/desorption cycles. The adsorption mechanism of lead ions on this material was linked to complexation interactions between the nitrogen and hydroxyl groups of UiO-66-RSA and lead ions.

Additionally, a significant challenge in the practical use of MOFs for heavy metal remediation is the large amounts of MOFs needed and the substantial waste generated from the complex separation of MOF particles from water. To address these issues, MOFs have been integrated into various substrates, including magnetic nanoparticles, polymers, and nanofibrous membranes[317],

[318], [319]. The integration of magnetic nanoparticles with MOFs or their derivatives has synergistically boosted adsorption efficiency. Furthermore, the frameworks incorporate magnetic particles, enabling easy removal with an external magnetic field. For this purpose, a series of nano-sized UiO-66-based composites, including $\text{Fe}_3\text{O}_4@\text{SiO}_2@\text{UiO-66}$, $\text{Fe}_3\text{O}_4@\text{SiO}_2@\text{UiO-66-NH}_2$, and $\text{Fe}_3\text{O}_4@\text{SiO}_2@\text{UiO-66-Urea}$, were studied[317]. Among them, and the parent MOFs, $\text{Fe}_3\text{O}_4@\text{SiO}_2@\text{UiO-66-NH}_2$ exhibited the highest adsorption capacity for Pb^{2+} ions at 102 mg/g, likely due to the abundant $-\text{NH}_2$ groups on its surface, which enhance interactions with lead ions. In another study, MIL-53 ($\text{Al}@100\text{aBDC}$), an aluminum-based MOF with a 2-amino-1,4-benzenedicarboxylic acid ligand, was introduced for the adsorption of Pb^{2+} ions. This MOF is distinguished by its water stability, structural flexibility, and excellent adsorption capacity, capable of adsorbing up to 492.4 mg/g of Pb^{2+} ions[320], [321]. Alternatively, to enhance the adsorption performance for Pb^{2+} ions, UiO-66 and UiO-66- NH_2 were grown in situ on the surface of cellulose aerogels (CA)[319]. CA was selected as the substrate due to its lightweight, high strength, water stability, low cost, non-toxicity, excellent processability, and flexibility. The maximum adsorption capacities for Pb^{2+} ions on $\text{UiO-66}@CA$ and $\text{UiO-66-NH}_2@CA$ were 81 mg/g and 89 mg/g, respectively, outperforming both the pure MOFs and the standalone CA.

1.8.1.2.1.2 Mercury (Hg)

Mercury (Hg) occurs in various chemical forms in the environment, primarily as inorganic mercury (Hg^{2+}) and methylmercury (MeHg). The most stable and common form of mercury is Hg^{2+} . The daily maximum permissible limit for lead is 0.002 mg/L[221]. Mercury contamination in the environment is driven by the erosion of natural deposits, discharges from refineries and factories, and runoff from landfills and croplands. Mercury can easily enter the human food chain through

INTRODUCTION

crops and water. It is recognized as a highly toxic heavy metal due to its ability to accumulate in the human body by binding strongly to thiol groups in proteins. Long-term consumption of mercury-contaminated food can lead to chronic mercury poisoning, causing severe health issues including damage to the brain, kidneys, nervous system, gastrointestinal system and other organs birth defects and potentially death. Taking everything into account, there is an increasingly urgent need to develop effective methods for removing mercury from wastewater[322].

Extensive exploration in the literature has delved into the removal of mercury through adsorption using MOFs, resulting in a spectrum of outcomes. Drawing from the HSAB theory, it is observed that soft bases demonstrate a heightened affinity for soft acids[323]. Numerous studies have highlighted the strong attraction of thiol- or thioether, acylamide, hydroxyl, and carboxyl groups to mercury, leading to the recognition of the functionalized with these groups MOFs as top candidates for extracting mercury ions from water sources[324], [325], [326], [327], [328], [329]. Amino acids can modify the surface of MOFs by virtue of their diverse functional groups, such as carboxyl, amine, and thiol, facilitating a potent chelating reaction with metal ions. Research has shown that nanoparticles of L-cysteine-functionalized $\text{NH}_2\text{-UiO-66}$ (Cys-UiO-66) have a high adsorption capacity of 350.14 mg/g for Hg^{2+} ions at room temperature and pH 5[330]. Additionally, Cys-UiO-66 exhibits a stronger affinity for Hg^{2+} compared to other coexisting ions in wastewater and can be regenerated for at least five cycles.

In another study a group of Zr-based MOFs, including UiO-66, UiO-66- NH_2 , UiO-66- SO_3H , and UiO-66-DMTD, were synthesized using post-synthetic modification techniques and applied in Hg^{2+} ion removal from wastewater[325]. Among others, UiO-66- NH_2 functionalized with 2,5-dimercapto-1,3,4-thiadiazole (UiO-66-DMTD), exhibited the highest adsorption capacity for Hg^{2+} ions, significantly surpassing that of pristine UiO-66 and other modified UiO-66 MOFs.

INTRODUCTION

Specifically, the maximum adsorption capacities of Hg^{2+} for UiO-66, UiO-66- NH_2 , UiO-66- SO_3H , and UiO-66-DMTD were recorded as 59.3 mg/g, 145.1 mg/g, 181.2 mg/g, and 670.5 mg/g, respectively. This represents a notable increase of 525.4 mg/g following the sulfhydryl-functionalization. Comparing these values with those reported in the literature, the adsorption capacity of UiO-66-DMTD surpasses that of other adsorbents, as illustrated in Table 1.8.1.2.1.2. This enhancement was attributed to the interaction between electron-rich functional groups, such as sulfur, nitrogen, and aromatic rings, on the modified MOF surface and Hg^{2+} via complexation reactions. Additionally, UiO-66-DMTD demonstrated notable selectivity in adsorbing Hg^{2+} ions over other competing metal ions. Consequently, UiO-66-DMTD exhibits significant potential for mercury removal.

Table 1.8.1.2.1.2 Comparison adsorption amount of different types of sorbents for Hg^{2+} ions.

Sorbents	Initial concentration (mg/L)	Adsorption amount (mg/g)	References
Romanian peat moss	40	98.94	[331]
TiO_2 -SG	100	121	[332]
MCA	2	172.61	[333]
Nanocomposite material of DDPP	0.25	179.74	[334]
SH@ SiO_2 /MOF nanocomposite	0.5	210	[335]
UiO-66-(SH) ₂	0.01	236.4	[336]
Acrylamide/hydroxyl-MOF	20	278	[337]
SH- Fe_3O_4 @ SiO_2 @UiO-66	20	282	[338]
MAF-SCMNPs	50	355	[339]
Aminated chitosan beads	100	461.36	[340]
UiO-66-DMTD	200	670.5	[325]

INTRODUCTION

Moreover, a magnetic MOF, $\text{Fe}_3\text{O}_4@\text{SiO}_2@\text{HKUST-1}$, with excellent mercury adsorption potential, was developed[341]. This material demonstrated rapid adsorption, reaching equilibrium in just 10 minutes, with a maximum uptake capacity of 264 mg/g. It achieved approximately 99% mercury removal from a 20 mg/L solution. Additionally, the MOF exhibited 23% adsorption for Pb^{2+} and 55% for Cr^{3+} when exposed to other metals.

1.8.1.2.1.3 Cadmium (Cd)

Cadmium, a toxic heavy metal ion in wastewater, exists in water as Cd^{2+} . The maximum permissible level of cadmium in water is 0.005 mg/L. Cadmium contamination in the environment is primarily caused by the corrosion of galvanized pipes, the erosion of natural deposits, discharges from metal refineries, and runoff from waste batteries and paints. Prolonged exposure to cadmium can severely impact the nervous, reproductive, renal, and skeletal systems and may also cause certain cancers. Numerous metal-organic frameworks (MOFs) are ideally used to remove cadmium ions through adsorption methods.

AMOF-1, an anionic metal-organic framework synthesized by combining Zn^{2+} with a tetra carboxylate linker, is water-stable and highly effective at capturing heavy metals, even at low concentrations[342]. Experiments revealed that AMOF-1 has a maximum uptake capacity of 41 mg/g for Cd^{2+} and an extraction efficiency of 98.2% for Cd ions in a 24h ion exchange process. Additionally, AMOF-1 demonstrates excellent extraction efficiencies for Hg^{2+} and Pb^{2+} , at 98.7% and 97.6% respectively, with maximum adsorption capacities of 78 mg/g for Hg^{2+} and 71 mg/g for Pb^{2+} . Moreover, AMOF-1 has a detection limit of 1 ppm for heavy metal ions in water.

INTRODUCTION

An outstanding MOF, named FJI-H9, was synthesized by reacting CaCl_2 with 2,5-thiophene carboxylate to reversibly capture Cd^{2+} , achieving an adsorption capacity of 286 mg/g[343]. Further research demonstrated that FJI-H9 does not absorb other metal ions such as Mg^{2+} , Co^{2+} , Ni^{2+} , Mn^{2+} , Zn^{2+} , Fe^{2+} , and Pb^{2+} . However, it showed slight capture of Hg, likely due to the presence of thiophenyl groups. Consequently, the authors concluded that this MOF is a highly selective adsorbent for Cd^{2+} ions.

1.8.1.2.2 Removal of oxyanions

1.8.1.2.2.1 Arsenic (As)

Arsenic is a significant water pollutant, extremely poisoning and highly hazardous to humans, primarily produced by fossil fuel combustion, semiconductor industry, pharmaceuticals, medical treatments, wood preservatives and metallurgical activities. In natural water, arsenic occurs as two oxyanion species: trivalent arsenite (As^{3+}) and pentavalent arsenate (As^{5+})[344]. According to the U.S.A Environmental Protection Agency, arsenic levels above the maximum contamination level (MCL) of 0.01 mg/L can cause skin, lungs, liver and kidney diseases, circulatory disorders, neurological disorders, nausea, severe immune system issues and increase cancer risk with long-term exposure[214], [220], [221]. Conversely, arsenic levels below 10 ppb in drinking water are considered safe. Because arsenic moves easily through water and accumulates readily in the food chain and the human body, its effective removal from water is a crucial topic in water treatment[345], [346], [347]. Traditional methods for removing arsenic include coagulation (co-precipitation), membrane filtration, adsorption, ion exchange, bioremediation, and biosand filtration. While these techniques are generally effective for As^{5+} removal, they are less effective

INTRODUCTION

for As^{3+} , which requires a pre-oxidation step, making the removal process more complex and demanding. Recently, increased attention has been given to the adsorptive removal using MOFs.

Due to its strong Zr-O bonding and hydrolytic stability, MOF-808 was employed to remove As^{5+} from water[348]. The adsorption capacity of MOF-808 for As^{5+} was measured at 24.80 mg/g with an initial arsenic concentration of 5 ppm, significantly outperforming traditional inorganic porous materials like hybrid silica and aluminum oxide. This high capacity is attributed to the low pH environment, which positively charges the surface of MOF-808, enhancing the interaction between As^{5+} and the adsorbent. Furthermore, cycling experiments revealed that MOF-808 demonstrates excellent stability and reproducibility, maintaining 82.10% of its removal efficiency after five cycles.

Besides anionic arsenates containing As^{5+} , inorganic arsenic can also be present in groundwater as neutral arsenites with As^{3+} . As highlighted in the literature, the toxicity of As^{3+} surpasses that of As^{5+} , necessitating the development of novel approaches to address this environmental hazard. Therefore, capturing toxic As^{3+} ions is equally essential. The simultaneous removal of As^{3+} using a combination of manganese oxide-based octahedral molecular sieves (K-OMS2) and iron-benzenetricarboxylate (Fe-BTC) was investigated[349]. This process involved both oxidation and adsorption, with K-OMS2 oxidizing As^{3+} to As^{5+} within the temperature range of 303-333 K, followed by adsorption of As^{5+} by Fe-BTC in the same batch. The maximum adsorption capacity was found to be 76.34 mg/g. When introduced together into a solution with an initial As^{3+} concentration of 5 mg/L, the combined K-OMS2 and Fe-BTC system completed the As^{3+} removal process within 60 minutes, shortening the process time compared to sequential addition.

In another study researchers introduced a series of UiO-MOF analogues, without the usage of oxidizing agents. These analogues incorporating a Zr_6 node with missing-linker sites and organic

INTRODUCTION

ligands based on thiolates within the same framework[350]. Thanks to the remarkable As^{5+} binding capability of the missing-linker-defect Zr_6 node and the selective capture of As^{3+} ions by thiolated linkers, these UiO-66 analogues achieved dual adsorption of both anionic arsenates and neutral arsenites.

Alternatively, Magnetic Metal-Organic Frameworks (MMOFs) comprising $\text{Fe}_3\text{O}_4@\text{ZIF-8}$, with Fe_3O_4 as the core and ZIF-8 as the shell, was investigated for the effective As^{3+} removal (Figure 1.8.1.2.2.1)[351]. $\text{Fe}_3\text{O}_4@\text{ZIF-8}$ exhibited a remarkable maximum adsorption capacity of 100 mg/g for As^{3+} , showcasing its exceptional adsorption efficiency. The study also investigated interference from other anions, revealing that chloride, sulfate, and nitrate have minimal effects on As^{3+} adsorption, whereas phosphate and carbonate significantly hinder it, likely owing to their chemical similarities.

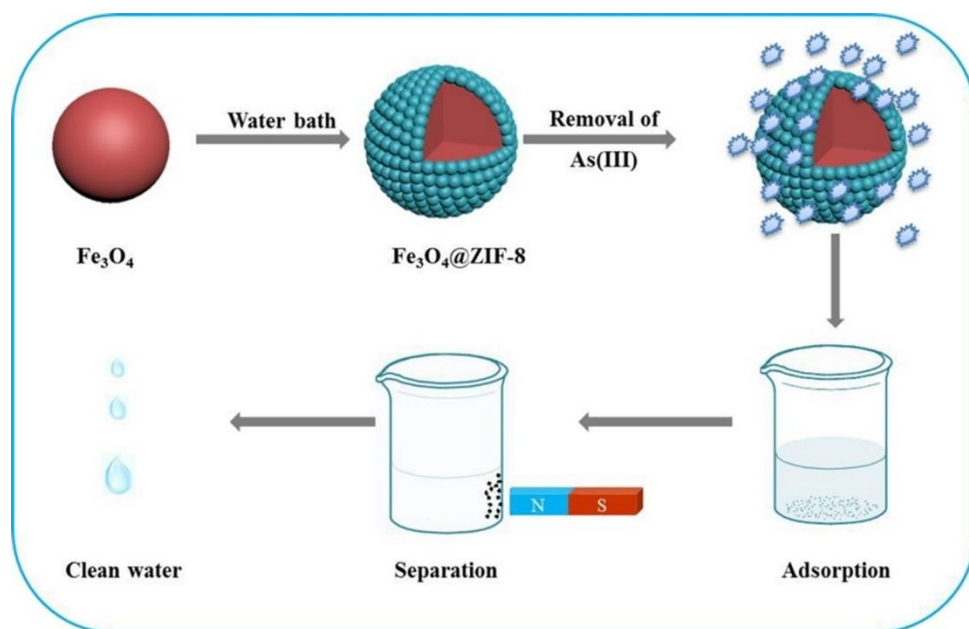


Figure 1.8.1.2.2.1 Schematic illustration of $\text{As}(\text{III})$ removal through adsorption using the $\text{Fe}_3\text{O}_4@\text{ZIF-8}$ MOF[351].

INTRODUCTION

In addition, Zn-MOF-74 was investigated for its effectiveness in removing As^{5+} and As^{3+} and their speciation based on pH values, owing to its open-metal sites that can coordinate with H_2AsO_4^- or H_2AsO_3 [352]. The optimal pH for adsorption was determined to be 7 for As^{5+} (H_2AsO_4^- species present) and 12 for As^{3+} (H_2AsO_3 species present). At an arsenate ion concentration of 800 mg/L, the adsorption capacity reached saturation, achieving ultrahigh capacities of up to 325 mg/g for As^{5+} and 211 mg/g for As^{3+} . Additionally, the impact of coexisting chlorate, nitrate, and phosphate, common in the hydrosphere, was assessed. Cl^- and NO_3^- were found to have minimal effect on the adsorption of both As^{3+} and As^{5+} species, whereas PO_4^{3-} significantly inhibited arsenic adsorption due to their chemical similarity.

1.8.1.2.2.2 Chromium (Cr)

Chromium is commonly found in wastewater, generally appears as anions such as CrO_4^{2-} , $\text{Cr}_2\text{O}_7^{2-}$, HCrO_4^- or cations (Cr^{3+})[234], [353]. Cr^{3+} is a vital nutrient found in numerous foods such as vegetables, fruits, meats, grains, and yeast. Cr^{6+} occurs naturally in the environment through the erosion of chromium deposits and is also produced by industrial activities like leather tanning, paint manufacturing, and cement production. Its rapid diffusion and carcinogenic nature have made chromium leakage a significant environmental concern[354]. The federal drinking water standard for total chromium is set at 0.1 mg/L[221]. This standard encompasses both Cr^{6+} and Cr^{3+} because they can interconvert depending on environmental conditions. The United States Environmental Protection Agency (EPA) assumes all total chromium is Cr^{6+} the more toxic form, to ensure comprehensive risk management. If tap water from a public system exceeds this standard, consumers will be informed accordingly. As a result, there is a rising interest in researching the use of MOFs for chromium removal.

INTRODUCTION

A cationic Zr-MOF (ZJU-101), derived from MOF-867 with modified methyl groups, was investigated for Cr^{6+} removal[355]. ZJU-101 demonstrated an impressive adsorption capacity of 245 mg/g for $\text{Cr}_2\text{O}_7^{2-}$, the highest recorded for any known porous solid. Furthermore, kinetic analysis using a pseudo-second-order model revealed an exceptionally high initial adsorption rate, 324 times greater than that of MOF-867, with a half adsorption time of just 0.41 minutes.

The maximum adsorption capacities for Cr^{6+} on Form-UiO-66 (formic acid-modified UiO-66) and Ac-UiO-66 (acetic acid-modified UiO-66) were 243.9 mg/g and 151.52 mg/g, respectively, which are significantly higher than the 36.4 mg/g observed for pristine UiO-66 [356]. Additionally, extensive research has focused on integrating UiO-66 into various supports, including nanofibers, polymers, and magnetic cores, for the removal of chromium[357], [358], [359]. More specific, a core-shell nanocomposite adsorbent featuring a UiO-66- NH_2 shell, and a silica gel core was developed to extract hexavalent chromium from water[356]. Silica, an inexpensive and abundant material with a large surface area, improved the packing efficiency of the ion-exchange column and increased the contact time between the adsorbent and adsorbate. As a result, the composite demonstrated a high adsorption capacity (>277 mg/g) for hexavalent chromium ($\text{Cr}_2\text{O}_7^{2-}$). Additionally, the presence of competing anions, such as bromide, chloride, sulfate, and nitrate, did not significantly affect the composite's ability to adsorb Cr^{6+} .

Alginic acid metal-organic frameworks (MOFs) like MOR-1-HA and MOR-2-HA have been thoroughly investigated, showing exceptional efficiency as adsorbents for $\text{Cr}_2\text{O}_7^{2-}$ [360], [361]. MOR-1-HA demonstrated an adsorption capacity of 280 mg/g within a pH range of 2-8, whereas MOR-2-HA showed a capacity of 162 mg/g within a pH range of 2-9 and could completely remove dichromate in just 1 minute. Detailed batch ion-exchange studies revealed that both MOFs possess high absorption capacities, rapid sorption kinetics, and outstanding selectivity for Cr^{6+} , even in the

presence of competing ions such as Cl^- , Br^- , NO_3^- , and SO_4^{2-} . Notably, columns incorporating a mixture of these MOFs and sand as the stationary phase, with only 1% wt. sorbent content, were highly effective in reducing moderate and trace Cr^{6+} concentrations to well below safe limits, even when high concentrations of competing anions were present. These columns also exhibited high breakthrough capacities, excellent regeneration capabilities, and reusability.

1.8.1.2.2.3 Selenate and selenite

Selenium (Se) is an essential trace element with significant roles in industry and human health[362]. It occurs naturally through the weathering of seleniferous soils and rocks, while human activities such as mining, metal refining, flue gas desulfurization, and other industrial processes contribute to Se pollution[363]. Se oxyanions, namely selenate (SeO_4^{2-}) and selenite (SeO_3^{2-}), are highly soluble in water and are known for their potential toxicity to organisms, even at very low concentrations. The maximum permissible level of selenium in water is 0.05 mg/L[221]. The primary concern regarding Se pollution is its bioaccumulative nature, leading to biomagnification and posing significant risks to aquatic ecosystems[364]. Several methods have been explored to remove selenite and selenate from water, including the use of advanced materials like MOFs.

Zirconium-based MOFs, such as hydrous zirconium oxides, possess ion exchange capabilities and a strong affinity of Zr^{4+} species towards various oxo-anions like selenite and selenate, which makes them highly selective for water purification. MOFs such as NU-1000, UiO-66, UiO-67, and their derivatives have been studied for their ability to adsorb selenite and selenate. Notably, NU-1000 exhibits impressive adsorption capacities of 85 mg/g for selenate and 95 mg/g for selenite[365].

INTRODUCTION

In our previous work, a bulk sorbent material composed of the MOF MOR-1 supported on cotton textiles was developed, thereby showcasing its efficacy in removing toxic oxyanions, including Se^{4+} oxyanions, from aquatic environments[366]. The new sorbent demonstrates exceptional capability in adsorbing both individual and competing As^{5+} and Se^{4+} oxyanionic species from water. This effectiveness stems from the strong binding affinity of these species to Zr^{4+} metal ions, combined with the fabric's high permeability and extensive surface area. MOR-1@cotton fabric exhibits maximum adsorption capacities for As^{5+} (459 mg g⁻¹) and Se^{4+} (325 mg g⁻¹), surpassing those of previously reported sorbents. Furthermore, it shows robust sorption performance across a broad pH range (3-7) and displays high selectivity for As^{5+} and Se^{4+} over various competing anions. Importantly, the fabric sorbent effectively removes As^{5+} and Se^{4+} from real water samples (lake, river, and well water) under realistic conditions, yielding highly satisfactory results. The ease of retrieving the bulk MOR-1@cotton fabric from water after use, unlike powdered sorbents, enhances its practicality for real-world water treatment applications.

1.8.1.2.3 Removal of halide ions

1.8.1.2.3.1 Fluoride

Adequate daily fluoride intake is crucial for maintaining bone integrity, but overconsumption can result in skeletal fluorosis and severe liver and kidney problems[367]. The maximum permissible level of fluoride in water is 4.0 mg/L[221]. Before the introduction of MOFs for fluoride adsorption, several methods such as precipitation, reverse osmosis, filtration, and adsorption using activated alumina and hydrous zirconium oxide[368], [369], [370], [371]. However, these techniques frequently suffer from low efficiency and difficulties in removing trace contaminants.

INTRODUCTION

It was found that MIL-96 effectively removes fluoride from solutions with low fluoride concentrations (1.5 mg/L), but it showed no effectiveness in solutions containing bicarbonate, sulfate, chloride, or nitrate[372]. Furthermore, column experiments on groundwater demonstrated MIL-96's potential for efficient water purification.

An innovative research describes a series of hydrolysis-stable MOFs, including MIL-53 (Fe, Cr, Al), MIL-68 (Al), CAU-1, CAU-6, UiO-66 (Zr, Hf), and ZIFs-7, -8, -9, and assesses their stability in fluoride solutions and their defluoridation performance[373]. Among the tested MOFs, UiO-66(Zr) showed the highest fluoride adsorption capacity at 40.09 mg/g, likely attributed to its inert metal with a high coordination number and suitable hydrophobicity, enhancing stability in fluoride solutions. This adsorption capacity was the highest reported among other adsorbents (α -Al₂O₃, hydrated cement, biochar) under neutral conditions[374], [375], [376].

Additionally, the aluminum fumarate (AlFu) MOF, similar in structure to MIL-53, demonstrates impressive water stability and boasts an exceptionally high fluoride uptake capacity[377]. Adsorption experiments demonstrated that AlFu MOF can reach a peak fluoride adsorption capacity of 600 mg/g at 293 K. Notably, there was a minor pH increase during the adsorption process, and the maximum adsorption capacity progressively declined at elevated temperatures.

1.8.1.2.4 Removal of radioactive substances

Nuclear energy, prized for its high energy density and zero greenhouse gas emissions, is regarded as an excellent source of clean energy[378]. Many nuclear reactors have been built globally to meet energy demands[379]. However, the development of nuclear energy brings significant environmental challenges, notably the generation of radioactive waste. Some radioactive elements,

due to their long half-lives, high solubility in water, and environmental mobility, can persist in groundwater for long periods, posing serious health risks, including cancer[380]. MOFs have been recognized as potential adsorbent materials for removing radioactive substances from wastewater, specifically targeting elements like ^{133}Ba , ^{137}Cs , ^{60}Co , ^{99}Tc , ^{129}I , ^{232}Th , ^{235}U , and ^{238}U .

1.8.1.2.4.1 Uranium (^{235}U)

Uranium is a crucial radioactive element, both valuable as a resource and dangerous as a toxic contaminant. The isotope ^{235}U , with a half-life of 7×10^8 years, is particularly notable. High levels of uranium in wastewater can cause irreversible kidney damage, DNA damage, and gene mutations[268]. In the nuclear industry, wastewater uranium concentrations can reach 5 mg/L, approximately 125 times the World Health Organization (WHO) limit[381]. As a result, efforts to remove uranium from water have significantly intensified over the past decade[382], [383]. Extensive research has focused on metal-organic frameworks (MOFs) and MOF-based composites for their ability to capture ^{235}U . Reported maximum sorption capacities (q_{max}) generally range from 100 to 350 mg/g [384]. For example, UiO-66 has a capacity of 109.09 mg/g, Co-SLUG-35 has 118 mg/g, Terbium(III)-based MOF has 179.8 mg/g, and MOF-76 has 314 mg/g[385], [386], [387], [388]. MIL-101-DETA stands out with the highest capacity of 350 mg/g at pH 5.5 [389]. Additionally, in this study ^{235}U can be easily desorbed by reducing the pH to 3.0 or lower. These materials also exhibit excellent selectivity for ^{235}U , even in solutions with various competing ions.

1.8.1.2.4.2 Barium (^{133}Ba)

INTRODUCTION

^{133}Ba , a radioactive barium isotope with a 10.5-year half-life, creates long-term environmental challenges due to its high water solubility and carcinogenic properties[390]. The concept of a barium "ion trap" using MOFs with highly accessible binding sites was introduced, significantly enhancing barium uptake[391]. In this study, MOF-808 and MIL-101(Cr) were modified with strong barium-chelating groups (sulfate and sulfonic acid groups), resulting in MOF-808-SO₄ and MIL-101-SO₃H(Cr), which exhibited high water stability and ultrahigh sorption rates (Figure 1.8.1.2.4.2). Adsorption experiments showed both MOFs achieved over 90% removal efficiency within the first 5 minutes, with MIL-101-SO₃H(Cr) displaying a kinetic rate constant vastly superior to other materials. The maximum adsorption capacities of MOF-808-SO₄ (131.1 mg/g) and MIL-101-SO₃H(Cr) (70.5 mg/g) were 328 and 60 times higher than their pristine forms, and they demonstrated high selectivity for barium even in the presence of other metal ions.

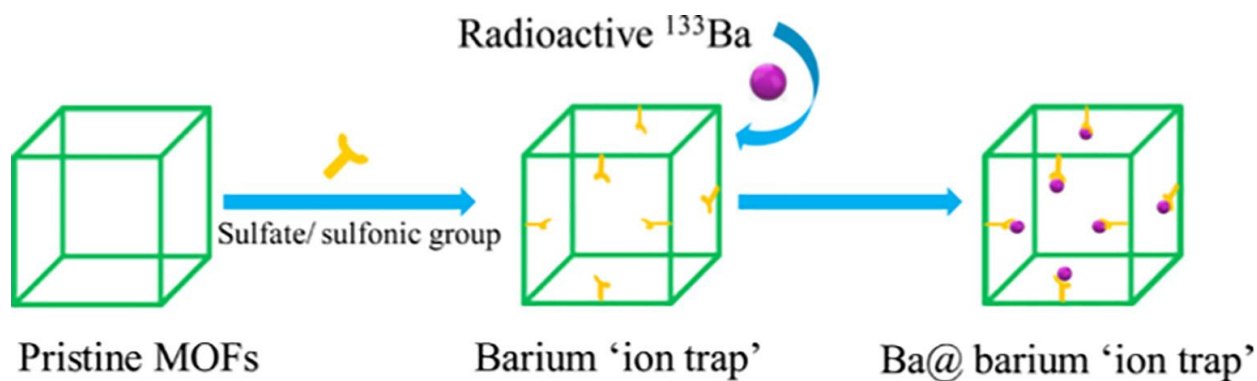


Figure 1.8.1.2.4.2 Illustration of barium capture by an "Ion Trap" based on MOFs with a chelating group[391].

1.8.1.2.4.3 Cobalt (^{60}Co)

^{60}Co is a significant component of radioactive waste, posing serious health risks to both humans and animals, such as aplastic anemia, lung irritation, and bone defects. Therefore, removing ^{60}Co from radioactive waste is of great theoretical and practical importance. It is primarily found in reactor cooling water as a corrosion byproduct and can easily migrate through soil and groundwater[268]. Efficient removal of ^{60}Co from wastewater relies on superior adsorbents with strong chemical stability, in-pore functionality, and outer-surface modifications[392]. The UiO-66-Schiff base achieved a maximum adsorption capacity of 256 mg/g for cobalt ions[393]. The selectivity of the UiO-66-Schiff base was tested in a solution containing Na^+ , K^+ , Mg^{2+} , Ca^{2+} , Co^{2+} , and Ni^{2+} , under optimal conditions (pH 8.4). The results indicated that most of these metals did not significantly affect Co^{2+} adsorption, with the exception of Ni^{2+} , likely due to the similar electron-shell structures and coordination conditions of Co^{2+} and Ni^{2+} with the UiO-66-Schiff base. Additionally, even after undergoing 5 cycles of reuse, the regenerated UiO-66-Schiff base retained its high sorption capacity, highlights its potential for effectively preconcentrating and removing cobalt (II) from aqueous solutions in real-world applications.

1.8.1.2.5 Removal of precious metals

The toxicological impacts of wastewater from precious metal mining, including gold, silver, platinum, palladium, iridium, ruthenium, and rhodium, are a growing global concern [394]. These rare earth metals are highly demanded in industries such as dental, electronics, automotive, and jewelry due to their economic value (Table 1.8.1.2.5)[395], [396]. This contamination not only has serious environmental impacts but also imposes financial penalties on industries and endangers human health and ecosystems. MOFs are notably versatile, finding numerous applications in the

separation and selective recovery of precious heavy metals such as platinum (Pt), palladium (Pd), silver (Ag) and gold (Au)[397], [398], [399].

Table 1.8.1.2.5 Major applications of precious metals. Retrieved from Ref [400].

Precious Metals	Applications
Gold	Jewellery, electronics, pharmaceuticals, superalloys and dental applications
Silver	Jewellery, catalyst, electronics, dental, oil, photovoltaics
Platinum	Superalloys, photovoltaics, pharmaceuticals, oil, dental ceramics, glass, fuel cells, electronics, chemistry, catalysts, jewellery
Palladium	Pharmaceuticals, dental, fuel cells, electronics, chemistry, catalysts, jewellery
Rhodium	Ceramics, glass, fuel cells, electronics, chemistry, catalysts
Iridium	Catalysts, electronics, dental
Ruthenium	Catalysts, electronics, fuel cells, pharmaceuticals, photovoltaics, superalloys

1.8.1.2.5.1 Gold (Au)

UiO-66-NH₂, an Zr-based MOF, was synthesized and employed to adsorb Au³⁺ from aqueous solutions[399]. Within just 6 minutes, it adsorbed around 50% of the Au³⁺, achieving a maximum adsorption capacity of up to 650 mg·g⁻¹ at room temperature, surpassing traditional adsorbents. The adsorption mechanism involved electrostatic attraction between -NH₃⁺ groups and Au³⁺, along with complexation with Zr-OH groups. Furthermore, the amino groups facilitated the reduction of Au³⁺ to Au⁰ through a redox reaction, as confirmed by X-ray photoelectron spectroscopy (XPS), powder X-ray diffraction (PXRD), and high-resolution transmission electron microscopy.

INTRODUCTION

Additionally, by modifying UiO-66-NH₂ nanoparticles with amidinothioura (UiO-66-ATU), the adsorption capacity increased from 166 mg/g to more than 227 mg/g at room temperature and pH 3[401]. UiO-66-ATU also displayed excellent selectivity towards Au³⁺ and demonstrated outstanding reusability after four adsorption-desorption cycles. The adsorption mechanisms were attributed to chelation and ion exchange interactions involving the N/S groups of UiO-66-ATU with Au³⁺.

1.8.1.2.5.2 Silver (Ag)

The thiol-functionalized MIL-53(Al) MOF is recognized for its high adsorption affinity for Ag⁺ ions, with a maximum capacity of 183 mg/g. After adsorption, the silver ions form clusters and develop into silver nanoparticles, which are stabilized by the thiol groups within the MOF framework[402]. Another framework, HKUST-1, has demonstrated significant potential for adsorbing Ag⁺ ions. This MOF effectively extracts silver nanoparticles from aqueous solutions, where the solution initially appears yellow. Upon adsorption by the blue HKUST-1 framework, the MOF's color changes to dark green. It is essential to maintain the temperature around 50°C during the adsorption process, as higher temperatures can lead to the degradation of the HKUST-1 framework[403].

1.8.1.2.5.3 Palladium (Pd)

A pyridyltriazol-functionalized UiO-66, referred to as UiO-66-Pyta, was employed for the solid-phase extraction of palladium ions from an aqueous solution[398]. UiO-66-Pyta exhibited remarkable selectivity and adsorption capacity for Pd²⁺, achieving a maximum sorption capacity

INTRODUCTION

of 294.1 mg g⁻¹ at an acidic pH of 4.5. Additionally, the adsorbent could be regenerated and reused for five cycles without significant loss in capacity or performance. Notably, as a case study, the palladium-loaded UiO-66-Pyta (UiO-66-Pyta-Pd) was used as an efficient catalyst for the Suzuki-Miyaura cross-coupling reaction. In another study, Zr(IV)-cluster-based MOFs were synthesized to selectively adsorb Pd²⁺ from acidic aqueous solutions containing Co²⁺, Ni²⁺, Pd²⁺, and Pt⁴⁺[397]. Among the synthesized Zr-MOFs (UiO-66, UiO-66-NH₂, and UiO-66-NHCOCH₃), UiO-66-NH₂ exhibited the highest adsorption capacity for Pd²⁺ at 166.4 mg g⁻¹ and remarkable selectivity. In mixed-metal solutions, UiO-66-NH₂'s uptake of Pd²⁺ was approximately 181 times greater than that of Pt⁴⁺, which had a maximum adsorption capacity of only 0.92 mg g⁻¹. This exceptional selectivity for Pd²⁺ is attributed to the stronger binding affinity of protonated amino groups (–NH₃⁺) for PdCl₄²⁻, and the more efficient diffusion of PdCl₄²⁻, through the well-suited pore sizes of UiO-66-NH₂, compared to Pt⁴⁺ ions (PtCl₆²⁻). Table 1.8.1.2 summarizes the adsorption of some inorganic pollutants by some selected MOFs

Table 1.8.1.2 Summary of inorganic pollutants adsorption from wastewater by some selected MOFs.

MOFs	Heavy Metal	Recyclability	Selectivity against	Reaction conditions	Maximum adsorption capacity(mg/g)	References
MCNC@ZN-BTC	Pb ²⁺	Reusable (5 cycles)	Zn ²⁺ , Cd ²⁺ , Cu ²⁺	pH=5.4, t=30min	558.66	[404]
Thiol-functionalized Fe ₃ O ₄ @Cu ₃ (BTC) ₂		Reusable (4 cycles)	Ni ²⁺ , Na ⁺ , Mg ²⁺ , Ca ²⁺ , Zn ²⁺ and Cd ²⁺	pH=5.9, t=2h	215.05	[405]
UiO-66-RSA		Reusable (5 cycles)	Zn ²⁺ , Co ⁴⁺ , Ni ²⁺ , Mg ²⁺ , Cd ²⁺ , Cu ²⁺ and Ca ²⁺	pH=5, t=2.5h	189.8	[315]
[Zn ₂ (oba) ₂ (bpfb)] · (DMF) ₅ (TMU-23)		Reusable (3 cycles)	Co ²⁺ , Hg ²⁺ , Cd ²⁺ , As ³⁺ , Ni ²⁺ , Pb ²⁺ and Cr ³⁺	pH=7, t=15min	434.70	[406]
Melamine-modified-MOFs		Reusable (5 cycles)	-	pH=5, t=120min, T=40°C	122.00	[407]

Cu ₃ (BTC) ₂ -SO ₃ H	Cd ²⁺	Reusable (6 cycles)	Na ⁺ , Mg ²⁺ , Ca ²⁺ , Pb ²⁺ , Cu ²⁺ , and Ni ²⁺	pH=6, t=10min	88.7	[408]
CD MOF-NPC		-	Na ⁺ , Ca ²⁺ , Mg ²⁺ , NO ₃ ⁻ , Cl ⁻ , SO ₄ ²⁻	pH=7, t=60min	140.85	[409]
UiO-66-NH ₂		Reusable (5 cycles)	-	pH=6, t=60min	415.6	[318]
UiO-66-SH	Hg ²⁺	Reusable (7 cycles)	Co ²⁺ , Cd ²⁺ , Cu ²⁺ , Ni ²⁺ , Ba ²⁺ and Mn ²⁺	pH=4, t=20min	785	[324]
FJI-H12		Reusable	Mn ²⁺ , Ba ²⁺ , Ni ²⁺ , Cd ²⁺	pH=7, t=50min	439.8	[322]
PCN-221		Reusable (3cycles)	No selective	pH=7.1, t=30min	233.3	[410]
Zr-DMBD		Reusable (5 cycles)	Co ²⁺ , Ni ²⁺ , Cu ²⁺ , Zn ²⁺ , Cd ²⁺ , Ca ²⁺ , Mg ²⁺	pH=6, t=10min	171.5	[328]
ZJU-101	Cr ₂ O ₇ ²⁻	-	Cl ⁻ , Br ⁻ , NO ₃ ⁻ , SO ₄ ²⁻ , I ⁻ and F ⁻	Ambient conditions, t=10min	245	[355]
FIR-54		Reusable (5 cycles)	No selective	Ambient conditions, t=10min	103	[411]
Fe ₃ O ₄ @UiO-66@UiO-67/CTAB		Reusable (5 cycles)	No selective	pH = 2.0, t=240min	932.1	[412]
MIL-100(Fe)	AsO ₄ ³⁻	Reusable (3 cycles)	Cl ⁻ , SO ₄ ²⁻ , NO ₃ ⁻ and CO ₃ ²⁻	T=1h	110	[413]
ZIF-8		Reusable (3 cycles)	Cl ⁻ , F ⁻ , NO ₃ ⁻ , SO ₄ ²⁻ , PO ₄ ³⁻	pH =4, t=7h	76.5	[414]
Zn-MOF-74		Reusable (3 cycles)	No selective	pH =7, t=150min	325	[352]
UiO-66(NH ₂)	As ³⁺	Reusable (6 cycles)	CO ₃ ²⁻ , NO ₃ ⁻ , Br ⁻ , Cl ⁻ , SO ₄ ²⁻ , Sb ⁵⁺ , Sb ³⁺ , HPO ₄ ²⁻ and H ₂ PO ₄ ⁻	pH =9.2, t=20min	205	[415]
Fe ₃ O ₄ @ZIF-8		No reusable	No selective	pH =5-9, t=240min	100	[351]
MOF-808-SO ₄	¹³³ Ba (Ba ²⁺)	-	Cs ⁺ , Zn ²⁺ , Ni ²⁺ , Co ²⁺ , Sr ²⁺ , La ³⁺ , Eu ³⁺	pH =5.8, t=5min	131.1	[391]
SZ-2	²³⁵ U (UO ₂ ²⁺)	-	Selective, except Ho ³⁺	pH=3-7, t=3h	58.18	[416]
SCU-100	⁹⁹ Tc (ReO ₄)	-	NO ₃ ⁻ , SO ₄ ²⁻ , CO ₃ ²⁻ , and PO ₄ ³⁻	T=30min	541	[417]
UiO-66(Zr)	F ⁻		Cl ⁻ , NO ₃ ⁻ , SO ₄ ²⁻ , except CO ₃ ²⁻	pH=6-9, t=80min	40.09	[373]
AlFu		Reusable	No selective	pH=6.5-7.5, t=24h	600	[377]
Cu-BMOFs	Au ³⁺	-	Ag ⁺ , Cr ³⁺ , Cd ²⁺ , Pb ²⁺ , Pd ²⁺ , Ni ⁺ , Al ³⁺ , Li ⁺ and Zn ²⁺	pH = 2.0, t=24h	933.0	[418]
UiO-66-NH ₂		-	No selective	pH =3, t=24h	166.33	[401]
UiO-66-ATU		Reusable (4 cycles)	Zn ²⁺ , Fe ³⁺ , Cu ²⁺ , Li ⁺ , Ni ²⁺ , Al ³⁺ , Mg ²⁺ and Cr ³⁺	pH =3, t=24h	227.68	[401]
UiO-66MAc	Ag ⁺	No reusable	-	pH =7	84	[15]

UiO-66	SeO ₃ ²⁻	Reusable	Relatively selective, except PO ₄ ³⁻	pH =6	59.9	[419]	
UiO-66-NH ₂		Reusable	Relatively selective, except PO ₄ ³	pH =6	26.8	[419]	
UiO-66	SeO ₄ ²⁻	Reusable	No selective	pH =6	37.3	[419]	
UiO-66-NH ₂		Reusable	No selective	pH =6	11.9	[419]	
Other Adsorbents							
Hydrochar	Pb ²⁺					38.31	[420]
Multiwall carbon nanotubes	Zn ²⁺	Cu ²⁺ , Fe ²⁺ , Pb ²⁺				250.00	[421]
Fly ash	Cd ²⁺					124.90	[422]
HAp-HA	Cu ²⁺	Reusable (4 cycles)	t=240min		35.20	[423]	

1.8.2 MOFs as adsorbents for soil remediation

Unlike aqueous contaminants, identifying and treating soil pollutants is particularly challenging due to their strong binding with soil organic matter (SOM). Nevertheless, given the harmful impacts of these pollutants, a variety of removal technologies have been developed. Among different technologies, in situ immobilization of metals is a promising soil remediation technology that effectively reduces risks of groundwater contamination, plant uptake, and exposure to living organisms. This method involves adding adsorbent materials (activated carbon, biochar, zeolites, MOFs, etc.) to contaminated soil to create insoluble, immobile, and low-toxicity compounds, reducing the migration of heavy metals to water, plants, and other environmental media[424]. The soil immobilization technique is valued for its simplicity, speed, cost effectiveness and high public acceptability.

In case of using a MOF as adsorbent, it has been reported the development of a multifunctional fertilizer, nZVI@MOF-g-DCUF, for the immobilization of Cr⁶⁺ in soil samples (Figure 1.8.2) [425]. This fertilizer was synthesized by combining nanoscale zero-valent iron-doped MOF(Mg)-

INTRODUCTION

74 (nZVI@MOF) as the core with a dialdehyde carboxymethylcellulose urea-formaldehyde (DCUF) coating. This innovative fertilizer initially enhanced the soil's water retention capacity. Soil remediation tests revealed that adding 1% (wt%) of nZVI@MOF-g-DCUF2.0 resulted in an impressive 84.40% removal rate of Cr^{6+} from contaminated soil, demonstrating significant remediation. The underlying mechanism involves immobilizing Cr^{6+} through hydrogen bonding, reduction, precipitation, and complexation on nZVI@MOF-g-DCUF. Therefore, MOFs and their derivatives show great promise as fertilizers for sustained nutrient release and effective Cr^{6+} immobilization in polluted soils.

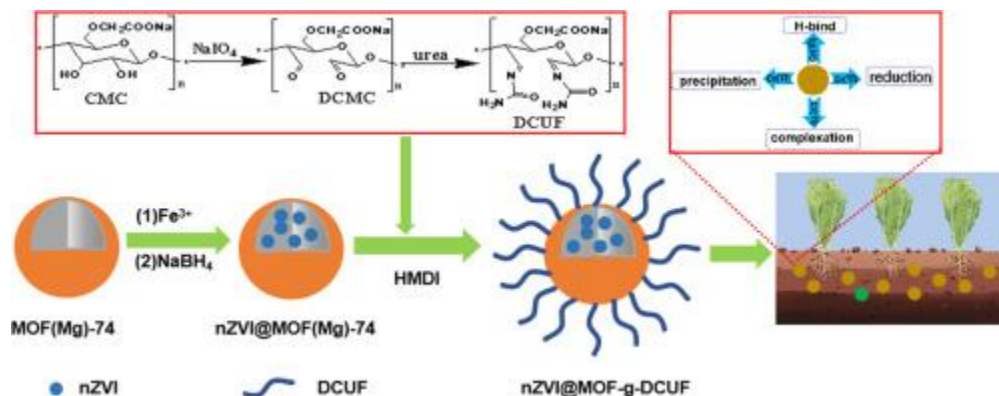


Figure 1.8.2 Schematic of the fabrication, release, and $\text{Cr}(\text{VI})$ immobilization of nZVI@MOF-g-DCUF[425].

However, because in situ immobilization is a temporary measure, contaminants remain in the environment, pollutants may become reactivated if soil physicochemical properties change. Therefore, ongoing monitoring of this process is crucial[426]. To address this limitation, the recovery of the adsorbent after deployment was proposed as a viable method to extract contaminants and prevent leaching. However, this approach has proven technically challenging because most sorbent materials are produced in powder form (i.e., as micro or nanoparticles),

which strongly adhere to and integrate with the soil matrix. One proposed solution to soil decontamination is using magnetic sorbents recoverable with an external magnetic field. However, these sorbents also adhere strongly to soil particles, making separation ineffective. To date, no significant studies have explored the use of **MOF-based recoverable adsorbent materials** for remediating environmental solids.

1.9 Fabric phase sorptive extraction

As previously mentioned, various extraction techniques have been developed and utilized as sample preparation techniques in environmental samples, such as solid phase extraction, solid phase microextraction, etc. (see paragraph 1.7.5)[427]. However, these methods come with several limitations, including lengthy procedures, the need for large volumes of organic solvents during conditioning, significant residual volumes, limited sorbent and sample capacities, a restricted range of commercially available stationary phases, and high costs. To address these issues, recent research has focused on miniaturization, aiming to develop more efficient methods that reduce solvent usage and save time. However, an analysis of various microextraction systems shows that their limitations stem from two main factors: (1) the coating technology used to immobilize the sorbent on the substrate, and (2) the physical design of the extraction system, which affects the primary contact surface area (PCSA)[428], [429]. The PCSA refers to the area of the extraction medium accessible to the sample matrix during extraction. To achieve high sensitivity and fast extraction, improvements are needed in both coating technology and PCSA.

Microextraction devices face challenges with sorbent coating technologies, which often use thin polymer films applied to substrates and then cross-linked[430]. This approach can lead to issues

INTRODUCTION

like high phase bleeding, polymer washout, long equilibrium times, limited selectivity, poor reproducibility, and swelling, mainly due to weak chemical bonding. Alternatives such as physical deposition, electrochemical deposition, adhesives, and sol-gel technology have been proposed[188], [428], [431], [432]. Sol-gel technology, is notably effective, providing a highly porous, chemically stable coating that enhances sensitivity and speeds up extraction equilibrium compared to traditional thick SPME coatings[188].

Despite significant efforts to boost the sensitivity of microextraction systems by increasing sorbent loading on conventional substrates like fused silica fibers or glass tubes, there has been relatively little focus on expanding the PCSA of the extraction device. Increasing the PCSA can enable higher sorbent loading without increasing coating thickness and can also substantially reduce the time needed to reach extraction equilibrium.

To address these challenges, a novel green sample preparation method called fabric phase sorptive extraction (FPSE) has been introduced[433]. This technique effectively overcomes many issues associated with conventional sample preparation methods. Figure 1.9 illustrates the standard protocol for applying fabric FPSE across various applications, including environmental analysis[434]. Specifically, a clean FPSE fabric, coated with the chosen sorbent, is submerged in a glass vial containing the sample under controlled conditions (such as pH, ionic strength, and volume) and stirred with a magnetic stirrer throughout the extraction period. After the extraction, the analytes retained by the FPSE media are back-extracted into a suitable solvent system by immersing the dry FPSE fabric in a vial with a minimal volume of solvent and allowing it to sit for a specified desorption time. The fabric is then removed, and the resulting extract can be either injected directly into a chromatographic system or evaporated to concentrate the solution or change

INTRODUCTION

the solvent. To ensure the FPSE fabric can be reused and to prevent contamination, it is cleaned with solvents, allowed to dry, and then stored until needed again.

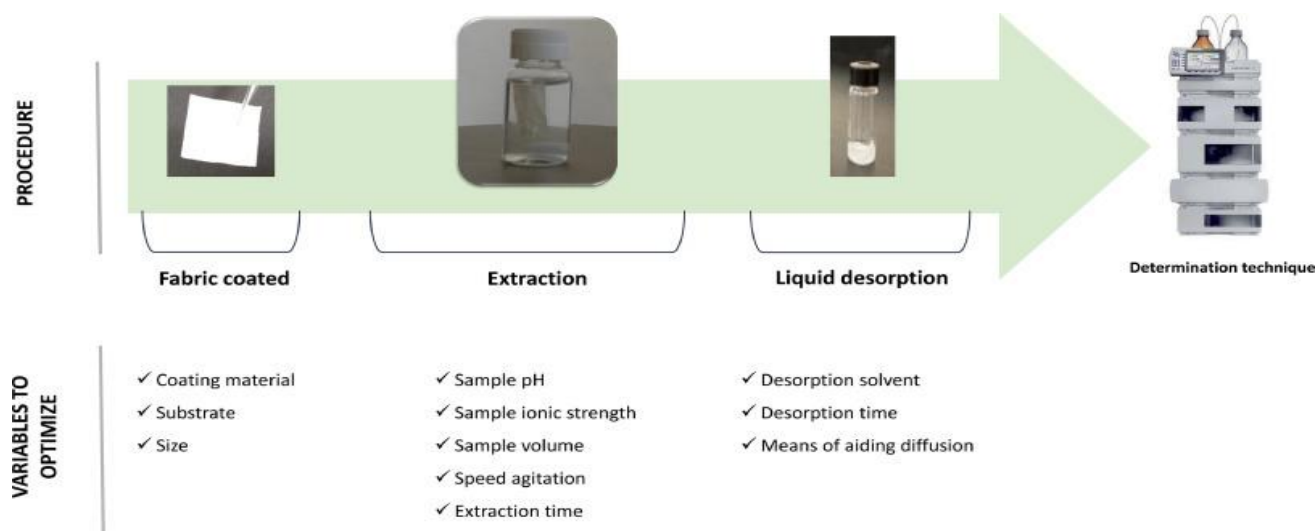


Figure 1.9 The steps of the traditional FPSE process for analyzing environmental samples and the key variables considered during optimization[434].

The procedure provides several key advantages[427]. It is easy to use with minimal solvent consumption, offers a wide variety of sorbents, and has a high surface area for effective sorbent-analyte interaction. It is also stable across a broad pH range (pH 1–12), allows for increased compound diffusion through magnetic stirring, enables quick back-extraction with small volumes of non-restricted solvents, reduces the number of sample preparation steps, minimizing potential errors, and is capable of extracting analytes at concentrations as low as ng L^{-1} .

As with other sorptive extraction techniques, the effectiveness of FPSE is highly dependent on the properties of the coating fabric[434]. Several coating materials with different chemical characteristics are currently available for FPSE. Table 1.9.a provides a list of the most commonly

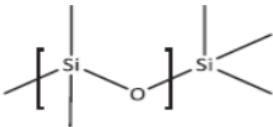
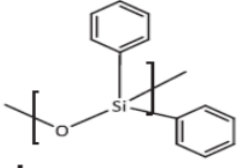
INTRODUCTION

used coatings, categorized by polarity and their chemical structures. The selection of an extraction material is directly tied to the nature of the compounds being extracted. Specifically, non-polar compounds require non-polar materials, while polar compounds necessitate polar materials.

Cellulose was frequently selected as the substrate because its hydrophilic nature aids in drawing water molecules toward the extraction device, making it effective for extracting non-polar compounds such as PAHs[435]. However, in other cases, polyester (hydrophobic), which also contains terminal hydroxyl groups that can engage in polycondensation during the sol-gel process, and silica fiber glass, which are ideal for subsequent thermal desorption, were utilized[427], [436], [437].

Table 1.9.b details the materials chosen for each example, along with the type of substrate used. The bold entries indicate where the material was selected after evaluating multiple options. To date, no significant studies have explored the use of MOF or MOF-based recoverable adsorbent materials, as FPSE media, for environmental remediation.

Table 2.9.a List of the most common FPSE sorbent coating and its classification [434].

Polarity	Name of the sorbent coating	Structure	Abbreviation
Non-polar	Sol-gel poly(dimethylsiloxane)		PDMS
	Sol-gel poly(dimethyldiphenylsiloxane)		PDMDPS

INTRODUCTION

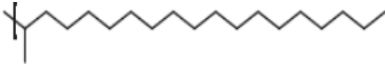
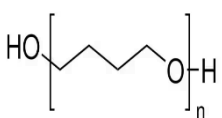
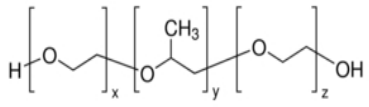
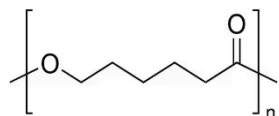
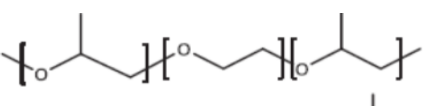
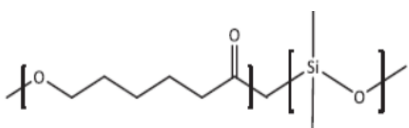
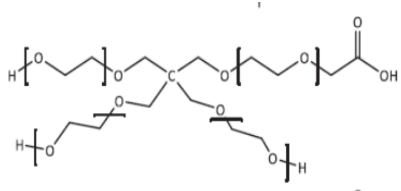
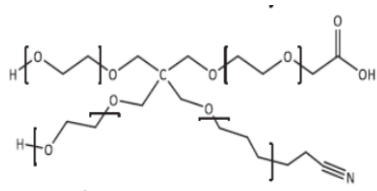
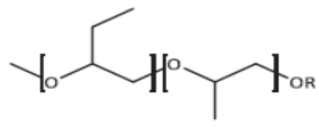
	Sol-gel octadecyl		Sol-gel C ₁₈
Medium polar	Sol-gel poly(tetrahydrofuran)		PTHF
	Sol-gel poly(ethylene glycol)-poly(propylene glycol)-poly(ethylene glycol)		PEG-PPG-PEG
	Sol-gel polycaprolactone		PCAP
	Sol-gel poly(propylene glycol)-poly(ethylene glycol)-poly(propylene glycol)		PPG-PEG-PPG
	Sol-gel poly(caprolactone)-poly(dimethylsiloxane)-poly(caprolactone)		PCAP-PDMS-PCAP
Polar	Sol-gel Carbowax 20M		Carbowax 20M
	Sol-gel cyanopropyl Carbowax 20M		CN-Carbowax20M
	Sol-gel polyalkylene glycol		UCON

Table 1.9.b Environmental applications of FPSE: details on the variables involved in the method development.

Compounds	Sample	Material (substrate) dimensions	Optimum FPSE conditions	% Recovery	Determination technique	Reference
CONVENTIONAL FPSE						
Alkyl phenols	Ground water River water Effluent WWTP Soil Sludge	Sol-gel PTHF (cellulose) n.d.	E: 10 mL pH 6.5, 1000 rpm, 25 min D: 0.5 mL MeOH, immersed, 6 min →direct injection	74-78	LC-UV	[438]
PPCPs	River water Effluent WWTP Influent WWTP	PDMDPS PTHF PEG-PPG-PEG Carbowax 20M (cellulose) 2.5 cm x 2 cm	E: 10 mL pH 6.5, 5% NaCl, 900 rpm, 240 min D: 1 mL MeOH, sonication, 6 min →evap dryness and resuspension in 1 mL mobile phase	%R app : 9-80 (river) 14-59 (effluent) 27-93 (influent) %ME: -16-39 (river) -17-38 (effluent) -29- + 48 (influent)	LC-MS/MS	[439]
Hormones	Tap water Effluent WWTP Hospital influent WWTP	Sol-gel PTHF (cellulose) n.d.	E: 10 mL pH 5.7, 0% NaCl, 1000 rpm, 20 min D: 0.75 mL MeOH, immersed, 3 min →direct injection	%RR: 73-120 (tap) 68-109 (effluent) 66-114 (influent) %ME: -10- + 37 (effluent)	LC-MS/MS	[440]
UV stabilizers	Seawater	PDMDPS PTHF PEG (polyester) n.d.	E: 25 mL pH 6, 5% NaCl, 1000 rpm, 150 min D: 1 mL MeOH, immersed, 10 min →direct injection	%R app : 32-51	LC-MS/MS	[427]
PAHs	Rain water River water Influent WWTP	Sol-gel C 18 (cellulose) 2.5 cm x 2 cm	E: 15 mL 0% NaCl, 1000 rpm, 30 min D: 0.3 mL ACN, sonication, 5 min →direct injection	88-92	LC-FD	[435]
Cytostatic drugs	Effluent WWTP Effluent WWTP Hospital influent WWTP	UCON Caprolactone Carbowax 20M CN-Carbowax 20M PEG 300 (cellulose) n.d.	E: 10 mL pH 8 or 10, 0% NaCl, 1000 rpm, 60 min D: 1 mL MeOH, immersed, 5 min → direct injection	%R app : 25-90 (ultrapure) %ME: -42- + 29 (effluent)	LC-MS/MS	[441]
Multiclass	Tap water	Sol-gel C 18	E: 10 mL pH 3, 10% NaCl, 1200 rpm, 25 min	95-99	GC-MS	[442]

INTRODUCTION

emerging organic compounds (2 parabens, 3 plastic additives, 1 antimicrobial, 2 anesthetic drugs)	Ground water Effluent WWTP Water sludge	PTHF Carbowax 20M (cellulose) 2.5 cm x 2 cm	D: 0.4 mL acetone, immersed, 10 min →direct injection			
Pesticides	River water Lake water Pound water	PCAP- PDMS-PCAP (cellulose) 1.5 cm x 1 cm	E: 50 mL, 1000 rpm, 30 min D: 0.4 mL MeOH/ACN (50/50, v/v), vortex, 0.5 min →direct injection	EF: 125	LC-DAD	[443]
Estrogens	Drinking water Ground water River water Effluent WWTP Hospital influent WWTP	PTHF (cellulose) 2.5 cm x 2 cm	E: 10 mL, 0% NaCl, 1200 rpm, 20 min D: 0.5 mL MeOH, immersed, 8 min + centrifugation 5 min →direct injection	EF: 14	LC-FD	[433]
Anthracyclines	WWTP	UCON PTHF250 Carbowax 20M CN-Carbowax 20M PEG 300 PCAP- PDMS-PCAP (cellulose) 1 cm x 1 cm	E: 20 mL pH 3, 1000 rpm, 15 min D: 2 × 1 mL 10% HCOOH in MeOH/ACN, (50/50, v/v), immersed 4 min →evap to dryness and reconstituted in 1 mL MeOH/ACN, (50/50, v/v)	39-60	LC-FL	[444]
RELATED FPSE APPROACHES						
Triazine herbicides	Stream water River wat	<u>Stir-FPSE</u> PDMDPS PTHF PEG (cellulose) n.d.	E: 100 mL, 5% NaCl, 1100 rpm, 60 min D: 1 mL MeOH, stirring, 5 min →evaporation and resuspension (50 or 100 µL)	%R app : 22-70 (ultrapure)	LC-DAD and LC-MS/MS	[445]
BFRs	Reservoir water Effluent WWTP	<u>Stir bar-FPSE</u> & <u>magnetic stir-FPSE</u> PDMDPS PTHF PEG (cellulose) n.d.	Stir bar-FPSE E: 10 mL, 15% NaCl, 300 rpm, 10 min D: 0.3 mL ACN, sonication, 10 min →direct injection Magnetic stir-FPSE E: 10 mL, 10% NaCl, 400 rpm, 15 min D: 0.3 mL ACN, sonication, 15 min →direct injection	87-96 (stir bar-FPSE) 85-95% (magnetic stir-FPSE) 82-89% (FPSE)	LC-DAD	[446]

INTRODUCTION

			FPSE E: 10 mL, 15% NaCl, 400 rpm, 20 min D: 0.3 mL ACN, sonication, 10 min →direct injection			
PPCPs	River water Effluent WWTP Influent WWTP	<u>DFPSE</u> Carbowax 20M (cellulose) ○ 47 mm i.d. 3 disks	E: 50 mL (25 mL influent) pH 3, 10% NaCl, 10 min D: 10 mL EtAc →evaporation and resuspension (1 mL mobile phase)	%R app : 10-76% (river) 5-64% (effluent) 3-45% (influent) %ME: -5-26% (river) + 9-36% (effluent) -7-52% (influent)	LC-MS/MS	[447]
Benzoyl urea insecticides	Drinking water Mineral water Tap water River water Lake water	<u>MI-FPSE</u> Carbowax 20M (cellulose) Circle ○ 1 " i.d.	E: 100 mL, 800 rpm, 40 min D: 1 mL MeOH, 2 min →evaporation and resuspended in 100 µL	50-73 EF: 501-731	LC-DAD	[448]
Fluoroquinolones	Reservoir water Lake water River water Wastewater	<u>Stir-bar FPSE</u> PEG PDMDPS PTHF (cellulose) n.d.	E: 10 Ml pH 6, 10% NaCl, 400 rpm, 10 min D: 0.3 mL Hac/ACN, sonication, 15 min →direct injection	28-32 RR: 90-100	LC-UV	[449]

ACN: acetonitrile; BFRs: brominated flame retardants; D: desorption; DAD: diode array detector; DFPSE: dynamic FPSE; E: extraction; EF: extraction factor; EtAc: ethyl acetate; FD: fluorescence detector; FPSE: fabric phase sorptive extraction; GC: gas chromatography; IMS: ion-mobility spectrometry; LC: liquid chromatography; ME: matrix effect; MeOH: methanol; MS: mass spectrometry; MS/MS: tandem mass spectrometry; n.d.: no data; NSAIDs: non-steroidal inflammatory drugs; PAHs: polycyclic aromatic hydrocarbons; PPCPs: pharmaceuticals and personal care products; PCAP: polycaprolactone; PDMS: polydimethyl siloxane; PDMDPS: poly(dimethyldiphenylsiloxane); PEG: polyethylene glycol; PPG: polypropylene glycol; PTHF: polytetrahydrofene; R app : apparent recoveries; RR: relative recoveries; UV: ultraviolet; WWTP: wastewater treatment plant.

1.9.1 FPSE approaches

1.9.1.1 *Stir-FPSE*

Enhanced versions of the traditional FPSE method have been developed and applied to environmental samples. To boost contact surface area and improve diffusion during extraction, some techniques involve simultaneously stirring the entire extraction system. This approach, known as stir-FPSE, integrates the FPSE medium with a magnetic stirring mechanism[445]. The stir-FPSE unit is constructed using four key components: (a) a section of a 3-mL polypropylene SPE cartridge, (b) an iron wire, (c) fabric phase sorptive extraction media, and (d) an external element cut from a 5 mL pipette tip. Figure 1.9.1.1 illustrates the assembly process and the individual components. The fabric phase sorptive extraction media is placed in the upper part of the internal cylinder, and the unit is sealed by sliding the external element over the internal one. The extraction medium, coated with the appropriate sol-gel sorbent, is securely fastened to prevent any movement during extraction. Finally, the device is pierced with an iron wire to facilitate magnetic stirring during use. Stir-FPSE has been successfully employed for extracting triazine herbicides from environmental samples, with specific conditions detailed in Table 1.9.b, achieving recoveries between 22% and 70%. The increased analyte diffusion and expanded contact surface area are key factors in the improved extraction efficiency and reduced analysis time.

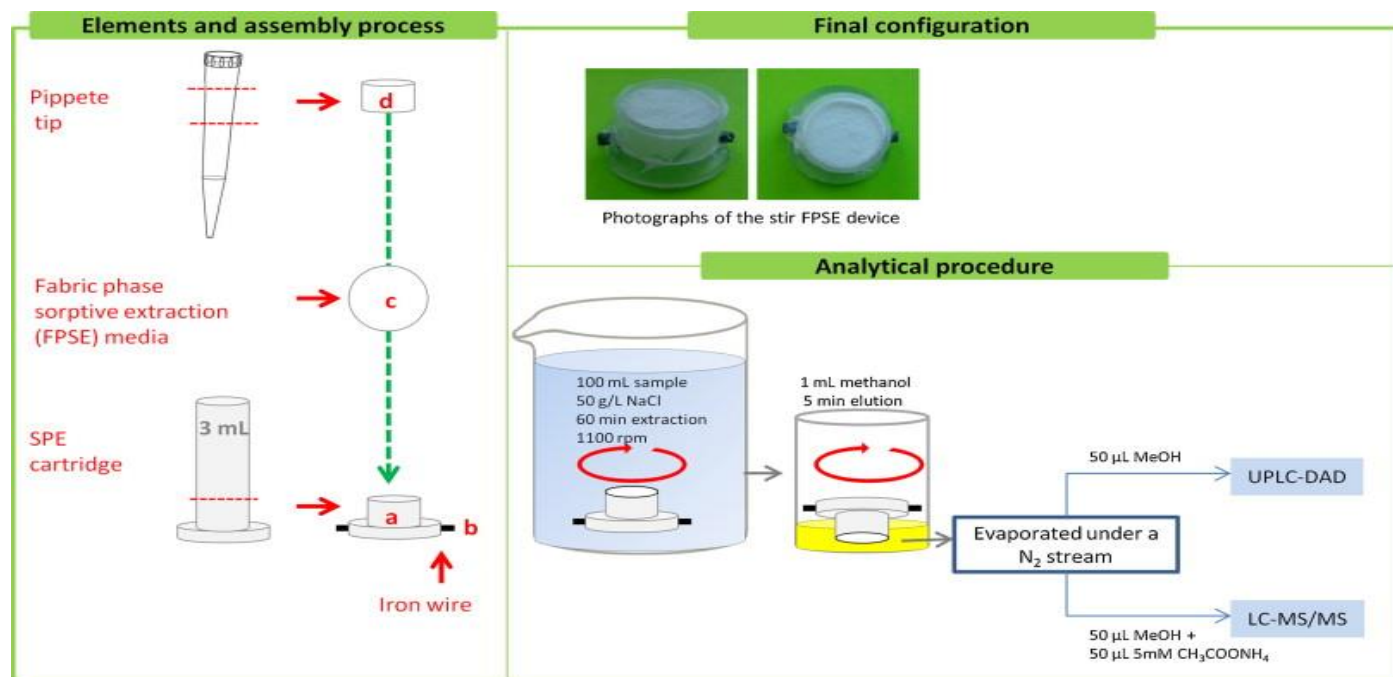


Figure 1.9.1.1 Stir fabric phase sorptive extraction device: components and assembly process[445].

1.9.1.2 Stir-bar FPSE

A novel technique called stir-bar FPSE, where the fabric phase media is cut into a house shape, clamped, and attached to a stir bar, was explored alongside magnetic stir-FPSE, which closely resembles the traditional stir-FPSE method[446]. Figure 1.9.1.2 illustrates these approaches. Both techniques, along with traditional FPSE, were evaluated for extracting brominated flame retardants (BFRs) from environmental samples. Notably, the optimal conditions varied slightly depending on the method used (details in Table 1.9.b). However, both stir-bar FPSE and magnetic FPSE showed improved extraction efficiency and reduced extraction times compared to conventional FPSE. Thanks to their large sorbent loading capacity and efficient stirring performance, both techniques demonstrated strong extraction capabilities and rapid extraction equilibrium. Under optimized

INTRODUCTION

conditions, they achieved high recovery rates (90-99%) and low limits of detection (LODs) ranging from 0.01 to 0.05 mg L⁻¹. Additionally, reproducibility was confirmed by assessing intraday and interday precisions, with relative standard deviations (RSDs) of less than 5.1% and 6.8%, respectively.

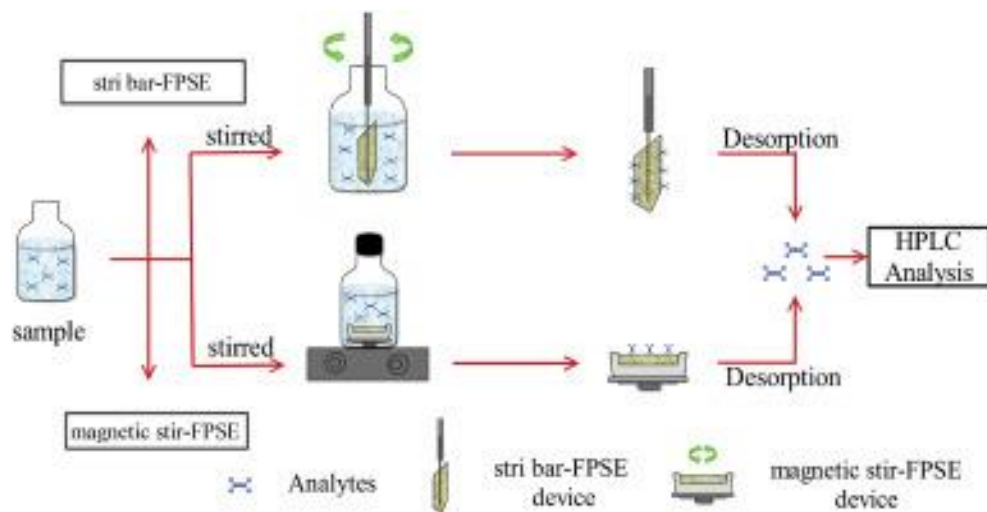


Figure 1.9.1.2 Schematic illustration of stir bar-FPSE and magnetic stir-FPSE procedure and analysis[446].

1.9.1.3 Magnet integrated (MI) FPSE

Additionally, a new technique called magnet integrated (MI)-FPSE, which combines the coating fabric and magnet into a single device, as shown in Fig.1.9.1.3, was recently introduced and successfully applied to extracting benzoyl urea insecticides from various environmental samples[448]. The proposed method allowed for the processing of relatively large sample volumes, leading to high preconcentration factors, between 501 and 731, and excellent sensitivity. Under optimal conditions, the limits of detection and quantification for benzoyl urea insecticides were

INTRODUCTION

0.06 ng mL⁻¹ and 0.20 ng mL⁻¹, respectively. Additionally, the method demonstrated good precision, with relative standard deviations below 6.1% for intra-day analysis and below 8.2% for inter-day analysis.

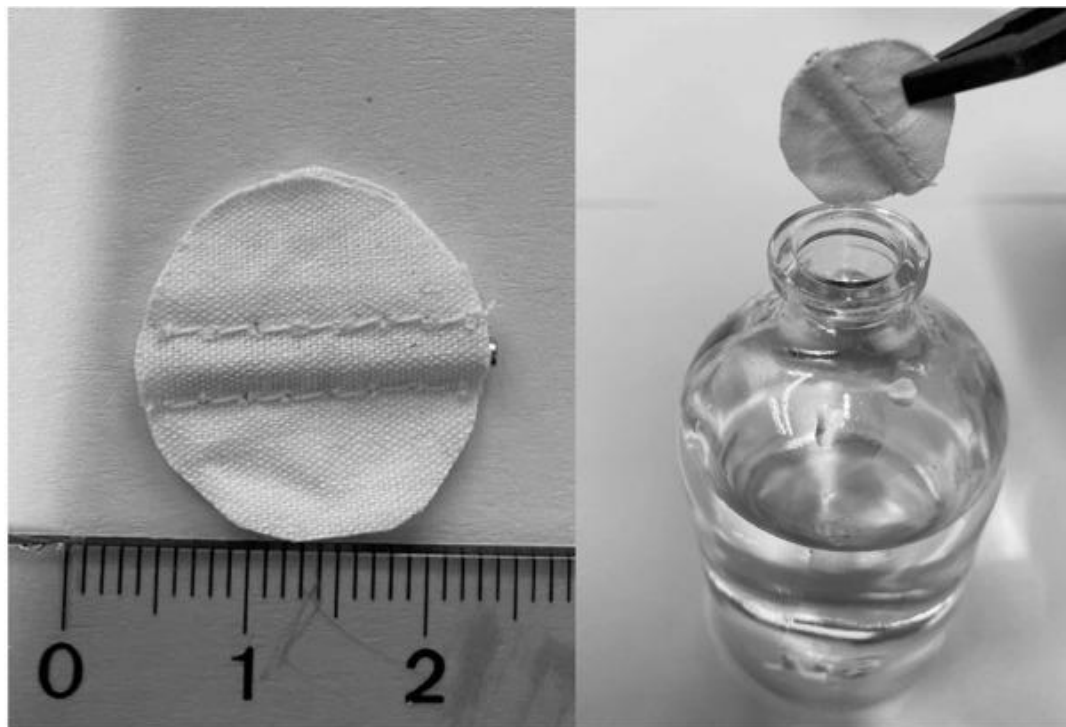


Figure 1.9.1.3 MI-FPSE of triazines from environmental water samples (a) clean MI-FPSE membrane; (b) immersing the MI-FPSE membrane in the sample solution[448].

1.9.1.4 Dynamic FPSE (DFPSE)

To shorten the lengthy FPSE extraction time, a new variation called dynamic FPSE (DFPSE) was introduced[447]. This method uses a 47 mm disk of FPSE medium within a filtration assembly (Fig.1.9.1.4), through which the sample is passed, followed by elution of the analytes with a desorption solvent. The dynamic mode significantly reduced the total extraction time. For instance, when comparing DFPSE and traditional FPSE for extracting a group of PPCPs using Carbowax-20M as the FPSE medium, the extraction time with FPSE was 240 minutes, whereas DFPSE

required only 10 minutes, despite processing a larger volume (50 mL for DFPSE versus 10 mL for FPSE). However, the desorption volume in DFPSE (using ethyl acetate) was ten times greater than in FPSE, making DFPSE less environmentally friendly as a sample extraction technique compared to FPSE.

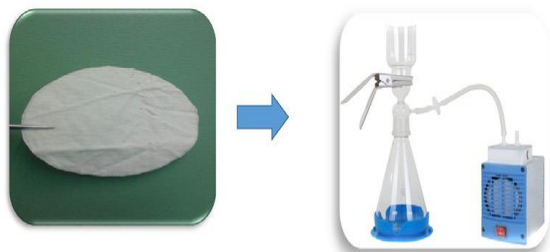


Figure 1.9.1.4 *Dynamic fabric phase sorptive extraction (DFPSE)*[447].

1.9.1.5 *Injection fabric disk sorptive extraction (FI-FDSE)*

On-line flow injection fabric disk sorptive extraction (FI-FDSE) was introduced to automate the process and significantly reduce extraction time[450]. The FDSE setup consists of a mini column fashioned from a polypropylene syringe body (1.5×4 mm i.d.), packed with 38 to 40 FPSE disks of identical diameter (4 mm). No frits or glass wool are required at either end of the column to secure the fabric disks. Figure 1.9.1.5 demonstrates the preparation of the FI-FDSE technique. The on-line formed complex of the metal with ammonium pyrrolidine dithiocarbamate (APDC) was retained on the fabric surface, and methyl isobutyl ketone (MIBK) was used to elute the analytes before atomization. With a preconcentration time of 90 seconds, enrichment factors of 140 for lead and 38 for cadmium were achieved, with detection limits (3σ) of 1.8 and $0.4 \mu\text{g L}^{-1}$, respectively, at a sampling frequency of 30 samples per hour. This mini column design allows for minimal back pressure due to the FPSE substrate's permeability, enabling the application of a high flow rate. As

INTRODUCTION

a result, the analysis time is shortened without compromising extraction efficiency. This technique was successfully applied to the extraction of cadmium and lead from river, coastal, and ditch water samples.



Figure 1.9.1.5 Configuration of on-line flow injection fabric disk sorptive extraction (FI-FDSE) with permission of Elsevier[450].

1.10 Purpose of the study

This PhD thesis aims to explore the application of water-stable zirconium-based metal-organic frameworks (MOFs) as coatings for cotton fabrics, in order to investigate their potential for remediating both aquatic and terrestrial environments from emerging pollutants, including UV filters and noble metal nanoparticles.

Specific Objectives:

1. Optimization of the **Fabric Phase Sorptive Extraction (FPSE)** conditions using MOF-coated cotton fabrics as adsorptive media.
2. Evaluation of the effectiveness of MOF-coated cotton fabrics in the **passive sampling of emerging pollutants** from aquatic environments.
3. Optimization of **soil remediation** processes using the retrievable cotton fabrics.

2 Experimental Part

2.1 Fabric phase sorptive extraction and passive sampling of ultraviolet filters from natural waters using a zirconium metal organic framework-cotton composite

2.1.1 Introduction

Fabric phase sorptive extraction (FPSE) is one of the newest sample preparation methods that has been receiving increasing attention, since its introduction in 2014[433]. This method combines the principles of exhaustive and equilibrium extraction and is based on partition of the analytes from the sample matrix (typically an aqueous phase) into a thin-film sorbent phase composed of a (sponge-like) porous, sol-gel organic-inorganic hybrid material, chemically coated on cellulose, polyester or fiberglass fabric [451]. The method is most commonly applied by stirring the sol-gel coated fabric into the aqueous solution so that the analytes can establish an equilibrium between the sorbent and the aqueous phase [452].

The main advantages of this method lay in the facts that a) the fabric support offers a very high primary contact surface area, b) the flexibility of using various sol-gel coatings that can favorably interact with the target analytes and c) the porosity of the fabric support which facilitates the penetration of the aqueous phase through the fabric pores, as opposed to non-porous phases where the flow is bounced back and redirected [453]. Typically, pieces of 2.5 cm x 2.0 cm of fabrics are used, having a surface area of 5 cm² in each side, which is 50–100 times higher than that of a typical solid phase microextraction (SPME) fiber and up to 10 times higher than that of a stir bar employed in stir bar sorptive extraction (SBSE) [454]. With regard to sorbent phases, various sol-gel chemistries have been used offering polar, nonpolar, ion exchange, or mixed mode analyte-sorbent interactions, utilizing polymers, carbon nanomaterials (such as carbon nanotubes,

EXPERIMENTAL

graphene, etc), ion exchange resins, polysaccharides and combinations of them [455], [456]. By exploiting these attributes, many FPSE analytical methodologies have been developed for the determination of analytes in environmental, food, pharmaceutical and biological samples.

Although great progress has been made so far, alternative fabric coatings that do not rely on sol-gel phases have not been reported despite the fact that a variety of sorbents have been successfully adopted in other microextraction methods [457], [458], [459]. Metal-organic frameworks (MOFs) are among the most popular sorbents in analytical sample preparation owing to their distinct properties such as large specific surface area, controlled pore size, excellent thermal and chemical stability and tunable chemistry. Since bulk powder MOFs are difficult to handle as dispersed sorbents and suffer from high back pressure or nanoparticle leaching in packed bed manifolds (such as SPE) [460], [461], many methods use either immobilized MOFs onto solid supports (e.g. SPME fibers, stirring bars, etc) or after magnetization, in order to facilitate their handling and collection [461], [462], [463]. Recently, the incorporation of MOF phases onto fabric supports has been receiving attention in order to form MOF-based fibrous composites with high flexibility and improved functionality over bulk powder MOFs. Such fiber-based composites have so far found applications in water purification [464], [465], [466] as well as in solid phase extraction of non-steroidal anti-inflammatory drugs [467], [468]. However, the potential utility of MOF-based fabrics as sorbent phases in FPSE has not been exploited yet while the use of MOFs for the extraction of UV filters is still limited [469], as compared to other sorbent phases.

In this work, we report for the first time the utilization of MOFs as novel sorbent phases of fabric phase sorptive extraction as well as for passive sampling of organic compounds from water samples. A Zr^{4+} MOF (the neutral form of UiO-66-NH_2 , hereinafter MOR-1) was decorated on the surface of cotton textiles using an aqueous phase synthetic route that involved the step-wise

in-situ growth of the MOF particles on the surface of the polydopamine (PDA) coated cotton textile. The MOF@cotton fabric was irreversibly immobilized on cotton enabling the extraction of non-polar UV filters, as model organic compounds, from water samples both under stirring as well as under flow-through conditions. Moreover, the MOF@cotton fiber composite could be used for the passive sampling of UV filters from natural water samples a feature that is not feasible with other microextraction methods. This work shows that the use of MOFs as sorbent phases on fabric solid supports could open new opportunities in the development of new porous sorbent phases for the extraction as well as the passive sampling of organic compounds in environmental systems.

2.1.2 Experimental

2.1.2.1 Chemicals and Materials

Pure cotton fabric sheets were purchased from local stores. Zirconium chloride 99.5%+, metal basis and 2-aminoterephthalic acid 99% (NH₂-H₂BDC) were obtained from Alfa-Aesar. 2-hydroxy-4-methoxybenzophenone (benzophenone-3 (BZ3)) 98%, 2-ethylhexyl 4-methoxycinnamate (EMC) 99.8% and 2-Ethylhexyl 4-(dimethylamino)benzoate (EDP)) 98%, tris(hydroxymethyl) aminomethane (tris-base) 99.9%, and glacial acetic acid $\geq 99.7\%$ were from Sigma-Aldrich (Steinheim, Germany). 3-hydroxytyraminium chloride $\geq 99.0\%$ was procured from Merck (Darmstadt, Germany), isoamyl 4-methoxycinnamate (IMC) 99.3%, was from Haarmann and Reimer Parets del Vallés, Spain), 3-(4-methylbenzylidene)camphor (MBC) 99.7% was obtained from Guinama S.L., (Valencia, Spain) and 2-ethylhexyl 2-cyano-3,3-diphenylacrylate (octocrylene (OCR)) $>98\%$ was purchased from F.Hoffman-La Roche Ltd. (Basel, Switzerland). HPLC-grade methanol, water, 2-propanol and analytical grade acetone were retrieved from Fisher

EXPERIMENTAL

Scientific (Loughborough, UK). Analytical grade inorganic salts (sodium chloride $\geq 99\%$, sodium nitrate $\geq 99\%$) were purchased from Scharlab (Barcelona, Spain).

2.1.2.2 Instrumentation

Power XRD (pXRD) diffraction patterns were recorded on a Bruker D2 Phaser X-ray diffractometer (CuK α radiation, wavelength=1.54184 Å). Scanning electron microscopy (SEM) images and energy dispersive spectroscopy (EDS) spectra were obtained on FEG-SEM Zeiss SUPRA 35VP (resolution 1.7 nm at 15kV) equipped with an EDS detector (QUANTA 200, Bruker AXS). IR spectra were recorded using a Perkin Elmer Spectrum Two attenuated total reflectance-IR (ATR-IR) spectrometer. Zeta potential measurements were carried with a Malvern Zetasizer Nano ZS (Malvern Panalytical, Worcestershire, UK) in a two-electrode capillary cell.

Liquid chromatographic analysis was carried out in a Shimadzu HPLC system (LC-20AD high-pressure solvent delivery pump, DGU-20A3 degasser, CTO-10A column oven) connected to a SPD-10AV UV/Vis detector. For the chromatographic analysis of UV filters 20 μ L of sample were injected into a Rheodyne® sample loop injector and separation was performed in a thermostated (45 °C) Hypersil ODS C18 column (250 mm length, 4.6 mm I.D., 5 μ m particle size) from MZ Analysentechnik (Mainz, Germany) under isocratic flow (1 mL min⁻¹) using MeOH and water as a mobile phase at a mixing ratio of 75:25 (v/v). All operations were controlled by LC Solution software (v.1.25-SP4). Peak area was monitored at 313 nm for all UV filters.

2.1.2.3 Synthesis of MOR-1@cotton fabric

A circular cotton fabric of 4 cm diameter (25.12 cm^2 area on both sides, 25.75 cm^2 surface area, 0.628 cm^3 volume) was sequentially washed under continuous flow with acetone and distilled water to remove impurities and dried at 80°C in an oven. The fabric was added in 20 mL tris-base (10 mM) solution containing 0.05 g of 3-Hydroxytyraminium chloride and reacted overnight under stirring. The PDA-coated fabric was rinsed with distilled water and acetone to remove any unreacted PDA and MOF deposition was accomplished by adding the fabric in a spherical flask containing a mixture of ZrCl_4 (0.125 g) and $\text{NH}_2\text{-H}_2\text{BDC}$ (0.136 g) dissolved in 20 mL H_2O and 5 mL CH_3COOH (glacial, 100%). The mixture was refluxed at $100\text{-}110^\circ\text{C}$ under stirring for 1 h in order to form MOR-1 particles *in-situ* on the surface of the PDA-coated fabric. A schematic illustration of the synthetic procedure is presented in Figure 2.1.2.3. The fabric was then removed from the flask and placed in another flask containing the same amount and volume of reactants and the MOF coating procedure was repeated as before (in total 2 times) to maximize the surface coating of the fabric with MOR-1 particles. The MOR-1@cotton fabric was washed under continuous flow with distilled water and its surface charge was neutralized with triethylamine (0.4 mL in 16 mL of methanol) for 1.5 h under stirring. The MOR-1@cotton fabric was finally washed with methanol and dried in an oven at 80°C . Before use the MOR-1@cotton fabric was rinsed with distilled water to ensure that the pH of the solution was between 6-7.

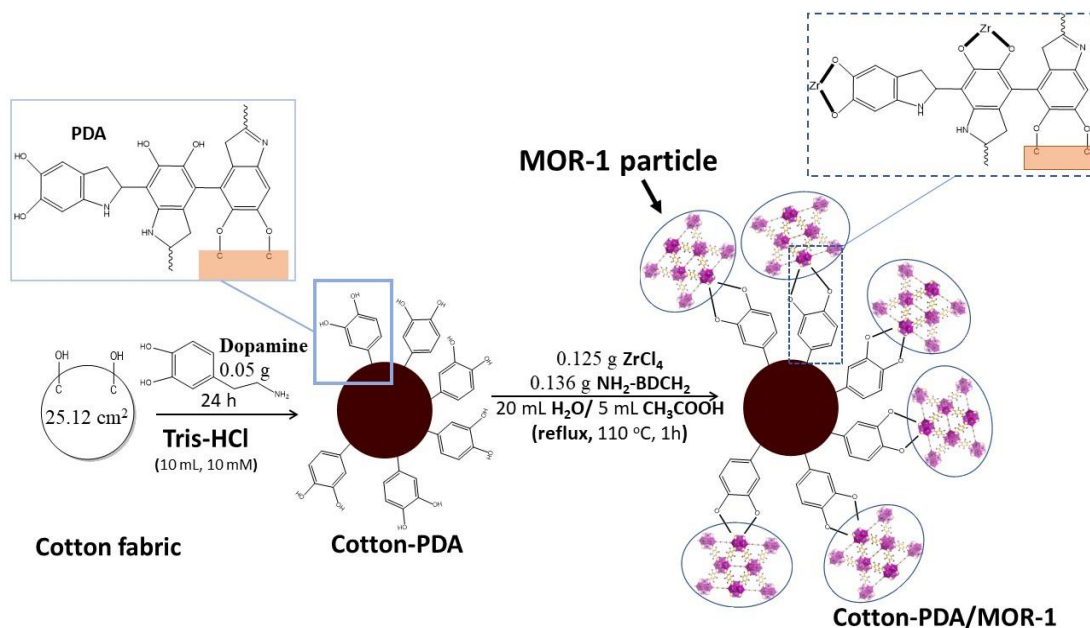


Figure 2.1.2.3 Schematic illustration of the synthetic procedure of MOR-1@Cotton.

2.1.2.4 Experimental procedure of static FPSE

An aliquot of aqueous sample solution (≤ 150 mL) was fortified with 3% (w/v) NaCl as ionic strength regulator and the pH was adjusted to 4 with dropwise addition of dilute HCl (0.025 M HCl in standard solutions and 0.05 M in real samples) using a pH-meter. One and a half pieces of fabrics (one circular and one semi-circular) were immersed into the sample and stirred for 60 min at 900 rpm with a Teflon coated stirring magnet. The fabrics were removed with the metallic tweezers and dried on blotting paper with the aid of Kimwipe disposable wipers.

The analytes extracted on the MOR-1@Cotton fabric were back-extracted into 3 mL of extraction solvent composed of MeOH:H₂O (75:25) for 15 min with interim vortex agitation. The extract was filtered through PTFE filters (13 mm, 0.22 μ m) to remove any particles of fabric residues and 20 μ L were injected directly into the LC system. In order to reuse the MOR-1@Cotton fabric, it was

EXPERIMENTAL

cleaned twice with 20 mL of MeOH under stirring for 5 min, thoroughly washed with distilled water under continuous flow and dried in an oven at 80°C.

2.1.2.5 Experimental procedure of dynamic FPSE

MOR-1@ cotton fabrics were cut into rectangular pieces of 2.5x2 cm (5 cm² area) and folded twice. The fabric was inserted into a 3 mL SPE cartridge which was placed in a SPE filtration assembly. Before use the fabrics were conditioned with 6 mL of water. For the extraction, 50 mL of sample adjusted to pH 4 and containing 3% of NaCl (w/v) were loaded and percolated through the fabric at a flow rate of 4 mL min⁻¹. The fabric was dried under vacuum and the retained analytes were eluted by passing 3 mL of MeOH:H₂O (75:25) from the cartridge. The extract was filtered through PTFE filters (13 mm, 0.22 µm) and a 20 µL aliquot was injected into the LC system.

2.1.2.6 Calibration of MOR-1@ cotton fabrics for passive sampling

The calibration of MOR-1@ cotton fabrics as passive samplers was performed by static renewal exposure of the fabrics to the target UV filters under stirred conditions (400 rev./min) at 20 °C. Six circular fabrics were fixed on a metallic holder (stainless steel mesh of 1 mm wire thickness and 6 mm mesh pore size) and immersed into 3 L aqueous solution fortified with 10 µg L⁻¹ of each UV filter. The water was renewed daily to ensure constant exposure conditions. To investigate the accumulation kinetics of UV filters in the MOR-1@ cotton fabric phase, one fabric sampler was removed from the tank weekly and analyzed for the uptake of UV filters. The calibration experiment was performed for 50 consecutive

EXPERIMENTAL

days. Based on these experiments, the sampling rate (R_s , L d⁻¹), which is the volume of water extracted per unit of time, was calculated by formulae:

$$R_s = \frac{M}{C_w \times t}$$

where M (μg) is the amount of a chemical accumulated in the sampler, C_w ($\mu\text{g L}^{-1}$) is the UV filter concentration in water and t (days) is the deployment time during the linear uptake phase [470]. Control experiments (water samples containing the samplers but not UV filters and water samples containing UV filters but not samplers) were also deployed daily, showing no contamination of the samplers ($<\text{LOD}$ of UV filters) and trivial loss of UV filters ($<2\%$). The absolute concentration of UV filters accumulated on the MOF@ cotton fabrics after deployment (as mg of UV filter per g of sorbent mass) was calculated using calibration curves prepared from standard solutions of the UV filters.

2.1.2.7 Real samples

Three genuine water samples with variable matrix composition (river, lake and seawater) were collected from random locations in Louros river, Lake Pamvotis and beaches of Amvrakikos gulf (NW Greece), respectively. The samples (1 L) were retrieved in amber glass vials and filtered through 0.45 μm filters to remove suspended solids. The samples were stored at 4°C before use which was performed by fortifying the samples with UV filters.

2.1.3 Results and Discussion

2.1.3.1 Preparation and Characterization of MOR-1@ cotton fabrics

The decoration of cotton with MOF particles was performed in two steps. The first involved the strong adherence of PDA on the cotton surface by strong covalent bonding via PDA carbon-O-cotton carbon groups (Figure 2.1.2.3)[471]. This step was applied in order to modify the cotton surface with the catechol functional groups of PDA, which enhance the immobilization of the MOF[472]. The coating of the cotton with PDA is simpler to perform as compared to other modification methods that rely on carboxymethylation of cotton which are more tedious and require the use of organic solvents[473] and provides stronger immobilization than direct coating on the fabric surface through Zr-carboxylate bonds (as evidenced by the reusability of the sorbent) [474]. Then, MOR-1 particles were immobilized on the PDA coating via strong bonding interactions involving the Zr^{4+} metal ions of the MOF and the catechol groups of PDA (Figure 2.1.2.3)[472]. By this method, the synthesis and immobilization of the MOF is performed *in-situ* in the aqueous solution, alleviating the need for organic solvents, which account for a significant portion in the production cost of MOFs[475].

The first feature of the MOR-1@ cotton fabric that was examined was its texture. The pore size of the cotton (60-100 μm) remains unaffected after synthesis, facilitating the permeation of the aqueous phase through the fabric during the extraction (Figure 2.1.3.1.1). This is important in FPSE for achieving high mass transfer rates, since permeable substrates facilitate the flow of the aqueous phase through the pores of the fabric without redirecting it or bouncing back to the reverse direction, as it occurs with impermeable substrates[476].

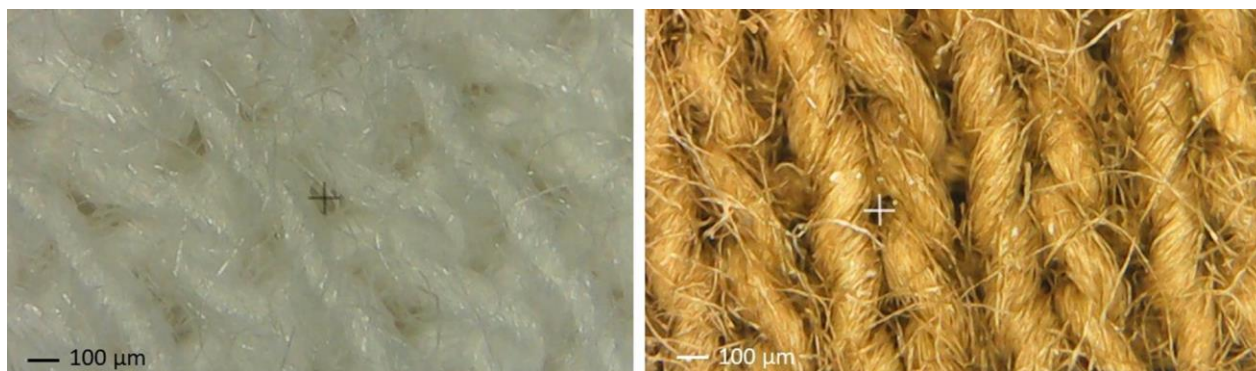


Figure 2.1.3.1.1 Stereoscopic images of plain cotton (left image) and MOR-1@ cotton (right image).

The characterization of MOR-1 immobilized on cotton fabrics was performed with XRD, FE-SEM, EDS, zeta potential measurements and IR analysis. The diffraction peaks of MOR-1 at 2θ of 7.3° , 8.5° and 12° , corresponding to (111), (200) and (220) planes (Figure 2.1.3.1.2.a), respectively, do not appear in the XRD spectra of cotton and PDA modified cotton (Figure 2.1.3.1.3.a) and agree with the calculated XRD pattern derived from the crystal structure of the UiO-NH₂ MOF (Figure 2.1.3.1.3.b), providing evidence to the successful immobilization of MOR-1 on the cotton surface. Further evidence to presence of MOR-1 particles on the fiber surface is also provided by the ATR-IR bands at 1570 and 1385 cm^{-1} assigned to the $\nu_{as}(\text{COO}^-)$ and $\nu_s(\text{COO}^-)$ modes[477], respectively, as well as to the Zr-O bond at 763 and 685 cm^{-1} (Figure 2.1.3.1.2.b)[478]. The FE-SEM images of the MOR-1@ cotton fabric show the coverage of the cotton fibers with octahedrally shaped MOR-1 particles of approximately $170 \pm 8\text{ nm}$ (Figure 2.1.3.1.4). Finally, the surface charge of the sorbent was explored by ζ -potential measurements and EDS analysis. The zeta potential of the MOR-1@ cotton fabric was close to zero ($-0.2 \pm 0.1\text{ mV}$ before extraction and $0.13 \pm 0.1\text{ mV}$ after extraction at pH 4) indicating that the immobilized MOR-1 particles have a neutral surface charge. This was further verified from

EDS analysis (Figure 2.1.3.1.2.d) which shows the absence of Cl^- anions (positively charged MOR-1 should contain 6 Cl^- per formula unit). Therefore, extraction of UV filters is attributed to hydrogen bonds and π -stacking interactions with MOR-1[23], [479].

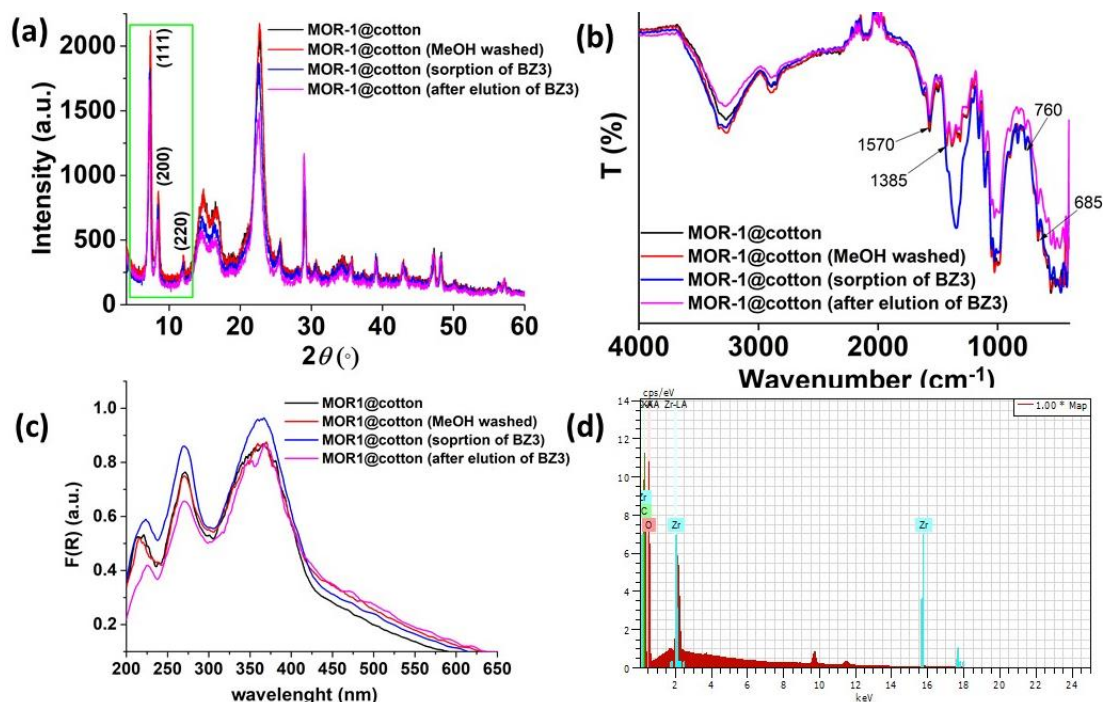


Figure 2.1.3.1.2 Comparison between the (a) pXRD patterns (b) ATR-IR spectra and (c) Absorbance spectra (Kubelka-Munk transformed diffuse reflectance spectra) of i) plain MOR-1@ cotton and after ii) treatment with methanol, iii) sorption of BZ3 and iv) elution of BZ3; (d) EDS analysis of MOR-1@ cotton fabric.

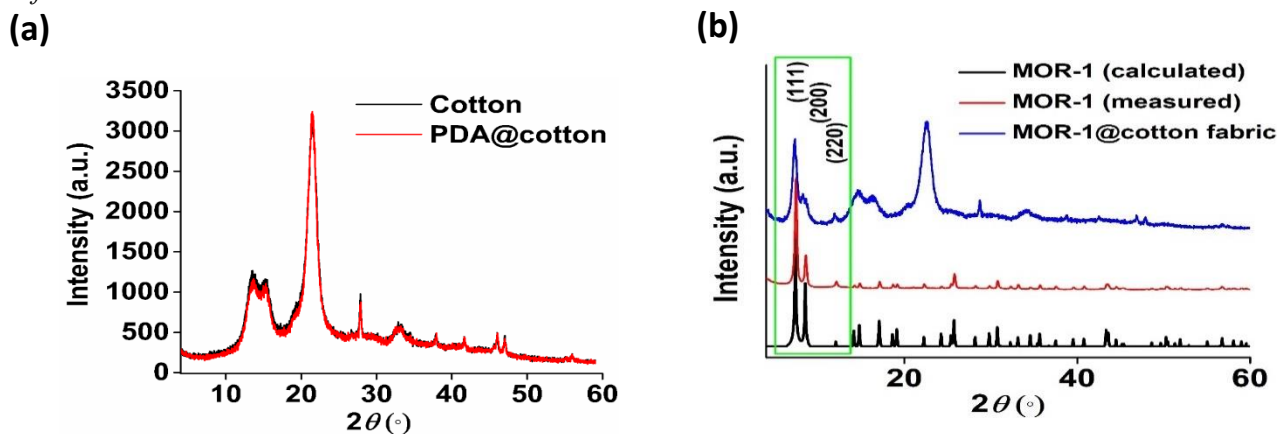


Figure 2.1.3.1.3 (a) pXRD pattern of plain cotton and PDA-modified cotton fabric. (b) Calculated (theoretical) pXRD pattern of MOR-1 (black line) in comparison to experimentally measured pXRD patterns of MOR-1 (red line) and MOR-1 immobilized on PDA-coated cotton fabric (blue line). The pXRD pattern of MOR-1 was calculated using the Mercury 4.0 software (<https://www.ccdc.cam.ac.uk/solutions/csd materials/Components/MercuryMaterials/>).

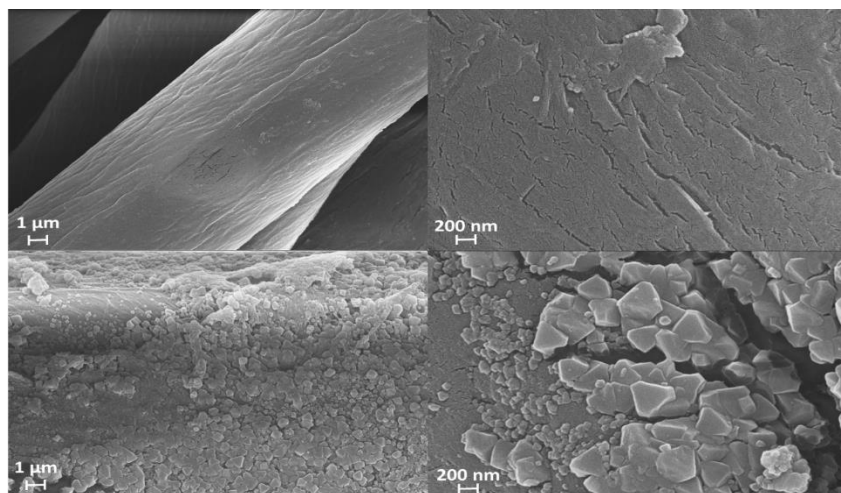


Figure 2.1.3.1.4 FE-SEM images of unmodified fabric (upper images) and MOR-1@ cotton fabric (lower images).

The stability of MOR-1@ cotton fabric during the extraction of UV filters was also examined. The XRD pattern of MOR-1 after extraction (i.e. after sorption of the UV filters) and back-extraction (Figure 2.1.3.1.2.a) displays that the MOF maintains its crystallinity. However, the intensity of diffraction after back-extraction appears slightly reduced suggesting that a small amount of MOR-1 may have been removed from the cotton surface. The ATR-IR (Figure 2.1.3.1.2.b) and the UV-Vis diffuse reflection spectra (Figure 2.1.3.1.2.c) of the MOR-1@ cotton fabric also concur to the loss of MOR-1 from the fabric surface after back-extraction. Specifically, the IR spectra of pristine, loaded (i.e after extraction/sorption of UV filters from water) and regenerated (i.e. after back-

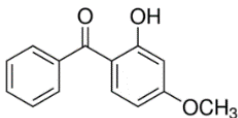
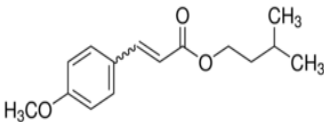
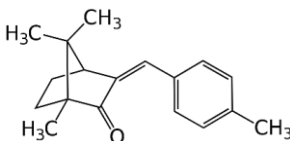
EXPERIMENTAL

extraction of UV filters into methanol) sorbents are very similar except for the IR band at 1340 cm^{-1} (which is assigned to C-H and O-H bending of the BZ3 that was used as a model UV filter) which appears after sorption (extraction) but disappears after elution (back-extraction). However, the intensity of IR bands is reduced for the regenerated sorbent, which may be attributed to a partial release of the MOF. Such a reduction of intensity is not observed when the pristine sorbent is treated with methanol. Thus, methanol alone cannot cause the removal of the MOF from the fabric. Therefore, we suggest that the strong interactions of UV-filter and immobilized MOF weaken the MOF-PDA bonding, resulting in leaching of the MOF upon methanol treatment of the loaded sorbent. The DRS spectra also follows the same pattern, exhibiting an increase in the absorbance in the UV region, due to the capture of BZ3 by the sorbent, and a decrease of absorbance after back-extraction. The reduction of absorbance is not observed when the fabric is treated only with methanol but only after back-extraction of the analytes from the MOR-1 material, a fact which is consistent with a partial release of the MOF as discussed above. The solubilization of MOF in organic solvents due to hydrophobic interactions with the target analytes has not been reported before and could be considered as a basis to design more stable MOF sorbents. However, as will be discussed further below, the reusability of the sorbent was not impaired and the MOR-1@ cotton could be re-used at least 15 times without loss of efficiency. This is both due to the relatively high amount of MOR-1 that was immobilized on the fabric surface ($\sim 30\text{ mg per fabric}$) and the very large specific surface area of ($1097\text{ m}^2\text{ g}^{-1}$) of MOR-1 [360], thus enabling the efficient sorption and reuse of the sorbent for multiple times.

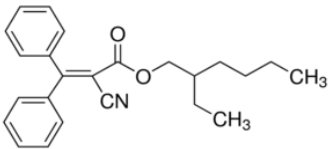
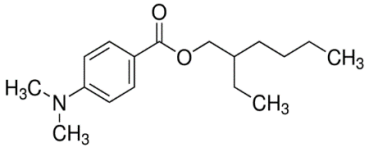
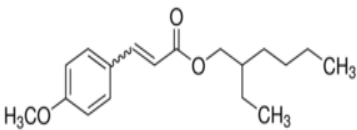
2.1.3.2 Optimization of FSPE experimental conditions

The experimental conditions that maximize the extraction efficiency of the method were optimized sequentially, by varying one parameter at a time. Specifically, the amount of MOR-1 immobilized per area of fabric, the dimensions of the fabric, the pH and ionic strength of the sample solution during extraction and the extraction time were optimized. The variables that determine the efficiency of the desorption step such as the composition of the organic solvent and desorption time were also investigated. Under the optimum conditions the breakthrough volume of the method and the reusability of the sorbent were also evaluated. All optimization studies were conducted in triplicate by extracting aqueous standard solutions containing 250 ng mL⁻¹ of six non-polar UV filters as model water contaminants. More information about the examined UV filters can be found in Table 2.1.3.2. For determining the optimum conditions, the extraction efficiencies were determined compared to a standard solution containing 5 µg mL⁻¹ of each analyte.

Table 2.1.3.2 Physicochemical properties of the examined UV filters.

UV filter	Chemical formulae	Structure	Molar mass (g/mol)	logKow
Benzophenone-3 (BZ3)	C ₁₄ H ₁₂ O ₃		228.247	3.79
Isoamyl 4-methoxycinnamate (IMC)	C ₁₅ H ₂₀ O ₃		248.32	4.33
3-(4-methylbenzylidene) camphor (MBC)	C ₁₈ H ₂₂ O		254.4	5.92

EXPERIMENTAL

Octocrylene (OCR)	$C_{24}H_{27}NO_2$		361.5	6.89
2-Ethylhexyl 4-(dimethylamino)benzoate (EDP)	$C_{17}H_{27}NO_2$		277.4	5.77
2-ethylhexyl 4-methoxycinnamate (EMC)	$C_{18}H_{26}O_3$		290.4	5.8-6.1

^a Data from Refs [478], [479]

2.1.3.2.1 Effect of MOR-1 amount and dimensions of the fabric phase

In FPSE, both the sorbent loading and the primary contact surface area play a significant role in the extraction efficiency and the mass transfer rate of the analytes from the donor to the acceptor phase. Therefore, both parameters were firstly optimized. Sorbent loading was evaluated by sequentially applying the MOR-1 synthetic procedure on the same fabric for several times using the same concentration of reactants (i.e. $ZrCl_4$ and NH_2 -H₂BDC in dilute acetic acid). This approach was found to be more suitable than applying the synthetic procedure once with higher concentration of reactants, because in the latter case a large amount of MOR-1 precipitated as solid and was not immobilized on the PDA@ cotton fabric. The results from the extraction of UV filters using fabrics that were exposed sequentially to the in-situ synthesis of MOR-1, show that the highest extraction efficiency was observed after 2 sequential synthetic cycles (Figure 2.1.3.2.1.a). Subjecting the fabric to a third synthetic step did not improve the extraction efficiency while at the fourth synthetic step the fabric exhibited visual signs of degradation due to the prolonged exposure at high temperatures and the friction with the stirring bar during reflux. Based on these data, the decoration of the fabric with MOR-1 was performed in two synthetic steps. Under these conditions,

EXPERIMENTAL

the amount of immobilized MOF was calculated by weighting the fabric before and after coating. Each fabric of 25.12 cm² area (on both sides) was found to host a mass of approximately 25 mg of MOR-1 corresponding to almost 1.0 mg MOR-1 /cm² fabric (or 100 mg of MOR-1 per gram of fabric). Although the amount of MOF deposited per fabric area is lower than that of sol-gel coatings [480], MOR-1 particles have a very large specific surface area of (1097 m² g⁻¹) [360], which imbues the sorbent with high extraction efficiency.

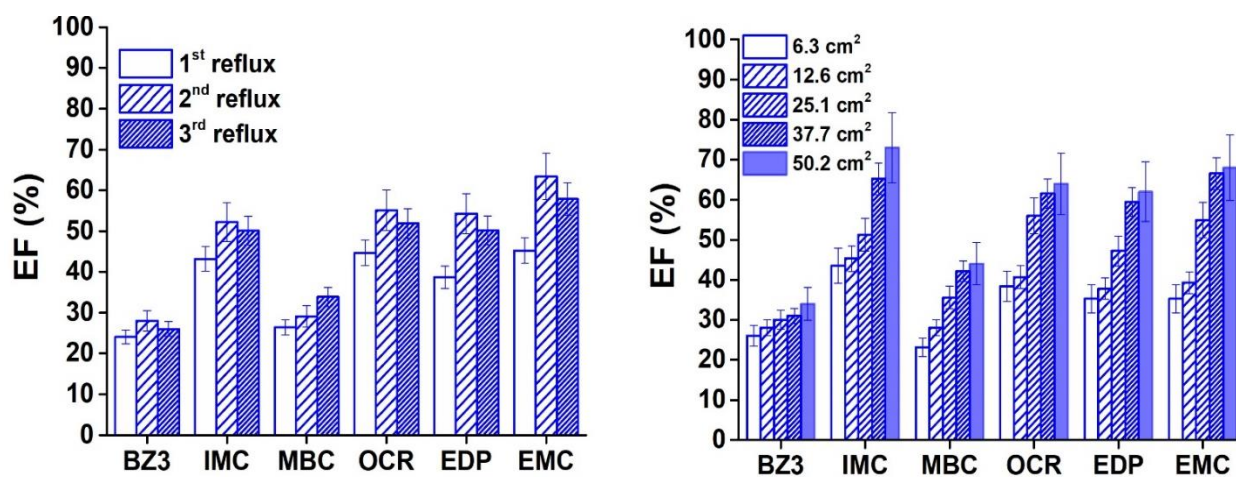


Figure 2.1.3.2.1 (a) Optimization of MOR-1 amount deposited on cotton surface and (b) effect of MOR-1@ cotton surface primary contact surface area on the extraction efficiency of UV filters.

The influence of the primary contact surface area of the sorbent was then investigated using MOR-1@ cotton fabrics of increasing area (from 6.3 to 50.2 cm²) by cutting circular fabrics to halves or quarters of circle and using them as appropriate. As shown in Figure 2.1.3.2.1.b, the increase in the area of the fabric has a beneficial effect in the extraction efficiency. However, when 2 fabrics were used simultaneously for extraction, the reproducibility of the measurements decreased. Therefore, 1.5 circular fabrics (37.7 cm²) were used as optimum for the extraction of UV filters.

2.1.3.2.2 Optimization of sample pH and ionic strength during extraction

The pH and the ionic strength of the solution are important parameters in sample preparation. On one hand, pH determines the ionization state of the analytes while, on the other hand, ionic strength affects their solubility in water; increasing ionic strength, decreases the solubility of non-polar analytes and enhances their partitioning onto the sorbent (salting-out effect). According to the results depicted in Figure 2.1.3.2.2.a, acidic pH values favor the extraction of UV filters an observation that agrees with previous studies. Since UV filters are non-polar compounds and the MOR-1 surface is neutralized before use, hydrophobic interactions between the MOR-1 particles should be the main extraction mechanism. At higher pH values, the ionization of some UV filters (e.g. $pK_{BZ3} = 7.1-7.56$, $pK_{EDP} = 2.38$ and 4.85) [481], [482] and the hydrolysis of UV filters has been reported to be the main reason for obtaining lower extraction yields with various extraction phases [483], [484], [485]. At highly alkaline conditions ($pH > 9$), MOR-1 particles become unstable which further contributes to the observed reduction in the extraction efficiency.

The influence of ionic strength of the aqueous phase on the extraction efficiency was investigated by using NaCl at concentrations from 1-10% (w/w). As shown in Figure 2.1.3.2.2.b, the efficiency of the method improves with increasing NaCl concentration up to 3% while at higher NaCl concentrations the extraction yield gradually decreases. Similar observations have been made in many studies and are ascribed to the increase in the viscosity of the aqueous phase, that reduces the diffusion rate of the analytes from water to the sorbent phase [476], [486], [487]. Based on these results, the extraction of UV filters was performed at pH 4 (using acetic acid/acetate buffer) and 3% NaCl (w/w) as ionic strength regulator.

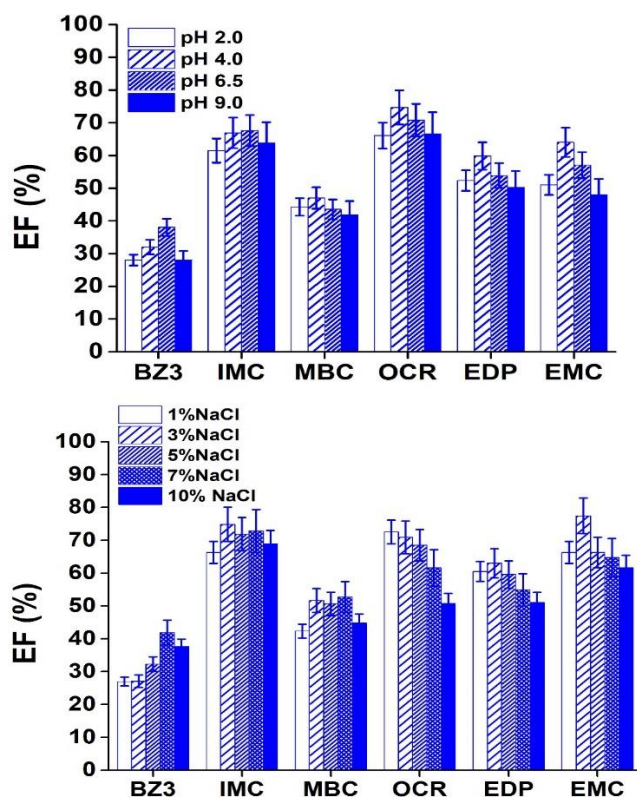


Figure 2.1.3.2.2. Effect of (a) pH and (b) ionic strength on the extraction efficiency of UV filters on MOR-1@ cotton fabric.

2.1.3.2.3 Extraction time

The importance of extraction time on the extraction of UV filters was investigated in the range of 15-90 min. For most analytes, a plateau in the extraction kinetic curve was reached after 45 min of stirring while for IMC and OCR the extraction yield further improved after 60 min of stirring. Extraction time longer than 60 min had a negative effect in the extraction efficiency of all UV filters possibly due to desorption of the analytes from the MOR-1 surface (Figure 2.1.3.2.3). This phenomenon is common in many microextraction methods [483] as well as FPSE [488]. As previously discussed, the sorption of UV filters on MOR-1 is attributed to hydrogen bonds and π -stacking interactions which are generally weak interactions (as compared to covalent bonds or

EXPERIMENTAL

electrostatic interactions). Moreover, the analytes, although hydrophobic, do exhibit a small solubility in water [480], [482]. The working concentrations of UV filters are below the solubility limits. Therefore, at prolonged mixing, the reduction in the EFs may be attributed to the establishment of an equilibrium among hydrogen bonds and π -stacking interactions with the MOR-1 surface and hydrogen bonds with water molecules, which are responsible for the aqueous solubility of organic compounds. The fact that BZ3 (which has the lowest $\log K_{ow}$ and the higher water solubility among the UV filters examined) exhibits higher desorption with increasing extraction time is supportive to this notion. Based on these findings, the extraction time was set at 60 min which lies in the middle of extraction times reported for other microextraction methods that typically range from a few minutes to 2 hours[35] [489].

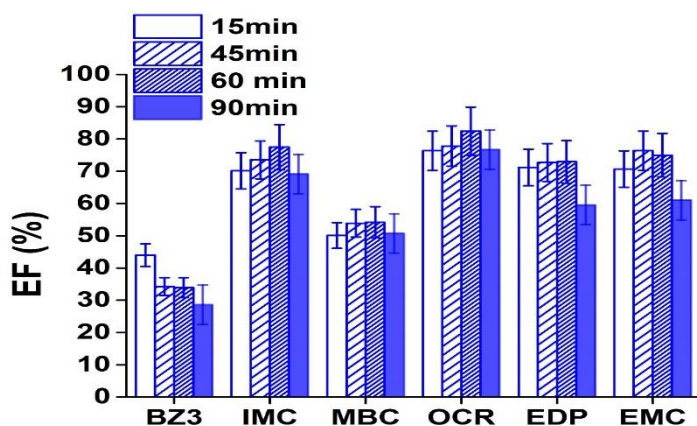


Figure 2.1.3.2.3. Optimization of the extraction time of UV filters on MOR-1@ cotton fabric.

2.1.3.2.4 Optimization of desorption conditions

To achieve the quantitative back-extraction of UV filters from the MOR-1@ cotton fabric, three factors were considered: the composition and volume of the elution solvent and the desorption time. To select the appropriate elution solvent methanol, propanol and mixtures of them with water

EXPERIMENTAL

at a ratio of 75:25 (similar to the mobile phase composition) was tested. A mixture of methanol:water (75:25) displayed the best performance (Fig 2.1.3.2.4.a) probably because this mixture had the lowest viscosity among the examined elution solvents. Less viscous solvents facilitate the penetration of the aqueous phase through the fabric pores thus maximizing the contact of the solvent with the MOF. BZ3 was the only exception since it was eluted more efficiency with both propanol and propanol:water (75:25), due to its higher solubility in propanol [490].

The volume of elution solvent was then studied by back-extracting the UV filters into variable volumes of methanol:water (75:25). Elution volumes lower than 2 mL were not adequate to completely immerse the fabrics, therefore, volumes equal to or higher than 3 mL were examined. Most analytes were effectively eluted with 3 mL of elution solvent (Figure 2.1.3.2.4.b) corresponding to 0.08 mL of elution solvent per cm^2 fabric area, which is similar to that of sol-gel coated fabric phases (typically 0.06-0.1 mL cm^{-2}) [451], [476]. Finally, desorption times from 5-20 min were examined (Figure 2.1.3.2.4.c) indicating that 15 min of desorption, with interim vortex mixing, could effectively desorb the analytes without further improvement at longer desorption times. Alternatively, ultrasound assisted extraction for 15 min was also efficient in desorbing the analytes. In the light of these results, the desorption of the UV filters was performed by exposing the MOR-1@ cotton fabric in 3 mL of methanol: water (75:25) for 15 min.

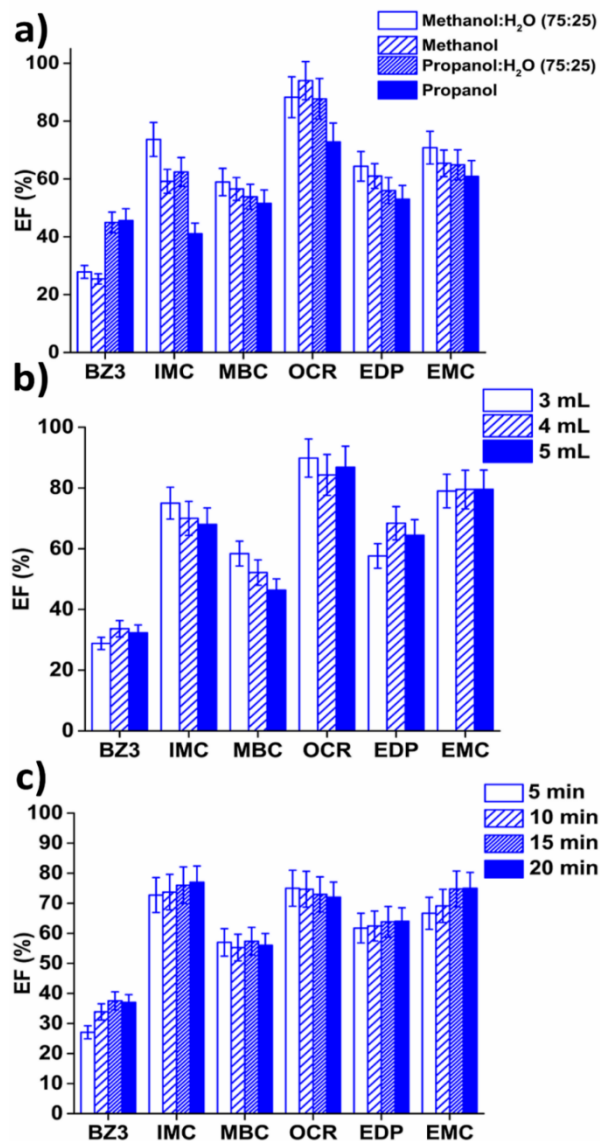


Figure 2.1.3.2.4. Optimization of desorption conditions for the FPSE of UV filters on MOR-1@ cotton fabric. (a) Effect of elution solvent composition, (b) Influence of elution solvent volume, and (c) Optimization of desorption time.

2.1.3.2.5 Sample volume

The maximal sample volume that can be extracted without impairing the EEs was examined by extracting UV filters from 50–750 mL of aqueous standard solutions using 1.5 circular MOR-

EXPERIMENTAL

1@cotton fabrics (corresponding to 0.05-0.75 cm² of fabric area per mL of sample) and considering that insufficient extraction occurs when the extraction efficiencies decreases more than 10% to that obtained from the extraction of 50 mL sample volume (that was used during the optimization study). As presented in Figure 2.1.3.2.5, for sample volumes up to 150 mL the extraction efficiency was not impaired. However, when the sample volume exceeded 150 mL, the extraction efficiency decreased. Since the (absolute) amount of UV filters that was extracted on the sorbent increased with sample volume up to 500 mL (and remained stable thereafter), we concluded that the decrease in the extraction efficiency was not due to sorbent saturation but due to the inadequate contact time of the MOR-1@cotton fabric with the aqueous donor phase. To verify this hypothesis, we extracted 250 mL of water samples for prolonged extraction times (2-4 h) and determined the extraction efficiency of the target UV filters. The extraction efficiency improved with increasing extraction time, an observation that led us to assume that the extraction of high sample volumes could be feasible at the expense of increasing the extraction time.

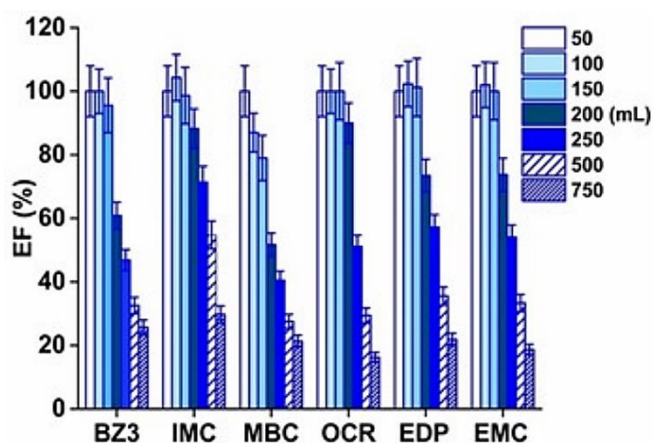


Figure 2.1.3.2.5 Influence of sample volume on the extraction efficiency of the method.

2.1.3.2.6 Reusability of the fabric

The reusability of the MOR-1@ cotton fabric was examined by repeatedly extracting 100 mL of aqueous standard solutions containing $10 \mu\text{g L}^{-1}$ of UV filters, under to the optimum experimental conditions. After each use the fabric was further cleaned with methanol to eliminate any UV filter residues and dried. The bar plots of Figure 2.1.3.2.6 show that the extraction efficiency, relatively to that obtained from the first time of use, remained satisfactory and within the range of 90 to 110% up to 15 times of reuse. This is explained by the quite high amount of MOR-1 immobilized in each fabric ($\sim 30 \text{ mg/fabric}$) and the high specific surface area of MOR-1 ($1097 \text{ m}^2 \text{ g}^{-1}$). After the 15th use, however, the extraction efficiency gradually declined, indicating that the loss of MOR-1 particles from the fabric surface, as previously discussed, became important.

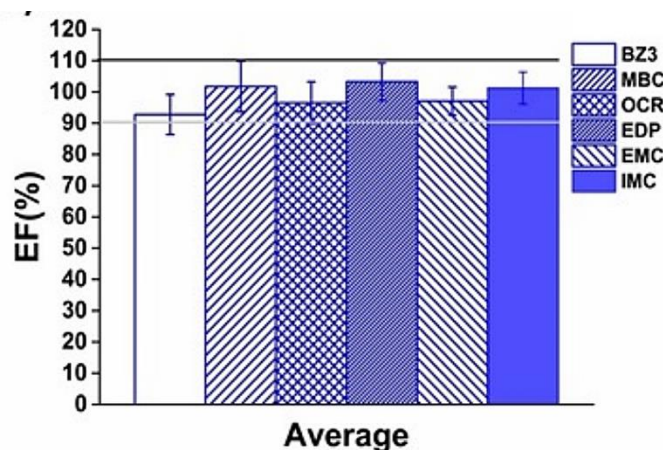


Figure 2.1.3.2.6 Average extraction efficiency of MOR-1@ cotton after 15 times of reuse.

2.1.3.2.7 Analytical figures of merit

The analytical figures of merit of the proposed method were determined by extracting 100 mL of aqueous standard solutions containing increasing concentrations of the target UV filters. According to the results shown in Table 2.1.3.2.7.a, the peak area increased linearly with concentration, from 10-250 ng mL^{-1} , with good linearity ($R^2 > 0.98$). The detection limits, calculated as $3S/b$ (where S and b are the residual standard deviation and the slope of the

EXPERIMENTAL

calibration curve, respectively) ranged from 2-10 ng mL⁻¹. The LODs are comparable to previous works reporting on the determination of UV filters with single-wavelength UV detection coupled to liquid chromatographic separation [489]. For the analysis of real samples, however, higher sensitivity should be pursued by using more sensitive detectors such as LC-MS or GC-MS and/or by evaporating the extraction solvent to lower volume [489].

Table 2.1.3.2.7.a Analytical merits of FPSE using the MOF@cotton sorbent phase in static (stirring assisted) extraction mode.

UV filter	Regression function	Regression Coefficient, R ²	Linear range (ng mL ⁻¹)	MLOD (ng mL ⁻¹)	EF (%) ^a	Precision (%RSD)	
						Repeatability (intra-day)	Reproducibility (inter-day)
BZ3	y=380±19 x-2434±1013	0.988	10 – 250	8.0	28.2	2.3	10.7
IMC	y=1136±45 x-7091±2425	0.993	10 – 250	6.4	69.5	7.2	10.1
MBC	y=1640±132 x+3160±2800	0.994	10 – 250	5.2	53.5	6.7	11.5
OCR	y=1195±84 x+5495±3600	0.980	10 – 250	9.1	71.8	5.0	10.4
EDP	y=3076±145 x-42843±10255	0.987	10 – 250	10.0	59.4	2.4	6.8
EMC	y=1453±120 x-18901±4845	0.988	10 – 250	10.0	67.5	8.4	7.6

^a EF: The slope of the calibration curve to the slope of the calibration curve obtained from standard solutions at the same concentration level.

The repeatability expressed as relative standard deviation (RSD %) was calculated from the analysis of five replicate aqueous standard solutions in the same day (intra-day repeatability) and 10 consecutive days (inter-day repeatability). The intra-day repeatability was found between 2.3 and 8.4 % showing the good precision of the method while inter-day repeatability ranged from 6.8-11.5%. The lower inter-day repeatability is attributed to the relatively high variability in the amount of MOR-1 immobilized on the fabric surface (25.4±6.6 mg, RSD=26.1%, n=250).

EXPERIMENTAL

However, such differences are statistically acceptable since only two fabrics contained such an amount of MOR-1 that fell outside the interquartile range rule and were excluded as outliers.

The analytical features of dynamic FPSE using MOR-1@ cotton fabrics were also assessed and the results are presented in Table 2.1.3.2.7.b. The data suggest that MOR-1@ cotton fabrics can be also used for flow-through extraction as an SPE sorbent. Due to the large pores of the fabric (60-100 μm) clogging associated with the use of SPE sorbent phases is minimized. In addition, the fabric support enables the use of a larger variety of nano-sized sorbent phases which are currently limited by high-back pressure or leaching problems. The linear range for all UV filters was the same to that obtained in static extraction mode but the slope of the calibration plots was lower. However, the method was not optimized for dynamic extractions, therefore, further improvement can be accomplished by optimizing the extraction conditions related to the application of the method in SPE mode.

Table 2.1.3.2.7.b Analytical merits of MOF@ cotton FPSE in dynamic extraction mode.

UV filter	Regression function	Regression Coefficient, R^2	Linear range (ng mL^{-1})	MLOD (ng mL^{-1})	Precision (%RSD) ^b
BZ3	$y=244x+4456$	0.988	10 – 250	10	4.6
IMC	$y=755x+6388$	0.987	10 – 250	10	6.8
MBC	$y=704x+4268$	0.985	10 – 250	10	7.3
OCR	$y=340x-4672$	0.990	10 – 250	8,3	8.2
EDP	$y=651x+7731$	0.986	10 – 250	10	6.7
EMC	$y=497x+4736$	0.992	10 – 250	9,0	7.8

2.1.3.2.8 Method application in real samples

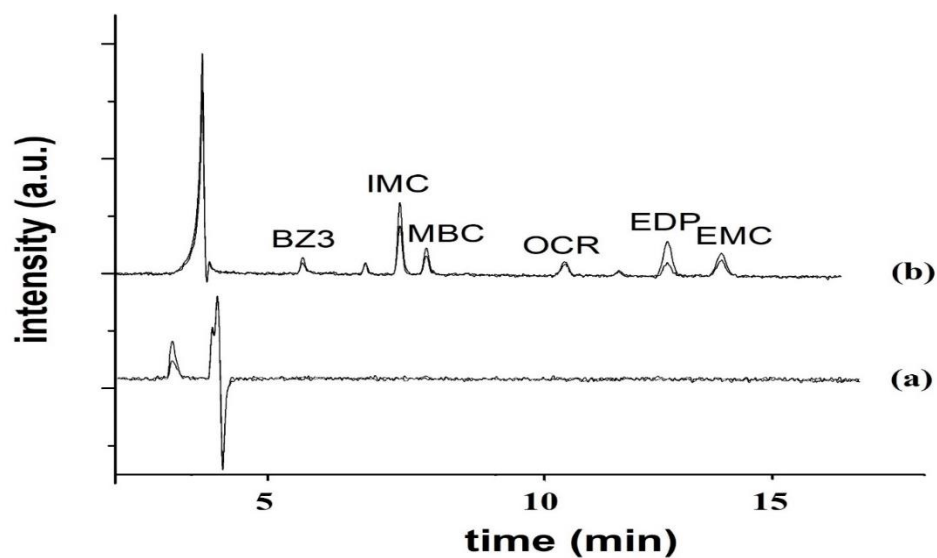
The applicability of the method was examined by analyzing a series of water samples of variable matrix complexity (river, lake and sea water). Since no UV filters were determined, spiking experiments at three concentration levels (low, medium, and high) were performed in order to calculate the recovery of UV filters. Due to the non-exhaustive extraction of the analytes, the relative recoveries, defined as the ratio of the concentration found in spiked water samples to that determined from the extraction of an aqueous standard solution of the same concentration level, were calculated. The results are presented in Table 2.1.3.2.8.a and Table 2.1.3.2.8.b and show that recoveries ranged from 85.6 to 118.8% in natural waters. These recoveries are similar to those accomplished by other microextraction methods [489]. A characteristic chromatograph from the analysis of real samples is presented in Figure 2.1.3.2.8.

Table 2.1.3.2.8.a Recoveries obtained by applying the method to real water samples spiked with $100 \mu\text{g L}^{-1}$ of UV filters.

UV filter	Recoveries \pm RSD (% , n=4)		
	River	Lake	Sea
BZ3	94.7 \pm 7.8	103.4 \pm 12.5	96.5 \pm 10.7
IMC	102.4 \pm 9.3	100.8 \pm 8.2	100.8 \pm 11.3
MBC	92.5 \pm 5.5	106.5 \pm 9.8	102.8 \pm 12.0
OCR	103 \pm 3.7	99.8 \pm 11.3	98.5 \pm 8.2
EDP	98.2 \pm 8.5	100.9 \pm 4.1	97.1 \pm 8.6
EMC	104.8 \pm 7.7	109.9 \pm 2.3	95.4 \pm 8.8

Table 2.1.3.2.8.b Recoveries of UV filters from spiked lake water at two concentration levels.

UV filter	Recoveries \pm RSD (% , n=3)	
	20 $\mu\text{g L}^{-1}$	200 $\mu\text{g L}^{-1}$
BZ3	114.4 \pm 11.0	113.2 \pm 12.5
IMC	85.6 \pm 8.1	94.8 \pm 8.2
MBC	87.0 \pm 9.0	118.8.5 \pm 9.8
OCR	91.8 \pm 10.0	103.8 \pm 11.3
EDP	116.2 \pm 13.4	97.2 \pm 4.1
EMC	88.4 \pm 7.6	108.2 \pm 2.3

*Figure 2.1.3.2.8 Chromatograph of lake water sample extracted with the developed method (a) before and (b) after spiking of UV filters.*

2.1.3.2.9 Method application to passive sampling of UV filters in natural waters

To evaluate the feasibility of using the MOR-1@ cotton fabrics for the passive sampling of UV filters from natural waters we measured the sampling rates by determining the uptake kinetics for a period of 50 days. The uptake kinetic curves of Figure 2.1.3.2.9 show that UV filter accumulation exhibited a linear (integrative) phase up to 35 days, except for BZ3 which exhibited desorption after the 14th day due to its higher solubility in water and lower hydrophobicity, compared to the other UV filters. The calculated sampling rates, summarized in the inset legend of Figure 2.1.3.2.9, ranged from 0.026 to 0.352 L d⁻¹ which are similar to those reported for other organic compounds using different passive sampling sorbent phases [491], [492], [493]. Moreover, the calculated sampling rates were positively correlated with the logK_{ow} of the UV filters ($r=0.70$). By excluding BZ3 which is the least hydrophobic of the UV filters examined (LogK_{ow}=3.79) and EDP which is a weak acid (pK_a=2.38 and pK_b=4.85) and is present in its ionized form in natural waters pH (6.5-7), there is a good linear relationship between the sampling rate and the hydrophobicity of the UV filters ($R_s = 0.24\log K_{ow} - 1.05$, $R^2=0.87$). Similar relationships between hydrophobicity and sampling rates have been commonly reported [491], [493]. All these data show that MOR-1@ cotton fabrics can be also used as an alternative sorbent phase for the passive sampling of UV filters in natural waters.

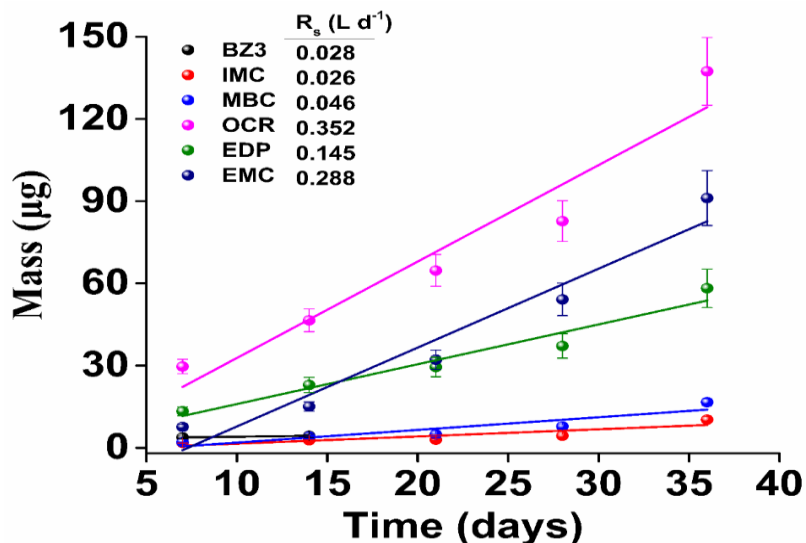


Figure 2.1.3.2.9 Uptake kinetic curves of UV filters on MOR-1@ cotton fabric.

2.1.4 Conclusions

This study demonstrates the use of MOF@ cotton fabrics as a new and versatile sorbent for the FPSE of organic compounds from water samples both under static (i.e. stirring assisted) and dynamic (i.e. vacuum assisted) extraction mode. The strong chemical bonding between the MOF and the substrate through polydopamine provides good chemical and solvent stability to the sorbent but the hydrophobic interactions between the analytes and the MOF ligand could lead to the gradual solubilization of the MOF. As a result of this finding, the MOF@ cotton sorbent could be re-used only 15 times without jeopardizing the extraction efficiency. The applicability of the material was demonstrated by the analysis of various spiked environmental water samples of variable complexity including river, lake and seawater. Moreover, the MOF@ cotton fabric was calibrated also as a passive sampling sorbent phase for the uptake of UV filters from natural waters over relatively long exposure times (up to 35 days) with sampling rates that are similar to other sorbent phases. All these results show that MOF@ cotton composites hold great promise as

EXPERIMENTAL

alternative sorbents for both FPSE and passive sampling, opening new opportunities in analytical sample preparation and environmental monitoring of organic micropollutants in the environment.

2.2 In-situ, extractive remediation of soil using retrievable bulk-supported nanosorbents composed of metal-organic framework-decorated cotton fabrics

2.2.1 Introduction

Soil is a valuable and non-renewable natural resource subject to widespread degradation due to anthropogenic activities [494]. For this reason, soil remediation has been at the forefront of academic research for many years, leading to various technologies based on two distinct methodological approaches: *ex-situ* and *in-situ* treatment [495], [496], [497], [498]. *Ex-situ* treatment (such as solid washing/flushing, wet oxidation, electrochemical separation, thermal treatment, solidification/stabilization, etc.) is a highly invasive method that is based on excavating the soil, transporting it in specialized facilities, extracting the pollutants, and then restabilizing the soil so that it can be safely returned to the field [495], [497], [499], [500]. Although efficient, *ex-situ* methods entail high operational and investment costs and significant energy requirements [499], [500]. *In-situ* methods, on the other hand, are minimally invasive, enabling the remediation of soils in the field without needing soil transportation or using specific infrastructures (e.g., soil flushing tanks) [496], [498], [499], [501]. As a result, they present cost-effective and relatively straightforward alternatives to *ex-situ* methods. Moreover, they offer high versatility since they can be utilized for contaminant removal (i.e., phytoremediation), degradation (i.e., bioremediation), or immobilization (i.e., sorbent amendments)" [496], [498], [499].

Among the *in-situ* remediation methods, sorbent amendment is an appealing option based on adding and mixing micro-meter-sized particles of sorbent materials, such as activated carbon, biochar, zeolites, MOFs, etc., into the soil. These particles bind and immobilize contaminants effectively, reducing their infiltration and bioretention and lowering their uptake and bioavailability to living organisms [502], [503], [504]. The limitation of this method is that the

EXPERIMENTAL

micro-sized sorbent firmly adheres to soil particles and cannot be physically separated and recovered from the soil. Although this would not be an issue if contaminant immobilization on the sorbent was permanent, several studies have shown that the efficiency of sorbents to retain contaminants diminishes over time. This degradation can occur due to the degradation of the sorbent or (bio)chemical transformation of the pollutants on the sorbent surface, leading to leaching back into the soil and inducing negative, mid- and long-term, ecotoxic effects on living organisms [505], [506].

Retrieval of the sorbent after deployment was suggested as a plausible way to extract the contaminants and avoid leaching. However, this is not technically feasible because most sorbent materials are produced in powder form (i.e., micro or nanoparticles), which firmly attach to and assimilate into the soil matrix. One proposed approach is to use magnetic sorbents that can be recovered from soil with an external magnetic field. In practice, however, the magnetic (micro/nano)sorbents also bind strongly to the soil particles and cannot be physically separated by magnetism. The dispersion of the soil-sorbent mixture in water and the magnetic separation of the sorbent is the only way to overcome this problem. However, excavating large amounts of soil and dispersing it in water tanks for *ex-situ* treatment entails high costs and generates large amounts of secondary waste, such as significant volumes of potentially contaminated water [507], [508], [509]. A more effective and practical solution proposed by our group is using granular magnetic sorbents [510]. Due to their large size, granular sorbents do not assimilate with soil particles. Thus, they can be directly retrieved from the solid matrix with an external magnetic field, producing a sorbent-free soil matrix. From our experience, the limitation of this method lies in the use of a relatively high amount of sorbent to accomplish efficient remediation ($\geq 10\%$ w/w) and the change in soil

pH, which may affect the activity of living (micro)organisms and enhance the hydrolysis of organic compounds.

In this study, we extend our previous work with granular sorbents to propose an *in-situ* soil remediation method that relies on nanosorbent materials incorporated onto bulk-solid supports for the minimally invasive, *in-situ* extraction of organic contaminants from soil. A metal-organic framework (MOF), namely $\text{Zr}_6\text{O}_4(\text{OH})_4(\text{NH}_3^+-\text{BDC})_6\text{Cl}_6$ (MOR-1, BDC^{2-} = terephthalate), was used as sorbent material due to its high surface area, good stability, and excellent sorption properties. Cotton fabric sheets were utilized as bulk support for the MOF due to their lightweight nature, low cost, and availability in variable qualities. Additionally, cotton fabrics occupy minimal space during storage and can be easily collected after use. The MOF-decorated sorbent could be added and removed from the soil with minimum effort, thus extracting the contaminants and relieving the soil from the contaminant-laden sorbent. Moreover, due to the excellent stability and inertness of the MOF, the sorbent could be reused several times while avoiding the leaching of the contaminants and enabling its safe disposal. As a demonstration, the remediation of soil contaminated with non-polar organic compounds was examined and optimized, accomplishing high recoveries.

2.2.2 Experimental

2.2.2.1 Chemicals and Materials

Cotton fabric sheets were purchased from local stores, washed with water and acetone, and air-dried. Zirconium chloride (99.5%+, metal basis), glacial acetic acid $\geq 99.7\%$ and 2-aminoterephthalic acid 99% ($\text{NH}_2\text{-H}_2\text{BDC}$) were obtained from Alfa-Aesar. Organic UV filters (2-hydroxy-4-methoxybenzophenone, BZ3, 98%, 2-ethylhexyl 4-methoxycinnamate, EMC,

EXPERIMENTAL

99.8%, and 2-Ethylhexyl 4-(dimethylamino)benzoate, EDP, 98%, were procured from Sigma-Aldrich (Steinheim, Germany), 3-(4-methylbenzylidene)camphor, MBC, 99.7% was from Guinama S.L., (Valencia, Spain), isoamyl 4-methoxycinnamate, IMC, 99.3%, was purchased from Haarmann and Reimer Parets del Vallés, Spain), and 2-ethylhexyl 2-cyano-3,3-diphenylacrylate, OCR, >98%, was obtained from F.Hoffman-La Roche Ltd. (Basel, Switzerland). HPLC-grade methanol and water were purchased from Scharlab (Barcelona, Spain). Anhydrous Na₂SO₃ was purchased from J.T. Baker Chemical (Leicestershire, U.K), and ethyl acetate (>99.5%) was procured from Honeywell (Charlotte, USA).

2.2.2.2 Instrumentation

Powder XRD (PXRD) diffraction patterns were recorded on a Bruker D2 Phaser X-ray diffractometer (CuK α radiation, wavelength=1.54184 Å). Scanning electron microscopy (SEM) measurements were performed with a Phenom Pharos G2 Desktop FEG-SEM (Thermo Fisher Scientific) on Cr sputtered specimens (Q150T ES Plus automatic sputter coater, Quorum Technologies Ltd.) IR spectra were recorded on a Perkin Elmer Spectrum Two attenuated total reflectance-IR (ATR-IR) spectrometer.

A Shimadzu HPLC composed of an LC-20AD high-pressure solvent delivery pump, a DGU-20A3 degasser, a CTO-10A column oven, and an SPD-10AV UV/Vis detector was used for the chromatographic analysis of UV filters. Analysis was performed by injecting 20 μ L of sample in a thermostated (45 °C) Hypersil ODS C18 column (250 mm length, 4.6 mm I.D., 5 μ m particle size) obtained from MZ Analysentechnik (Mainz, Germany) under isocratic flow conditions (1

mL min⁻¹) using MeOH and water at a mixing ratio of 75:25 (v/v) as a mobile phase. The peak area for all UV filters was recorded at 313 nm.

2.2.2.3 Synthesis of MOR-1@ cotton fabrics

The synthesis of **MOR-1@ cotton fabric** was performed according to the procedure described in our previous work [511].

2.2.2.4 Batch sorption studies of UV filters on MOR-1@ cotton fabric

Rectangle **MOR-1@PDA-cotton** and **PDA@ cotton fabrics** (2.2 × 3.0 cm) with a surface area of 13.2 cm² (6.6 cm² on each side) was added in an aqueous solution containing 5 mg/L of UV filter and stirred at 100 rpm in an orbital shaker. At a given time intervals, an aliquot of 20 µL of the sample was withdrawn and analyzed by HPLC.

2.2.2.5 Preparation of the contaminated soil

Non-polluted soil was collected and air-dried from a remote area from the top 20-25 cm of the topsoil profile. To remove debris and larger particles the sample was dry-sieved to through 2 mm stainless steel sieves and manually milled to homogenize the soil. The soil properties (particle size distribution and composition) were determined to be as follows: 1-2 mm: 17.6%, 0.5-1 mm: 38.4%, 0.25-0.5 mm: 21.2%, 0.063-0.25 mm: 15.4% and <0.063mm: 7.4%, organic matter=8.1±1.7 % (w/w), electrical conductivity=188±21 µS cm⁻¹, pH=7.6±0.3, CaCO₃=16.0±2.5% w/w.

Contaminated soil was prepared by spiking a methanolic solution of UV filters (BZ3, IMC, MBC, OCR, EDP, and EMC) to soil under mixing to achieve a nominal UV filter concentration of 5 mg kg⁻¹ for each UV filter (total 30 mg kg⁻¹ for all UV filters). The slurry was initially aged overnight

in an air-sealed vessel while mixed in an orbital shaker (100 rpm) and dried at room conditions (~18-20 °C, humidity ~50-60%). To facilitate drying and homogenize the sample so that UV filters can reach a pseudo-equilibrium with the soil, the slurry was mixed with a glass rod.

2.2.2.6 Soil remediation studies with MOR-1@PDA-cotton fabrics

Soil remediation studies were performed in Amber glass vessels to avoid light exposure and minimize moisture fluctuations throughout the study. **MOR-1@PDA-cotton fabrics** of variable surface area (from 6.5 to 51.5 cm²) were added to 20 g of water-saturated contaminated soil (i.e., moisture 50% or higher) containing 1 g/L NaN₃ to inhibit microbial activity. The cotton fabric was mixed with the soil and incubated for a period ranging from 5 to 60 days. Weekly, the fabric was mixed with the soil to enhance contact, and the gross weight of each vessel was measured to calculate moisture loss. When the gross weight decreased more than 10% of the initial weight recorded at the beginning of the experiment, a small aliquot of distilled water was added dropwise and mixed with soil to restore moisture content and ensure constant humidity conditions throughout the remediation period. Finally, the **MOR-1@PDA-cotton fabric** sorbent was pulled out of the soil, and the soil as well as the **MOR-1@PDA-cotton fabric** were dried in air.

2.2.2.7 Extraction of residual UV filters from soil

The extraction of UV filters from the soil matrix was performed by ultrasound-assisted solvent extraction, as described in our previous work[512]. Specifically, 2 g of dry soil and 1 g of anhydrous Na₂SO₄ were mixed in a glass centrifuge vial. Then, 8 mL of the extraction solvent composed of ethyl acetate: methanol (9:1) was added and placed in an ultrasonic bath for 15 min. The vials were centrifuged at 6000 rpm for 20 min, and the supernatant solution was collected.

EXPERIMENTAL

The same procedure was repeated three times, and the combined extracts were mixed and evaporated to dryness in a rotary evaporator at a temperature <30 °C. The residue was re-dissolved in 2 mL HPLC grade methanol, filtered through 0.22 µm PTFE filters, and 20 µL were injected into the liquid chromatograph for analysis. The efficiency of the extraction method was tested by extracting soil samples spiked with 2 mg Kg⁻¹ of the examined UV filters. Recoveries ranged from 86.5-94.4%, which were considered satisfactory.

The remediation efficiency was calculated by determining the remaining concentration of UV filters in the soil according to the formulae:

$$E(\%) = \left(1 - \frac{\text{residual concentration after remediation}}{\text{initial concentration}}\right) \times 100$$

2.2.3 Results and Discussion

2.2.3.1 Characterization of MOR-1@cotton fabrics

The efficiency of the synthetic method to immobilize MOR-1 particles on cotton fabrics has been demonstrated in our previous works, along with extensive characterization data concerning the properties of the MOR-1-coated cotton fabrics [513], [514], [515]. The successful synthesis was confirmed through PXRD and IR analysis, while SEM evidenced the formation of MOR-1 particles. Figure 2.2.3.1a shows the diffraction peaks of MOR-1 at 2θ of 7.3°, 8.5° and 12°, corresponding to (111), (200) and (220) planes, respectively, while Figure 2.2.3.1.b depicts the characteristic IR bands at 1570 and 1385 cm⁻¹ assigned to the $\nu_{as}(\text{COO}^-)$ and $\nu_{sym}(\text{COO}^-)$ modes, respectively, as well as to the Zr-O bond at 763 and 685 cm⁻¹ [516]. The FE-SEM images also verify the successful immobilization of the octahedrally shaped MOR-1 particles on the cotton surface (Figures 2.2.3.1.c, d).

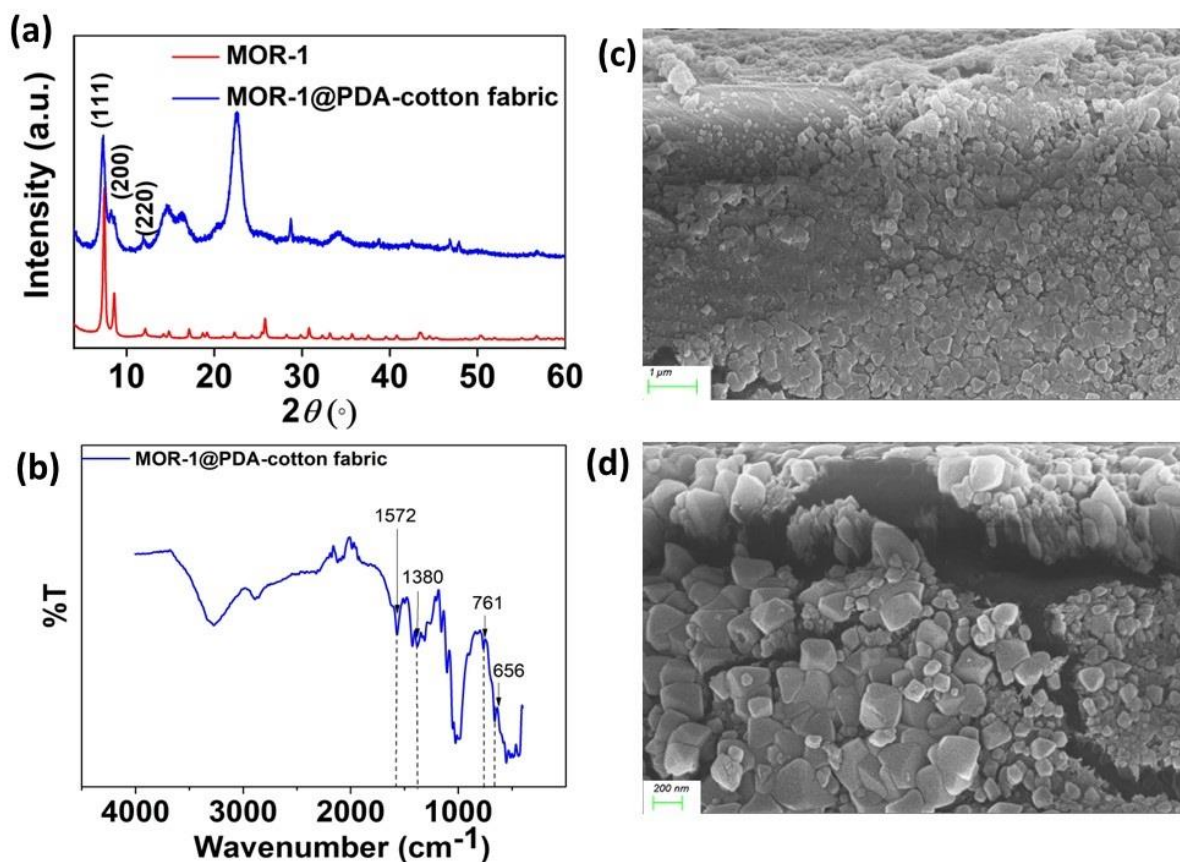


Figure 2.2.3.1. (a) PXRD pattern, (b) ATR-IR spectrum, and (c), (d) SEM images of **MOR-1@PDA-cotton fabric**.

Thermogravimetric analysis (TGA) of the **MOR-1@PDA-cotton fabric** was not possible because cotton fabric residues remaining after thermal treatment did not enable the accurate and reproducible determination of the pure amount of MOR-1 (as ZrO_2) that was deposited on the cotton. Therefore, an estimate of the amount of MOR-1 deposited on cotton was determined gravimetrically by weighting the cotton sheet before and after the deposition of MOF. Through this procedure, the estimated amount of MOR-1 deposited per 25.75 cm^2 surface area of cotton was $25.6 \pm 5 \text{ mg}$ (average mass determined by weighting 200 **MOR-1@PDA-cotton fabrics**), which means that approximately $1 \pm 0.04 \text{ mg}$ of MOR-1 was deposited per 1 cm^2 of cotton fabric.

2.2.3.2 UV filter sorption on MOR-1@PDA-cotton fabric

The kinetic data for the sorption of UV filters on **MOR-1@PDA-cotton fabric** and **PDA@cotton fabric** are shown in Figure 2.2.3.2.a. The sorption efficiency is expressed as mg of UV filter per fabric area (13.2 cm²) to compare the performance of **MOR-1@PDA-cotton fabric** with that of cotton-PDA (i.e., fabric not loaded with MOF). The Ho-Mckay pseudo-second-order (PSO) kinetic model can describe the sorption kinetics data optimally. This reveals that chemical sorption is the primary removal mechanism, attributed in the case of UV filters to hydrophobic interactions, H-bonding, and π -stacking interactions.

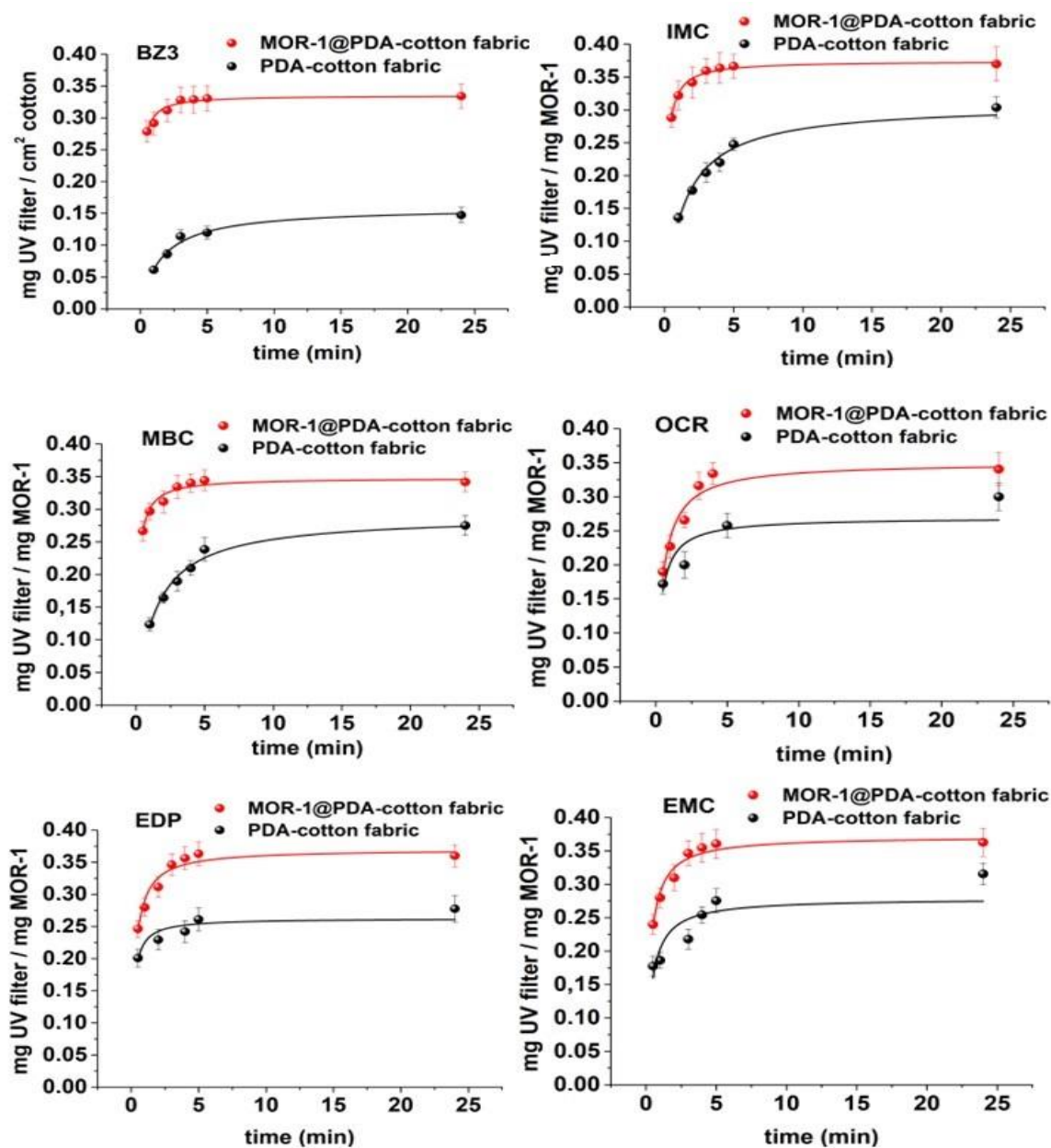


Figure 2.2.3.2.a Fitting of the UV filter sorption on *MOR-1@PDA-cotton fabric* to Ho-Mckay's pseudo-second-order kinetic model.

Since in Ho-Mckay's PSO kinetic model, the adsorption rate depends on the adsorption capacity rather than the adsorbate concentration, the equilibrium adsorption capacity can also be estimated

EXPERIMENTAL

from this model [517], [518]. This benefits the sorption of organic compounds with limited aqueous solubility, such as UV filters, because sorption isotherms cannot be performed over a wide concentration gradient necessary to establish equilibrium. From these data (Table 2.2.3.2.a), it can be calculated that the UV filters exhibit maximum sorption capacities from 0.34-0.37 mg UV filter/cm² of **MOR-1@PDA-cotton fabric**, which is 1.5-3.5 higher than those of plain **PDA-cotton fabric** (Table 2.2.3.2.b). Considering that 1 cm² of fabric contains approximately 1 mg of MOR-1, as discussed above, the sorption capacity per mass of sorbent is 0.34-0.37 mg UV filter/mg MOR-1, which is very satisfactory considering that, e.g., a 100 cm² cotton may uptake 340-370 mg of UV filters. Moreover, the sorption of all UV filters exhibited very rapid sorption kinetics with PDA- and **MOR-1@PDA-cotton fabrics**, reaching equilibrium within only 5 minutes. In addition to the high surface area of MOR-1 (~ 581 m²/g for the MOR-1 immobilized on cotton fabric) and its NH₂-BDC²⁻ ligands, capable of forming strong hydrogen bonds and enabling π -stacking interactions with UV-filters [366], as well as the reactive sites of PDA that may also facilitate π -stacking and hydrogen-bonding interactions [519], [520], the high sorption capacity and the fast reaction kinetics may also be attributed to the use of fabric as support of MOR-1 and PDA. Fabric is a substrate that facilitates the flow of the aqueous phase through its large pores (60–100 μ m) without redirecting it or bouncing back to the reverse direction, as it occurs with impermeable substrates or solid sorbents [476], which has been proven to facilitate the high mass transfer rates [521]. However, it was impossible to calculate the surface coverage of the cotton fabric with PDA (for the above reasons); therefore, the contribution of PDA and MOR-1 to the sorption of UV filters could not be discriminated. Notably, Pearson correlation analysis of the (pseudo-second order) rate constant (K) with the LogKow of the UV filters yielded a negative

EXPERIMENTAL

correlation coefficient ($r = -0.85$), statistically significant at the $p=0.05$ confidence level, suggesting that less hydrophobic compounds exhibit faster sorption kinetics.

Table 2.2.3.2.a Parameters of pseudo-second-order and intra-particle diffusion kinetic models for the adsorption of UV filters on MOR-1@PDA-cotton fabric.

UV filter	Pseudo-second order			Intra-particle diffusion			
	q_e (mg / cm ²)	K (cm ² / mg × min)	R^2	K_1 (mg / cm ² × min ^{1/2})	R^2	K_2 (mg / cm ² × min ^{1/2})	R^2
BZ3	0.33	26.2	0.93	0.04	0.97	0.002	0.89
EDP	0.37	9.9	0.95	0.08	0.97	-	-
EMC	0.37	9.2	0.97	0.08	0.96	0.0008	0.99
IMC	0.37	17.4	0.99	0.05	0.91	0.001	0.99
MBC	0.34	18.1	0.96	0.05	0.94	-	-
OCR	0.35	6.14	0.94	0.11	0.99	0.002	0.99

Table 2.2.3.2.b Parameters of pseudo-second-order and intra-particle diffusion kinetic models for the adsorption of UV filters on PDA@cotton fabric.

UV filter	Pseudo-second order			Intra-particle kinetic diffusion			
	q_e (mg / cm ²)	K (cm ² / mg × min)	R^2	K_1 (mg / cm ² × min ^{1/2})	R^2	K_2 (mg / cm ² × min ^{1/2})	R^2
BZ3	0.16	3.96	0.98	0.072	0.98	0.01	0.99
EDP	0.26	22.8	0.8	0.036	0.96	0.006	0.99
EMC	0.28	9.6	0.71	0.063	0.93	0.015	0.99
IMC	0.31	2.32	0.98	0.088	0.99	0.02	0.99
MBC	0.29	2.41	0.99	0.09	0.99	0.014	0.99
OCR	0.27	11.1	0.66	0.056	0.96	0.016	0.99

EXPERIMENTAL

To further examine the diffusion mechanism in the adsorption of UV filters on **MOR-1@PDA-cotton fabric** and **PDA@cotton fabric**, the intraparticle mass transfer diffusion model of Weber-Morris, $q_t = k_i \times t^{0.5} + C_i$, where q_t is the amount of the compound adsorbed at time t , k_i is the intraparticle diffusion rate and C_i is an empirical parameter related to the thickness of the boundary layer, was investigated. The plots of q_t as a function of $t^{0.5}$ depicted in Figure 2.2.3.2.b are not represented by straight lines, meaning that intraparticle diffusion was not the rate-limiting step in the sorption of UV filters. Since the intraparticle diffusion constants in the first stage were higher than those determined in the second stage ($K_1 > K_2$) (Table 2.2.3.2.a), the second stage (i.e., film diffusion) was the rate-limiting step in the sorption process, which means that the external surface of the sorbent is the primary site for sorption. This is reasonable since the size of UV filters is estimated to be ≥ 10 Å (Figure 2.2.3.2.c), which is larger than the pores of MOR-1 (i.e., 8-9 Å)[360].

EXPERIMENTAL

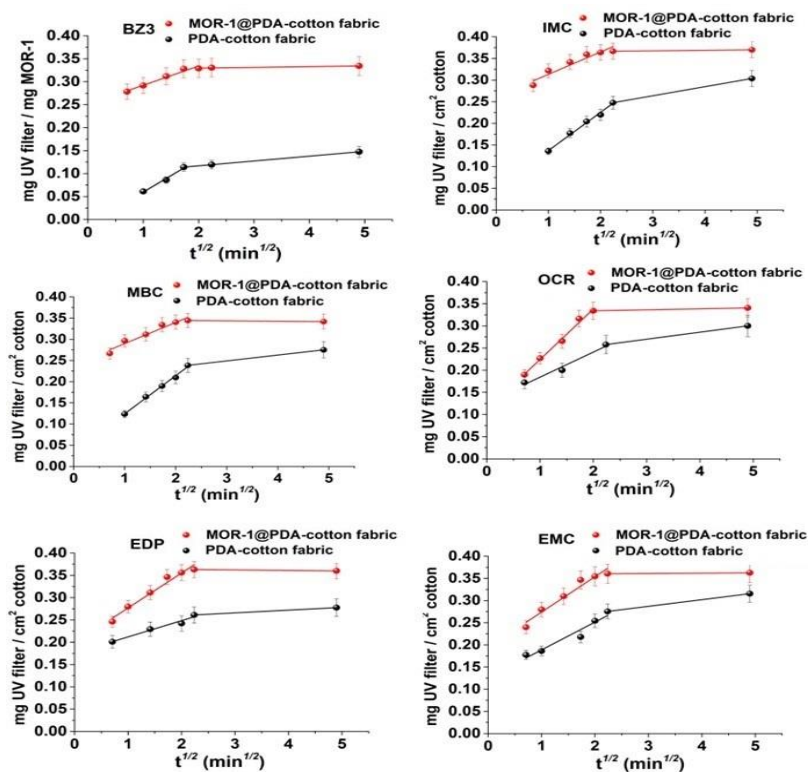


Figure 2.2.3.2.b Intraparticle diffusion model plots of UV filter sorption on *MOR-1@cotton fabric* and *PDA-cotton fabric*.

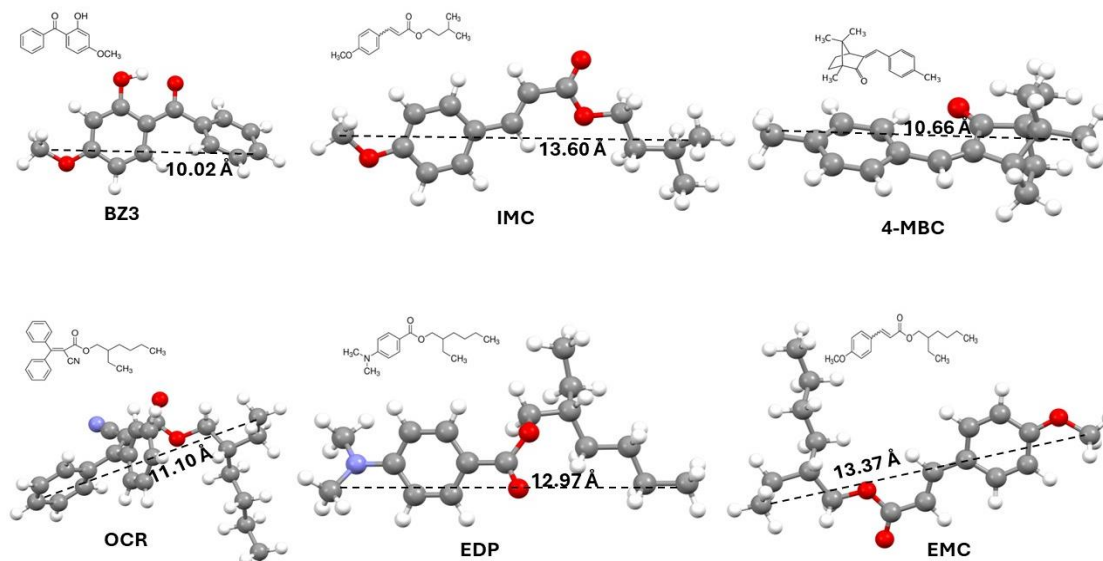


Figure 2.2.3.2.c Structures of UV filters after minimization at the B3LYP/6-31+G(d,p) level of theory in aqueous solution using Gaussian 09, version D.01 program suite.

2.2.3.3 Remediation of soil with MOR-1@PDA-cotton fabrics

The efficiency of **MOR-1@PDA-cotton fabrics** in removing UV filters from soil was optimized by varying the bulk sorbent's surface area, the soil's moisture content, and the remediation time. In each study, the total remediation efficiency was calculated by determining the concentration of UV filters remaining in the remediated soil.

The removal efficiency of UV filters in relation to the surface area of the **MOR-1@PDA-cotton fabrics** is depicted in Figure 2.2.3.3.a. From these data, it can be inferred that increasing the surface area of the sorbent from 6.3 to 50.2 cm² per 20 g of soil (or 0.32-2.51 cm² / g of soil) the removal efficiency of UV filters improves for surface area up to 1.88 cm²/g soil. This is due to the larger contact area of the sorbent with the soil and the higher mass of MOR-1, which increases the available sorption sites and reaches a plateau at higher values. Regarding soil moisture, the results presented in Fig. 2.2.3.3.b show no significant influence of moisture on the removal efficiency. This is advantageous because the sorbent can be used effectively over various soil moisture conditions, including water-saturated soils such as those found in wetlands, river or lake shores, and sediments. Finally, the effect of the incubation time of the sorbent with the soil was investigated from 5-60 days. The remediation efficiency improves with time for all UV filters with increasing incubation time (Figure 2.2.3.3.c). Under the optimum conditions, the removal of UV filters ranged from 43-90% for most compounds, except for the highly hydrophobic OCR (logK_{ow}=6.9) which was removed by 25%. In fact, the removal efficiency was negatively correlated to the logK_{ow} of the UV filters ($r = -0.97$, $p=0.05$), suggesting that **MOR-1@PDA-**

EXPERIMENTAL

cotton fabric more effectively sorbs less hydrophobic compounds. This may be attributed to the hydrophilicity of the fabric sorbent (water contact angle $< 10^0$) that facilitates the permeation of water through its pores. Importantly, compared to control samples (contaminated soil incubated for the same time intervals without **MOR-1@PDA-cotton fabric**) no significant change in the pH of the soils was recorded during the remediation period ($\Delta\text{pH} \leq 0.5$). This is advantageous compared to other sorbents because it does not induce secondary reactions with organic compounds (e.g., protonation at acidic pH and hydrolysis at alkaline conditions) that may alter the interaction of the contaminants with the soil and their fractionation or speciation inside the soil matrix.

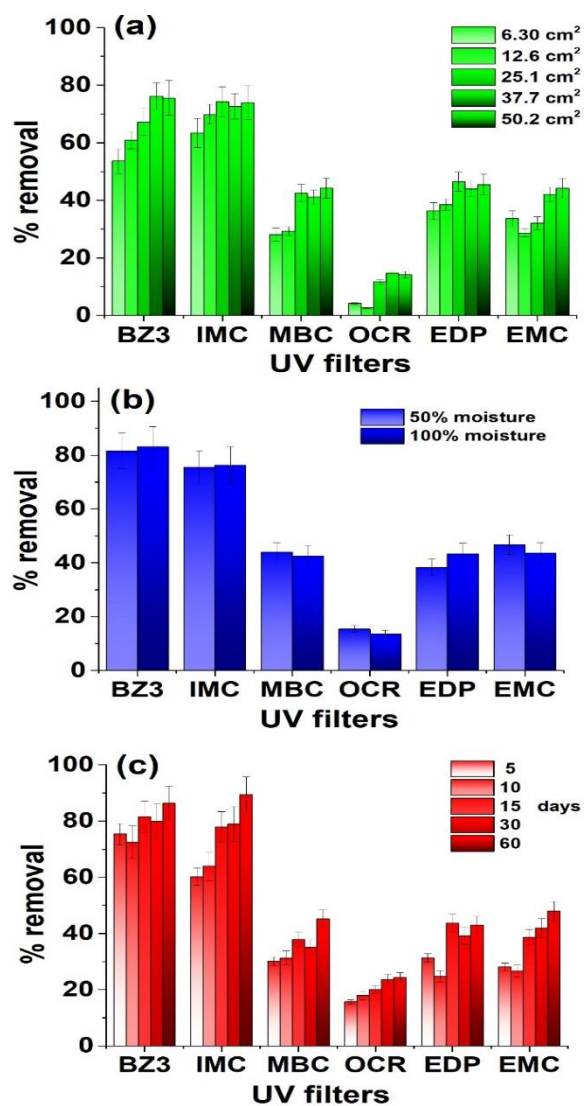


Figure 2.2.3.3 Removal (%) of UV filters from the soil as a function of (a) sorbent surface area (50% moisture capacity for 10 days), (b) soil moisture content (50.2 cm² MOR-1@PDA-cotton fabric for ten days), and (c) remediation time (50.2 cm² MOR-1@PDA-cotton fabric in water-saturated soil).

2.2.3.4 Regeneration and stability of MOR-1@PDA-cotton fabric

While investigating the efficiency of remediation with increasing incubation time, the stability of **MOR-1@PDA-cotton fabric** was also monitored. After retrieving the **MOR-1@PDA-cotton fabric** from the soil, the UV filters were eluted with MeOH:H₂O (75:25) after 15 min of agitation, as described in our previous work [521], and their XRD and IR patterns were measured and compared to that of pristine **MOR-1@PDA-cotton fabric** (Figure 2.2.3.4). The XRD pattern and the IR spectra show that the diffraction peaks and the IR bands of MOR-1 are maintained throughout the remediation period, indicating that MOR-1 retains its stability.

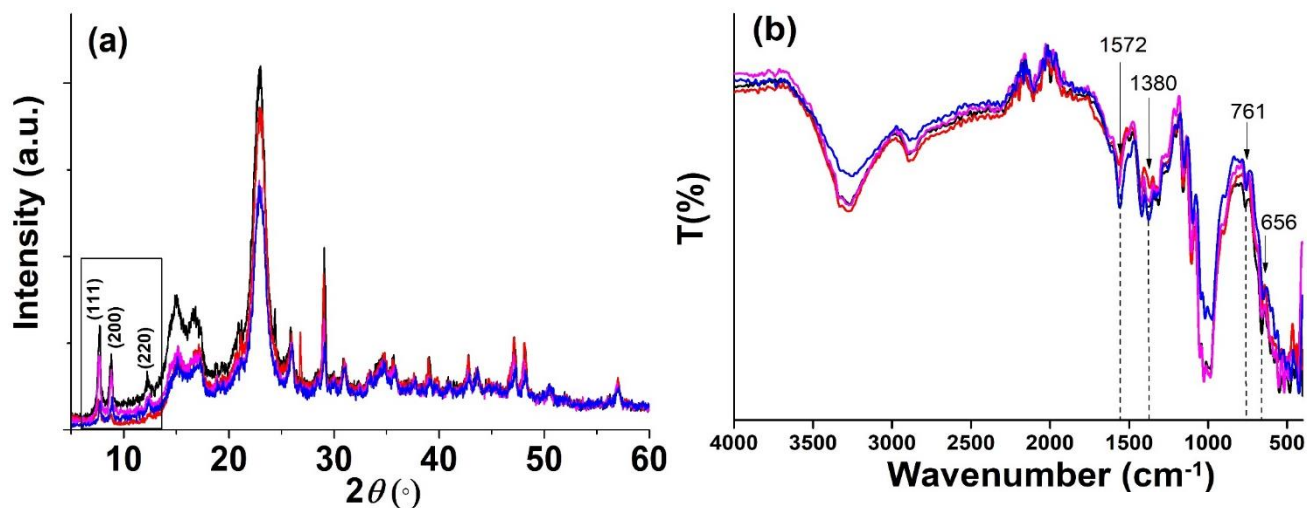


Figure 2.2.3.4. (a) pXRD pattern and (b) ATR-IR spectra of MOR-1@cotton fabric sorbent after soil remediation for — 5, — 15, — 30, and — 60 days.

On the grounds of this observation, the reusability of the sorbent was evaluated by reusing the sorbent several consecutive times. To enable a direct comparison, 10 g of water-saturated soil, spiked with the same UV filter concentration, was remediated with 50.2 cm² of **MOR-1@PDA-cotton fabric** for 15 days. After use, the UV filters were eluted, and the sorbent was re-used in

EXPERIMENTAL

new soil. The results in Fig. 2.2.3.4.c show that the sorbent can be efficiently reused five times without losing its efficiency for most UV filters. This feature is advantageous as the sorbent can be reused to reduce the overall cost of the application.

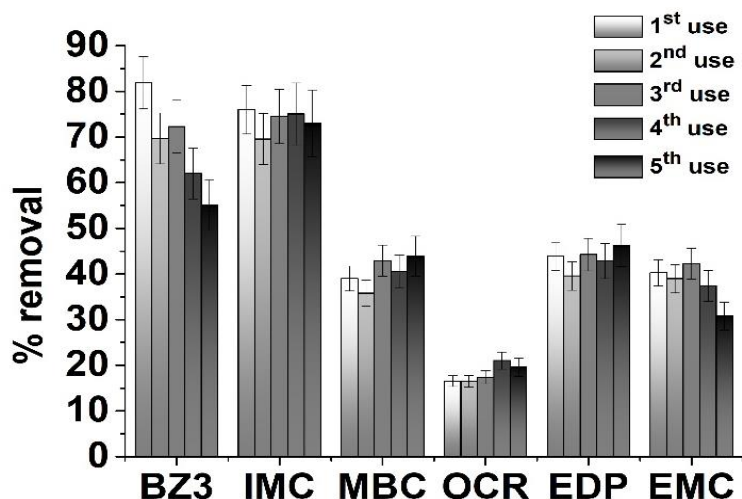


Figure 2.2.3.4.c. Re-usability of MOR-1@PDA-cotton fabric in soil remediation.

Finally, the stability of UV filters sorbed on the **MOR-1@PDA-cotton fabric** was evaluated by leaching tests to assess the potential hazards associated with the disposal of the UV filter-laden sorbent phase. First, **MOR-1@PDA-cotton fabrics** were brought in contact with a 20 mL solution containing a mixture of UV filters (1 mg/L each UV filter) for one hour under orbital shaking (150 rpm) to establish equilibrium. Leaching of UV filters was examined by immersing the UV filter-laden fabrics into a) distilled water, b) a dilute acetic acid solution (pH~4), and c) a NaOH (0.05 M) solution while agitated (50 rpm) for 24 h. No leaching of UV filters was observed in distilled water and diluted acetic acid solutions. In NaOH, on the other hand, most UV filters leached into the solution due to NaOH digestion of the MOR-1[522]. Still, no quantitative calculation could be

performed because several unidentified peaks appeared (more peaks may have been present and could not be detected by the UV detector), possibly due to the alkaline hydrolysis of the UV filters. Based on these results, it can be inferred that storing and disposing of contaminated cotton in non-alkaline media poses no threat to the environment.

2.2.4 Conclusions

This work demonstrates a new remediation method that amalgamates the principles of *in-situ* remediation by sorbent amendment and extraction. Incorporating nanosorbent materials on bulk supports addresses the challenges associated with the addition of sorbents in soil by enabling not only the easy addition of the sorbent medium into the soil to sorb the contaminants but also its retrieval, thus accomplishing both the extraction of the contaminants from soil and the removal of the contaminant-laden sorbent. Using cotton fabrics decorated with MOFs, we demonstrate the remediation of soils from hydrophobic organic compounds, achieving satisfactory removal efficiencies within relatively short periods. The remediation efficiency could likely be further enhanced by increasing the mixing frequency to maximize contact, using simple mechanical means such as plowing. Notably, the sorbent can be reused several times, decreasing the remediation cost or safely disposed of without specialized treatment. Another advantage of the method is that adding bulk-supported nanosorbents may also contribute to preventing future pollution. Both applications (remediation and prevention) may be particularly interesting for managing sediments, where *ex-situ* treatment methods have been the only available option, often with limited success due to the secondary implications in water quality and biota.

2.3 Extraction and passive sampling of gold nanoparticles and gold ions using a Zr (IV) MOF-cotton composite with thiophene functional groups

2.3.1 Introduction

The exponential increase in the use of nanomaterials in many consumer products and industrial processes has raised concerns regarding their release into the environment and their potential risks to humans and living organisms [523], [524]. These concerns were initially supported by probabilistic and material flow algorithms, that predicted the release of nanomaterials in the environment [525], [526], [527] and verified when trace levels (i.e. ng/L or pg/L) of several nanoparticle species, such as Ag, Au, Ce, Ti, Cu and Zn, were determined in various environmental waters (surface waters, seawater, drinking water, wastewater), as well as in biota [528], [529], [530], [531], [532], [533].

Although the levels of nanomaterials in natural waters appear to be low, the reported concentrations were determined in samples collected by grab sampling from various aquatic systems. This approach, only provides a “snapshot” of the levels of the contaminants at the time and place of sampling without accounting for temporal fluctuations (seasonal or diurnal) and for spatial variations as well as for acute pollution events [534], [535]. This fact, along with the limited number of extensive monitoring surveys for nanoparticle species in the environment [528], [529], [530], [531] may contribute to the underestimation of their presence in aquatic systems and wastewater streams.

The technique of passive sampling is a plausible way to overcome the limitations of grab (spot) sampling while perform continues monitoring over long periods of time. The principle of passive sampling is based on the use of a sorbent (receiving phase) that is exposed into the

EXPERIMENTAL

environmental medium (donor phase) for a period of many days or weeks so that it can passively sorb and retain the contaminants. The sorbent phase is then extracted to determine the concentration of the contaminants accumulated during the duration of sampling and averaged over the total sampling period to calculate a time-weighted average concentration (TWA) [534], [535], [536]. In that manner, passive sampling can be used for screening the presence of waterborne contaminants for long periods of time, monitor temporal trends in water quality, investigate spatial distribution of pollution sources and identify acute pollution events. Another advantage of this technique is that it measures the soluble concentrations of the target contaminants that are related to organism exposure and potential bioaccumulation [536]. Due to these advantages, a large research effort has been devoted to passive sampling of inorganic and organic pollutants resulting in the commercialization of many devices (DGTs, POCIS, Chemcatcher, etc) [534], [535], [536], [537]. However, no receiving phases for the passive sampling for nanosized particle species have been developed yet.

In this work, aiming to address the lack of passive sampling sorbent phases for nanoparticle species, we designed a new sorbent phase consisting of a novel Zr-MOF material with thiophene functional groups and immobilized it onto a bulk support comprised of cotton fabrics. We used MOFs, over other sorbent phases, due to their exceptional sorption properties stemming from the high surface area, the tunable porosity and tailor-made surface modification [538], [539], while thiophene functionalization was employed because of its good stability and high affinity of most metals for sulfur. The new sorbent offers several advantages compared to previous sorbents for nanoparticles as a) it does not use thiols, which are easily oxidized in water and air [540], b) it does not rely on the entrapment of nanoparticle inside the pores of the sorbent, thus avoiding limitations imposed by the size of nanoparticles [541], [542], and c) it does not rely on electrostatic

interactions which can only attract oppositely charged nanoparticles [543], [544]. The immobilization of the MOF-thiophene on cotton fabric offer several additional benefits to its use as a receiving (extraction) phase: a) it enhances sorption and the mass transfer rates due to the improved permeability of water through the fabric pores and the large primary contact surface area of the cotton substrate [545] b) it facilitates handling, because cotton is a lightweight and flexible material that can be easily adjusted to various sizes and shapes, fitted to sampling devices and easily processed after use. Overall, this work paves the way towards the development of passive sampling sorbent phases for nanoparticle species, using bulk supported nanosorbents. Moreover, the modified fabrics can be used also as a sorbent for benchtop sample preparation and extraction of metal nanoparticles; a proof-of-concept demonstration of this application is also presented.

2.3.2 Experimental procedure

2.3.2.1 Chemical and Materials

Thiophene-2-carboxaldehyde, 98+% was from Thermo Fisher Scientific (Kandel, Germany). Zirconium chloride (99.5%+, metal basis) was obtained from Alfa-Aesar (Kandel, Germany). 2-aminoterephthalic 99% (NH₂-BDC) was from Acros Organics (Geel, Belgium). Hydrogen tetrachloroaurate trihydrate ($\geq 99.9\%$ trace metals basis), sodium borohydride, tri-sodium citrate, polyvinyl pyrrolidone (PVP₁₀, MW 10,000), cetyltrimethylammonium bromide (CTAB), tris(hydroxymethyl) aminomethane (tris-base) 99.9%, L-Cysteine 96%, L- ascorbic acid and glacial acetic acid $\geq 99.7\%$ were obtained from Sigma-Aldrich (Steinheim, Germany). 3-hydroxytyraminium chloride $\geq 99.0\%$, hydrogen peroxide solution 30%, N, N-Dimethylformamid (for synthesis) and acetone were procured from Merck (Darmstadt, Germany). Glycine (analytical grade) was obtained from Serva Fein Biochemica (Heidelberg, New York). HPLC- grade

EXPERIMENTAL

methanol was retrieved from Fisher Scientific (Loughborough, UK). Hydrochloric acid (puriss. p.a.) and diethyl ether were obtained from Honeywell Fluka (Seelze, Germany). Nitric acid 65% G.R. was obtained from Lachner (Neratovice, Czech Republic). Sodium hydroxide was from Mallinckrodt (Dublin, Ireland).

2.3.2.2 Instrumentation

A Shimadzu AA-6800 (Shimadzu Corp., Kyoto, Japan) flame atomic absorption spectrophotometer (FAAS) with a self-reversal hollow cathode lamp (Heraeus, Hanau, Germany) operating at 10 mA was used for the measurements of gold ions and AuNPs which were made at 242.8 nm. Instrumental calibration was performed according to the specifications of the manufacturer using standard solutions of gold ions in the range of 0-20 mg L⁻¹. To estimate the nanoparticles size spectrophotometric measurements were performed in a Jenway 6405 UV/Vis spectrophotometer (Essex, UK) with matched quartz cells of 1 cm path length.

Power XRD (pXRD) diffraction patterns were recorded on a Bruker D2 Phaser X-ray diffractometer (CuK α radiation, wavelength = 1.54184 Å). Scanning electron microscopy (SEM) measurements were performed with a Phenom Pharos G2 Desktop FEG-SEM (Thermo Fisher Scientific) on Cr sputtered specimens (Q150T ES Plus automatic sputter coater, Quorum Technologies Ltd.) IR spectra were recorded on a Perkin Elmer Spectrum Two attenuated total reflectance-IR (ATR-IR) spectrometer. Zeta potential measurements were carried with a Malvern Zetasizer Nano ZS (Malvern Panalytical, Worcestershire, UK) in a two-electrode capillary cell.

2.3.2.3 Synthesis of 2-((thiophene-2-ylmethyl) amino) terephthalate (TATP2)

The formation of the TATP2 ligand is based on the formation of a Schiff (imine) base between the amino group of 2-terephthalic acid and the carbonyl group of 2-thiophene-carboxaldehyde which is reduced to form an amine. In detail, 2-thiophenecarboxaldehyde (1.5ml, 16.5mmol) was added in 60ml of a methanol containing 1.2 g (6.6 mol) of 2-amino terephthalic acid and stirred for 2h until a milky pale-yellow solution was formed. Solid sodium borohydride, as a reductant (2.5g, 66.08mmol) was added to the solution in small portions to avoid excessive bubbling, the vials were sealed, and the reaction was left to proceed overnight at room temperature under stirring. Then, 60ml of diethyl ether were added solution and a white precipitate was formed which was isolated by filtration. The precipitate was dried (60-80°C), redissolved in 50ml distilled water, precipitated again by acid treatment by the dropwise addition of 6M acetic acid until the pH of the solution was 5. The yellow organic ligand, 2-((thiophene)-2ylmethyl) amino) terephthalic acid (TATP2) was finally isolated by filtration, washed twice with 5ml of distilled water, once with a mixture of 1:5 methanol/water and dried at 60-80°C for 24h. The yield of this synthesis was 0.9g.

2.3.2.4 Fabrication of MOR-3@ cotton fabric

The in-situ synthesis and deposition of the MOF ($\text{H}_{16}[\text{Zr}_6\text{O}_{16}(\text{TATP})_{3.54}(\text{NH}_2\text{-BDC})_{0.46}]$, MOR-3) on the PDA-coated fabric was performed by the addition of the PDA-coated fabric into a 50ml conical flask containing ZrCl_4 (0.06g, 0.257mmol) and TATP2 (0.1g, 0.36mmol) in 8ml dimethylformamide / 1.2ml glacial acetic acid. The flask was sealed and heated at $85\pm 3^\circ\text{C}$ for 4h to form and in-situ deposit the MOR-3 particles on the surface of the PDA-coated fabric. The MOR-3@ cotton fabric was washed sequentially with distilled water and acetone, dried at 80°C and stored in a desiccator until use. The amount of MOR-3 deposited on the fabric was calculated

by accurately weighting the fabric before and after deposition of MOR-3 yielding a mass of 1 mg MOR-3 per 1 cm² fabric.

2.3.2.5 Synthesis of AuNPs

2.3.2.5.1 Citrate capped AuNPs (CA@AuNPs) with different size distributions

Citrate capped AuNPs (CA@AuNPs) of variable average size distribution were synthesized by reduction of AuCl₄⁻ from NaBH₄ in the presence of tri-sodium citrate as stabilizer or by using tri-sodium citrate both as a reducing agent and as a stabilizer, using standard procedures reported in the literature[546], [547], [548].

2.3.2.5.2 CA@AuNPs 4nm in diameter

Citrate capped AuNPs (CA@AuNPs, **~4nm in diameter**) were synthesized by reduction of AuCl₄⁻ from NaBH₄ in the presence of tri-sodium citrate as stabilizer[547]. For the synthesis of 20mL AuNP stock solution, 0.5mL of tri-sodium citrate (10.0mM) and 0.5mL of HAuCl₄.3H₂O (10.0mM) standard solution were mixed with 18.5mL of distilled water. To this mixture 0.5mL of a freshly prepared solution of NaBH₄ (0.1M) was added rapidly under stirring. The color of the solution changes immediately from slightly yellow to wine-red upon the addition of borohydride signified the formation of CA@AuNPs, 4nm. The mixture was stirred for another 10min and stored in dark for 24h before use to allow aging of the particles and establishment of a stable solution.

2.3.2.5.3 CA@AuNPs 7nm in diameter

Larger AuNPs were prepared by controlling the composition of the reactants. Specifically, for the preparation of CA@AuNPs (**~7nm in diameter**), 250μL of a HAuCl₄.3H₂O (25.4mM) standard solution was quickly added into 24.75ml of a boiling tris-sodium citrate (1.22mM)

aqueous solution under constant stirring. The solution was kept gently boiling until a wine-red color appeared.

2.3.2.5.4 CA@AuNPs 15nm in diameter

For the preparation of CA@AuNPs (**~15nm in diameter**), 150mL of aqueous solution of $\text{HAuCl}_4 \cdot 3\text{H}_2\text{O}$ (0.25mM) was brought to boil under constant stirring and 2.8mL of tris-sodium citrate (1.0% w/v) was quickly added. The solution was kept gently boiling until a wine-red color appeared [546].

2.3.2.5.5 CA@AuNPs 25nm in diameter

CA@AuNPs (**~25nm in diameter**) were prepared by bringing to boil 100mL of $\text{HAuCl}_4 \cdot 3\text{H}_2\text{O}$ (0.25 mM) followed by the addition of 1.0mL of 1.0% w/v aqueous solution of tris-sodium citrate. The solution was kept gently boiling until a wine-red color appeared[547].

2.3.2.5.6 CA@AuNPs 40, 60 and 80nm in diameter

To prepare CA@AuNPs (**~40, 60 and 80nm in diameter**) 50mL of $\text{HAuCl}_4 \cdot 3\text{H}_2\text{O}$ (0.25mM) solution was heated to boiling while stirring. Then, 330, 230 and 210 μL of 1.0% w/v tris-sodium citrate was quickly added to form CA@AuNPs with sizes 40, 60 and 80nm, respectively, and the color of the solution changed to purple red[548]. The larger the size of the CA@AuNPs the more purple the color of the solution. All suspensions were aged for 24h at room temperature and stored at 4°C for 15 days.

2.3.2.6 AuNPs with different coatings

Using the as synthesized CA@AuNPs, various AuNPs with different coatings were prepared according to previous methods[549], [550].

2.3.2.6.1 PVP₁₀ coated AuNPs (PVP₁₀@AuNPs)

PVP₁₀ coated AuNPs were prepared by mixing 10mL of an aqueous CA@AuNPs suspension with 1.1mL of PVP₁₀ (0.02mM in distilled water), stirred for 20h.

2.3.2.6.2 Cysteine coated AuNPs (Cys@AuNPs)

Cysteine coated AuNPs (Cys@AuNPs) were prepared by mixing 10ml of a CA@AuNPs suspension with 200μL cysteine solution (1.0mM), stirred for 10 min and aged for 24h in dark.

2.3.2.6.3 Glycine coated AuNPs (Gly@AuNPs)

Glycine capped AuNPs (Gly@AuNPs,) were prepared by adding 200μL of glycine (1mM) to 10mL of an aqueous CA@AuNPs suspension under continuous stirring for 20 min at 1000rpm. This solution then allowed to age overnight.

2.3.2.6.4 CTAB coated AuNPs (CTAB@AuNPs)

Synthesis of CTAB stabilized AuNPs (CTAB@AuNPs), was performed according to the seeding growth method [550], [551]. Briefly, CA@AuNPs (~4nm in diameter) were prepared as described above and were used as seeds. A growth solution was then prepared by mixing 200mL of 0.1M CTAB with 5mL of HAuCl₄.3H₂O (10.0mM) standard solution. Growth mixture was prepared by mixing 9mL of the growth solution with 50mL of 0.1M ascorbic acid. Then, 2.5mL of CA@AuNPs seeds were added to the growth mixture to prepare CTAB@AuNPs of 5.5nm in diameter.

The average size distribution and the molar concentration of the synthesized AuNPs were calculated from their UV-Vis spectra[552]. Specifically, the average size distribution in each AuNP suspension was first calculated by the ratio of the absorbance of AuNPs at the surface plasmon resonance peak to the absorbance at 450 nm. Based on the estimated size

distribution, the concentration of AuNPs was calculated by dividing the absorbance at 450 nm with the molar decadic extinction coefficient at $\lambda=450$ nm[552].

2.3.2.7 Batch sorption studies

Batch sorption experiments were conducted at room temperature with a volume-to-mass (MOR-3) ratio (V:m) of 6000 mL/g. Sorption kinetics of AuNPs were studied using 50 mL aqueous solutions and a semicircular (12.56 cm^2) MOR-3@fabric at pH 3 using 5.6 nM PVP@Au NPs (4nm) (3 mg/L as AuCl_4^- ions) while the sorption kinetics of AuCl_4^- ions was studied at pH 6, also at 3 mg/L of AuCl_4^- ions. The solutions were agitated at different reaction times ranging from 1 to 1440 min in an orbital shaker at 150 rpm. At specific time intervals, the aqueous supernatant was analyzed for its content in AuNPs or AuCl_4^- ions (expressed as mg/L AuCl_4^- ions) by atomic absorption spectroscopy (AAS).

The uptake of AuNPs by MOR-3@fabric was investigated at pH 3 by determining the sorption efficiency of PVP@AuNPs (5nm) (0.84-134.4 nM PVP@AuNPs containing 0.5–80 mg/L AuCl_4^- ions, respectively) after 3h of mixing in an orbital shaker at 150 rpm. The sorption of AuCl_4^- ions was studied at pH 6 in the presence of 0.5–500 mg/L AuCl_4^- ions after 1h of orbital mixing at 150 rpm. All experiments were run in triplicate and the results were averaged.

The above batch sorption experiments were also performed using 8 mg of MOR-3 powder to compare the sorption properties of MOR-3 with MOR-3@fabric.

2.3.2.8 Calibration of MOR-3@ cotton fabric as passive sampling receiving phase

The calibration of MOR-3@ cotton fabrics for passive sampling was performed by static renewal exposure experiments[553]. Eight semi-circular fabrics of 12.56cm² surface area each, were fixed on a metallic holder (stainless steel mesh of 1mm wire thickness and 6mm mesh pore size) and immersed into 3L aqueous sample solution fortified with 0.094 nM PVP@AuNPs (50µg L⁻¹ AuCl₄⁻). The sample was mixed by stirring at 300 rev/min, at 20°C and renewed daily to ensure constant exposure conditions. To investigate the accumulation kinetics of AuNPs in the MOR-3@ fabric phase, one fabric was removed from the vial every other week and analyzed for the uptake of AuNPs. The calibration of the passive sampler was performed for 110 consecutive days and the data were used to calculate the sampling rate (R_s , L d⁻¹), which is the volume of water extracted per a unit of time and is represented by the formulae:

$$R_s = \frac{M}{C_w \times t}$$

where $M(\mu\text{g})$ is the amount of a chemical accumulated in the sampler, $C_w (\mu\text{g L}^{-1})$ is the concentration of AuNPs in water and t (days) is the deployment time during the linear uptake phase. The calculation of R_s was performed in the linear uptake phase of the uptake profile, by taking the slope of M/C_w versus deployment time. Control experiments (water samples containing the fabric samplers but not PVP@AuNPs, and water samples containing PVP@AuNPs but not fabric samplers) were deployed to account for contamination of the samplers or loss of analytes, not attributed to PVP@AuNPs, respectively. The results showed no contamination of the samplers and trivial loss of PVP@AuNPs (<5%), therefore, correction to the calculated concentrations was not deemed necessary.

2.3.2.9 Extraction and determination of AuNPs in water samples based on fabric phase sorptive extraction

For the extraction of AuNPs, Au ions or their mixture a 50 mL aliquot of an aqueous sample solution was adjusted to pH 3 with dilute HCl (0.05M) using a pH-meter. A semicircular MOR-3@fabric (12.56 cm²) was immersed into the sample and mixed for 1h, at room temperature in an orbital shaker at 150 rpm.

After sorption, the fabrics were removed with the plastic tweezers and dried on blotting paper at ambient conditions with the aid of Kimwipe disposable wipers. The desorption of AuNPs was accomplished by immersing the semicircular fabrics in 5 mL of elution solvent (0.1 M NaOH/H₂O₂) for 1 h with interim vortex agitation. The extract was centrifuged at 1500 rpm for 10 min (to remove any fabric impurities) without precipitating AuNPs, and directly analyzed by AAS.

2.3.2.10 Application of MOR-3@cotton as solid phase extraction disks

MOR-3@cotton fabrics were cut into pieces of 2.5 × 2 cm and folded. The fabric was inserted into a 3 mL SPE cartridge which was placed in a SPE filtration apparatus. The fabrics were firstly conditioned with 6 mL of water and 50 mL of aqueous sample, containing PVP@AuNPs (4 nm) adjusted to pH 3 were percolated through the fabric at a flow rate of 5 mL min⁻¹. The fabric was dried under vacuum and the retained AuNPs were eluted with 3 mL of NaOH:H₂O₂ (0.1M). The extract was centrifuged at 1500 rpm for 10 min, and directly analyzed by AAS.

2.3.2.11 *Real samples*

The efficiency of the MOR-3@fabric as a sorbent for sample preparation, was examined using four genuine water samples with variable matrix complexity (tap, seawater, lake, and river) that were collected from the local water supply network, Kiani Akti beach (Preveza, Greece), Lake Pamvotis (Ioannina, Greece) and Louros river (Epirus region, NW Greece), respectively. The samples (1,5L) were retrieved in plastic vials and filtered through 0.45 μm filters to remove suspended solids and stored at 4°C. Before analysis the samples were fortified with known concentrations of AuNPs.

2.3.3 Results and discussion

Since MOR-3 is a new MOF, the sorption properties of MOR-3@fabric for AuNPs were firstly evaluated using batch sorption studies. We used PVP coated AuNPs due to their high stability stemming from the bulky polymer coating that can stereochemically protect AuNPs, minimizing interactions (such as electrostatic, formation of chemical bonds, etc) not only with other sample components but also between AuNPs. Because of the high affinity of noble metals for sulfur, the reactivity of the sorbent for AuCl_4^- ions was also examined.

2.3.3.1 *Characterization of MOR-3@cotton fabrics*

The PXRD patterns of Figure 2.3.3.1.a reveal that MOR-3 was successfully synthesized and immobilized on the cotton, as evidenced by the characteristic diffraction peaks of MOR-3 at 2θ of 7.3° and 8.5° corresponding to (111) and (200) planes, respectively.

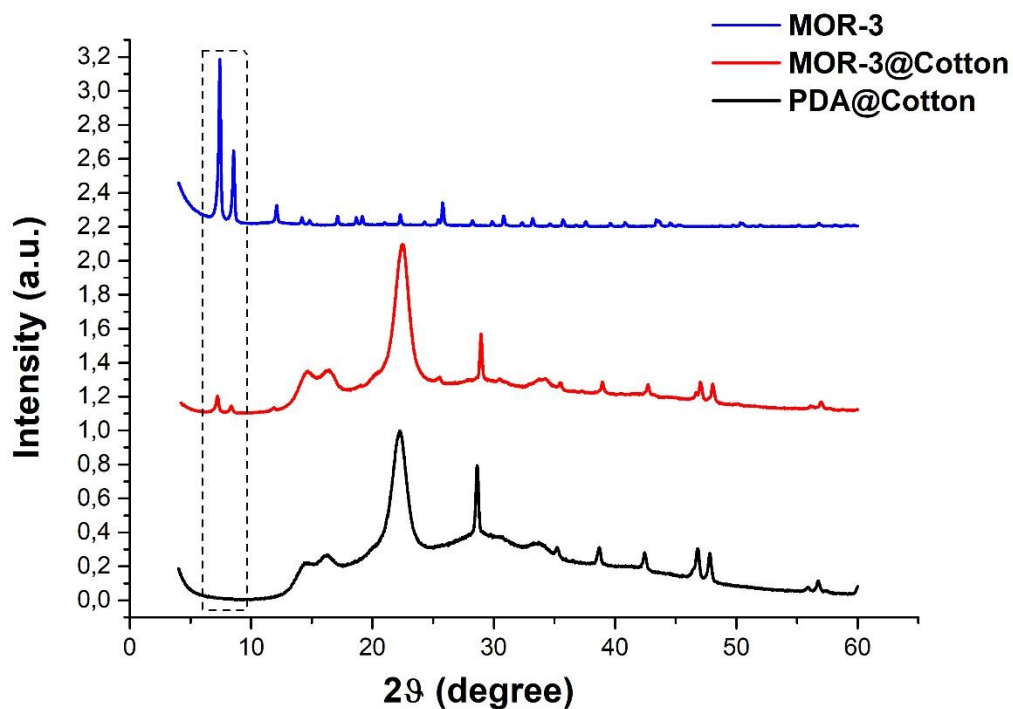


Figure 2.3.3.1.a XRD pattern of PDA@cotton, MOR-3@cotton and MOR-3 powder.

Additional evidence to the incorporation of MOR-3 on the cotton surface was obtained from the ATR-IR spectra of MOR-3@cotton fabric, which shows the most characteristic bands of MOR-3 such as the stretching vibration of N-H at 3375 cm^{-1} and the asymmetric $\nu_{\text{as}}(\text{COO}^-)$ and symmetric $\nu_{\text{s}}(\text{COO}^-)$ stretching vibrations of carboxylate anions at 1565 and 1386 cm^{-1} , respectively (Figure 2.3.3.1.b). The distance in the wavenumbers of these two vibrations is 179 cm^{-1} , corresponding to bidentate interaction of carboxylate anions[554].

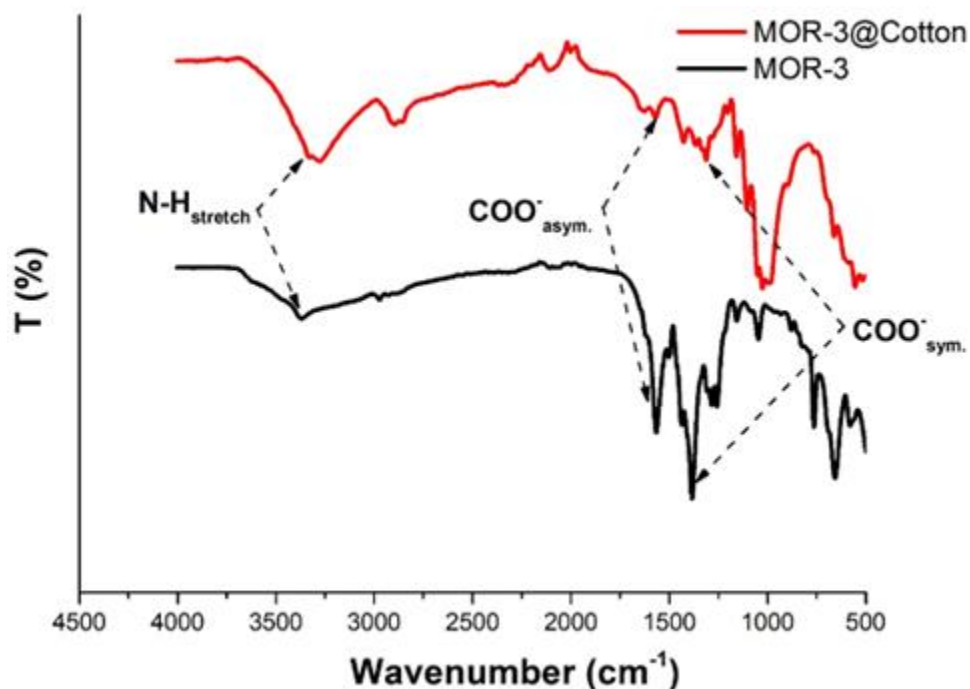


Figure 2.3.3.1.b IR spectra MOR-3@cotton and MOR-3 powder.

FE-SEM images show that MOR-3 in powder form appears as uniformly sized cubic particles of 160-220 nm while the SEM images of MOR-3@cotton fabric show the high coverage of the cotton fibers with MOR-3 particles (Figure 2.3.3.1.c(a),(b)). Finally, the surface charge of the sorbent was explored by ζ -potential measurements. The zeta potential of the MOR-3 powder was +26.2 mV indicating that the sorbent has a positive surface charge.

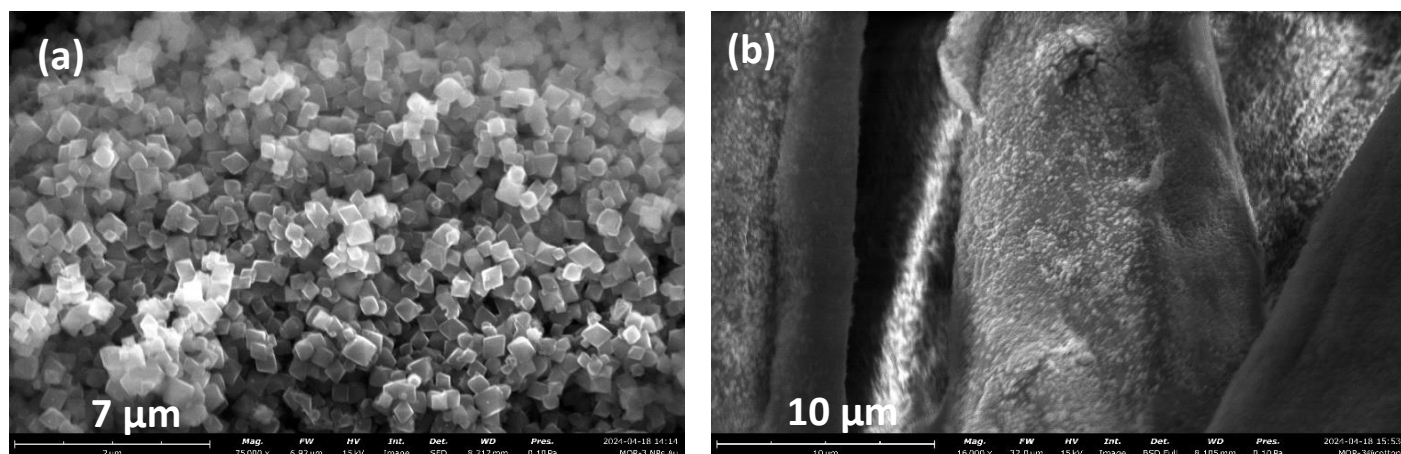


Figure 2.3.3.1.c SEM images of (a) MOR-3 powder and (b) MOR-3@ cotton.

After sorption of AuNPs and Au ions the yellow color of the MOR-3 powder turned to pale brown and purple in the presence of AuNPs and Au ions, respectively (Figure 2.3.3.1.d(a)). These color transitions were not evident in the MOR-3@ cotton, however, due to the blank coloration of the cotton fabric after treatment with PDA (Figure 2.3.3.1.d(a)). The diffuse reflectance spectra of the MOR-3 powder depicted in Figure 2.3.3.1.e shows the appearance of two absorption bands at 525 and 545 nm, which are characteristic of AuNPs. This observation also indicates that during sorption, Au ions are reduced to AuNPs.

EXPERIMENTAL

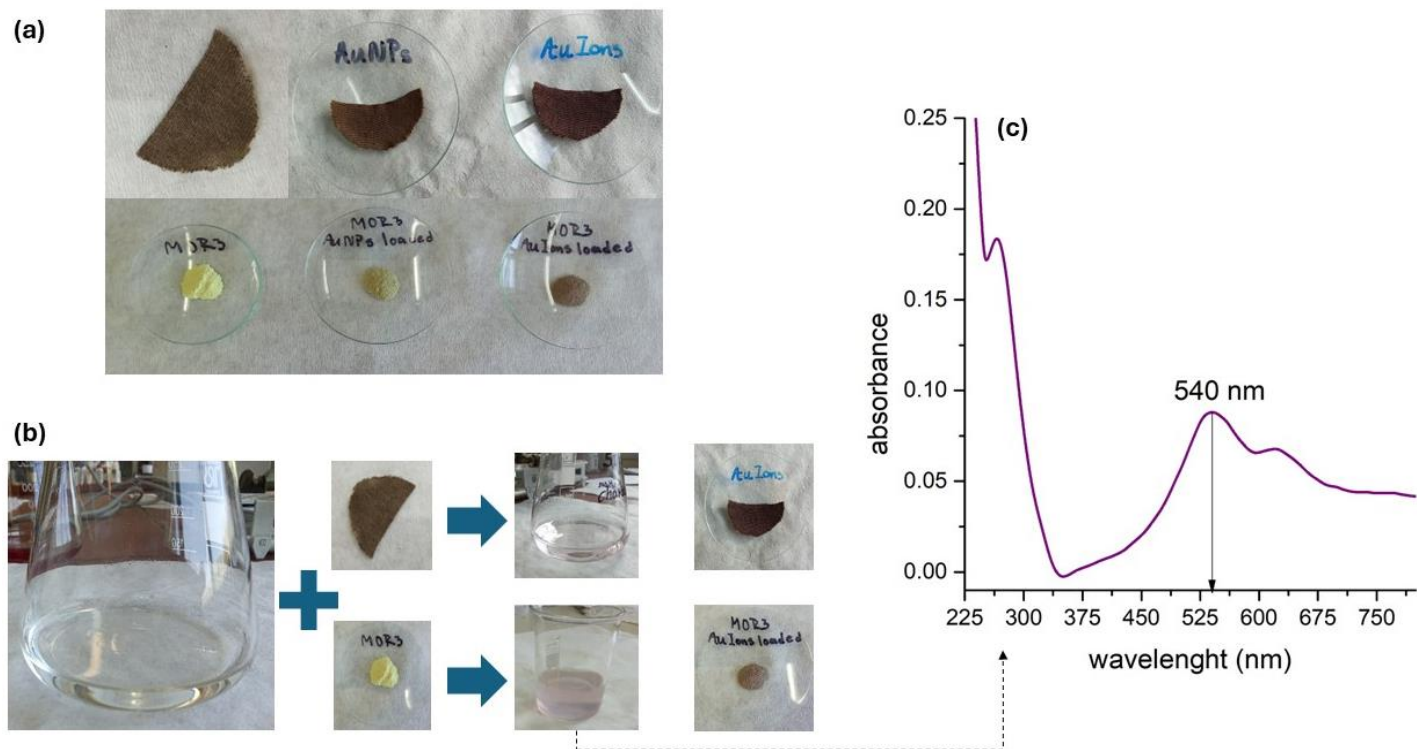


Figure 2.3.3.1.d (a) MOR-3@fabric (upper image) and MOR-3 powder after sorption of PVP@AuNPs and AuCl_4^- ions, (b) color of the solutions and the sorbents after sorption of AuCl_4^- ions on MOR-3@fabric (upper image) and MOR-3 powder (lower image), (c) UV-Vis spectra of the aqueous solution after sorption of 50 mg/L of AuCl_4^- ions on MOR-3 powder.

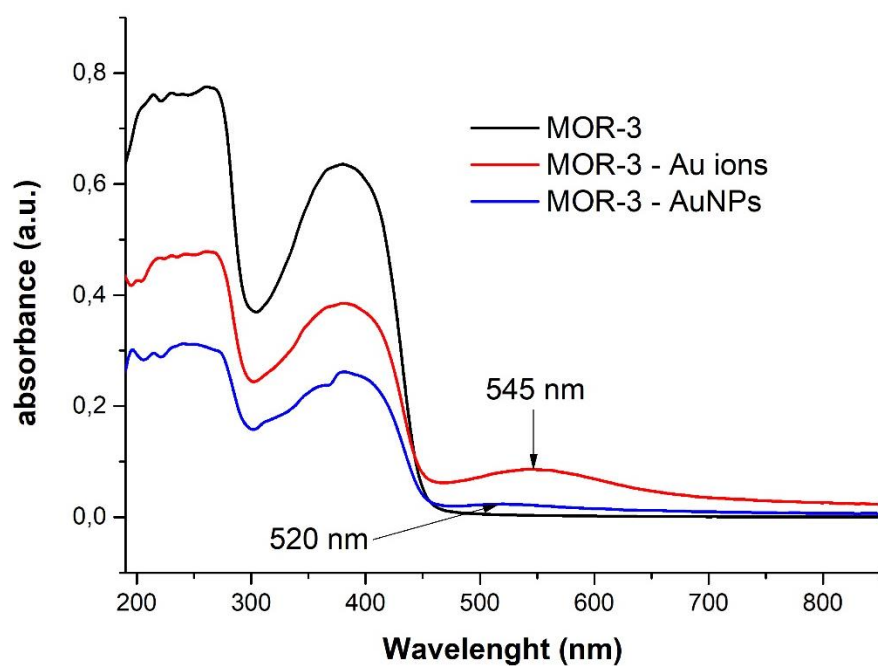


Figure 2.3.3.1.e Absorbance spectra (Kubelka-Munk transformed diffuse reflectance spectra) of MOR-3 powder after sorption of AuNPs and Au ions.

FE-SEM, EDS spectra and TEM images of the MOR-3 powder confirm the sorption of AuNPs and Au ions as well as the reduction of Au ions on MOR-3 (Figure 2.3.3.1.f).

EXPERIMENTAL

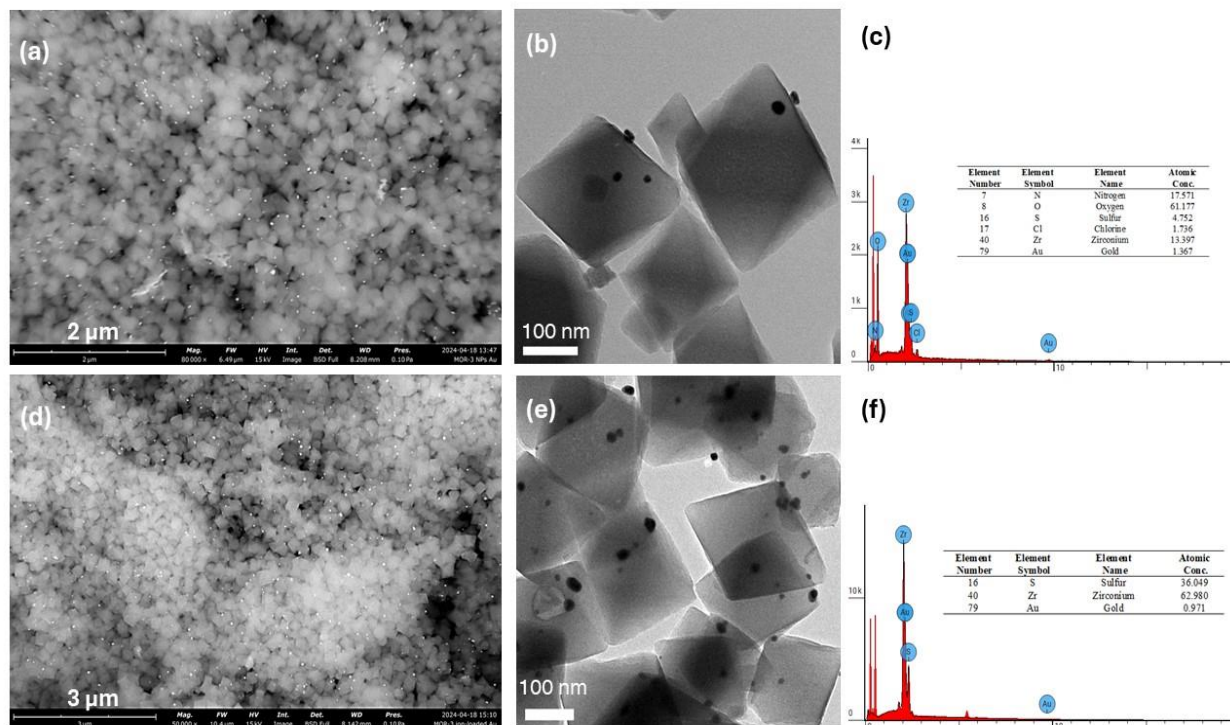
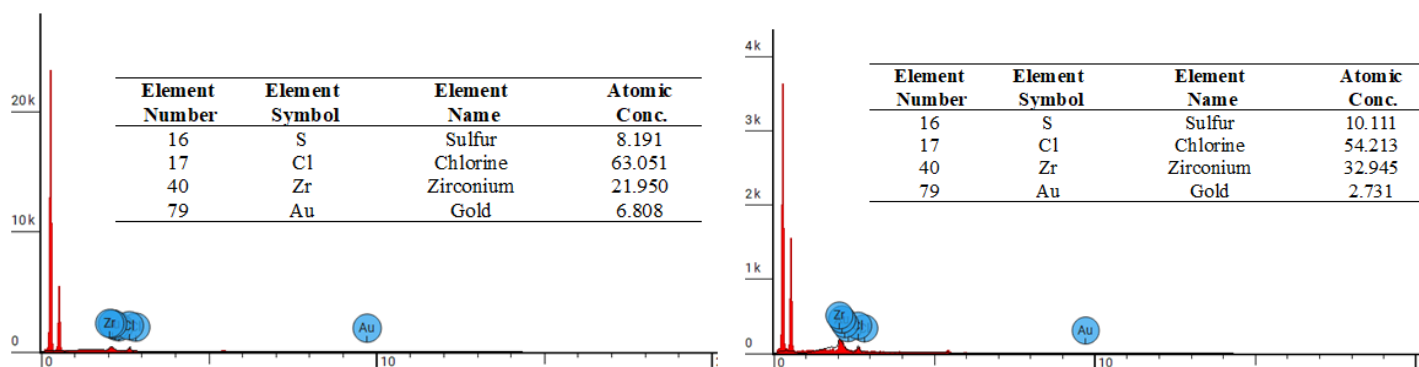


Figure 2.3.3.1.f SEM and TEM images and EDS spectra of MOR-3 powder after sorption of PVP@AuNPs (a,b,c) and Au ions (d,e,f).

The sorption of AuNPs and Au ions on MOR-3@ cotton was not visible in SEM and TEM but the EDS spectra confirm their presence on the sorbent surface (Figure 2.3.3.1.g).



EXPERIMENTAL

Figure 2.3.3.1.g EDS spectra of MOR-3@cotton after sorption of (a) PVP@AuNPs and (b) Au ions.

Following these observations, the stability of MOR-3@cotton fabric during the sorption was investigated. Both the pXRD pattern and the IR spectra of MOR-3 and MOR-3@cotton after sorption of AuNPs and Au ions show no changes indicating that the sorbent, either in powder form or immobilized on cotton, retains its stability during sorption (Figure 2.3.3.1.h).

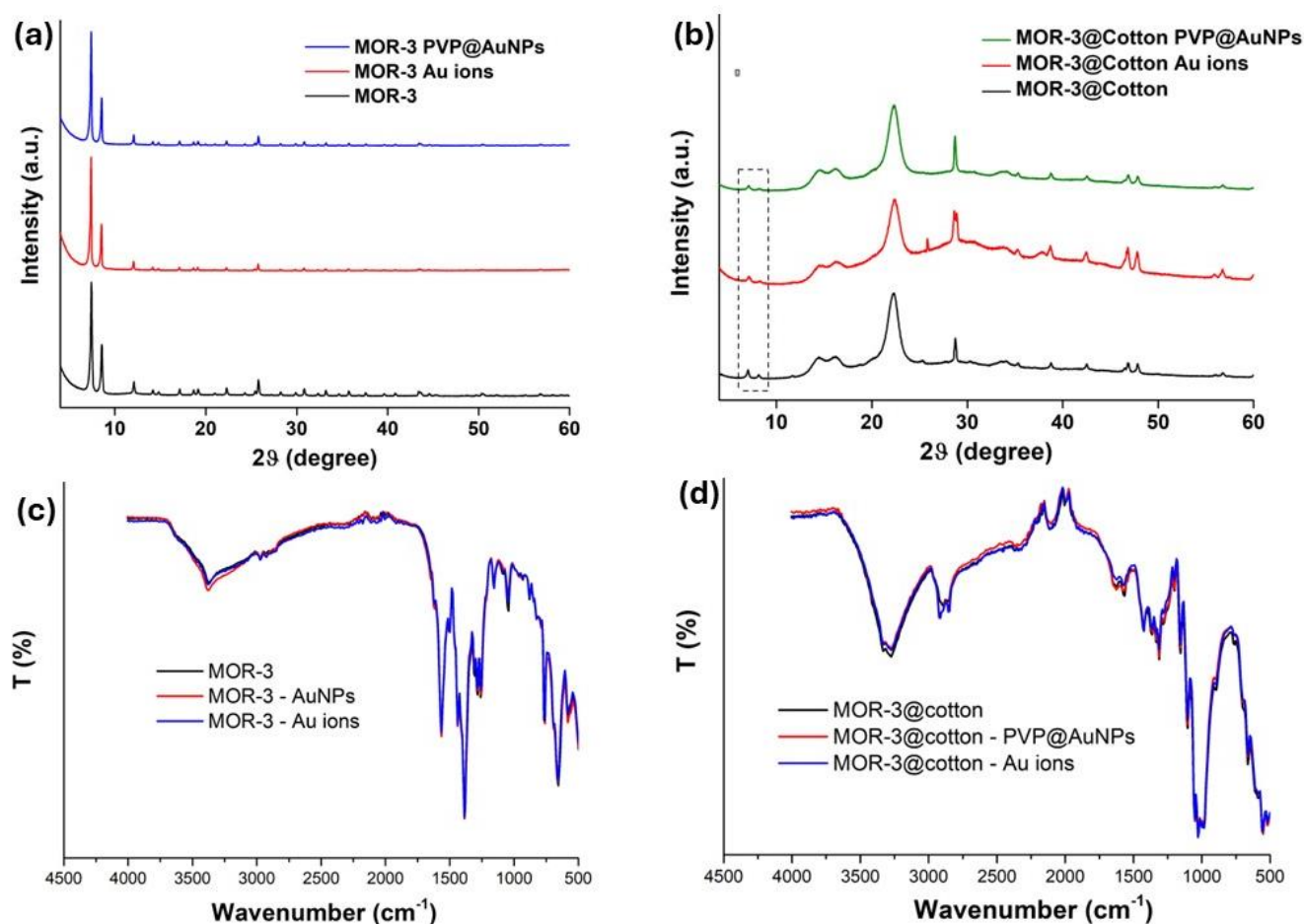


Figure 2.3.3.1.h pXRD patterns and IR spectra of (a,c) MOR-3 and (b,d) MOR-3@cotton after sorption of PVP@AuNPs and Au ions.

2.3.3.2 Effect of pH on sorption

The optimum pH that maximizes the sorption of AuNPs and AuCl_4^- ions was surveyed by adjusting the pH of the sample solutions from 3 to 8 using dilute HCl and NaOH solutions. Experiments were performed in 50 mL aqueous solutions containing each species separately to avoid co-extraction. A semicircular MOR-3@fabric was immersed into each sample and mixed at room temperature, in an orbital shaker at 150rpm, overnight. The residual concentration of AuNPs and Au ions in solution were determined by FAAS. When the residual concentration was below the measurable range by FAAS, sorption efficiency was determined by extracting either species from the MOR-3@cotton fabric with 5mL of aqua regia (diluted by 2-fold) by stirring the MOR-3@fabric at 900rpm overnight.

The results of Figure 2.3.3.2 show that the MOR-3@fabric exhibits pH-dependent selectivity against AuNPs and AuCl_4^- ions. At acidic pH values both AuNPs and AuCl_4^- ions are effectively extracted but at pH 6 the sorption efficiency of AuNPs deteriorates dramatically (from 85% to 10%). This observation imbues the material with some selectivity against AuNPs and AuCl_4^- ions by adjusting the pH of the solution, however, co-sorption is not totally avoided. The observed pH-dependent selectivity may be a complex phenomenon related to a planar-to-nonplanar transition of the thiophene backbone[555], [556] and π - π stacking of adjacent thiophene units [557], with decreasing pH (from neutral to acidic) [558]. The non-planar structure and the stacking of thiophene chains at acidic pH values leads to the formation of a three-dimensional arrangement that favors the interaction with AuNPs and AuCl_4^- ions. At higher pH these structural transitions are not favored and the interaction with AuNPs is less efficient (the bulk polymer coating of AuNPs probably also contributes to the lower interaction with MOR-3). On the contrary, AuCl_4^- ions are

not affected by pH because its sorption occurs both by electrostatic interactions with the positively charged MOR-3 surface (z-potential=+26.2 mV) as well as by the formation of Au-S bonds.

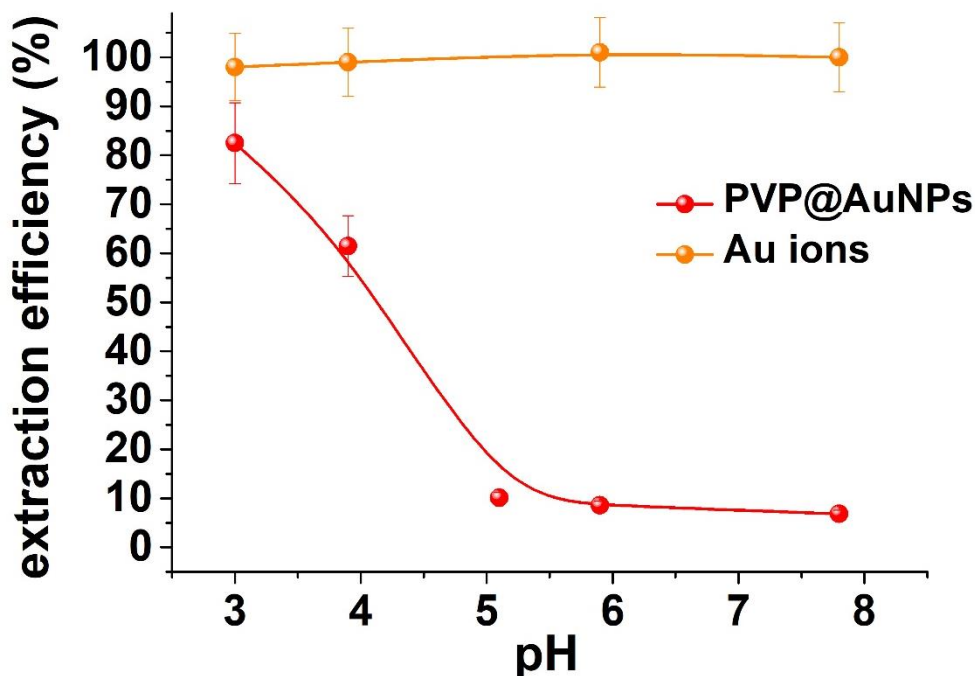


Figure 2.3.3.2 Effect of pH on the extraction efficiency of MOR3@fabric for the uptake of PVP@AuNPs and Au ions.

2.3.3.3 Investigation of the sorption kinetics

Considering the influence of pH on the sorption behavior of AuNPs and AuCl_4^- , the investigation of sorption kinetics was studied through batch sorption experiments at pH 3 for PVP@AuNPs (5 nm, 3 mg/L Au) and at pH 6 for AuCl_4^- ions (3 mg/L), at separate aqueous solutions, using a semi-circular MOR-3@fabric at variable time intervals. The sorption kinetics were then fitted to the pseudo-first order (PFO) and pseudo-second order (PSO) kinetic models (Figure 2.3.3.3, panels a and b).

The sorption kinetics of PVP@AuNPs could only be described by the Ho McKay pseudo-second order (PSO) kinetic model which means that chemical sorption is the main removal

EXPERIMENTAL

mechanism and is attributed to the formation of AuNP-thiophene bonds. With regard to AuCl_4^- ions, although fitting with the Ho McKay pseudo-second order (PSO) kinetic model was satisfactory ($R^2=0.97$) the kinetic sorption data could better be described by the Lagergren's pseudo-first-order (PFO) model ($R^2=0.99$) indicating that the sorption of AuCl_4^- ions is a multi-stage process that occurs mainly through physical mechanisms while chemical sorption contributes to a lesser extent. The contribution of physical sorption may be explained by a) the electrostatic interactions of AuCl_4^- with the positively charged MOR-3 surface and b) the oxidative polymerization of thiophene from AuCl_4^- which occurs through the reduction of AuCl_4^- towards the formation of AuNPs [559], [560], increasing the heterogeneity on the MOR-3 surface.

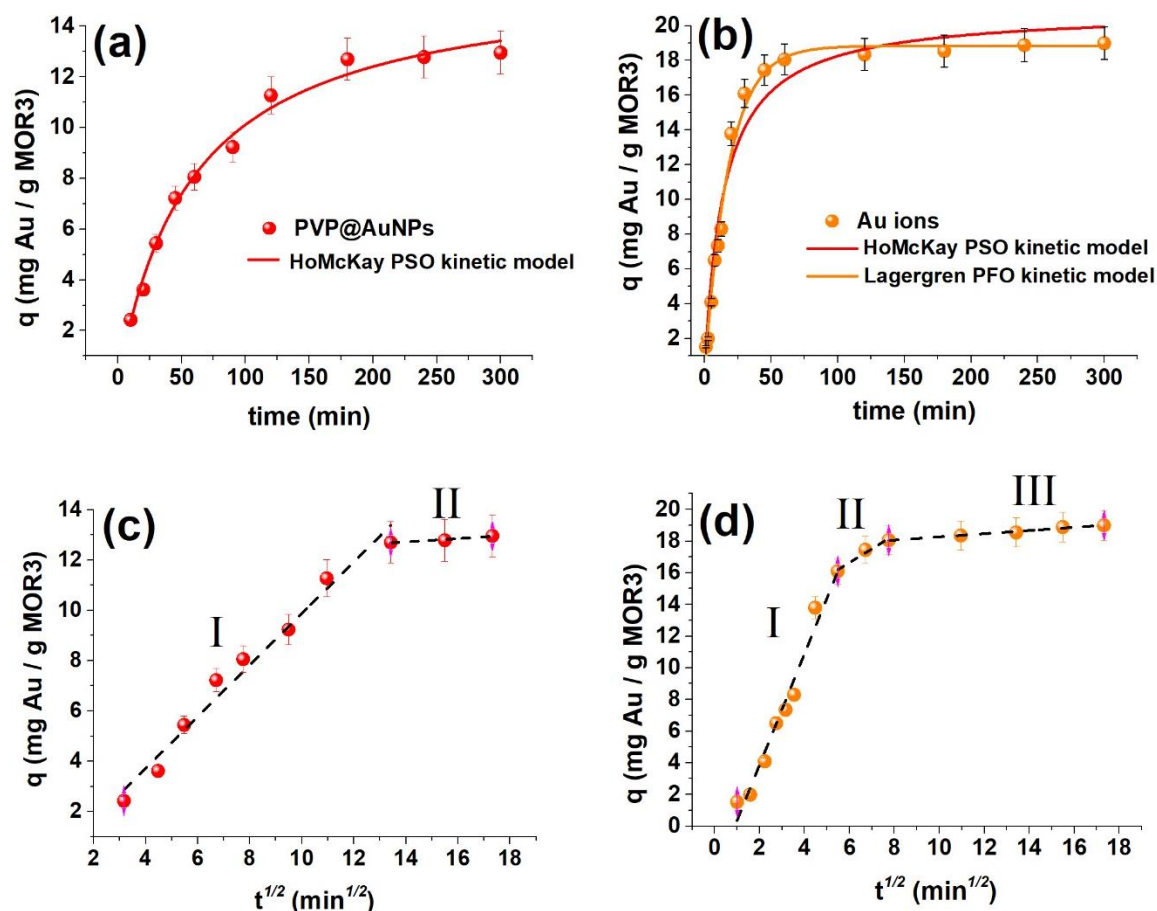


Figure 2.3.3.3 *Fitting of the kinetic data with the Ho-Mckay's pseudo-second-order equations (red lines) and Lagergren's pseudo-first order (orange line) for the sorption of (a) PVP@AuNPs, and (b) Au ions by MOR-3@fabric. Weber-Morris plots for the sorption of (c) PVP@AuNPs, and (d) Au ions by MOR-3@fabric.*

To further investigate the steps associated with the sorption process, the kinetic data were fitted to the intraparticle diffusion model of Weber and Morris (Figure 2.3.3.3 panels c and d). The sorption of AuNPs was manifested in two stages: boundary layer (film) diffusion (stage I) and intraparticle diffusion (stage II) while in the case of AuCl_4^- ions the intraparticle diffusion model presented three stages, an observation which is consistent with the sorption of AuCl_4^- ions also in other sorbents[561]. In the first stage, sorption occurs rapidly, due to the large availability of sorption sites but slows down at the second state as the sorption sites become saturated. The third stage (for AuCl_4^- ions only) implies that sorption has reached equilibrium. Across all plots, the sorption rate decreased ($K_{diff,1} > K_{diff,2} > K_{diff,3}$) and the intercepting lines have not gone through the origin. These findings suggest that intraparticle diffusion was not the rate limiting step in the sorption of PVP@AuNPs and AuCl_4^- ions. Moreover, for AuCl_4^- ions the decrease of $K_{diff,3}$ value, suggests that in addition to liquid film diffusion and intraparticle diffusion, diffusion in the interior of the sorbent is also a rate limiting step.

2.3.3.4 Sorption isotherms

To describe the interaction of AuNPs and AuCl_4^- ions with MOR-3@fabric, and to calculate the maximum sorption capacity of the sorbent, batch sorption isotherm studies were conducted at pH 3 for PVP@AuNPs (5 nm) and pH 6 for AuCl_4^- ions (Figure 2.3.3.4.a). The sorption of PVP@AuNPs fitted to the modified Langmuir-Freundlich isotherm model

EXPERIMENTAL

which accounts for both monolayer and multilayer adsorption on heterogeneous surfaces. According to this model, during sorption, the adsorbed species can occupy more than one binding sites without adsorbate-adsorbate interactions. Both assumptions may be valid for PVP@AuNPs that may bind to more than one thiophene moieties while their size and surface coating (PVP polymer) exerts stereochemical repulsion between AuNPs. The sorption of AuCl_4^- ions, was also predicted by the modified Langmuir-Freundlich ($R^2=0.99$) isotherm but the $1/n$ value was higher than 1 ($1/n=1.38$) indicating cooperativity in sorbate-sorbent interactions[562]. This cooperativity is attributed to the electrostatic attraction of AuCl_4^- ions on the MOR-3 surface and the reduction of AuCl_4^- ions on the surface of MOR-3@fabric, as previously discussed (Figure 2.3.3.3). Furthermore, the reduction of AuCl_4^- ions and oxidation of thiophene monomers may be repeated, causing the gold nuclei to grow [560]. Therefore, sorption starts with the cooperative action between the electrostatic attraction of AuCl_4^- ions and the formation of Au-S bonds, followed by reduction to AuNPs on the surface of MOR-3@fabric and reaches completion with the growth of AuNPs. The maximum sorption capacity calculated using the modified Langmuir - Freundlich model was 43.4 mg Au/g MOR-3 for PVP@AuNPs (or 50.2 nmole PVP@AuNPs /g MOR-3) and 883.5 mg Au/g MOR-3 for AuCl_4^- ions.

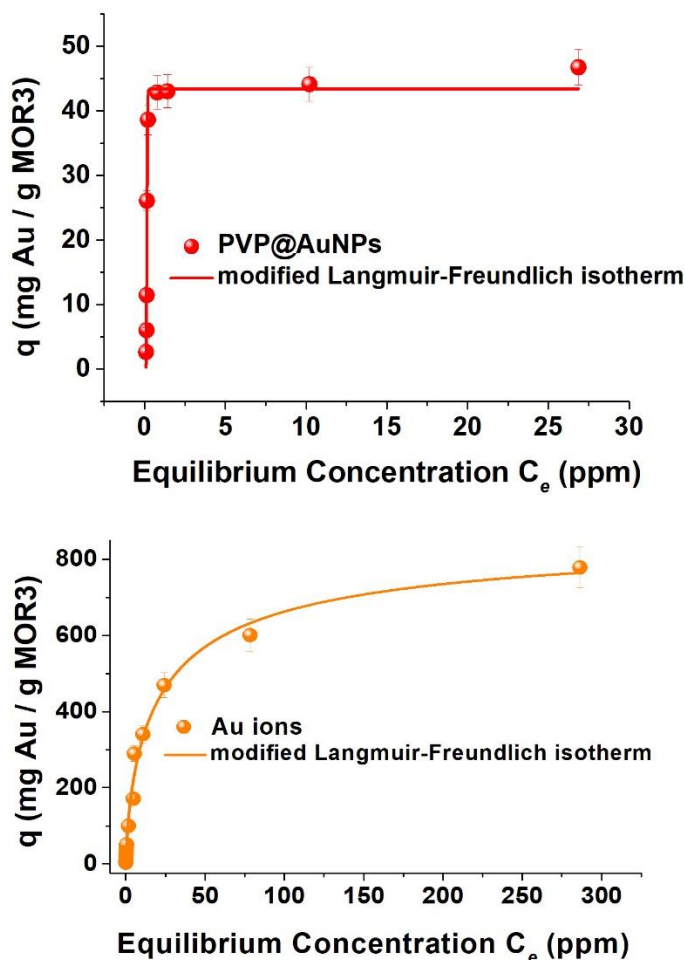


Figure 2.3.3.4.a Fitting of the modified Langmuir-Freundlich isotherm model to the sorption of PVP@AuNPs and Au ions on MOR-3@fabric.

The sorption capacity of MOR-3@fabric was also compared to that of MOR-3 particles. The mass of MOR-3 deposited on the fabric could not be accurately measured by TGA (because the thermal degradation of the fabric affected weight loss and could not be discriminated from the thermal decomposition of MOR-3), therefore an estimate of MOR-3 was obtained by weighting the fabric before and after deposition of MOR-3. Roughly (not accounting for fabric degradation during synthesis) the weight of MOR-3 was calculated at 16 mg per 25.12 cm² of fabric, which is in agreement with the deposition of Zr-based MOFs on cotton surfaces observed in our previous work [521]. Therefore, 8 mg of MOR-3 were used as a reasonable estimate of the mass of MOR-3 on

EXPERIMENTAL

the semi-circular MOR-3@fabric. Before use, MOR-3 was deprotonated three times in a methanolic solution of triethylamine for 4 h to enable a direct comparison with MOR-3@fabric. This was made because freely dispersed, protonated, MOR-3 particles decreased the pH from 6 to 4.5, a pattern that was much less evident with MOR-3@fabric ($\Delta\text{pH}=-0.5$).

The sorption of PVP@AuNPs and AuCl_4^- ions on MOR-3 could be described by the modified Langmuir-Freundlich isotherm models, which agrees with the observations made with MOR3@fabric (Figure 2.3.3.4.b). Interestingly, as the concentration of $[\text{AuCl}_4]^-$ ions in solution increased above 20 mg/L, the surplus of AuCl_4 ions could be reduced in also solution leading to the formation of freely dispersed AuNPs, as witnessed by the appearance of a pale purple coloration with a corresponding absorption band at ~ 540 nm (Figure 2.3.3.1.d). This phenomenon was not observed with MOR₃@fabric (at pH 6) at any AuCl_4^- concentration level.

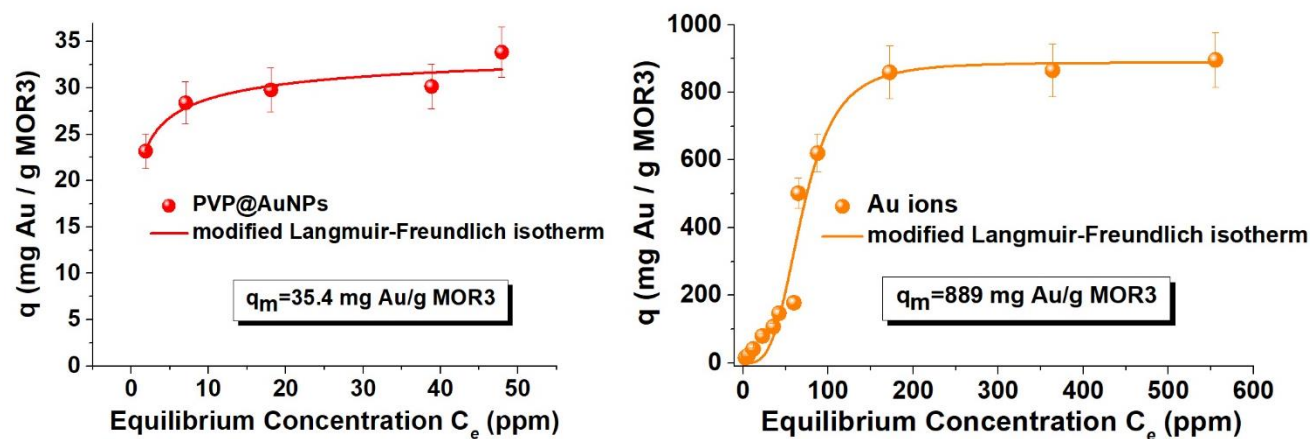


Figure 2.3.3.4.b Fitting of the modified Langmuir-Freundlich isotherm model to the sorption of PVP@AuNPs and Au ions on MOR-3 powder.

EXPERIMENTAL

From the isotherms of Figure 2.3.3.4.b, the maximum sorption capacity of AuCl_4^- on MOR-3 powder was 889 mg Au/g MOR-3 which is in excellent agreement with the sorption capacity calculated for MOR-3@fabric. For PVP@AuNPs the sorption capacity of MOR-3 powder (35.4 mg Au/g MOR-3) was lower than that determined for MOR-3@fabric. We attribute this difference to the fabric support of MOR-3@fabric which offers a very high primary contact surface area (defined as the surface area of the sorbent that can be accessed directly by the sample matrix)[476], while the porosity of the fabric facilitates the penetration of the aqueous phase through the fabric pores (60-100 μm), as opposed to non-porous phases where the flow is bounced back and collides with the incoming flow stream, causing some of the flow to redirect away from the substrate surface[476], [521], [563]. These features imbue fabric-based sorbent phases with improved mass transfer rates and improved sorption efficiency[476], [521].

2.3.3.5 Sorption of AuNPs of various sizes and surface coatings

As a result of the widespread use of AuNPs in many different applications, their presence in industrial wastewater and the environment may occur in various sizes, morphologies and surface coatings. Moreover, AuNPs may undergo various transformations in environmental systems or during wastewater treatment that may cause morphological transformations and changes in their surface properties[564]. Therefore, it is necessary to determine the total concentration of AuNPs, irrespective of their size, shape and surface functionalization.

The efficiency of MOR-3@fabric to remove AuNPs of different sizes and surface functionalization was evaluated using PVP₁₀@AuNPs of various sizes (5-80 nm) and AuNPs (4 nm) coated with small molecules (citrate), polymers (PVP₁₀), thiols (cysteine), amino acids (glycine) and surfactants (CTAB). According to the results shown in panel A of Figure 2.3.3.5, the sorption

EXPERIMENTAL

efficiency of MOR-3@fabric for AuNPs of various sizes (5-80 nm) improved with increasing size and ranged from 88.6-98.8%, while the sorption of AuNPs with different surface coatings (panel B, Figure 2.3.3.5) ranged from 85.6-95.0%, except for CTAB@AuNPs which were removed by 66.2%. These data indicate that MOR-3@fabric can effectively uptake AuNPs of different sizes and coatings and hence, it is suitable for the sorption of the total amount of AuNPs in environmental samples.

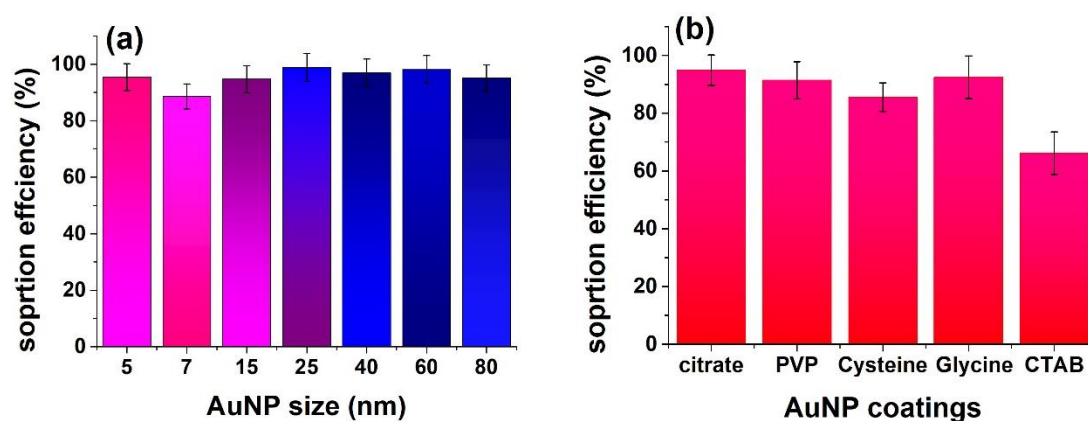


Figure 2.3.3.5 Sorption efficiency of MOR-3@fabric for the removal of AuNPs of different (a) sizes and, (b) surface coatings.

2.3.3.6 Optimization of desorption conditions

The elution of AuNPs and Au ions from the MOR-3@fabric was examined using two different elution solvents consisting of aqua regia and an equimolar (0.1M) mixture of NaOH/H₂O₂. Aqua regia was tested because it can dissolve AuNPs to AuCl₄⁻ ions[565], while strongly alkaline media and H₂O₂ can decompose MOFs (oxidation of the ligand and formation of the insoluble zirconium(IV) hydroxide precipitates) and release the extracted species[566]. In all experiments,

EXPERIMENTAL

5 mL of elution solvent was used to ensure that the elution volume is adequate for aspiration in FAAS.

The efficiency of aqua regia and NaOH/H₂O₂ was tested at different concentrations, elution times and elution methods. As shown in panel A of Figure 2.3.3.6, the dissolution efficiency declines with decreasing aqua regia acidity but remains constant for NaOH/H₂O₂ concentrations 0.1 and higher. Due to the strong acidity of the aqua regia, the elution time did not have any effect on the extraction efficiency of AuNPs while 50 min of incubation in NaOH/H₂O₂ was necessary to completely digest the MOF and release the AuNPs (Figure 2.3.3.6, panel B). Finally mixing of the elution solvent with the sorbent provided the best results without the need for heating (Figure 2.3.3.6, Panel C). Overall, NaOH-H₂O₂ provided improved recoveries, by almost 10%, compared to those obtained with aqua regia. Both elution solvents were efficient in recovering AuCl₄⁻ ions (recovery>94%) (Figure 2.3.3.6, Panel D), however, neither elution solvent enabled the reuse of MOR-3@fabric; at alkaline solutions the MOR-3 was digested to ZrO₂ while under strongly acidic conditions, MOR-3 did not maintain its crystallinity.

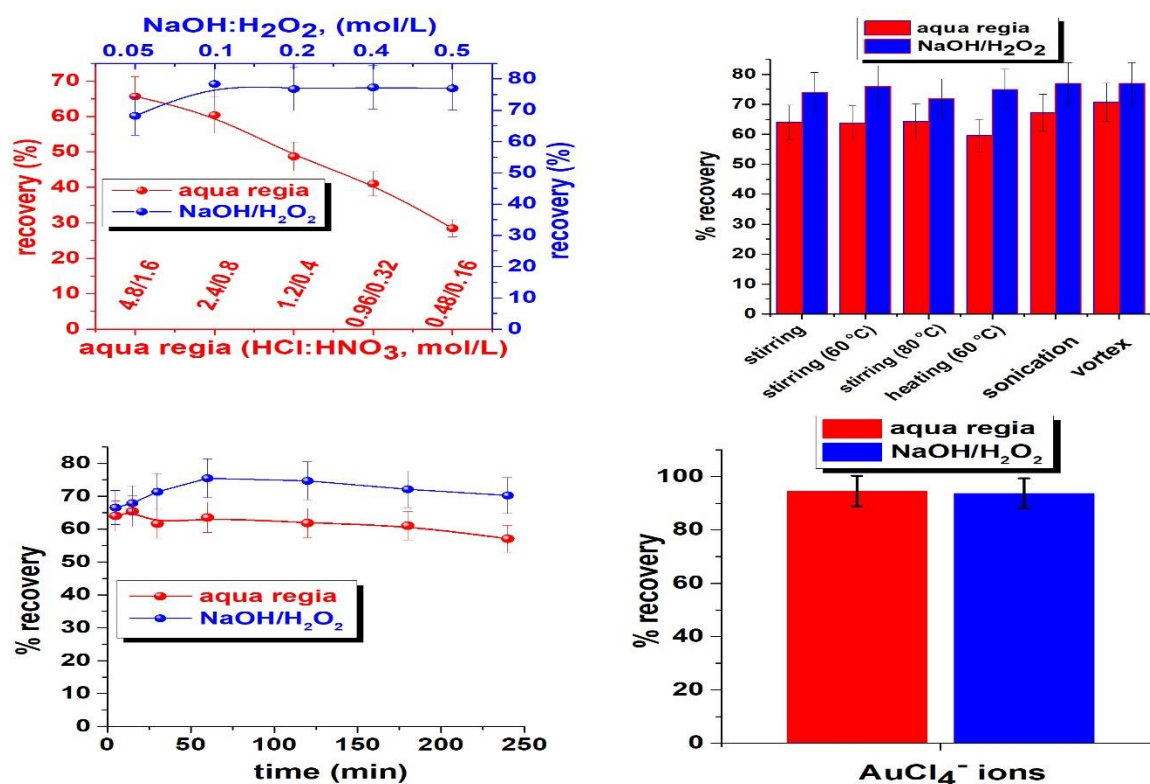


Figure 2.3.3.6 Optimization of experimental conditions for the elution of AuNPs from MOR-3@cotton fabric. (A) Effect of elution solvent strength and composition, (B) Influence of elution time, (C) Effect of elution method and (D) efficiency of eluting Au ions under the optimum conditions, and recovery of AuNPs of different.

2.3.3.7 Application of MOR-3@fabric

2.3.3.7.1 Evaluation of MOR-3@cotton fabrics as passive sampling receiving phase

As previously discussed, the sorption efficiency of MOR-3 for AuNPs depends on pH exhibiting its maximum value ($q_{\max}=43.3$ mg/g) at pH 3. At the usual pH values of most environmental waters (6.5-8.0), the efficiency of MOR-3@fabric is limited to almost 10% of its maximum value, which corresponds to a value of ≤ 4.3 mg/g. This value is more than adequate for passive sampling applications considering that the measured environmental concentrations of nanoparticles lie at the

EXPERIMENTAL

ng/L levels[567], [568], [569]. Even if the predictions of probabilistic and material flow algorithms are verified and the concentration of AuNPs raise to a few $\mu\text{g/L}$ [570], [571], the sorption capacity of MOR-3@fabric would still be adequate. The uptake kinetic curves of Figure 2.3.3.7.1 show that AuNP accumulation exhibited a linear (integrative) phase up to 110 days, which is significantly higher than most passive samples used for inorganic ions (Table 2.3.3.7.1). This attribute is particularly important due to the low levels of AuNPs in natural waters[567], [568], [569], which may necessitate long-term monitoring surveys to obtain measurable concentrations of AuNPs on the MOR-3@fabric sorbent phase. The efficiency of MOR-3@fabrics for the passive sampling of AuNPs from natural waters was also evidenced by the good sampling rate ($R_s=2.1 \text{ mL/h}$) which is comparable to those obtained with commercial passive samplers for metal ions[572], [573], [574], [575]. From these data it can be concluded that MOR-3@cotton fabrics are very efficient materials for the passive sampling of AuNPs in natural waters. However, to differentiate between AuNPs and Au ions and accomplish their speciation, a commercial passive sampling phase for

EXPERIMENTAL

metal ions (e.g. DGTS, Chemcatchers, etc) should be employed simultaneously with MOR-3@fabric since the latter exhibits no selectivity for Au species.

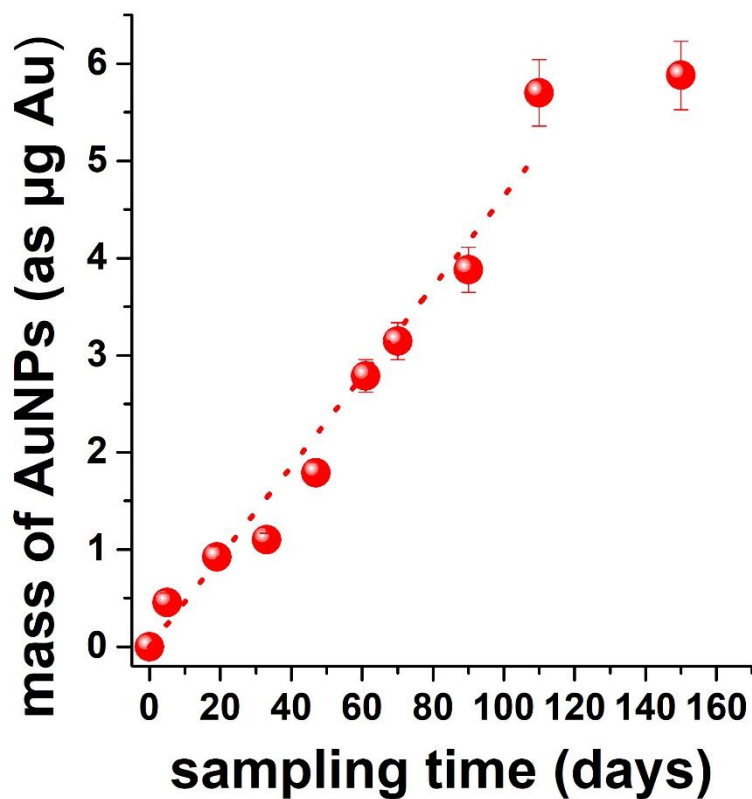


Figure 2.3.3.7.1 Passive sampler (MOR-3@fabric) uptake curve for PVP@AuNPs.

Table 2.3.3.7.1 Uptake kinetic curves of commercial passive samples used for inorganic ions.

Sampler	Inorganic species	Rs (mL/h)	Linear uptake phase time (days)	Reference
Chemcatcher	Cd	5.1	28	[575]
	Cu	4.9		
	Ni	5.7		
	Pb	0.7		
	Zn	5.3		
Chemcatcher	Cd	3.1	14	[574]
	Ni	2.7		

	Zn	2.9		
Chemcatcher	Rare earth elements	0.92-2.15	14	[573]
Chemcatcher	Hg	1.3-3.8	14	[572]
MOR3@fabric	AuNPs	2.1	110	This work

2.3.3.7.2 Application of MOR-3@fabric for the fabric phase sorptive extraction of AuNPs

The use of MOR-3@fabric was also examined as a sorbent phase for the extraction of AuNPs based on the principles of fabric phase sorptive extraction (FPSE). The method of FPSE was developed for the extraction of organic compounds in a membrane, constituted with a flexible fabric substrate and a sol-gel-derived high-efficiency sorbent coating, immobilized on the surface of the substrate[476]. Our group demonstrated that MOF@fabrics can be also used as a sorbent in FPSE for the extraction of organic compounds[521]. In that regard, we expanded the use of MOR-3@fabric phase as a sorbent for the extraction of AuNPs. A simplified representation of the experimental procedure is depicted in Figure 2.3.3.7.2.

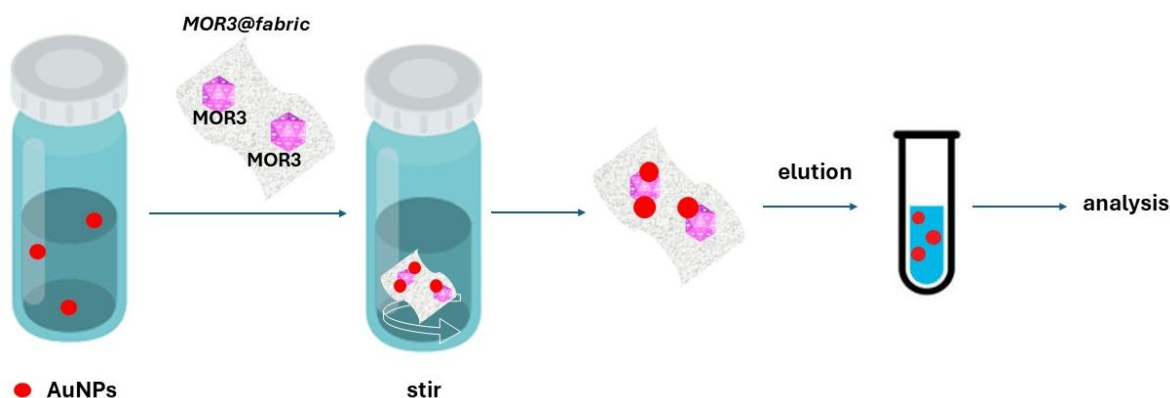


Figure 2.3.3.7.2 Simplified sketch of the experimental procedure for the FPSE of AuNPs from water samples.

EXPERIMENTAL

First, the performance of the MOR-3@fabric was evaluated by preparing calibration curves of AuNPs using standard solutions of PVP₁₀@AuNP (4nm) at pH 3 where the sorbent exhibits its maximum sorption capacity for AuNPs. The response is described by the equation $y=0.0375x+0.0081$, $R^2=0.9991$ and is rectilinear in the range of 0.2-20 nM of 4 nm PVP@AuNPs (or to 0.05-8.0 $\mu\text{g Au /mL}$), yielding detection limits (defined as three times the standard deviation of the intercept divided by the slope) of 0.18 nM (0.045 $\mu\text{g Au /mL}$). These data indicate that the MOR-3@fabric could also serve as a sorbent for the analytical determination of AuNPs in natural waters. However, due to their low concentrations in real samples more sensitive detectors, such as ICP-MS, are required to bring the detection limits to the ng/L and pg/L levels[567], [568], [576], [577]. Further improvement in sensitivity may be also pursued by increasing the preconcentration factor either by extracting larger sample volumes and/or by using a lower volume of elution solvent. Not least, speciation of AuNPs and Au ions could be accomplished by separating AuNPs before extraction using physical methods, such as ultracentrifugation[578], ultrafiltration[579] and nanoparticle imprinted matrices' (NAIMs)[580], thus further expanding the utility of MOR-3@fabric for analytical and sample preparation purposes.

The reproducibility of the FPSE method, expressed as the relative standard deviation (RSD, %) of three measurements at an equivalent concentration of 0.5 nM PVP@AuNPs (0.25 $\mu\text{g Au /mL}$) was 8.8%, indicating the good precision of the method.

Based on these results, the FPSE method was evaluated by recovery experiments in environmental water samples of different matrix complexity (i.e. river water, lake water and seawater). Since the sorbent effectively extracts both AuNPs and Au ions, the recoveries in mixtures of both species were also examined. The results gathered in Table 2.3.3.7.2 show that the method effectively extracts both AuNPs and Au ions with recoveries

EXPERIMENTAL

ranging from 80.8% to 115% which are very satisfactory and within the range of values reported from other methods[581], [582] and within the acceptable range for trace analysis[583].

Table 2.3.3.7.2 Summary of results from the analysis of real samples and recovery rates from fortified water samples. Standard deviation for $n=3$.^a

Sample	Total AuNPs and Au ($\mu\text{g Au / mL}$) ^{a,b}			AuNPs ($\mu\text{g Au / mL}$) ^a		
	spiked	determined	recovery (%)	spiked	calculated	recovery (%)
Tap water	2.40±0.05	2.39±0.07	99.9±2.9	1.15±0.18	1.27±0.10	110.4±7.8
River water	2.25±0.03	2.59±0.03	115±1.2	0.97±0.15	0.89±0.01	91.7±1.1
Lake water	1.61±0.19	1.58±0.11	97.7±6.9	1.27±0.23	1.25±0.22	98.4±17.6
Seawater	2.60±0.46	2.1±0.26	80.8±12	1.10±0.15	1.04±0.16	94.5±15.4

^a Spiking levels of AuNPs were initially calculated based on volumetric dilution of the AuNP stock solutions and verified by AAS because AuNP suspensions are not homogeneous solutions and the dilution low may deviate from ideal conditions. ^b Values were calculated from the calibration plots obtained by extracting mixtures of AuNP and Au ions at equal concentrations of Au ions at pH 3, respectively.

2.3.3.7.3 Application of MOR-3@fabric for the solid phase extraction of AuNPs

Except for FPSE, MOR-3@cotton was also be used as SPE disks for the on-line extraction of AuNPs from aqueous solutions. The calibration plot of Figure 2.3.3.7.3 shows a linear response (0.18-7.5 nM or 0.1-4 mg Au/L) expanding more than an order of magnitude with acceptable reproducibility (10.5%, $n=3$). The linear range was lower to that obtained in FPSE but the slope of the calibration plot was similar, suggesting that further improvement can be accomplished by optimizing the extraction conditions related to the application of the method in SPE mode.

EXPERIMENTAL

Not the least, the use of MOR-3@ cotton as an SPE disk may offer several advantages. Firstly, the large pores of the fabric (60–100 μm) minimizes clogging which is a common problem associated with the use of SPE sorbents which currently find limited use in SPE due to high-back pressure or leaching problems.

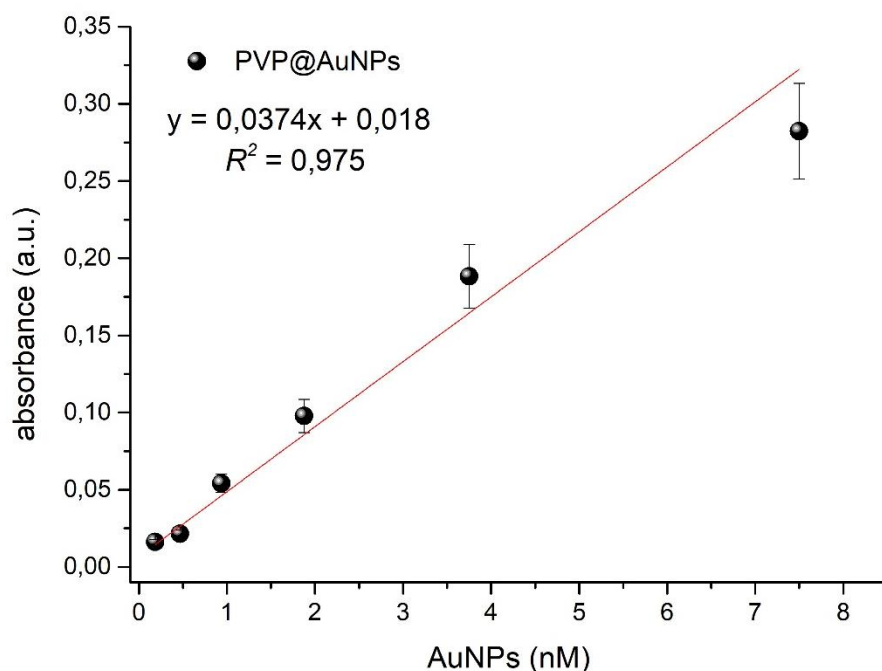


Figure 2.3.3.7.3 Calibration plot of PVP@AuNPs (4-nm) extracted with MOR-3@ cotton in SPE mode.

2.3.4 Conclusions

This study demonstrates the use of MOF@ cotton fabrics as a new and versatile sorbent for the FPSE of noble metal nanoparticles from water samples both under static (i.e. stirring assisted) and dynamic (i.e. vacuum assisted) extraction mode. The results show that the MOR-3@ fabric exhibits pH-dependent selectivity against AuNPs and AuCl_4^- ions. At acidic pH values both AuNPs and AuCl_4^- ions are effectively extracted but at pH 6 the sorption efficiency of AuNPs deteriorates

EXPERIMENTAL

dramatically (from 85% to 10%), however, co-sorption is not totally avoided. The efficiency of MOR-3@fabric to remove AuNPs of different sizes and surface functionalization was evaluated. These data indicate that MOR-3@fabric can effectively uptake AuNPs of different sizes and coatings and hence, it is suitable for the sorption of the total amount of AuNPs in environmental samples. Moreover, the MOF@cotton fabric was calibrated also as a passive sampling sorbent phase for the uptake of gold nanoparticles from natural waters over relatively long exposure times (up to 110 days) with sampling rates that are similar to other sorbent phases. The applicability of the material was demonstrated by the analysis of various spiked environmental water samples of variable complexity including river, lake and seawater. The results show that the method effectively extracts both AuNPs and Au ions with recoveries ranging from 80.8% to 115% which are very satisfactory and within the range of values reported from other method. -All these results show that MOF@cotton composites hold great promise as alternative sorbents for both FPSE and passive sampling, opening new opportunities in analytical sample preparation and environmental monitoring of noble nanoparticles in the environment.

3 REFERENCES

- [1] Y. Song, J. Phipps, C. Zhu, and S. Ma, "Porous Materials for Water Purification," Mar. 06, 2023, *John Wiley and Sons Inc.* doi: 10.1002/anie.202216724.
- [2] J. Abdi, M. Vossoughi, N. M. Mahmoodi, and I. Alemzadeh, "Synthesis of metal-organic framework hybrid nanocomposites based on GO and CNT with high adsorption capacity for dye removal," *Chemical Engineering Journal*, vol. 326, pp. 1145–1158, 2017, doi: 10.1016/j.cej.2017.06.054.
- [3] F. Ahmadijokani *et al.*, "UiO-66 metal–organic frameworks in water treatment: A critical review," Apr. 01, 2022, *Elsevier Ltd.* doi: 10.1016/j.pmatsci.2021.100904.
- [4] Y. Cao, X. Chen, X. Li, and B. Wang, "Tuning Surface Functionalization and Pore Structure of UiO-66 Metal-Organic Framework Nanoparticles for Organic Pollutant Elimination," *ACS Appl Nano Mater*, vol. 4, no. 5, pp. 5486–5495, May 2021, doi: 10.1021/acsanm.1c00796.
- [5] M. Gao *et al.*, "Recent advances in metal-organic frameworks/membranes for adsorption and removal of metal ions," Apr. 01, 2021, *Elsevier B.V.* doi: 10.1016/j.trac.2021.116226.
- [6] E. Torabi *et al.*, "Advanced materials in sorbent-based analytical sample preparation," May 01, 2024, *Elsevier B.V.* doi: 10.1016/j.ccr.2024.215680.
- [7] S. Kumar *et al.*, "Concomitant role of metal clusters and ligands in the synthesis and control of porosity in Metal-Organic Frameworks: A literature review," *Results Chem*, vol. 6, Dec. 2023, doi: 10.1016/j.rechem.2023.101206.
- [8] D. Y. Heo, H. H. Do, S. H. Ahn, and S. Y. Kim, "Metal-organic framework materials for perovskite solar cells," *Polymers (Basel)*, vol. 12, no. 9, Sep. 2020, doi: 10.3390/POLYM12092061.
- [9] H. C. J. Zhou and S. Kitagawa, "Metal-Organic Frameworks (MOFs)," Aug. 21, 2014, *Royal Society of Chemistry*. doi: 10.1039/c4cs90059f.
- [10] H. C. Zhou, J. R. Long, and O. M. Yaghi, "Introduction to metal-organic frameworks," Feb. 08, 2012. doi: 10.1021/cr300014x.
- [11] S. Yuan *et al.*, "Stable Metal–Organic Frameworks: Design, Synthesis, and Applications," Sep. 13, 2018, *Wiley-VCH Verlag*. doi: 10.1002/adma.201704303.
- [12] S. Y. Ding and W. Wang, "Covalent organic frameworks (COFs): From design to applications," *Chem Soc Rev*, vol. 42, no. 2, pp. 548–568, Dec. 2013, doi: 10.1039/c2cs35072f.
- [13] Y. Song, Q. Sun, B. Aguila, and S. Ma, "Opportunities of Covalent Organic Frameworks for Advanced Applications," Jan. 23, 2019, *John Wiley and Sons Inc.* doi: 10.1002/advs.201801410.
- [14] Y. Zhang and S. N. Riduan, "Functional porous organic polymers for heterogeneous catalysis," *Chem Soc Rev*, vol. 41, no. 6, pp. 2083–2094, Feb. 2012, doi: 10.1039/c1cs15227k.
- [15] B. Moll *et al.*, "Modulated synthesis of thiol-functionalized fcu and hep UiO-66(Zr) for the removal of silver(i) ions from water," *Mater Adv*, vol. 2, no. 2, pp. 804–812, Jan. 2021, doi: 10.1039/d0ma00555j.
- [16] S. Dalai, "Coordination Polymers," 2011. [Online]. Available: www.vidyasagar.ac.in/journal
- [17] S. Carrasco, "Metal-organic frameworks for the development of biosensors: A current overview," Oct. 16, 2018, *MDPI*. doi: 10.3390/bios8040092.

- [18] C. P. Raptopoulou, "Metal-organic frameworks: Synthetic methods and potential applications," Jan. 02, 2021, *MDPI AG*. doi: 10.3390/ma14020310.
- [19] C. Janiak, "Engineering coordination polymers towards applications," *Journal of the Chemical Society. Dalton Transactions*, vol. 3, no. 14, pp. 2781–2804, Jun. 2003, doi: 10.1039/b305705b.
- [20] R. S. Salama, E. S. M. El-Sayed, S. M. El-Bahy, and F. S. Awad, "Silver nanoparticles supported on UiO-66 (Zr): As an efficient and recyclable heterogeneous catalyst and efficient adsorbent for removal of indigo carmine," *Colloids Surf A Physicochem Eng Asp*, vol. 626, Oct. 2021, doi: 10.1016/j.colsurfa.2021.127089.
- [21] J. L. C. Rowsell and O. M. Yaghi, "Metal-organic frameworks: A new class of porous materials," Aug. 06, 2004. doi: 10.1016/j.micromeso.2004.03.034.
- [22] S. Kitagawa, R. Kitaura, and S. I. Noro, "Functional porous coordination polymers," Apr. 26, 2004. doi: 10.1002/anie.200300610.
- [23] M. Bazargan, F. Ghaemi, A. Amiri, and M. Mirzaei, "Metal–organic framework-based sorbents in analytical sample preparation," Oct. 15, 2021, *Elsevier B.V.* doi: 10.1016/j.ccr.2021.214107.
- [24] V. R. Bakuru, M. E. DMello, and S. B. Kalidindi, "Metal-Organic Frameworks for Hydrogen Energy Applications: Advances and Challenges," May 16, 2019, *Wiley-VCH Verlag*. doi: 10.1002/cphc.201801147.
- [25] S. Henke, "Metal-Organic Frameworks with Additional Flexible Substituents-Modulating Responsiveness, Gas Sorption Selectivity & Network Topologies." [Online]. Available: <https://www.researchgate.net/publication/280923901>
- [26] H. Mena, "Synthesis and characterization of metal-organic and supramolecular compounds based on the 1,2-bis(1,2,4-triazol-4-yl)ethane ligand," 2008.
- [27] H. Furukawa *et al.*, "Ultrahigh porosity in metal-organic frameworks," *Science (1979)*, vol. 329, no. 5990, pp. 424–428, Jul. 2010, doi: 10.1126/science.1192160.
- [28] S. K. Elsaïdi, M. H. Mohamed, D. Banerjee, and P. K. Thallapally, "Flexibility in Metal–Organic Frameworks: A fundamental understanding," Mar. 01, 2018, *Elsevier B.V.* doi: 10.1016/j.ccr.2017.11.022.
- [29] C. Mellot-Draznieks, C. Serre, S. Surblé, N. Audebrand, and G. Férey, "Very large swelling in hybrid frameworks: A combined computational and powder diffraction study," *J Am Chem Soc*, vol. 127, no. 46, pp. 16273–16278, Nov. 2005, doi: 10.1021/ja054900x.
- [30] D. N. Dybtsev, H. Chun, and K. Kim, "Rigid and flexible: A highly porous metal-organic framework with unusual guest-dependent dynamic behavior," *Angewandte Chemie - International Edition*, vol. 43, no. 38, pp. 5033–5036, Sep. 2004, doi: 10.1002/anie.200460712.
- [31] G. Férey and C. Serre, "Large breathing effects in three-dimensional porous hybrid matter: Facts, analyses, rules and consequences," *Chem Soc Rev*, vol. 38, no. 5, pp. 1380–1399, Apr. 2009, doi: 10.1039/b804302g.
- [32] J. Seo, R. Matsuda, H. Sakamoto, C. Bonneau, and S. Kitagawa, "A pillared-layer coordination polymer with a rotatable pillar acting as a molecular gate for guest molecules," *J Am Chem Soc*, vol. 131, no. 35, pp. 12792–12800, Sep. 2009, doi: 10.1021/ja904363b.

- [33] S. Sahoo, R. Kumar, G. Dhakal, and J. J. Shim, "Recent advances in synthesis of metal-organic frameworks (MOFs)-derived metal oxides and its composites for electrochemical energy storage applications," Dec. 25, 2023, *Elsevier Ltd.* doi: 10.1016/j.est.2023.109427.
- [34] Y. Bian, N. Xiong, and G. Zhu, "Technology for the remediation of water pollution: A review on the fabrication of metal organic frameworks," *Processes*, vol. 6, no. 8, Aug. 2018, doi: 10.3390/pr6080122.
- [35] N. Al Amery, H. R. Abid, S. Al-Saadi, S. Wang, and S. Liu, "Facile directions for synthesis, modification and activation of MOFs," Sep. 01, 2020, *Elsevier Ltd.* doi: 10.1016/j.mtchem.2020.100343.
- [36] R. Ameloot *et al.*, "Direct patterning of oriented metal-organic framework crystals via control over crystallization kinetics in clear precursor solutions," Jun. 25, 2010. doi: 10.1002/adma.200903867.
- [37] D. J. Tranchemontagne, J. R. Hunt, and O. M. Yaghi, "Room temperature synthesis of metal-organic frameworks: MOF-5, MOF-74, MOF-177, MOF-199, and IRMOF-0," *Tetrahedron*, vol. 64, no. 36, pp. 8553–8557, Sep. 2008, doi: 10.1016/j.tet.2008.06.036.
- [38] R. Q. Zou, L. Jiang, H. Senoh, N. Takeichi, and Q. Xu, "Rational assembly of a 3D metal-organic framework for gas adsorption with predesigned cubic building blocks and 1D open channels," *Chemical Communications*, no. 28, pp. 3526–3528, 2005, doi: 10.1039/b503667d.
- [39] G. H. Wang, Z. G. Li, H. Q. Jia, N. H. Hu, and J. W. Xu, "Metal-organic frameworks based on the pyridine-2,3-dicarboxylate and a flexible bispyridyl ligand: Syntheses, structures, and photoluminescence," *CrystEngComm*, vol. 11, no. 2, pp. 292–297, 2009, doi: 10.1039/b809557d.
- [40] G. H. Wang, Z. G. Li, H. Q. Jia, N. H. Hu, and J. W. Xu, "Metal-organic frameworks based on the pyridine-2,3-dicarboxylate and a flexible bispyridyl ligand: Syntheses, structures, and photoluminescence," *CrystEngComm*, vol. 11, no. 2, pp. 292–297, 2009, doi: 10.1039/b809557d.
- [41] T. W. T. Muesmann, A. Mietrach, J. Christoffers, and M. S. Wickleder, "Synthesis of 1,2,4,5-benzenetetrasulfonic acid (H4B4S) and its implementation as a linker for building metal-organic frameworks on the example of [Cu₂(B4S)(H₂O)₈]·0.5H₂O," *Z Anorg Allg Chem*, vol. 636, no. 7, pp. 1307–1312, Jul. 2010, doi: 10.1002/zaac.201000056.
- [42] T. W. Murinzi, E. Hosten, and G. M. Watkins, "Synthesis and characterization of a cobalt-2,6-pyridinedicarboxylate MOF with potential application in electrochemical sensing," *Polyhedron*, vol. 137, pp. 188–196, 2017, doi: 10.1016/j.poly.2017.08.030.
- [43] A. N. Amenaghawon *et al.*, "A comprehensive review of recent advances in the synthesis and application of metal-organic frameworks (MOFs) for the adsorptive sequestration of pollutants from wastewater," Apr. 15, 2023, *Elsevier B.V.* doi: 10.1016/j.seppur.2023.123246.
- [44] B. Chen, Z. Yang, Y. Zhu, and Y. Xia, "Zeolitic imidazolate framework materials: Recent progress in synthesis and applications," Oct. 28, 2014, *Royal Society of Chemistry*. doi: 10.1039/c4ta02984d.
- [45] M. Y. Zorainy, M. Sheashea, S. Kaliaguine, M. Gobara, and D. C. Boffito, "Facile solvothermal synthesis of a MIL-47(V) metal-organic framework for a high-performance Epoxy/MOF coating with improved anticorrosion properties," *RSC Adv*, vol. 12, no. 15, pp. 9008–9022, Mar. 2022, doi: 10.1039/d1ra08950a.
- [46] M. Fiaz, M. Athar, S. Rani, M. Najam-ul-Haq, and M. A. Farid, "One pot solvothermal synthesis of Co₃O₄@UiO-66 and CuO@UiO-66 for improved current density towards hydrogen evolution reaction," *Mater Chem Phys*, vol. 239, Jan. 2020, doi: 10.1016/j.matchemphys.2019.122320.

- [47] R. M. Main *et al.*, “Solvothermal synthesis of a novel calcium metal-organic framework: High temperature and electrochemical behaviour,” *Molecules*, vol. 26, no. 22, Nov. 2021, doi: 10.3390/molecules26227048.
- [48] M. Schlesinger, S. Schulze, M. Hietschold, and M. Mehring, “Evaluation of synthetic methods for microporous metal-organic frameworks exemplified by the competitive formation of [Cu₂(btc)₃(H₂O)₃] and [Cu₂(btc)(OH)(H₂O)],” *Microporous and Mesoporous Materials*, vol. 132, no. 1–2, pp. 121–127, Jul. 2010, doi: 10.1016/j.micromeso.2010.02.008.
- [49] W. Cheng, Y. Wang, S. Ge, X. Ding, Z. Cui, and Q. Shao, “One-step microwave hydrothermal preparation of Cd/Zr-bimetallic metal–organic frameworks for enhanced photochemical properties,” *Adv Compos Hybrid Mater*, vol. 4, no. 1, pp. 150–161, Mar. 2021, doi: 10.1007/s42114-020-00199-5.
- [50] L. Stewart, W. Lu, Z. W. Wei, D. Ila, C. Padilla, and H. C. Zhou, “A zirconium metal-organic framework with an exceptionally high volumetric surface area,” *Dalton Transactions*, vol. 46, no. 41, pp. 14270–14276, 2017, doi: 10.1039/c7dt03394j.
- [51] V. H. Nguyen, L. Van Tan, T. Lee, and T. D. Nguyen, “Solvothermal synthesis and photocatalytic activity of metal-organic framework materials based on bismuth and trimesic acid,” *Sustain Chem Pharm*, vol. 20, May 2021, doi: 10.1016/j.scp.2021.100385.
- [52] H. Guan, Y. Yang, H. Luo, H. Chen, and H. Zhou, “Improved Electrochemical Performance of a Li_{1.2}Ni_{0.2}Mn_{0.6}O₂ Cathode by a Hydrothermal Method with a Metal-Organic Framework as a Precursor,” *ACS Appl Energy Mater*, vol. 4, no. 3, pp. 2506–2513, Mar. 2021, doi: 10.1021/acsaem.0c03020.
- [53] J. Campbell and B. Tokay, “Controlling the size and shape of Mg-MOF-74 crystals to optimise film synthesis on alumina substrates,” *Microporous and Mesoporous Materials*, vol. 251, pp. 190–199, 2017, doi: 10.1016/j.micromeso.2017.05.058.
- [54] T. T. Wang *et al.*, “Solvothermal Preparation of a Lanthanide Metal-Organic Framework for Highly Sensitive Discrimination of Nitrofurantoin and L-Tyrosine,” *Molecules*, vol. 26, no. 12, Jun. 2021, doi: 10.3390/molecules26123673.
- [55] X. H. Zhou, L. Li, H. H. Li, A. Li, T. Yang, and W. Huang, “A flexible Eu(III)-based metal-organic framework: Turn-off luminescent sensor for the detection of Fe(III) and picric acid,” *Dalton Transactions*, vol. 42, no. 34, pp. 12403–12409, Sep. 2013, doi: 10.1039/c3dt51081f.
- [56] M. D. Olawale, J. O. Obaleye, and E. O. Oladele, “Solvothermal synthesis and characterization of novel [Ni(II)(Tpy)(Pydc)]·2H₂O metal-organic framework as an adsorbent for the uptake of caffeine drug from aqueous solution,” *New Journal of Chemistry*, vol. 44, no. 43, pp. 18780–18791, Nov. 2020, doi: 10.1039/d0nj04316h.
- [57] G. S. Deiko, V. I. Isaeva, and L. M. Kustov, “New Molecular Sieve Materials: Composites Based on Metal–Organic Frameworks and Ionic Liquids,” *Petroleum Chemistry*, vol. 59, no. 8, pp. 770–787, Aug. 2019, doi: 10.1134/S096554411908005X.
- [58] Z. H. Zhang, L. Xu, and H. Jiao, “Ionothermal synthesis, structures, properties of cobalt-1,4-benzenedicarboxylate metal-organic frameworks,” *J Solid State Chem*, vol. 238, pp. 217–222, Jun. 2016, doi: 10.1016/j.jssc.2016.03.028.

- [59] L. Xu, E. Y. Choi, and Y. U. Kwon, "Ionothermal synthesis of a 3D Zn-BTC metal-organic framework with distorted tetranuclear $[\text{Zn}_4(\mu_4\text{-O})]$ subunits," *Inorg Chem Commun*, vol. 11, no. 10, pp. 1190–1193, Oct. 2008, doi: 10.1016/j.inoche.2008.07.001.
- [60] L. Xu, Y. U. Kwon, B. De Castro, and L. Cunha-Silva, "Novel mn(II)-based metal-organic frameworks isolated in ionic liquids," *Cryst Growth Des*, vol. 13, no. 3, pp. 1260–1266, Mar. 2013, doi: 10.1021/cg301725z.
- [61] J. H. Liao and W. C. Huang, "Ionic liquid as reaction medium for the synthesis and crystallization of a metal-organic framework: $(\text{BMIM})_2[\text{Cd}_3(\text{BDC})_3\text{Br}_2]$ (BMIM = 1-butyl-3-methylimidazolium, BDC = 1,4-benzenedicarboxylate)," *Inorg Chem Commun*, vol. 9, no. 12, pp. 1227–1231, Dec. 2006, doi: 10.1016/j.inoche.2006.07.041.
- [62] Z. H. Zhang, B. Liu, L. Xu, and H. Jiao, "Combination effect of ionic liquid components on the structure and properties in 1,4-benzenedicarboxylate based zinc metal-organic frameworks," *Dalton Transactions*, vol. 44, no. 41, pp. 17980–17989, 2015, doi: 10.1039/c5dt02672e.
- [63] Z. F. Wu, M. L. Feng, B. Hu, B. Tan, and X. Y. Huang, "Ionothermal synthesis of a metal-organic framework constructed by magnesium(II) and 4,4'-oxybis(benzoic acid) ligand," *Inorg Chem Commun*, vol. 24, pp. 166–169, Oct. 2012, doi: 10.1016/j.inoche.2012.06.024.
- [64] J. Zhang, S. Chen, and X. Bu, "Multiple functions of ionic liquids in the synthesis of three-dimensional low-connectivity homochiral and achiral frameworks," *Angewandte Chemie - International Edition*, vol. 47, no. 29, pp. 5434–5437, Jul. 2008, doi: 10.1002/anie.200801838.
- [65] K. Jin, X. Huang, L. Pang, J. Li, A. Appel, and S. Wherland, "[Cu(I)(bpp)]BF₄: The first extended coordination network prepared solvothermally in an ionic liquid solvent," *Chemical Communications*, vol. 23, pp. 2872–2873, 2002, doi: 10.1039/b209937n.
- [66] Z. Lin, A. M. Z. Slawin, and R. E. Morris, "Chiral induction in the ionothermal synthesis of a 3-D coordination polymer," *J Am Chem Soc*, vol. 129, no. 16, pp. 4880–4881, Apr. 2007, doi: 10.1021/ja070671y.
- [67] H. Y. Cao, Q. Y. Liu, M. J. Gao, Y. L. Wang, L. L. Chen, and Y. Liu, "Ionothermal syntheses, crystal structures and luminescence of three three-dimensional lanthanide-1,4-benzenedicarboxylate frameworks," *Inorganica Chim Acta*, vol. 414, pp. 226–233, Apr. 2014, doi: 10.1016/j.ica.2014.02.014.
- [68] R. Lalawmpuia, M. Lalhruaitluangi, D. Tiwari, and J.-K. Yang, "Metal Organic Framework (MOF): Synthesis and Fabrication for the Application of Electrochemical Sensing," 2023, doi: 10.20944/preprints202309.0192.v1.
- [69] M. F. Thorne, M. L. R. Gómez, A. M. Bumstead, S. Li, and T. D. Bennett, "Mechanochemical synthesis of mixed metal, mixed linker, glass-forming metal-organic frameworks," *Green Chemistry*, vol. 22, no. 8, pp. 2505–2512, Apr. 2020, doi: 10.1039/d0gc00546k.
- [70] P. A. Julien *et al.*, "In Situ Monitoring and Mechanism of the Mechanochemical Formation of a Microporous MOF-74 Framework," *J Am Chem Soc*, vol. 138, no. 9, pp. 2929–2932, Mar. 2016, doi: 10.1021/jacs.5b13038.
- [71] G. Wang *et al.*, "Metal-organic frameworks template-directed growth of layered double hydroxides: A fantastic conversion of functional materials," Jun. 01, 2022, *Elsevier B.V.* doi: 10.1016/j.ccr.2022.214467.

- [72] M. Taheri, I. Di Bernardo, A. Lowe, D. R. Nisbet, and T. Tsuzuki, “Green Full Conversion of ZnO Nanopowders to Well-Dispersed Zeolitic Imidazolate Framework-8 (ZIF-8) Nanopowders via a Stoichiometric Mechanochemical Reaction for Fast Dye Adsorption,” *Cryst Growth Des*, vol. 20, no. 4, pp. 2761–2773, Apr. 2020, doi: 10.1021/acs.cgd.0c00129.
- [73] Z. Wang, Z. Li, M. Ng, and P. J. Milner, “Rapid mechanochemical synthesis of metal-organic frameworks using exogenous organic base,” *Dalton Transactions*, vol. 49, no. 45, pp. 16238–16244, Dec. 2020, doi: 10.1039/d0dt01240h.
- [74] R. Zhang, C. A. Tao, R. Chen, L. Wu, X. Zou, and J. Wang, “Ultrafast synthesis of Ni-MOF in one minute by ball milling,” *Nanomaterials*, vol. 8, no. 12, Dec. 2018, doi: 10.3390/NANO8121067.
- [75] M. Taheri, T. G. Enge, and T. Tsuzuki, “Water stability of cobalt doped ZIF-8: a quantitative study using optical analyses,” *Mater Today Chem*, vol. 16, Jun. 2020, doi: 10.1016/j.mtchem.2019.100231.
- [76] J. Beamish-Cook, K. Shankland, C. A. Murray, and P. Vaqueiro, “Insights into the Mechanochemical Synthesis of MOF-74,” *Cryst Growth Des*, vol. 21, no. 5, pp. 3047–3055, May 2021, doi: 10.1021/acs.cgd.1c00213.
- [77] Y. Chen *et al.*, “Highly efficient mechanochemical synthesis of an indium based metal-organic framework with excellent water stability,” *Chem Eng Sci*, vol. 158, pp. 539–544, Feb. 2017, doi: 10.1016/j.ces.2016.11.009.
- [78] Y. Sun, X. Jia, H. Huang, X. Guo, Z. Qiao, and C. Zhong, “Solvent-free mechanochemical route for the construction of ionic liquid and mixed-metal MOF composites for synergistic CO₂ fixation,” *J Mater Chem A Mater*, vol. 8, no. 6, pp. 3180–3185, Feb. 2020, doi: 10.1039/c9ta10409g.
- [79] I. Brekalo *et al.*, “Manometric real-time studies of the mechanochemical synthesis of zeolitic imidazolate frameworks,” *Chem Sci*, vol. 11, no. 8, pp. 2141–2147, Feb. 2020, doi: 10.1039/c9sc05514b.
- [80] M. Pilloni *et al.*, “Liquid-assisted mechanochemical synthesis of an iron carboxylate Metal Organic Framework and its evaluation in diesel fuel desulfurization,” *Microporous and Mesoporous Materials*, vol. 213, pp. 14–21, Sep. 2015, doi: 10.1016/j.micromeso.2015.04.005.
- [81] H. Liu, Y. Zhao, C. Zhou, B. Mu, and L. Chen, “Microwave-assisted synthesis of Zr-based metal–organic framework (Zr-fum-fcu-MOF) for gas adsorption separation,” *Chem Phys Lett*, vol. 780, Oct. 2021, doi: 10.1016/j.cplett.2021.138906.
- [82] Y. Thi Dang *et al.*, “Microwave-assisted synthesis of nano Hf- and Zr-based metal-organic frameworks for enhancement of curcumin adsorption,” *Microporous and Mesoporous Materials*, vol. 298, May 2020, doi: 10.1016/j.micromeso.2020.110064.
- [83] S. Gaikwad, S. J. Kim, and S. Han, “Novel metal–organic framework of UTSA-16 (Zn) synthesized by a microwave method: Outstanding performance for CO₂ capture with improved stability to acid gases,” *Journal of Industrial and Engineering Chemistry*, vol. 87, pp. 250–263, Jul. 2020, doi: 10.1016/j.jiec.2020.04.015.
- [84] Y. K. Seo, G. Hundal, I. T. Jang, Y. K. Hwang, C. H. Jun, and J. S. Chang, “Microwave synthesis of hybrid inorganic-organic materials including porous Cu₃(BTC)₂ from Cu(II)-trimesate mixture,” *Microporous and Mesoporous Materials*, vol. 119, no. 1–3, pp. 331–337, Mar. 2009, doi: 10.1016/j.micromeso.2008.10.035.

- [85] S. Laha, A. Chakraborty, and T. K. Maji, "Synergistic Role of Microwave and Perturbation toward Synthesis of Hierarchical Porous MOFs with Tunable Porosity," *Inorg Chem*, vol. 59, no. 6, pp. 3775–3782, Mar. 2020, doi: 10.1021/acs.inorgchem.9b03422.
- [86] A. Arenas-Vivo, D. Avila, and P. Horcajada, "Phase-selective microwave assisted synthesis of iron(III) aminoterephthalate MOFs," *Materials*, vol. 13, no. 6, Mar. 2020, doi: 10.3390/ma13061469.
- [87] H. Mao *et al.*, "Furfural separation from aqueous solution by pervaporation membrane mixed with metal organic framework MIL-53(Al) synthesized via high efficiency solvent-controlled microwave," *Sep Purif Technol*, vol. 272, Oct. 2021, doi: 10.1016/j.seppur.2021.118813.
- [88] Q. Li *et al.*, "Microwave-assisted rapid synthesis and activation of ultrathin trimetal–organic framework nanosheets for efficient electrocatalytic oxygen evolution," *J Colloid Interface Sci*, vol. 603, pp. 148–156, Dec. 2021, doi: 10.1016/j.jcis.2021.06.102.
- [89] L. N. Appelhans *et al.*, "Facile microwave synthesis of zirconium metal-organic framework thin films on gold and silicon and application to sensor functionalization," *Microporous and Mesoporous Materials*, vol. 323, Aug. 2021, doi: 10.1016/j.micromeso.2021.111133.
- [90] R. Vakili, S. Xu, N. Al-Janabi, P. Gorgojo, S. M. Holmes, and X. Fan, "Microwave-assisted synthesis of zirconium-based metal organic frameworks (MOFs): Optimization and gas adsorption," *Microporous and Mesoporous Materials*, vol. 260, pp. 45–53, Apr. 2018, doi: 10.1016/j.micromeso.2017.10.028.
- [91] H. T. T. Nguyen *et al.*, "Microwave-assisted solvothermal synthesis of bimetallic metal-organic framework for efficient photodegradation of organic dyes," *Mater Chem Phys*, vol. 272, Nov. 2021, doi: 10.1016/j.matchemphys.2021.125040.
- [92] M. Shen *et al.*, "Cyclodextrin metal–organic framework by ultrasound-assisted rapid synthesis for caffeic acid loading and antibacterial application," *Ultrason Sonochem*, vol. 86, May 2022, doi: 10.1016/j.ultsonch.2022.106003.
- [93] M. Stawowy *et al.*, "The impact of synthesis method on the properties and CO₂ sorption capacity of UiO-66(Ce)," *Catalysts*, vol. 9, no. 4, Apr. 2019, doi: 10.3390/catal9040309.
- [94] H. X. Tian, M. Zha, J. G. Ding, L. M. Zhu, B. L. Li, and B. Wu, "Visible-light-driven and ultrasonic-assisted copper metal-organic frameworks and graphene oxide nanocomposite for decolorization of dyes," *J Solid State Chem*, vol. 304, Dec. 2021, doi: 10.1016/j.jssc.2021.122627.
- [95] P. Hayati *et al.*, "Photocatalytic activity of new nanostructures of an Ag(i) metal-organic framework (Ag-MOF) for the efficient degradation of MCPA and 2,4-D herbicides under sunlight irradiation," *New Journal of Chemistry*, vol. 45, no. 7, pp. 3408–3417, Feb. 2021, doi: 10.1039/d0nj02460k.
- [96] D. A. Yang, H. Y. Cho, J. Kim, S. T. Yang, and W. S. Ahn, "CO₂ capture and conversion using Mg-MOF-74 prepared by a sonochemical method," *Energy Environ Sci*, vol. 5, no. 4, pp. 6465–6473, 2012, doi: 10.1039/c1ee02234b.
- [97] C. X. Yu *et al.*, "Highly efficient and selective removal of anionic dyes from aqueous solution by using a protonated metal-organic framework," *J Alloys Compd*, vol. 853, Feb. 2021, doi: 10.1016/j.jallcom.2020.157383.

- [98] P. Abdolalian, A. Morsali, and S. K. Tizhoush, "Sono-synthesis of basic metal-organic framework for reusable catalysis of organic reactions in the eco-friendly conditions," *J Solid State Chem*, vol. 303, Nov. 2021, doi: 10.1016/j.jssc.2021.122525.
- [99] Z. Q. Li *et al.*, "Ultrasonic synthesis of the microporous metal-organic framework Cu₃(BTC)₂ at ambient temperature and pressure: An efficient and environmentally friendly method," *Mater Lett*, vol. 63, no. 1, pp. 78–80, Jan. 2009, doi: 10.1016/j.matlet.2008.09.010.
- [100] D. Chen, Y. Cao, N. Chen, and P. Feng, "Synthesis and Characterization of Cobalt Metal Organic Frameworks Prepared by Ultrasonic Wave-Assisted Ball Milling for Adsorptive Removal of Congo Red Dye from Aqueous Solutions," *J Inorg Organomet Polym Mater*, vol. 31, no. 3, pp. 1231–1240, Mar. 2021, doi: 10.1007/s10904-020-01832-y.
- [101] B. Yao *et al.*, "Rapid ultrasound-assisted synthesis of controllable Zn/Co-based zeolitic imidazolate framework nanoparticles for heterogeneous catalysis," *Microporous and Mesoporous Materials*, vol. 314, Feb. 2021, doi: 10.1016/j.micromeso.2020.110777.
- [102] N. Campagnol *et al.*, "On the electrochemical deposition of metal-organic frameworks," *J Mater Chem A Mater*, vol. 4, no. 10, pp. 3914–3925, 2016, doi: 10.1039/c5ta10782b.
- [103] V. M. V. and G. Nageswaran, "Review—Direct Electrochemical Synthesis of Metal Organic Frameworks," *J Electrochem Soc*, vol. 167, no. 15, p. 155527, Dec. 2020, doi: 10.1149/1945-7111/abc6c6.
- [104] U. Mueller, M. Schubert, F. Teich, H. Puetter, K. Schierle-Arndt, and J. Pastré, "Metal-organic frameworks - Prospective industrial applications," in *Journal of Materials Chemistry*, 2006, pp. 626–636. doi: 10.1039/b511962f.
- [105] Ö. H. Demirel, T. Rijnaarts, P. De Wit, J. A. Wood, and N. E. Benes, "Electroforming of a metal-organic framework on porous copper hollow fibers," *J Mater Chem A Mater*, vol. 7, no. 20, pp. 12616–12626, 2019, doi: 10.1039/c8ta11296g.
- [106] W. W. Lestari, I. D. Winarni, and F. Rahmawati, "Electrosynthesis of Metal-Organic Frameworks (MOFs) Based on Nickel(II) and Benzene 1,3,5-Tri Carboxylic Acid (H₃BTC): An Optimization Reaction Condition," in *IOP Conference Series: Materials Science and Engineering*, Institute of Physics Publishing, Feb. 2017. doi: 10.1088/1757-899X/172/1/012064.
- [107] J. L. Hauser, M. Tso, K. Fitchmun, and S. R. J. Oliver, "Anodic Electrodeposition of Several Metal Organic Framework Thin Films on Indium Tin Oxide Glass," *Cryst Growth Des*, vol. 19, no. 4, pp. 2358–2365, Apr. 2019, doi: 10.1021/acs.cgd.9b00054.
- [108] H. M. Yang, X. Liu, X. L. Song, T. L. Yang, Z. H. Liang, and C. M. Fan, "In situ electrochemical synthesis of MOF-5 and its application in improving photocatalytic activity of BiOBr," *Transactions of Nonferrous Metals Society of China (English Edition)*, vol. 25, no. 12, pp. 3987–3994, Dec. 2015, doi: 10.1016/S1003-6326(15)64047-X.
- [109] L. Han *et al.*, "Preparation of multivariate zirconia metal-organic frameworks for highly efficient adsorption of endocrine disrupting compounds," *J Hazard Mater*, vol. 424, Feb. 2022, doi: 10.1016/j.jhazmat.2021.127559.

- [110] K. Okada, Y. Tanaka, T. Inose, H. Ujii, H. Yoshikawa, and D. Tanaka, "Electrolytic synthesis of porphyrinic Zr-metal-organic frameworks with selective crystal topologies," *Dalton Transactions*, vol. 50, no. 16, pp. 5411–5415, Apr. 2021, doi: 10.1039/d1dt00491c.
- [111] T. Zhang *et al.*, "Rapid synthesis of UiO-66 by means of electrochemical cathode method with electrochemical detection of 2,4,6-TCP," *Inorg Chem Commun*, vol. 111, Jan. 2020, doi: 10.1016/j.inoche.2019.107671.
- [112] B. Habibi, S. Pashazadeh, L. A. Saghatforoush, and A. Pashazadeh, "Direct electrochemical synthesis of the copper based metal-organic framework on/in the heteroatoms doped graphene/pencil graphite electrode: Highly sensitive and selective electrochemical sensor for sertraline hydrochloride," *Journal of Electroanalytical Chemistry*, vol. 888, May 2021, doi: 10.1016/j.jelechem.2021.115210.
- [113] A. M. Antonio, J. Rosenthal, and E. D. Bloch, "Electrochemically Mediated Syntheses of Titanium(III)-Based Metal-Organic Frameworks," *J Am Chem Soc*, vol. 141, no. 29, pp. 11383–11387, Jul. 2019, doi: 10.1021/jacs.9b05035.
- [114] F. Zhang, T. Zhang, X. Zou, X. Liang, G. Zhu, and F. Qu, "Electrochemical synthesis of metal organic framework films with proton conductive property," *Solid State Ion*, vol. 301, pp. 125–132, Mar. 2017, doi: 10.1016/j.ssi.2017.01.022.
- [115] K. K. Tanabe and S. M. Cohen, "Postsynthetic modification of metal–organic frameworks—a progress report," *Chem Soc Rev*, vol. 40, no. 2, pp. 498–519, Jan. 2011, doi: 10.1039/c0cs00031k.
- [116] W. He, D. Lv, Y. Guan, and S. Yu, "Post-synthesis modification of metal-organic frameworks: synthesis, characteristics, and applications," Nov. 01, 2023, *Royal Society of Chemistry*. doi: 10.1039/d3ta05158g.
- [117] A. M. Shultz, A. A. Sarjeant, O. K. Farha, J. T. Hupp, and S. T. Nguyen, "Post-synthesis modification of a metal-organic framework to form metallosalen-containing MOF materials," *J Am Chem Soc*, vol. 133, no. 34, pp. 13252–13255, Aug. 2011, doi: 10.1021/ja204820d.
- [118] M. Kim and S. M. Cohen, "Discovery, development, and functionalization of Zr(IV)-based metal-organic frameworks," *CrystEngComm*, vol. 14, no. 12, pp. 4096–4104, Jun. 2012, doi: 10.1039/c2ce06491j.
- [119] J. Canivet, S. Aguado, G. Bergeret, and D. Farrusseng, "Amino acid functionalized metal-organic frameworks by a soft coupling-deprotection sequence," *Chemical Communications*, vol. 47, no. 42, pp. 11650–11652, Nov. 2011, doi: 10.1039/c1cc15541e.
- [120] T. Zhou *et al.*, "Post-synthesis modification of a metal-organic framework to construct a bifunctional photocatalyst for hydrogen production," *Energy Environ Sci*, vol. 6, no. 11, pp. 3229–3234, Nov. 2013, doi: 10.1039/c3ee41548a.
- [121] Q. Cheng *et al.*, "Chiral metal-organic frameworks materials for racemate resolution," Jun. 01, 2023, *Elsevier B.V.* doi: 10.1016/j.ccr.2023.215120.
- [122] R. Rani, A. Deep, B. Mizaikoff, and S. Singh, "Enhanced hydrothermal stability of Cu MOF by post synthetic modification with amino acids," *Vacuum*, vol. 164, pp. 449–457, Jun. 2019, doi: 10.1016/j.vacuum.2019.01.011.
- [123] J. Lim *et al.*, "Amine-Tagged Fragmented Ligand Installation for Covalent Modification of MOF-74," *Angewandte Chemie - International Edition*, vol. 60, no. 17, pp. 9296–9300, Apr. 2021, doi: 10.1002/anie.202100456.

- [124] M. Ding, W. Liu, and R. Gref, “Nanoscale MOFs: From synthesis to drug delivery and theranostics applications,” Nov. 01, 2022, *Elsevier B.V.* doi: 10.1016/j.addr.2022.114496.
- [125] Y. An *et al.*, “The stability of MOFs in aqueous solutions—research progress and prospects,” Jun. 01, 2024, *KeAi Communications Co.* doi: 10.1016/j.gce.2023.07.004.
- [126] B. Pramanik, R. Sahoo, and M. C. Das, “pH-stable MOFs: Design principles and applications,” Oct. 15, 2023, *Elsevier B.V.* doi: 10.1016/j.ccr.2023.215301.
- [127] B. Wang, Q. Yang, C. Guo, Y. Sun, L. H. Xie, and J. R. Li, “Stable Zr(IV)-Based Metal-Organic Frameworks with Predesigned Functionalized Ligands for Highly Selective Detection of Fe(III) Ions in Water,” *ACS Appl Mater Interfaces*, vol. 9, no. 11, pp. 10286–10295, Mar. 2017, doi: 10.1021/acsami.7b00918.
- [128] L. H. Xie, X. M. Liu, T. He, and J. R. Li, “Metal-Organic Frameworks for the Capture of Trace Aromatic Volatile Organic Compounds,” *Chem*, vol. 4, no. 8, pp. 1911–1927, Aug. 2018, doi: 10.1016/j.chempr.2018.05.017.
- [129] X. L. Lv *et al.*, “Ligand Rigidification for Enhancing the Stability of Metal-Organic Frameworks,” *J Am Chem Soc*, vol. 141, no. 26, pp. 10283–10293, Jul. 2019, doi: 10.1021/jacs.9b02947.
- [130] Y. Chen, P. Li, J. A. Modica, R. J. Drout, and O. K. Farha, “Acid-Resistant Mesoporous Metal-Organic Framework toward Oral Insulin Delivery: Protein Encapsulation, Protection, and Release,” *J Am Chem Soc*, vol. 140, no. 17, pp. 5678–5681, May 2018, doi: 10.1021/jacs.8b02089.
- [131] Y. Y. Xue, S. N. Li, Y. C. Jiang, M. C. Hu, and Q. G. Zhai, “Quest for 9-connected robust metal-organic framework platforms based on [M 3 (O/OH)(COO) 6 (pyridine) 3] clusters as excellent gas separation and asymmetric supercapacitor materials,” *J Mater Chem A Mater*, vol. 7, no. 9, pp. 4640–4650, 2019, doi: 10.1039/c8ta09080g.
- [132] F. Leng, H. Liu, M. Ding, Q. P. Lin, and H. L. Jiang, “Boosting Photocatalytic Hydrogen Production of Porphyrinic MOFs: The Metal Location in Metalloporphyrin Matters,” *ACS Catal*, vol. 8, no. 5, pp. 4583–4590, May 2018, doi: 10.1021/acscatal.8b00764.
- [133] K. Leus *et al.*, “Systematic study of the chemical and hydrothermal stability of selected ‘stable’ Metal Organic Frameworks,” *Microporous and Mesoporous Materials*, vol. 226, pp. 110–116, May 2016, doi: 10.1016/j.micromeso.2015.11.055.
- [134] J. Aguilera-Sigalat and D. Bradshaw, “A colloidal water-stable MOF as a broad-range fluorescent pH sensor via post-synthetic modification,” *Chemical Communications*, vol. 50, no. 36, pp. 4711–4713, Apr. 2014, doi: 10.1039/c4cc00659c.
- [135] S. Ghosh and S. Biswas, “Ultrafast and nanomolar level detection of H₂S in aqueous medium using a functionalized UiO-66 metal-organic framework based fluorescent chemosensor,” *Dalton Transactions*, vol. 50, no. 33, pp. 11631–11639, Sep. 2021, doi: 10.1039/d1dt01456k.
- [136] N. Seal, M. Singh, S. Das, R. Goswami, B. Pathak, and S. Neogi, “Dual-functionalization actuated trimodal attribute in an ultra-robust MOF: Exceptionally selective capture and effectual fixation of CO₂ with fast-responsive, nanomolar detection of assorted organo-contaminants in water,” *Mater Chem Front*, vol. 5, no. 2, pp. 979–994, Jan. 2021, doi: 10.1039/d0qm00721h.

- [137] Z. B. Sun, Y. N. Si, S. N. Zhao, Q. Y. Wang, and S. Q. Zang, "Ozone Decomposition by a Manganese-Organic Framework over the Entire Humidity Range," *J Am Chem Soc*, vol. 143, no. 13, pp. 5150–5157, Apr. 2021, doi: 10.1021/jacs.1c01027.
- [138] L. Liang *et al.*, "Carbon dioxide capture and conversion by an acid-base resistant metal-organic framework," *Nat Commun*, vol. 8, no. 1, Dec. 2017, doi: 10.1038/s41467-017-01166-3.
- [139] Y. Y. Fu, C. X. Yang, and X. P. Yan, "Metal-organic framework MIL-100(Fe) as the stationary phase for both normal-phase and reverse-phase high performance liquid chromatography," *J Chromatogr A*, vol. 1274, pp. 137–144, Jan. 2013, doi: 10.1016/j.chroma.2012.12.015.
- [140] D. Evangelou, A. Pournara, C. Tziasiou, E. Andreou, G. S. Armatas, and M. J. Manos, "Robust Al³⁺ MOF with Selective As(V) Sorption and Efficient Luminescence Sensing Properties toward Cr(VI)," *Inorg Chem*, vol. 61, no. 4, pp. 2017–2030, Jan. 2022, doi: 10.1021/acs.inorgchem.1c03199.
- [141] M. T. Hang *et al.*, "Rational synthesis of isomorphic rare earth metal-organic framework materials for simultaneous adsorption and photocatalytic degradation of organic dyes in water," *CrystEngComm*, vol. 24, no. 3, pp. 552–559, Jan. 2022, doi: 10.1039/d1ce01411k.
- [142] X. Han *et al.*, "Water-Stable Eu⁶⁺-Cluster-Based fcu-MOF with Exposed Vinyl Groups for Ratiometric and Fluorescent Visual Sensing of Hydrogen Sulfide," *Inorg Chem*, vol. 61, no. 12, pp. 5067–5075, Mar. 2022, doi: 10.1021/acs.inorgchem.2c00019.
- [143] X. Q. Wang *et al.*, "A water-stable zinc(ii)-organic framework as a multiresponsive luminescent sensor for toxic heavy metal cations, oxyanions and organochlorine pesticides in aqueous solution," *Dalton Transactions*, vol. 48, no. 44, pp. 16776–16785, 2019, doi: 10.1039/c9dt03195b.
- [144] Q. R. Liu, B. Liu, M. M. Qiu, W. N. Miao, and L. Xu, "A Europium MOF-based turn-off fluorescent sensor for tryptophan detection in human serum, urine and lake water," *J Solid State Chem*, vol. 311, Jul. 2022, doi: 10.1016/j.jssc.2022.123138.
- [145] H. Atallah, M. Elcheikh Mahmoud, F. M. Ali, A. Lough, and M. Hmadeh, "A highly stable indium based metal organic framework for efficient arsenic removal from water," *Dalton Transactions*, vol. 47, no. 3, pp. 799–806, 2018, doi: 10.1039/c7dt03705h.
- [146] C. Zhang *et al.*, "Water Stable Metal-Organic Framework Based on Phosphono-containing Ligand as Highly Sensitive Luminescent Sensor toward Metal Ions," *Cryst Growth Des*, vol. 18, no. 12, pp. 7683–7689, Dec. 2018, doi: 10.1021/acs.cgd.8b01535.
- [147] A. Pankajakshan, D. Kuznetsov, and S. Mandal, "Ultrasensitive Detection of Hg(II) Ions in Aqueous Medium Using Zinc-Based Metal-Organic Framework," *Inorg Chem*, vol. 58, no. 2, pp. 1377–1381, Jan. 2019, doi: 10.1021/acs.inorgchem.8b02898.
- [148] X. Wang *et al.*, "A stable interpenetrated Zn-MOF with efficient light hydrocarbon adsorption/separation performance," *Cryst Growth Des*, vol. 20, no. 9, pp. 5670–5675, Sep. 2020, doi: 10.1021/acs.cgd.0c00925.
- [149] S. Gai *et al.*, "Highly Stable Zinc-Based Metal-Organic Frameworks and Corresponding Flexible Composites for Removal and Detection of Antibiotics in Water," *ACS Appl Mater Interfaces*, vol. 12, no. 7, pp. 8650–8662, Feb. 2020, doi: 10.1021/acsami.9b19583.

- [150] Q. Huang *et al.*, “A highly stable polyoxometalate-based metal-organic framework with π - π Stacking for enhancing lithium ion battery performance,” *J Mater Chem A Mater*, vol. 5, no. 18, pp. 8477–8483, 2017, doi: 10.1039/c7ta00900c.
- [151] S. M. Moosavi, P. G. Boyd, L. Sarkisov, and B. Smit, “Improving the Mechanical Stability of Metal-Organic Frameworks Using Chemical Caryatids,” *ACS Cent Sci*, vol. 4, no. 7, pp. 832–839, Jul. 2018, doi: 10.1021/acscentsci.8b00157.
- [152] B. Li, H. M. Wen, Y. Cui, W. Zhou, G. Qian, and B. Chen, “Emerging Multifunctional Metal–Organic Framework Materials,” Oct. 26, 2016, *Wiley-VCH Verlag*. doi: 10.1002/adma.201601133.
- [153] S. S. Kaye, A. Dailly, O. M. Yaghi, and J. R. Long, “Impact of preparation and handling on the hydrogen storage properties of $\text{Zn}_4\text{O}(1,4\text{-benzenedicarboxylate})_3$ (MOF-5),” *J Am Chem Soc*, vol. 129, no. 46, pp. 14176–14177, Nov. 2007, doi: 10.1021/ja076877g.
- [154] J. D. Termine *et al.*, “Hydrogen Storage in Microporous Metal-Organic Frameworks,” 1973. [Online]. Available: <http://science.sciencemag.org/>
- [155] R. V. Morris *et al.*, “Identification of carbonate-rich outcrops on Mars by the spirit rover,” *Science (1979)*, vol. 329, no. 5990, pp. 421–424, Jul. 2010, doi: 10.1126/science.1189667.
- [156] D. Gygi *et al.*, “Hydrogen Storage in the Expanded Pore Metal-Organic Frameworks $\text{M}_2(\text{dobpdc})$ ($\text{M} = \text{Mg}, \text{Mn}, \text{Fe}, \text{Co}, \text{Ni}, \text{Zn}$),” *Chemistry of Materials*, vol. 28, no. 4, pp. 1128–1138, Feb. 2016, doi: 10.1021/acs.chemmater.5b04538.
- [157] H. R. Abid, H. Tian, H. M. Ang, M. O. Tade, C. E. Buckley, and S. Wang, “Nanosize Zr-metal organic framework (UiO-66) for hydrogen and carbon dioxide storage,” *Chemical Engineering Journal*, vol. 187, pp. 415–420, Apr. 2012, doi: 10.1016/j.cej.2012.01.104.
- [158] R. P. Ojha, P. A. Lemieux, P. K. Dixon, A. J. Liu, and D. J. Durian, “Statistical mechanics of a gas-fluidized particle,” *Nature*, vol. 427, no. 6974, pp. 521–523, Feb. 2004, doi: 10.1038/nature02294.
- [159] J. R. Li, J. Sculley, and H. C. Zhou, “Metal-organic frameworks for separations,” Feb. 08, 2012. doi: 10.1021/cr200190s.
- [160] J. R. Li, R. J. Kuppler, and H. C. Zhou, “Selective gas adsorption and separation in metal-organic frameworks,” *Chem Soc Rev*, vol. 38, no. 5, pp. 1477–1504, 2009, doi: 10.1039/b802426j.
- [161] E. D. Bloch *et al.*, “Selective binding of O_2 over N_2 in a redox-active metal-organic framework with open iron(II) coordination sites,” *J Am Chem Soc*, vol. 133, no. 37, pp. 14814–14822, Sep. 2011, doi: 10.1021/ja205976v.
- [162] L. J. Murray *et al.*, “Highly-selective and reversible O_2 binding in $\text{Cr}_3(1,3,5\text{-benzenetricarboxylate})_2$,” *J Am Chem Soc*, vol. 132, no. 23, pp. 7856–7857, Jun. 2010, doi: 10.1021/ja1027925.
- [163] G. Dubois, R. Tripier, S. Brandès, F. Denat, and R. Guilard, “Cyclam complexes containing silica gels for dioxygen adsorption,” *J Mater Chem*, vol. 12, no. 8, pp. 2255–2261, Aug. 2002, doi: 10.1039/b203372k.
- [164] B. Castro-Domínguez, P. Leelachaikul, A. Takagaki, T. Sugawara, R. Kikuchi, and S. T. Oyama, “Perfluorocarbon-based supported liquid membranes for O_2/N_2 separation,” *Sep Purif Technol*, vol. 116, pp. 19–24, 2013, doi: 10.1016/j.seppur.2013.05.023.
- [165] G. T. Rochelle, “Amine Scrubbing for CO_2 Capture,” 2009. doi: 10.1126/science.1176731.

- [166] B. P. Mandal and S. S. Bandyopadhyay, "Absorption of carbon dioxide into aqueous blends of 2-amino-2-methyl-1-propanol and monoethanolamine," *Chem Eng Sci*, vol. 61, no. 16, pp. 5440–5447, Aug. 2006, doi: 10.1016/j.ces.2006.04.002.
- [167] S. R. Caskey, A. G. Wong-Foy, and A. J. Matzger, "Dramatic tuning of carbon dioxide uptake via metal substitution in a coordination polymer with cylindrical pores," *J Am Chem Soc*, vol. 130, no. 33, pp. 10870–10871, Aug. 2008, doi: 10.1021/ja8036096.
- [168] Z. R. Herm, E. D. Bloch, and J. R. Long, "Hydrocarbon separations in metal-organic frameworks," Jan. 14, 2014. doi: 10.1021/cm402897c.
- [169] E. D. Bloch, W. L. Queen, R. Krishna, J. M. Zadrozny, C. M. Brown, and J. R. Long, "Hydrocarbon separations in a metal-organic framework with open iron(II) coordination sites," *Science (1979)*, vol. 335, no. 6076, pp. 1606–1610, Mar. 2012, doi: 10.1126/science.1217544.
- [170] Y. He, R. Krishna, and B. Chen, "Metal-organic frameworks with potential for energy-efficient adsorptive separation of light hydrocarbons," *Energy Environ Sci*, vol. 5, no. 10, pp. 9107–9120, Oct. 2012, doi: 10.1039/c2ee22858k.
- [171] S. Yang *et al.*, "Supramolecular binding and separation of hydrocarbons within a functionalized porous metal-organic framework," *Nat Chem*, vol. 7, no. 2, pp. 121–129, 2015, doi: 10.1038/nchem.2114.
- [172] B. Li *et al.*, "Introduction of π -complexation into porous aromatic framework for highly selective adsorption of ethylene over ethane," *J Am Chem Soc*, vol. 136, no. 24, pp. 8654–8660, Jun. 2014, doi: 10.1021/ja502119z.
- [173] B. Chen *et al.*, "A microporous metal-organic framework for gas-chromatographic separation of alkanes," *Angewandte Chemie - International Edition*, vol. 45, no. 9, pp. 1390–1393, Feb. 2006, doi: 10.1002/anie.200502844.
- [174] C.-T. He *et al.*, "Exceptional Hydrophobicity of a Large-Pore Metal-Organic Zeolite," *J. Am. Chem. Soc.*, pp. 137(22):7217–23., May 2015, doi: 10.1021/jacs.5b03727.
- [175] B. Chen, S. Xiang, and G. Qian, "Metal-organic frameworks with functional pores for recognition of small molecules," *Acc Chem Res*, vol. 43, no. 8, pp. 1115–1124, Aug. 2010, doi: 10.1021/ar100023y.
- [176] A. Lan *et al.*, "A luminescent microporous metal-organic framework for the fast and reversible detection of high explosives," *Angewandte Chemie - International Edition*, vol. 48, no. 13, pp. 2334–2338, Mar. 2009, doi: 10.1002/anie.200804853.
- [177] B. Chen, Y. Yang, F. Zapata, G. Lin, G. Qian, and E. B. Lobkovsky, "Luminescent open metal sites within a metal-organic framework for sensing small molecules," *Advanced Materials*, vol. 19, no. 13, pp. 1693–1696, Jul. 2007, doi: 10.1002/adma.200601838.
- [178] C.-T. He *et al.*, "Convenient detection of Pd(II) by a metal-organic framework with sulfur and olefin functions," *J. Am. Chem. Soc.*, 2015, [Online]. Available: <http://pubs.acs.org>
- [179] H. L. Jiang *et al.*, "An exceptionally stable, porphyrinic Zr metal-organic framework exhibiting pH-dependent fluorescence," *J Am Chem Soc*, vol. 135, no. 37, pp. 13934–13938, Sep. 2013, doi: 10.1021/ja406844r.

- [180] M. H. Beyzavi *et al.*, “A hafnium-based metal-organic framework as an efficient and multifunctional catalyst for facile CO₂ fixation and regioselective and enantioselective epoxide activation,” *J Am Chem Soc*, vol. 136, no. 45, pp. 15861–15864, Nov. 2014, doi: 10.1021/ja508626n.
- [181] J. E. Mondloch *et al.*, “Destruction of chemical warfare agents using metal-organic frameworks,” *Nat Mater*, vol. 14, no. 5, pp. 512–516, May 2015, doi: 10.1038/nmat4238.
- [182] Jung S *et al.*, “A homochiral metal-organic porous material for enantioselective separation and catalysis”.
- [183] M. Wang, M. H. Xie, C. De Wu, and Y. G. Wang, “From one to three: A serine derivate manipulated homochiral metal-organic framework,” *Chemical Communications*, no. 17, pp. 2396–2398, 2009, doi: 10.1039/b823323c.
- [184] D. Feng *et al.*, “Stable metal-organic frameworks containing single-molecule traps for enzyme encapsulation,” *Nat Commun*, vol. 6, 2015, doi: 10.1038/ncomms6979.
- [185] P. Horcajada, C. Serre, M. Vallet-Regí, M. Sebban, F. Taulelle, and G. Férey, “Metal-organic frameworks as efficient materials for drug delivery,” *Angewandte Chemie - International Edition*, vol. 45, no. 36, pp. 5974–5978, Sep. 2006, doi: 10.1002/anie.200601878.
- [186] Y. Zhong *et al.*, “Recent advances in MOF-based nanoplatforms generating reactive species for chemodynamic therapy,” Aug. 28, 2020, *Royal Society of Chemistry*. doi: 10.1039/d0dt01882a.
- [187] X. Gao, M. Zhai, W. Guan, J. Liu, Z. Liu, and A. Damirin, “Controllable synthesis of a smart multifunctional nanoscale metal-organic framework for magnetic resonance/optical imaging and targeted drug delivery,” *ACS Appl Mater Interfaces*, vol. 9, no. 4, pp. 3455–3462, Feb. 2017, doi: 10.1021/acsami.6b14795.
- [188] A. Kabir, K. G. Furton, and A. Malik, “Innovations in sol-gel microextraction phases for solvent-free sample preparation in analytical chemistry,” 2013, *Elsevier B.V.* doi: 10.1016/j.trac.2012.11.014.
- [189] A. Andrade-Eiroa, M. Canle, V. Leroy-Cancellieri, and V. Cerdà, “Solid-phase extraction of organic compounds: A critical review. part ii,” Jun. 01, 2016, *Elsevier B.V.* doi: 10.1016/j.trac.2015.08.014.
- [190] A. Andrade-Eiroa, M. Canle, V. Leroy-Cancellieri, and V. Cerdà, “Solid-phase extraction of organic compounds: A critical review (Part I),” Jun. 01, 2016, *Elsevier B.V.* doi: 10.1016/j.trac.2015.08.015.
- [191] Y. Y. Zhou, X. P. Yan, K. N. Kim, S. W. Wang, and M. G. Liu, “Exploration of coordination polymer as sorbent for flow injection solid-phase extraction on-line coupled with high-performance liquid chromatography for determination of polycyclic aromatic hydrocarbons in environmental materials,” *J Chromatogr A*, vol. 1116, no. 1–2, pp. 172–178, May 2006, doi: 10.1016/j.chroma.2006.03.061.
- [192] G. Gao, Y. Xing, T. Liu, J. Wang, and X. Hou, “UiO-66(Zr) as sorbent for porous membrane protected micro-solid-phase extraction androgens and progestogens in environmental water samples coupled with LC-MS/MS analysis: The application of experimental and molecular simulation method,” *Microchemical Journal*, vol. 146, pp. 126–133, May 2019, doi: 10.1016/j.microc.2018.12.050.
- [193] H. Duo, Y. Wang, L. Wang, X. Lu, and X. Liang, “Zirconium(IV)-based metal-organic frameworks (UiO-67) as solid-phase extraction adsorbents for extraction of phenoxyacetic acid herbicides from vegetables,” *J Sep Sci*, vol. 41, no. 22, pp. 4149–4158, Nov. 2018, doi: 10.1002/jssc.201800784.

- [194] Q. Han, T. Aydan, L. Yang, X. Zhang, Q. Liang, and M. Ding, "In-syringe solid-phase extraction for on-site sampling of pyrethroids in environmental water samples," *Anal Chim Acta*, vol. 1009, pp. 48–55, Jun. 2018, doi: 10.1016/j.aca.2018.01.001.
- [195] X. Zhang, P. Wang, Q. Han, H. Li, T. Wang, and M. Ding, "Metal–organic framework based in-syringe solid-phase extraction for the on-site sampling of polycyclic aromatic hydrocarbons from environmental water samples," *J Sep Sci*, vol. 41, no. 8, pp. 1856–1863, Apr. 2018, doi: 10.1002/jssc.201701383.
- [196] A. Amiri, R. Tayebbe, A. Abdar, and F. Narenji Sani, "Synthesis of a zinc-based metal-organic framework with histamine as an organic linker for the dispersive solid-phase extraction of organophosphorus pesticides in water and fruit juice samples," *J Chromatogr A*, vol. 1597, pp. 39–45, Jul. 2019, doi: 10.1016/j.chroma.2019.03.039.
- [197] X. Mao, A. Yan, Y. Wan, D. Luo, and H. Yang, "Dispersive solid-phase extraction using microporous sorbent UiO-66 coupled to gas chromatography-tandem mass spectrometry: A QuEChERS-Type method for the determination of organophosphorus pesticide residues in edible vegetable oils without matrix interference," *J Agric Food Chem*, vol. 67, no. 6, pp. 1760–1770, Feb. 2019, doi: 10.1021/acs.jafc.8b04980.
- [198] M. Gao *et al.*, "Hydrogen-bonding-induced efficient dispersive solid phase extraction of bisphenols and their derivatives in environmental waters using surface amino-functionalized MIL-101(Fe)," *Microchemical Journal*, vol. 145, pp. 1151–1161, Mar. 2019, doi: 10.1016/j.microc.2018.12.013.
- [199] F. Maya, C. Palomino Cabello, R. M. Frizzarin, J. M. Estela, G. Turnes Palomino, and V. Cerdà, "Magnetic solid-phase extraction using metal-organic frameworks (MOFs) and their derived carbons," May 01, 2017, *Elsevier B.V.* doi: 10.1016/j.trac.2017.03.004.
- [200] G. Mínguez Espallargas and E. Coronado, "Magnetic functionalities in MOFs: From the framework to the pore," Jan. 21, 2018, *Royal Society of Chemistry*. doi: 10.1039/c7cs00653e.
- [201] L. Fan *et al.*, "A multifunctional composite Fe₃O₄/MOF/l-cysteine for removal, magnetic solid phase extraction and fluorescence sensing of Cd(II)," *RSC Adv*, vol. 8, no. 19, pp. 10561–10572, 2018, doi: 10.1039/c8ra00070k.
- [202] W. Filipiak and B. Bojko, "SPME in clinical, pharmaceutical, and biotechnological research – How far are we from daily practice?," Jun. 01, 2019, *Elsevier B.V.* doi: 10.1016/j.trac.2019.02.029.
- [203] W. Guo, H. Tao, H. Tao, Q. Shuai, and L. Huang, "Recent progress of covalent organic frameworks as attractive materials for solid-phase microextraction: A review," Jan. 25, 2024, *Elsevier B.V.* doi: 10.1016/j.aca.2023.341953.
- [204] X. Y. Cui, Z. Y. Gu, D. Q. Jiang, Y. Li, H. F. Wang, and X. P. Yan, "In situ hydrothermal growth of metal-organic framework 199 films on stainless steel fibers for solid-phase microextraction of gaseous benzene homologues," *Anal Chem*, vol. 81, no. 23, pp. 9771–9777, Dec. 2009, doi: 10.1021/ac901663x.
- [205] M. Cruz-Vera, R. Lucena, S. Cárdenas, and M. Valcárcel, "Sorptive microextraction for liquid-chromatographic determination of drugs in urine," Nov. 2009. doi: 10.1016/j.trac.2009.07.010.
- [206] L. Q. Yu and X. P. Yan, "Covalent bonding of zeolitic imidazolate framework-90 to functionalized silica fibers for solid-phase microextraction," *Chemical Communications*, vol. 49, no. 21, pp. 2142–2144, Feb. 2013, doi: 10.1039/c3cc00123g.

- [207] X. Liu, F. Suo, M. He, B. Chen, and B. Hu, "Imidazole functionalized organic monoliths for capillary microextraction of Co(II), Ni(II) and Cd(II) from urine prior to on-line ICP-MS detection," *Microchimica Acta*, vol. 184, no. 3, pp. 927–934, Mar. 2017, doi: 10.1007/s00604-017-2087-5.
- [208] C. L. Lin, S. Lirio, Y. T. Chen, C. H. Lin, and H. Y. Huang, "A novel hybrid metal-organic framework-polymeric monolith for solid-phase microextraction," *Chemistry - A European Journal*, vol. 20, no. 12, pp. 3317–3321, Mar. 2014, doi: 10.1002/chem.201304458.
- [209] C. Wang, W. Zhou, X. Liao, X. Wang, and Z. Chen, "Covalent immobilization of metal organic frameworks onto chemical resistant poly(ether ether ketone) jacket for stir bar extraction," *Anal Chim Acta*, vol. 1025, pp. 124–133, Sep. 2018, doi: 10.1016/j.aca.2018.04.056.
- [210] R. Jiang and J. Pawliszyn, "Thin-film microextraction offers another geometry for solid-phase microextraction," Oct. 2012. doi: 10.1016/j.trac.2012.07.005.
- [211] F. Alipour, J. B. Raoof, and M. Ghani, "Hierarchical zeolitic imidazolate framework-67 derived from in-situ synthesized CO-Al layered double hydroxide embedded within porous-anodized aluminum foil for thin film microextraction of caffeine followed by its high performance liquid chromatography-ultraviolet detection," *J Chromatogr A*, vol. 1626, Aug. 2020, doi: 10.1016/j.chroma.2020.461358.
- [212] Y. Zhang, B. Wang, and R. Wang, "Functionally decorated metal-organic frameworks in environmental remediation," Jan. 01, 2023, *Elsevier B.V.* doi: 10.1016/j.cej.2022.140741.
- [213] J. Bikash Baruah, "Coordination polymers in adsorptive remediation of environmental contaminants," Nov. 01, 2022, *Elsevier B.V.* doi: 10.1016/j.ccr.2022.214694.
- [214] H. Shayegan, G. A. M. Ali, and V. Safarifard, "Recent Progress in the Removal of Heavy Metal Ions from Water Using Metal-Organic Frameworks," Jan. 09, 2020, *Wiley-Blackwell*. doi: 10.1002/slct.201904107.
- [215] R. Al-Wafi, M. K. Ahmed, and S. F. Mansour, "Tuning the synthetic conditions of graphene oxide/magnetite/ hydroxyapatite/cellulose acetate nanofibrous membranes for removing Cr(VI), Se(IV) and methylene blue from aqueous solutions," *Journal of Water Process Engineering*, vol. 38, Dec. 2020, doi: 10.1016/j.jwpe.2020.101543.
- [216] T. Rasheed, M. Adeel, F. Nabeel, M. Bilal, and H. M. N. Iqbal, "TiO₂/SiO₂ decorated carbon nanostructured materials as a multifunctional platform for emerging pollutants removal," Oct. 20, 2019, *Elsevier B.V.* doi: 10.1016/j.scitotenv.2019.06.200.
- [217] T. Rasheed, F. Nabeel, and S. Shafi, "Chromogenic vesicles for aqueous detection and quantification of Hg²⁺ /Cu²⁺ in real water samples," *J Mol Liq*, vol. 282, pp. 489–498, May 2019, doi: 10.1016/j.molliq.2019.03.048.
- [218] T. Rasheed, F. Nabeel, C. Li, and Y. Zhang, "Rhodol assisted alternating copolymer based chromogenic vesicles for the aqueous detection and quantification of hydrazine via switch-on strategy," *J Mol Liq*, vol. 274, pp. 461–469, Jan. 2019, doi: 10.1016/j.molliq.2018.11.014.
- [219] T. Rasheed, F. Nabeel, M. Adeel, M. Bilal, and H. M. N. Iqbal, "'Turn-on' fluorescent sensor-based probing of toxic Hg(II) and Cu(II) with potential intracellular monitoring," *Biocatal Agric Biotechnol*, vol. 17, pp. 696–701, Jan. 2019, doi: 10.1016/j.bcab.2019.01.032.
- [220] S. Li *et al.*, "Water Purification: Adsorption over Metal-Organic Frameworks," Feb. 01, 2016, *Shanghai Institute of Organic Chemistry*. doi: 10.1002/cjoc.201500761.

- [221] “Drinking Water Contaminants,” United States Environmental Protection Agency. Accessed: Jun. 01, 2024. [Online]. Available: <http://water.epa.gov/drink/contaminants/index.cfm>
- [222] S. Rojas and P. Horcajada, “Metal-Organic Frameworks for the Removal of Emerging Organic Contaminants in Water,” Aug. 26, 2020, *American Chemical Society*. doi: 10.1021/acs.chemrev.9b00797.
- [223] E. K. Richmond *et al.*, “A diverse suite of pharmaceuticals contaminates stream and riparian food webs,” *Nat Commun*, vol. 9, no. 1, Dec. 2018, doi: 10.1038/s41467-018-06822-w.
- [224] F. Fu and Q. Wang, “Removal of heavy metal ions from wastewaters: A review,” 2011, *Academic Press*. doi: 10.1016/j.jenvman.2010.11.011.
- [225] M. M. Khin, A. S. Nair, V. J. Babu, R. Murugan, and S. Ramakrishna, “A review on nanomaterials for environmental remediation,” 2012, *Royal Society of Chemistry*. doi: 10.1039/c2ee21818f.
- [226] T. Robinson, G. McMullan, R. Marchant, and P. Nigam, “Remediation of dyes in textile e,uent: a critical review on current treatment technologies with a proposed alternative.”
- [227] P. Hayati *et al.*, “Photocatalytic activity of new nanostructures of an Ag(i) metal-organic framework (Ag-MOF) for the efficient degradation of MCPA and 2,4-D herbicides under sunlight irradiation,” *New Journal of Chemistry*, vol. 45, no. 7, pp. 3408–3417, Feb. 2021, doi: 10.1039/d0nj02460k.
- [228] H. Lebig-Elhadi, Z. Frontistis, H. Ait-Amar, S. Amrani, and D. Mantzavinos, “Electrochemical oxidation of pesticide thiamethoxam on boron doped diamond anode: Role of operating parameters and matrix effect,” *Process Safety and Environmental Protection*, vol. 116, pp. 535–541, May 2018, doi: 10.1016/j.psep.2018.03.021.
- [229] X. Zheng, Z. P. Shen, L. Shi, R. Cheng, and D. H. Yuan, “Photocatalytic membrane reactors (PMRs) in water treatment: Configurations and influencing factors,” Aug. 01, 2017, *MDPI*. doi: 10.3390/catal7080224.
- [230] F. Mansour, M. Al-Hindi, R. Yahfoufi, G. M. Ayoub, and M. N. Ahmad, “The use of activated carbon for the removal of pharmaceuticals from aqueous solutions: a review,” Mar. 01, 2018, *Springer Netherlands*. doi: 10.1007/s11157-017-9456-8.
- [231] Z. A. Allothman, “A review: Fundamental aspects of silicate mesoporous materials,” 2012. doi: 10.3390/ma5122874.
- [232] B. Huang, X. Li, C. Fu, Y. Wang, and H. Cheng, “Study rheological behavior of polymer solution in different-medium-injection-tools,” *Polymers (Basel)*, vol. 11, no. 2, Feb. 2019, doi: 10.3390/polym11020319.
- [233] S. Dhaka, R. Kumar, A. Deep, M. B. Kurade, S. W. Ji, and B. H. Jeon, “Metal–organic frameworks (MOFs) for the removal of emerging contaminants from aquatic environments,” Feb. 01, 2019, *Elsevier B.V.* doi: 10.1016/j.ccr.2018.10.003.
- [234] T. Rasheed, A. A. Hassan, M. Bilal, T. Hussain, and K. Rizwan, “Metal-organic frameworks based adsorbents: A review from removal perspective of various environmental contaminants from wastewater,” Nov. 01, 2020, *Elsevier Ltd.* doi: 10.1016/j.chemosphere.2020.127369.
- [235] W. Zhang *et al.*, “Effects of multi–walled carbon nanotubes on pyrene adsorption and desorption in soils: The role of soil constituents,” *Chemosphere*, vol. 221, pp. 203–211, Apr. 2019, doi: 10.1016/j.chemosphere.2019.01.030.

- [236] Z. Peng *et al.*, “Advances in the application, toxicity and degradation of carbon nanomaterials in environment: A review,” Jan. 01, 2020, *Elsevier Ltd.* doi: 10.1016/j.envint.2019.105298.
- [237] D. Yang and B. C. Gates, “Catalysis by Metal Organic Frameworks: Perspective and Suggestions for Future Research,” Mar. 01, 2019, *American Chemical Society*. doi: 10.1021/acscatal.8b04515.
- [238] Q. Wang and D. Astruc, “State of the Art and Prospects in Metal-Organic Framework (MOF)-Based and MOF-Derived Nanocatalysis,” Jan. 22, 2020, *American Chemical Society*. doi: 10.1021/acs.chemrev.9b00223.
- [239] L. Joseph *et al.*, “Removal of contaminants of emerging concern by metal-organic framework nanoadsorbents: A review,” Aug. 01, 2019, *Elsevier B.V.* doi: 10.1016/j.ccej.2019.03.173.
- [240] G. Liu *et al.*, “Adsorption and removal of organophosphorus pesticides from environmental water and soil samples by using magnetic multi-walled carbon nanotubes @ organic framework ZIF-8,” *J Mater Sci*, vol. 53, no. 15, pp. 10772–10783, Aug. 2018, doi: 10.1007/s10853-018-2352-y.
- [241] W. Yao, Z. Fan, and S. Zhang, “Preparation of metal-organic framework UiO-66-incorporated polymer monolith for the extraction of trace levels of fungicides in environmental water and soil samples,” *J Sep Sci*, vol. 42, no. 16, pp. 2679–2686, 2019, doi: 10.1002/jssc.201900168.
- [242] S. Pai, & M. S. Kini, and R. Selvaraj, “ENVIRONMENTAL AND ENERGY MANAGEMENT A review on adsorptive removal of dyes from wastewater by hydroxyapatite nanocomposites”, doi: 10.1007/s11356-019-07319-9/Published.
- [243] “Textiles and Clothing.” [Online]. Available: <https://onlinelibrary.wiley.com/doi/>
- [244] E. Haque, V. Lo, A. I. Minett, A. T. Harris, and T. L. Church, “Dichotomous adsorption behaviour of dyes on an amino-functionalised metal-organic framework, amino-MIL-101(Al),” *J Mater Chem A Mater*, vol. 2, no. 1, pp. 193–203, Jan. 2014, doi: 10.1039/c3ta13589f.
- [245] S. Mohd, A. A. Wani, and A. M. Khan, “ZnO/POA functionalized metal-organic framework ZIF-8 nanomaterial for dye removal,” *Cleaner Chemical Engineering*, vol. 3, p. 100047, Sep. 2022, doi: 10.1016/j.clce.2022.100047.
- [246] D. Pattappan, S. Vargheese, K. V. Kavya, R. T. R. Kumar, and Y. Haldorai, “Metal-organic frameworks with different oxidation states of metal nodes and aminoterephthalic acid ligand for degradation of Rhodamine B under solar light,” *Chemosphere*, vol. 286, Jan. 2022, doi: 10.1016/j.chemosphere.2021.131726.
- [247] X. L. Li, W. Zhang, Y. Q. Huang, Q. Wang, and J. M. Yang, “Superior adsorptive removal of azo dyes from aqueous solution by a Ni(II)-doped metal–organic framework,” *Colloids Surf A Physicochem Eng Asp*, vol. 619, Jun. 2021, doi: 10.1016/j.colsurfa.2021.126549.
- [248] C. X. Yu *et al.*, “Highly efficient and selective removal of anionic dyes from aqueous solution by using a protonated metal-organic framework,” *J Alloys Compd*, vol. 853, Feb. 2021, doi: 10.1016/j.jallcom.2020.157383.
- [249] N. M. Mahmoodi, M. Taghizadeh, A. Taghizadeh, J. Abdi, B. Hayati, and A. A. Shekarchi, “Bio-based magnetic metal-organic framework nanocomposite: Ultrasound-assisted synthesis and pollutant (heavy metal and dye) removal from aqueous media,” *Appl Surf Sci*, vol. 480, pp. 288–299, Jun. 2019, doi: 10.1016/j.apsusc.2019.02.211.

- [250] H. M. Abd El Salam and T. Zaki, "Removal of hazardous cationic organic dyes from water using nickel-based metal-organic frameworks," *Inorganica Chim Acta*, vol. 471, pp. 203–210, Feb. 2018, doi: 10.1016/j.ica.2017.10.040.
- [251] D. Li *et al.*, "Multifunctional adsorbent based on metal-organic framework modified bacterial cellulose/chitosan composite aerogel for high efficient removal of heavy metal ion and organic pollutant," *Chemical Engineering Journal*, vol. 383, Mar. 2020, doi: 10.1016/j.cej.2019.123127.
- [252] S. S. Lam *et al.*, "Microwave-assisted pyrolysis with chemical activation, an innovative method to convert orange peel into activated carbon with improved properties as dye adsorbent," *J Clean Prod*, vol. 162, pp. 1376–1387, Sep. 2017, doi: 10.1016/j.jclepro.2017.06.131.
- [253] S. M. Prabhu, A. Khan, M. Hasmath Farzana, G. C. Hwang, W. Lee, and G. Lee, "Synthesis and characterization of graphene oxide-doped nano-hydroxyapatite and its adsorption performance of toxic diazo dyes from aqueous solution," *J Mol Liq*, vol. 269, pp. 746–754, Nov. 2018, doi: 10.1016/j.molliq.2018.08.044.
- [254] A. I. Abd-Elhamid, E. A. Kamoun, A. A. El-Shanshory, H. M. A. Soliman, and H. F. Aly, "Evaluation of graphene oxide-activated carbon as effective composite adsorbent toward the removal of cationic dyes: Composite preparation, characterization and adsorption parameters," *J Mol Liq*, vol. 279, pp. 530–539, Apr. 2019, doi: 10.1016/j.molliq.2019.01.162.
- [255] L. Ding *et al.*, "Adsorption of Rhodamine-B from aqueous solution using treated rice husk-based activated carbon," *Colloids Surf A Physicochem Eng Asp*, vol. 446, pp. 1–7, Apr. 2014, doi: 10.1016/j.colsurfa.2014.01.030.
- [256] Y. Wang, Y. Li, H. Li, H. Zheng, and Q. Du, "Equilibrium, Kinetic and Thermodynamic Studies on Methylene Blue Adsorption by Konjac Glucomannan/Activated Carbon Aerogel," *J Polym Environ*, vol. 27, no. 6, pp. 1342–1351, Jun. 2019, doi: 10.1007/s10924-019-01420-3.
- [257] L. A. M. Mahmoud, R. A. Dos Reis, X. Chen, V. P. Ting, and S. Nayak, "Metal-Organic Frameworks as Potential Agents for Extraction and Delivery of Pesticides and Agrochemicals," Dec. 20, 2022, *American Chemical Society*. doi: 10.1021/acsomega.2c05978.
- [258] A. Miodovnik and M. S. Wolff, "Prenatal Exposure to Industrial Chemicals and Pesticides and Effects on Neurodevelopment."
- [259] Q. Hong, Z. Zhang, Y. Hong, and S. Li, "A microcosm study on bioremediation of fenitrothion-contaminated soil using Burkholderia sp. FDS-1," *Int Biodeterior Biodegradation*, vol. 59, no. 1, pp. 55–61, Jan. 2007, doi: 10.1016/j.ibiod.2006.07.013.
- [260] K. N. Baer and B. J. Marcel, "Glyphosate," in *Encyclopedia of Toxicology: Third Edition*, Elsevier, 2014, pp. 767–769. doi: 10.1016/B978-0-12-386454-3.00148-2.
- [261] S. Karanth, "Chlorophenoxy Herbicides," in *Encyclopedia of Toxicology: Third Edition*, Elsevier, 2014, pp. 900–902. doi: 10.1016/B978-0-12-386454-3.00114-7.
- [262] R. C. Gupta, "Carbamate Pesticides," in *Encyclopedia of Toxicology: Third Edition*, Elsevier, 2014, pp. 661–664. doi: 10.1016/B978-0-12-386454-3.00106-8.
- [263] S. C. Gad and T. Pham, "Phenothrin," in *Encyclopedia of Toxicology: Third Edition*, Elsevier, 2014, pp. 884–886. doi: 10.1016/B978-0-12-386454-3.01198-2.

- [264] J. Seifert, “Neonicotinoids,” in *Encyclopedia of Toxicology: Third Edition*, Elsevier, 2014, pp. 477–482. doi: 10.1016/B978-0-12-386454-3.00168-8.
- [265] M. Toda, K. D. Beer, K. M. Kuivila, T. M. Chiller, and B. R. Jackson, “Trends in agricultural triazole fungicide use in the united states, 1992–2016 and possible implications for antifungal-resistant fungi in human disease,” May 01, 2021, *Public Health Services, US Dept of Health and Human Services*. doi: 10.1289/EHP7484.
- [266] J. Cooper and H. Dobson, “The benefits of pesticides to mankind and the environment,” Sep. 2007. doi: 10.1016/j.cropro.2007.03.022.
- [267] B. Eskenazi *et al.*, “The pine river statement: Human health consequences of DDT use,” 2009. doi: 10.1289/ehp.11748.
- [268] Q. Gao, J. Xu, and X. H. Bu, “Recent advances about metal–organic frameworks in the removal of pollutants from wastewater,” Jan. 01, 2019, *Elsevier B.V.* doi: 10.1016/j.ccr.2018.03.015.
- [269] V. Bervia Lunardi *et al.*, “Pesticide elimination through adsorption by metal-organic framework and their modified forms,” May 01, 2022, *Elsevier B.V.* doi: 10.1016/j.enmm.2021.100638.
- [270] B. K. Jung, Z. Hasan, and S. H. Jhung, “Adsorptive removal of 2,4-dichlorophenoxyacetic acid (2,4-D) from water with a metal-organic framework,” *Chemical Engineering Journal*, vol. 234, pp. 99–105, Sep. 2013, doi: 10.1016/j.cej.2013.08.110.
- [271] C. De Smedt, P. Spanoghe, S. Biswas, K. Leus, and P. Van Der Voort, “Comparison of different solid adsorbents for the removal of mobile pesticides from aqueous solutions,” *Adsorption*, vol. 21, no. 3, pp. 243–254, Apr. 2015, doi: 10.1007/s10450-015-9666-8.
- [272] Y. S. Seo, N. A. Khan, and S. H. Jhung, “Adsorptive removal of methylchlorophenoxypropionic acid from water with a metal-organic framework,” *Chemical Engineering Journal*, vol. 270, pp. 22–27, Jun. 2015, doi: 10.1016/j.cej.2015.02.007.
- [273] B. K. Jung, Z. Hasan, and S. H. Jhung, “Adsorptive removal of 2,4-dichlorophenoxyacetic acid (2,4-D) from water with a metal-organic framework,” *Chemical Engineering Journal*, vol. 234, pp. 99–105, Sep. 2013, doi: 10.1016/j.cej.2013.08.110.
- [274] S. M. Mirsoleimani-Azizi, P. Setoodeh, F. Samimi, J. Shadmehr, N. Hamed, and M. R. Rahimpour, “Diazinon removal from aqueous media by mesoporous MIL-101(Cr) in a continuous fixed-bed system,” *J Environ Chem Eng*, vol. 6, no. 4, pp. 4653–4664, Aug. 2018, doi: 10.1016/j.jece.2018.06.067.
- [275] Y. S. Seo, N. A. Khan, and S. H. Jhung, “Adsorptive removal of methylchlorophenoxypropionic acid from water with a metal-organic framework,” *Chemical Engineering Journal*, vol. 270, pp. 22–27, Jun. 2015, doi: 10.1016/j.cej.2015.02.007.
- [276] X. Zhu *et al.*, “Effective adsorption and enhanced removal of organophosphorus pesticides from aqueous solution by Zr-Based MOFs of UiO-67,” *ACS Appl Mater Interfaces*, vol. 7, no. 1, pp. 223–231, Jan. 2015, doi: 10.1021/am5059074.
- [277] A. Jamali, F. Shemirani, and A. Morsali, “A comparative study of adsorption and removal of organophosphorus insecticides from aqueous solution by Zr-based MOFs,” *Journal of Industrial and Engineering Chemistry*, vol. 80, pp. 83–92, Dec. 2019, doi: 10.1016/j.jiec.2019.07.034.

- [278] I. Akpınar, R. J. Drout, T. Islamoglu, S. Kato, J. Lyu, and O. K. Farha, “Exploiting π - π Interactions to Design an Efficient Sorbent for Atrazine Removal from Water,” *ACS Appl Mater Interfaces*, vol. 11, no. 6, pp. 6097–6103, Feb. 2019, doi: 10.1021/acsami.8b20355.
- [279] Y. Su, S. Wang, N. Zhang, P. Cui, Y. Gao, and T. Bao, “Zr-MOF modified cotton fiber for pipette tip solid-phase extraction of four phenoxy herbicides in complex samples,” *Ecotoxicol Environ Saf*, vol. 201, Sep. 2020, doi: 10.1016/j.ecoenv.2020.110764.
- [280] G. Liu *et al.*, “Metal–organic framework preparation using magnetic graphene oxide- β -cyclodextrin for neonicotinoid pesticide adsorption and removal,” *Carbohydr Polym*, vol. 175, pp. 584–591, Nov. 2017, doi: 10.1016/j.carbpol.2017.06.074.
- [281] Q. Yang *et al.*, “Interface engineering of metal organic framework on graphene oxide with enhanced adsorption capacity for organophosphorus pesticide,” *Chemical Engineering Journal*, vol. 313, pp. 19–26, 2017, doi: 10.1016/j.cej.2016.12.041.
- [282] X. Huang *et al.*, “Removal of organic herbicides from aqueous solution by ionic liquid modified chitosan/metal-organic framework composite,” *Int J Biol Macromol*, vol. 149, pp. 882–892, Apr. 2020, doi: 10.1016/j.ijbiomac.2020.01.165.
- [283] C. Liu, P. Wang, X. Liu, X. Yi, Z. Zhou, and D. Liu, “Supporting Information Multifunctional β -cyclodextrin MOF derived porous carbon as efficient herbicides adsorbent and potassium fertilizer.”
- [284] D. Chen *et al.*, “MOF-derived magnetic porous carbon-based sorbent: Synthesis, characterization, and adsorption behavior of organic micropollutants,” *Advanced Powder Technology*, vol. 28, no. 7, pp. 1769–1779, Jul. 2017, doi: 10.1016/j.appt.2017.04.018.
- [285] T. Rasheed *et al.*, “Environmental threatening concern and efficient removal of pharmaceutically active compounds using metal-organic frameworks as adsorbents,” Jun. 01, 2020, *Academic Press Inc.* doi: 10.1016/j.envres.2020.109436.
- [286] J. R. De Andrade, M. F. Oliveira, M. G. C. Da Silva, and M. G. A. Vieira, “Adsorption of Pharmaceuticals from Water and Wastewater Using Nonconventional Low-Cost Materials: A Review,” Mar. 07, 2018, *American Chemical Society*. doi: 10.1021/acs.iecr.7b05137.
- [287] P. Klimaszyk and P. Rzymiski, “Water and Aquatic Fauna on Drugs: What are the Impacts of Pharmaceutical Pollution?,” 2018, pp. 255–278. doi: 10.1007/978-3-319-79014-5_12.
- [288] “Pharmaceuticals in drinking-water.”
- [289] D. Kanakaraju, B. D. Glass, and M. Oelgemöller, “Advanced oxidation process-mediated removal of pharmaceuticals from water: A review,” Aug. 01, 2018, *Academic Press*. doi: 10.1016/j.jenvman.2018.04.103.
- [290] S. O. Ganiyu, E. D. Van Hullebusch, M. Cretin, G. Esposito, and M. A. Oturan, “Coupling of membrane filtration and advanced oxidation processes for removal of pharmaceutical residues: A critical review,” *Sep Purif Technol*, vol. 156, pp. 891–914, Dec. 2015, doi: 10.1016/j.seppur.2015.09.059.
- [291] A. Kumar *et al.*, “Wide spectral degradation of Norfloxacin by Ag@BiPO₄/BiOBr/BiFeO₃ nano-assembly: Elucidating the photocatalytic mechanism under different light sources,” *J Hazard Mater*, vol. 364, pp. 429–440, Feb. 2019, doi: 10.1016/j.jhazmat.2018.10.060.

- [292] A. S. Oberoi, Y. Jia, H. Zhang, S. K. Khanal, and H. Lu, "Insights into the Fate and Removal of Antibiotics in Engineered Biological Treatment Systems: A Critical Review," *Environ Sci Technol*, vol. 53, no. 13, pp. 7234–7264, Jul. 2019, doi: 10.1021/acs.est.9b01131.
- [293] M. B. Ahmed, J. L. Zhou, H. H. Ngo, and W. Guo, "Adsorptive removal of antibiotics from water and wastewater: Progress and challenges," Nov. 01, 2015, *Elsevier*. doi: 10.1016/j.scitotenv.2015.05.130.
- [294] K. Ikehata, N. Jodeiri Naghashkar, and M. Gamal El-Din, "Degradation of aqueous pharmaceuticals by ozonation and advanced oxidation processes: A review," Dec. 01, 2006. doi: 10.1080/01919510600985937.
- [295] B. Liu, K. Vikrant, K. H. Kim, V. Kumar, and S. K. Kailasa, "Critical role of water stability in metal-organic frameworks and advanced modification strategies for the extension of their applicability," May 01, 2020, *Royal Society of Chemistry*. doi: 10.1039/c9en01321k.
- [296] Z. Hasan, N. A. Khan, and S. H. Jhung, "Adsorptive removal of diclofenac sodium from water with Zr-based metal–organic frameworks," *Chemical Engineering Journal*, vol. 284, pp. 1406–1413, 2016, doi: 10.1016/j.cej.2015.08.087.
- [297] X. Zhao *et al.*, "A metal-organic framework with large 1-D channels and rich –OH sites for high-efficiency chloramphenicol removal from water," *J Colloid Interface Sci*, vol. 526, pp. 28–34, Sep. 2018, doi: 10.1016/j.jcis.2018.04.095.
- [298] K. W. Jung, J. H. Kim, and J. W. Choi, "Synthesis of magnetic porous carbon composite derived from metal-organic framework using recovered terephthalic acid from polyethylene terephthalate (PET) waste bottles as organic ligand and its potential as adsorbent for antibiotic tetracycline hydrochloride," *Compos B Eng*, vol. 187, Apr. 2020, doi: 10.1016/j.compositesb.2020.107867.
- [299] Z. Hasan, J. Jeon, and S. H. Jhung, "Adsorptive removal of naproxen and clofibric acid from water using metal-organic frameworks," *J Hazard Mater*, vol. 209–210, pp. 151–157, Mar. 2012, doi: 10.1016/j.jhazmat.2012.01.005.
- [300] Y. Peng, Y. Zhang, H. Huang, and C. Zhong, "Flexibility induced high-performance MOF-based adsorbent for nitroimidazole antibiotics capture," *Chemical Engineering Journal*, vol. 333, pp. 678–685, Feb. 2018, doi: 10.1016/j.cej.2017.09.138.
- [301] M. R. Azhar, H. R. Abid, H. Sun, V. Periasamy, M. O. Tadé, and S. Wang, "Excellent performance of copper based metal organic framework in adsorptive removal of toxic sulfonamide antibiotics from wastewater," *J Colloid Interface Sci*, vol. 478, pp. 344–352, Sep. 2016, doi: 10.1016/j.jcis.2016.06.032.
- [302] M. R. Azhar, H. R. Abid, V. Periasamy, H. Sun, M. O. Tade, and S. Wang, "Adsorptive removal of antibiotic sulfonamide by UiO-66 and ZIF-67 for wastewater treatment," *J Colloid Interface Sci*, vol. 500, pp. 88–95, Aug. 2017, doi: 10.1016/j.jcis.2017.04.001.
- [303] Mehdi Sadeghi, Majid Moradian, Habib-Allah Tayebi, and Ali Mirabi, "Removal of Penicillin G from aqueous medium by PPI@SBA-15/ZIF-8 super adsorbent: Adsorption isotherm, thermodynamic, and kinetic studies," *Chemosphere*, vol. 311, p. 136887, 2023, Accessed: Jun. 08, 2024. [Online]. Available: <https://doi.org/10.1016/j.chemosphere.2022.136887>
- [304] S. Zhuang, R. Cheng, and J. Wang, "Adsorption of diclofenac from aqueous solution using UiO-66-type metal-organic frameworks," *Chemical Engineering Journal*, vol. 359, pp. 354–362, Mar. 2019, doi: 10.1016/j.cej.2018.11.150.

- [305] S. Saghir and Z. Xiao, "Synthesis of novel Ag@ZIF-67 rhombic dodecahedron for enhanced adsorptive removal of antibiotic and organic dye," *J Mol Liq*, vol. 328, Apr. 2021, doi: 10.1016/j.molliq.2021.115323.
- [306] W. Liu *et al.*, "Selective adsorption and removal of drug contaminants by using an extremely stable Cu(II)-based 3D metal-organic framework," *Chemosphere*, vol. 215, pp. 524–531, Jan. 2019, doi: 10.1016/j.chemosphere.2018.10.075.
- [307] Y. Li, H. Zhang, Y. Chen, L. Huang, Z. Lin, and Z. Cai, "Core-Shell Structured Magnetic Covalent Organic Framework Nanocomposites for Triclosan and Triclocarban Adsorption," *ACS Appl Mater Interfaces*, vol. 11, no. 25, pp. 22492–22500, Jun. 2019, doi: 10.1021/acsami.9b06953.
- [308] J. Tang, L. Zong, B. Mu, Y. Kang, and A. Wang, "Attapulgit/carbon composites as a recyclable adsorbent for antibiotics removal," *Korean Journal of Chemical Engineering*, vol. 35, no. 8, pp. 1650–1661, Aug. 2018, doi: 10.1007/s11814-018-0066-0.
- [309] H. T. Nguyen *et al.*, "Low-cost hydrogel derived from agro-waste for veterinary antibiotic removal: Optimization, kinetics, and toxicity evaluation," *Environ Technol Innov*, vol. 20, Nov. 2020, doi: 10.1016/j.eti.2020.101098.
- [310] M. Mon, R. Bruno, J. Ferrando-Soria, D. Armentano, and E. Pardo, "Metal-organic framework technologies for water remediation: Towards a sustainable ecosystem," 2018, *Royal Society of Chemistry*. doi: 10.1039/c8ta00264a.
- [311] A. Kumar *et al.*, "Lead toxicity: Health hazards, influence on food Chain, and sustainable remediation approaches," Apr. 01, 2020, *MDPI AG*. doi: 10.3390/ijerph17072179.
- [312] G. Flora, D. Gupta, and A. Tiwari, "Toxicity of lead: A review with recent updates," 2012. doi: 10.2478/v10102-012-0009-2.
- [313] E. Tahmasebi, M. Y. Masoomi, Y. Yamini, and A. Morsali, "Application of mechanosynthesized azine-decorated zinc(II) metal-organic frameworks for highly efficient removal and extraction of some heavy-metal ions from aqueous samples: A comparative study," *Inorg Chem*, vol. 54, no. 2, pp. 425–433, Jan. 2015, doi: 10.1021/ic5015384.
- [314] Q. Qin, Q. Wang, D. Fu, and J. Ma, "An efficient approach for Pb(II) and Cd(II) removal using manganese dioxide formed in situ," *Chemical Engineering Journal*, vol. 172, no. 1, pp. 68–74, Aug. 2011, doi: 10.1016/j.cej.2011.05.066.
- [315] L. Fu *et al.*, "Post-modification of UiO-66-NH₂ by resorcylic aldehyde for selective removal of Pb(II) in aqueous media," *J Clean Prod*, vol. 229, pp. 470–479, Aug. 2019, doi: 10.1016/j.jclepro.2019.05.043.
- [316] K. Wang, J. Gu, and N. Yin, "Efficient Removal of Pb(II) and Cd(II) Using NH₂-Functionalized Zr-MOFs via Rapid Microwave-Promoted Synthesis," *Ind Eng Chem Res*, vol. 56, no. 7, pp. 1880–1887, Feb. 2017, doi: 10.1021/acs.iecr.6b04997.
- [317] L. Huang, M. He, B. Chen, and B. Hu, "Magnetic Zr-MOFs nanocomposites for rapid removal of heavy metal ions and dyes from water," *Chemosphere*, vol. 199, pp. 435–444, May 2018, doi: 10.1016/j.chemosphere.2018.02.019.

- [318] S. Jamshidifard *et al.*, “Incorporation of UiO-66-NH₂ MOF into the PAN/chitosan nanofibers for adsorption and membrane filtration of Pb(II), Cd(II) and Cr(VI) ions from aqueous solutions,” *J Hazard Mater*, vol. 368, pp. 10–20, Apr. 2019, doi: 10.1016/j.jhazmat.2019.01.024.
- [319] C. Lei *et al.*, “Fabrication of metal-organic frameworks@cellulose aerogels composite materials for removal of heavy metal ions in water,” *Carbohydr Polym*, vol. 205, pp. 35–41, Feb. 2019, doi: 10.1016/j.carbpol.2018.10.029.
- [320] S. Ramanayaka, M. Vithanage, A. Sarmah, T. An, K. H. Kim, and Y. S. Ok, “Performance of metal-organic frameworks for the adsorptive removal of potentially toxic elements in a water system: A critical review,” 2019, *Royal Society of Chemistry*. doi: 10.1039/c9ra06879a.
- [321] R. Ricco *et al.*, “Lead(II) uptake by aluminium based magnetic framework composites (MFCs) in water,” *J Mater Chem A Mater*, vol. 3, no. 39, pp. 19822–19831, Aug. 2015, doi: 10.1039/c5ta04154f.
- [322] L. Liang *et al.*, “In situ large-scale construction of sulfur-functionalized metal-organic framework and its efficient removal of Hg(II) from water,” *J Mater Chem A Mater*, vol. 4, no. 40, pp. 15370–15374, 2016, doi: 10.1039/c6ta04927c.
- [323] P. K. Chattaraj, P. W. Ayers, and J. Melin, “Further links between the maximum hardness principle and the hard/soft acid/base principle: Insights from hard/soft exchange reactions,” *Physical Chemistry Chemical Physics*, vol. 9, no. 29, pp. 3853–3856, 2007, doi: 10.1039/b705742c.
- [324] J. Li, Y. Liu, Y. Ai, A. Alsaedi, T. Hayat, and X. Wang, “Combined experimental and theoretical investigation on selective removal of mercury ions by metal organic frameworks modified with thiol groups,” Dec. 15, 2018, *Elsevier B.V.* doi: 10.1016/j.ccej.2018.08.041.
- [325] H. Saleem, U. Rafique, and R. P. Davies, “Investigations on post-synthetically modified UiO-66-NH₂ for the adsorptive removal of heavy metal ions from aqueous solution,” *Microporous and Mesoporous Materials*, vol. 221, pp. 238–244, Feb. 2016, doi: 10.1016/j.micromeso.2015.09.043.
- [326] L. Fu *et al.*, “Post-functionalization of UiO-66-NH₂ by 2,5-Dimercapto-1,3,4-thiadiazole for the high efficient removal of Hg(II) in water,” *J Hazard Mater*, vol. 368, pp. 42–51, Apr. 2019, doi: 10.1016/j.jhazmat.2019.01.025.
- [327] F. S. Awad, A. M. Bakry, A. A. Ibrahim, A. Lin, and M. S. El-Shall, “Thiol- And Amine-Incorporated UIO-66-NH₂ as an Efficient Adsorbent for the Removal of Mercury(II) and Phosphate Ions from Aqueous Solutions,” *Ind Eng Chem Res*, vol. 60, no. 34, pp. 12675–12688, Sep. 2021, doi: 10.1021/acs.iecr.1c01892.
- [328] L. Ding, X. Luo, P. Shao, J. Yang, and D. Sun, “Thiol-Functionalized Zr-Based Metal-Organic Framework for Capture of Hg(II) through a Proton Exchange Reaction,” *ACS Sustain Chem Eng*, vol. 6, no. 7, pp. 8494–8502, Jul. 2018, doi: 10.1021/acssuschemeng.8b00768.
- [329] X. P. Zhou, Z. Xu, M. Zeller, and A. D. Hunter, “Reversible uptake of HgCl₂ in a porous coordination polymer based on the dual functions of carboxylate and thioether,” *Chemical Communications*, no. 36, pp. 5439–5441, 2009, doi: 10.1039/b910265e.
- [330] M. Zhao, Z. Huang, S. Wang, L. Zhang, and Y. Zhou, “Design of l -Cysteine Functionalized UiO-66 MOFs for Selective Adsorption of Hg(II) in Aqueous Medium,” *ACS Appl Mater Interfaces*, vol. 11, no. 50, pp. 46973–46983, Dec. 2019, doi: 10.1021/acsami.9b17508.

- [331] L. Bulgariu, M. Ratoi, D. Bulgariu, and M. MacOveanu, "Adsorption potential of mercury(II) from aqueous solutions onto Romanian peat moss," *J Environ Sci Health A Tox Hazard Subst Environ Eng*, vol. 44, no. 7, pp. 700–706, Jun. 2009, doi: 10.1080/10934520902847836.
- [332] M. J. López-Muñoz, A. Arencibia, L. Cerro, R. Pascual, and Á. Melgar, "Adsorption of Hg(II) from aqueous solutions using TiO₂ and titanate nanotube adsorbents," *Appl Surf Sci*, vol. 367, pp. 91–100, Mar. 2016, doi: 10.1016/j.apsusc.2016.01.109.
- [333] K. Abbas, H. Znad, and M. R. Awual, "A ligand anchored conjugate adsorbent for effective mercury(II) detection and removal from aqueous media," *Chemical Engineering Journal*, vol. 334, pp. 432–443, Feb. 2018, doi: 10.1016/j.cej.2017.10.054.
- [334] M. R. Awual, "Novel nanocomposite materials for efficient and selective mercury ions capturing from wastewater," *Chemical Engineering Journal*, vol. 307, pp. 456–465, Jan. 2017, doi: 10.1016/j.cej.2016.08.108.
- [335] M. R. Sohrabi, "Preconcentration of mercury(II) using a thiol-functionalized metal-organic framework nanocomposite as a sorbent," *Microchimica Acta*, vol. 181, no. 3–4, pp. 435–444, Feb. 2014, doi: 10.1007/s00604-013-1133-1.
- [336] K. Leus *et al.*, "UiO-66-(SH)₂ as stable, selective and regenerable adsorbent for the removal of mercury from water under environmentally-relevant conditions," 2017, *Royal Society of Chemistry*. doi: 10.1039/c7fd00012j.
- [337] F. Luo *et al.*, "High-performance Hg₂⁺ removal from ultra-low-concentration aqueous solution using both acylamide- and hydroxyl-functionalized metal-organic framework," *J Mater Chem A Mater*, vol. 3, no. 18, pp. 9616–9620, May 2015, doi: 10.1039/c5ta01669j.
- [338] L. Huang, M. He, B. Chen, and B. Hu, "A mercapto functionalized magnetic Zr-MOF by solvent-assisted ligand exchange for Hg₂⁺ removal from water," *J Mater Chem A Mater*, vol. 4, no. 14, pp. 5159–5166, 2016, doi: 10.1039/c6ta00343e.
- [339] S. Bao, K. Li, P. Ning, J. Peng, X. Jin, and L. Tang, "Highly effective removal of mercury and lead ions from wastewater by mercaptoamine-functionalised silica-coated magnetic nano-adsorbents: Behaviours and mechanisms," *Appl Surf Sci*, vol. 393, pp. 457–466, Jan. 2017, doi: 10.1016/j.apsusc.2016.09.098.
- [340] C. Jeon and W. H. Höll, "Chemical modification of chitosan and equilibrium study for mercury ion removal," *Water Res*, vol. 37, no. 19, pp. 4770–4780, 2003, doi: 10.1016/S0043-1354(03)00431-7.
- [341] L. Huang, M. He, B. Chen, and B. Hu, "A designable magnetic MOF composite and facile coordination-based post-synthetic strategy for the enhanced removal of Hg₂⁺ from water," *J Mater Chem A Mater*, vol. 3, no. 21, pp. 11587–11595, Jun. 2015, doi: 10.1039/c5ta01484k.
- [342] A. Chakraborty, S. Bhattacharyya, A. Hazra, A. C. Ghosh, and T. K. Maji, "Post-synthetic metalation in an anionic MOF for efficient catalytic activity and removal of heavy metal ions from aqueous solution," *Chemical Communications*, vol. 52, no. 13, pp. 2831–2834, 2016, doi: 10.1039/c5cc09814a.
- [343] H. Xue *et al.*, "A regenerative metal-organic framework for reversible uptake of Cd(II): From effective adsorption to: In situ detection," *Chem Sci*, vol. 7, no. 9, pp. 5983–5988, 2016, doi: 10.1039/c6sc00972g.

- [344] D. Haldar, P. Duarah, and M. K. Purkait, "MOFs for the treatment of arsenic, fluoride and iron contaminated drinking water: A review," Jul. 01, 2020, *Elsevier Ltd.* doi: 10.1016/j.chemosphere.2020.126388.
- [345] C. Wang, J. Luan, and C. Wu, "Metal-organic frameworks for aquatic arsenic removal," Jul. 01, 2019, *Elsevier Ltd.* doi: 10.1016/j.watres.2019.04.043.
- [346] R. Singh, S. Singh, P. Parihar, V. P. Singh, and S. M. Prasad, "Arsenic contamination, consequences and remediation techniques: A review," Feb. 01, 2015, *Academic Press.* doi: 10.1016/j.ecoenv.2014.10.009.
- [347] A. Sarkar and B. Paul, "The global menace of arsenic and its conventional remediation - A critical review," Sep. 01, 2016, *Elsevier Ltd.* doi: 10.1016/j.chemosphere.2016.05.043.
- [348] Z. Q. Li, J. C. Yang, K. W. Sui, and N. Yin, "Facile synthesis of metal-organic framework MOF-808 for arsenic removal," *Mater Lett*, vol. 160, pp. 412–414, Aug. 2015, doi: 10.1016/j.matlet.2015.08.004.
- [349] J. Phanthasri, P. Khamdahsag, P. Jutaporn, K. Sorachoti, K. Wantala, and V. Tanboonchuy, "Enhancement of arsenite removal using manganese oxide coupled with iron (III) trimesic," *Appl Surf Sci*, vol. 427, pp. 545–552, Jan. 2018, doi: 10.1016/j.apsusc.2017.09.032.
- [350] C. O. Audu *et al.*, "The dual capture of AsV and AsIII by UiO-66 and analogues," *Chem Sci*, vol. 7, no. 10, pp. 6492–6498, 2016, doi: 10.1039/c6sc00490c.
- [351] J. B. Huo, L. Xu, J. C. E. Yang, H. J. Cui, B. Yuan, and M. L. Fu, "Magnetic responsive Fe₃O₄-ZIF-8 core-shell composites for efficient removal of As(III) from water," *Colloids Surf A Physicochem Eng Asp*, vol. 539, pp. 59–68, Feb. 2018, doi: 10.1016/j.colsurfa.2017.12.010.
- [352] W. Yu *et al.*, "Metal-organic framework (MOF) showing both ultrahigh As(V) and As(III) removal from aqueous solution," *J Solid State Chem*, vol. 269, pp. 264–270, Jan. 2019, doi: 10.1016/j.jssc.2018.09.042.
- [353] E. A. Katayev, Y. A. Ustynyuk, and J. L. Sessler, "Receptors for tetrahedral oxyanions," Dec. 2006. doi: 10.1016/j.ccr.2006.04.013.
- [354] A. M. Zayed and N. Terry, "Chromium in the environment: factors affecting biological remediation," 2003.
- [355] Q. Zhang *et al.*, "A porous Zr-cluster-based cationic metal-organic framework for highly efficient Cr₂O₇²⁻ removal from water," *Chemical Communications*, vol. 51, no. 79, pp. 14732–14734, Aug. 2015, doi: 10.1039/c5cc05927e.
- [356] Z. Wang, J. Yang, Y. Li, Q. Zhuang, and J. Gu, "Simultaneous Degradation and Removal of CrVI from Aqueous Solution with Zr-Based Metal–Organic Frameworks Bearing Inherent Reductive Sites," *Chemistry - A European Journal*, vol. 23, no. 61, pp. 15415–15423, Nov. 2017, doi: 10.1002/chem.201702534.
- [357] W. A. El-Mehalmey *et al.*, "Metal-organic framework@silica as a stationary phase sorbent for rapid and cost-effective removal of hexavalent chromium," *J Mater Chem A Mater*, vol. 6, no. 6, pp. 2742–2751, 2018, doi: 10.1039/c7ta08281a.
- [358] K. Wang, X. Tao, J. Xu, and N. Yin, "Novel chitosan-MOF composite adsorbent for the removal of heavy metal ions," *Chem Lett*, vol. 45, no. 12, pp. 1365–1368, 2016, doi: 10.1246/cl.160718.

- [359] H. Wang *et al.*, “Synthesis of core-shell UiO-66-poly(m-phenylenediamine) composites for removal of hexavalent chromium,” *Environmental Science and Pollution Research*, vol. 27, no. 4, pp. 4115–4126, Feb. 2020, doi: 10.1007/s11356-019-07070-1.
- [360] S. Rapti *et al.*, “Rapid, green and inexpensive synthesis of high quality UiO-66 amino-functionalized materials with exceptional capability for removal of hexavalent chromium from industrial waste,” *Inorg Chem Front*, vol. 3, no. 5, pp. 635–644, May 2016, doi: 10.1039/c5qi00303b.
- [361] S. Rapti *et al.*, “All in one porous material: Exceptional sorption and selective sensing of hexavalent chromium by using a Zr⁴⁺ MOF,” *J Mater Chem A Mater*, vol. 5, no. 28, pp. 14707–14719, 2017, doi: 10.1039/c7ta04496h.
- [362] S. Ećimović *et al.*, “Acute toxicity of selenate and selenite and their impacts on oxidative status, efflux pump activity, cellular and genetic parameters in earthworm *Eisenia andrei*,” *Chemosphere*, vol. 212, pp. 307–318, Dec. 2018, doi: 10.1016/j.chemosphere.2018.08.095.
- [363] D. M. Walters, E. Rosi-Marshall, T. A. Kennedy, W. F. Cross, and C. V. Baxter, “Mercury and selenium accumulation in the Colorado River food web, Grand Canyon, USA,” *Environ Toxicol Chem*, vol. 34, no. 10, pp. 2385–2394, Oct. 2015, doi: 10.1002/etc.3077.
- [364] Y. V. Nancharaiah and P. N. L. Lens, “Selenium biomineralization for biotechnological applications,” Jun. 01, 2015, *Elsevier Ltd*. doi: 10.1016/j.tibtech.2015.03.004.
- [365] A. J. Howarth *et al.*, “High Efficiency Adsorption and Removal of Selenate and Selenite from Water Using Metal-Organic Frameworks,” *J Am Chem Soc*, vol. 137, no. 23, pp. 7488–7494, Jun. 2015, doi: 10.1021/jacs.5b03904.
- [366] A. D. Pournara, E. Moisiadis, V. Gouma, M. J. Manos, and D. L. Giokas, “Cotton fabric decorated by a Zr⁴⁺MOF for selective As(V) and Se(IV) removal from aqueous media,” *J Environ Chem Eng*, vol. 10, no. 3, Jun. 2022, doi: 10.1016/j.jece.2022.107705.
- [367] M. K. So *et al.*, “Health risks in infants associated with exposure to perfluorinated compounds in human breast milk from Zhoushan, China,” *Environ Sci Technol*, vol. 40, no. 9, pp. 2924–2929, May 2006, doi: 10.1021/es060031f.
- [368] M. Mahramanlioglu, I. Kizilcikli, and I. O. Bicer, “Adsorption of fluoride from aqueous solution by acid treated spent bleaching earth \$.”
- [369] X. Fan, D. J. Parker, and M. D. Smith, “Adsorption kinetics of fluoride on low cost materials,” *Water Res*, vol. 37, no. 20, pp. 4929–4937, 2003, doi: 10.1016/j.watres.2003.08.014.
- [370] M. Mohapatra, S. Anand, B. K. Mishra, D. E. Giles, and P. Singh, “Review of fluoride removal from drinking water,” 2009, *Academic Press*. doi: 10.1016/j.jenvman.2009.08.015.
- [371] A. Bhatnagar, E. Kumar, and M. Sillanpää, “Fluoride removal from water by adsorption-A review,” Jul. 15, 2011. doi: 10.1016/j.cej.2011.05.028.
- [372] N. Zhang *et al.*, “Al-1,3,5-benzenetricarboxylic metal-organic frameworks: A promising adsorbent for defluoridation of water with pH insensitivity and low aluminum residual,” *Chemical Engineering Journal*, vol. 252, pp. 220–229, Sep. 2014, doi: 10.1016/j.cej.2014.04.090.

- [373] X. Zhao, D. Liu, H. Huang, W. Zhang, Q. Yang, and C. Zhong, "The stability and defluoridation performance of MOFs in fluoride solutions," *Microporous and Mesoporous Materials*, vol. 185, pp. 72–78, Feb. 2014, doi: 10.1016/j.micromeso.2013.11.002.
- [374] J. L. R. Bahena, A. R. Cabrera, A. L. Valdivieso, and R. H. Urbina, "Fluoride adsorption onto α -Al₂O₃ and its effect on the zeta potential at the alumina-aqueous electrolyte interface," *Sep Sci Technol*, vol. 37, no. 8, pp. 1973–1987, 2002, doi: 10.1081/SS-120003055.
- [375] S. Kagne, S. Jagtap, P. Dhawade, S. P. Kamble, S. Devotta, and S. S. Rayalu, "Hydrated cement: A promising adsorbent for the removal of fluoride from aqueous solution," *J Hazard Mater*, vol. 154, no. 1–3, pp. 88–95, Jun. 2008, doi: 10.1016/j.jhazmat.2007.09.111.
- [376] D. Mohan, R. Sharma, V. K. Singh, P. Steele, and C. U. Pittman, "Fluoride removal from water using bio-char, a green waste, low-cost adsorbent: Equilibrium uptake and sorption dynamics modeling," in *Industrial and Engineering Chemistry Research*, American Chemical Society, Jan. 2012, pp. 900–914. doi: 10.1021/ie202189v.
- [377] S. karmakar, J. Dechnik, C. Janiak, and S. De, "Aluminium fumarate metal-organic framework: A super adsorbent for fluoride from water," *J Hazard Mater*, vol. 303, pp. 10–20, Feb. 2016, doi: 10.1016/j.jhazmat.2015.10.030.
- [378] "Dresselhaus," 2001. [Online]. Available: www.nature.com
- [379] A. Adamantiades and I. Kessides, "Nuclear power for sustainable development: Current status and future prospects," *Energy Policy*, vol. 37, no. 12, pp. 5149–5166, Dec. 2009, doi: 10.1016/j.enpol.2009.07.052.
- [380] "tubiana2000".
- [381] S. H. Frisbie, E. J. Mitchell, and B. Sarkar, "World Health Organization increases its drinking-water guideline for uranium," Oct. 2013. doi: 10.1039/c3em00381g.
- [382] C. C. Fuller, J. R. Bargar, J. A. Davis, and M. J. Piana, "Mechanisms of uranium interactions with hydroxyapatite: Implications for groundwater remediation," *Environ Sci Technol*, vol. 36, no. 2, pp. 158–165, Jan. 2002, doi: 10.1021/es0108483.
- [383] C. Jing, Y. L. Li, and S. Landsberger, "Review of soluble uranium removal by nanoscale zero valent iron," Nov. 01, 2016, *Elsevier Ltd*. doi: 10.1016/j.jenvrad.2016.06.027.
- [384] M. Feng, P. Zhang, H. C. Zhou, and V. K. Sharma, "Water-stable metal-organic frameworks for aqueous removal of heavy metals and radionuclides: A review," Oct. 01, 2018, *Elsevier Ltd*. doi: 10.1016/j.chemosphere.2018.06.114.
- [385] B. C. Luo, L. Y. Yuan, Z. F. Chai, W. Q. Shi, and Q. Tang, "U(VI) capture from aqueous solution by highly porous and stable MOFs: UiO-66 and its amine derivative," *J Radioanal Nucl Chem*, vol. 307, no. 1, pp. 269–276, Jan. 2016, doi: 10.1007/s10967-015-4108-3.
- [386] J. Q. Li *et al.*, "Direct extraction of U(VI) from alkaline solution and seawater via anion exchange by metal-organic framework," *Chemical Engineering Journal*, vol. 316, pp. 154–159, 2017, doi: 10.1016/j.cej.2017.01.046.
- [387] W. Liu *et al.*, "Highly Sensitive and Selective Uranium Detection in Natural Water Systems Using a Luminescent Mesoporous Metal-Organic Framework Equipped with Abundant Lewis Basic Sites: A

- Combined Batch, X-ray Absorption Spectroscopy, and First Principles Simulation Investigation,” *Environ Sci Technol*, vol. 51, no. 7, pp. 3911–3921, Apr. 2017, doi: 10.1021/acs.est.6b06305.
- [388] W. Yang *et al.*, “MOF-76: From a luminescent probe to highly efficient Uvi sorption material,” *Chemical Communications*, vol. 49, no. 88, pp. 10415–10417, Oct. 2013, doi: 10.1039/c3cc44983a.
- [389] Z. Q. Bai *et al.*, “Introduction of amino groups into acid-resistant MOFs for enhanced U(vi) sorption,” *J Mater Chem A Mater*, vol. 3, no. 2, pp. 525–534, Jan. 2015, doi: 10.1039/c4ta04878d.
- [390] B. K. Singh, R. Tomar, S. Kumar, A. Jain, B. S. Tomar, and V. K. Manchanda, “Sorption of ^{137}Cs , ^{133}Ba and ^{154}Eu by synthesized sodium aluminosilicate (Na-AS),” *J Hazard Mater*, vol. 178, no. 1–3, pp. 771–776, Jun. 2010, doi: 10.1016/j.jhazmat.2010.02.007.
- [391] Y. Peng, H. Huang, D. Liu, and C. Zhong, “Radioactive Barium Ion Trap Based on Metal-Organic Framework for Efficient and Irreversible Removal of Barium from Nuclear Wastewater,” *ACS Appl Mater Interfaces*, vol. 8, no. 13, pp. 8527–8535, Apr. 2016, doi: 10.1021/acsami.6b00900.
- [392] G. Yuan *et al.*, “Glycine derivative-functionalized metal-organic framework (MOF) materials for Co(II) removal from aqueous solution,” *Appl Surf Sci*, vol. 466, pp. 903–910, Feb. 2019, doi: 10.1016/j.apsusc.2018.10.129.
- [393] Guoyuan Yuan *et al.*, “Schiff base anchored on metal-organic framework for Co (II) removal from aqueous solution,” *Chemical Engineering Journal*, vol. 326, pp. 691–699, 2017, Accessed: Jun. 16, 2024. [Online]. Available: <http://dx.doi.org/10.1016/j.cej.2017.06.024>
- [394] Z. S. Birungi, E. M. Nkhambayausi Chirwa, N. Shen, and M. Roestorff, “Recovery of Rare Earths, Precious Metals and Bioreduction of Toxic Metals from Wastewater Using Algae,” 2020, pp. 267–297. doi: 10.1007/978-981-15-1390-9_12.
- [395] H. Umeda, A. Sasaki, K. Takahashi, K. Haga, Y. Takasaki, and A. Shibayama, “Recovery and concentration of precious metals from strong acidic wastewater,” *Mater Trans*, vol. 52, no. 7, pp. 1462–1470, Jul. 2011, doi: 10.2320/matertrans.M2010432.
- [396] J. He and A. Kappler, “Recovery of precious metals from waste streams,” *Microb Biotechnol*, vol. 10, no. 5, pp. 1194–1198, Sep. 2017, doi: 10.1111/1751-7915.12759.
- [397] S. Lin *et al.*, “Selective adsorption of Pd(II) over interfering metal ions (Co(II), Ni(II), Pt(IV)) from acidic aqueous phase by metal-organic frameworks,” *Chemical Engineering Journal*, vol. 345, pp. 337–344, Aug. 2018, doi: 10.1016/j.cej.2018.03.173.
- [398] S. Daliran *et al.*, “A Pyridyltriazol Functionalized Zirconium Metal-Organic Framework for Selective and Highly Efficient Adsorption of Palladium,” *ACS Appl Mater Interfaces*, vol. 12, no. 22, pp. 25221–25232, Jun. 2020, doi: 10.1021/acsami.0c06672.
- [399] Z. Chang, F. Li, X. Qi, B. Jiang, J. Kou, and C. Sun, “Selective and efficient adsorption of Au (III) in aqueous solution by Zr-based metal-organic frameworks (MOFs): An unconventional way for gold recycling,” *J Hazard Mater*, vol. 391, Jun. 2020, doi: 10.1016/j.jhazmat.2020.122175.
- [400] A. O. Adeeyo *et al.*, “Recovery of precious metals from processed wastewater: conventional techniques nexus advanced and pragmatic alternatives,” *Water Reuse*, vol. 13, no. 2, pp. 134–161, Jun. 2023, doi: 10.2166/wrd.2023.068.

- [401] M. Zhao, Z. Huang, S. Wang, L. Zhang, and C. Wang, “Experimental and DFT study on the selective adsorption mechanism of Au(III) using amidinothiourea-functionalized UiO-66-NH₂,” *Microporous and Mesoporous Materials*, vol. 294, Mar. 2020, doi: 10.1016/j.micromeso.2019.109905.
- [402] X. Cheng *et al.*, “Size-controlled silver nanoparticles stabilized on thiol-functionalized MIL-53(Al) frameworks,” *Nanoscale*, vol. 7, no. 21, pp. 9738–9745, Jun. 2015, doi: 10.1039/c5nr01292a.
- [403] J. E. Conde-González, E. M. Peña-Méndez, S. Rybáková, J. Pasán, C. Ruiz-Pérez, and J. Havel, “Adsorption of silver nanoparticles from aqueous solution on copper-based metal organic frameworks (HKUST-1),” *Chemosphere*, vol. 150, pp. 659–666, May 2016, doi: 10.1016/j.chemosphere.2016.02.005.
- [404] K. Wang, J. Gu, and N. Yin, “Efficient Removal of Pb(II) and Cd(II) Using NH₂-Functionalized Zr-MOFs via Rapid Microwave-Promoted Synthesis,” *Ind Eng Chem Res*, vol. 56, no. 7, pp. 1880–1887, Feb. 2017, doi: 10.1021/acs.iecr.6b04997.
- [405] Fei Ke, Jing Jiang, Yizhi Li, Jing Liang, Xiaochun Wan, and Sanghoon Ko, “Highly selective removal of Hg²⁺ and Pb²⁺ by thiol-functionalized Fe₃O₄@metal-organic framework core-shell magnetic microspheres,” *Appl Surf Sci*, vol. 413, pp. 266–274, 2017, Accessed: Jun. 17, 2024. [Online]. Available: <https://doi.org/10.1016/j.apsusc.2017.03.303>
- [406] H. Shayegan, G. A. M. Ali, and V. Safarifard, “Amide-Functionalized Metal–Organic Framework for High Efficiency and Fast Removal of Pb(II) from Aqueous Solution,” *J Inorg Organomet Polym Mater*, vol. 30, no. 8, pp. 3170–3178, Aug. 2020, doi: 10.1007/s10904-020-01474-0.
- [407] N. Yin, K. Wang, Y. Xia, and Z. Li, “Novel melamine modified metal-organic frameworks for remarkably high removal of heavy metal Pb (II),” *Desalination*, vol. 430, pp. 120–127, Mar. 2018, doi: 10.1016/j.desal.2017.12.057.
- [408] Y. Wang, G. Ye, H. Chen, X. Hu, Z. Niu, and S. Ma, “Functionalized metal-organic framework as a new platform for efficient and selective removal of cadmium(II) from aqueous solution,” *J Mater Chem A Mater*, vol. 3, no. 29, pp. 15292–15298, Jun. 2015, doi: 10.1039/c5ta03201f.
- [409] C. Liu, P. Wang, X. Liu, X. Yi, D. Liu, and Z. Zhou, “Ultrafast removal of cadmium(II) by green cyclodextrin metal–organic-framework-based nanoporous carbon: Adsorption mechanism and application,” *Chem Asian J*, vol. 14, no. 2, pp. 261–268, 2019, doi: 10.1002/asia.201801431.
- [410] Z. Seyfi Hasankola, R. Rahimi, H. Shayegan, E. Moradi, and V. Safarifard, “Removal of Hg²⁺ heavy metal ion using a highly stable mesoporous porphyrinic zirconium metal-organic framework,” *Inorganica Chim Acta*, vol. 501, Feb. 2020, doi: 10.1016/j.ica.2019.119264.
- [411] H. R. Fu, Z. X. Xu, and J. Zhang, “Water-stable metal-organic frameworks for fast and high dichromate trapping via single-crystal-to-single-crystal ion exchange,” *Chemistry of Materials*, vol. 27, no. 1, pp. 205–210, Jan. 2015, doi: 10.1021/cm503767r.
- [412] L. Li, Y. Xu, D. Zhong, and N. Zhong, “CTAB-surface-functionalized magnetic MOF@MOF composite adsorbent for Cr(VI) efficient removal from aqueous solution,” *Colloids Surf A Physicochem Eng Asp*, vol. 586, Feb. 2020, doi: 10.1016/j.colsurfa.2019.124255.
- [413] J. Cai, X. Wang, Y. Zhou, L. Jiang, and C. Wang, “Selective adsorption of arsenate and the reversible structure transformation of the mesoporous metal-organic framework MIL-100(Fe),” *Physical Chemistry Chemical Physics*, vol. 18, no. 16, pp. 10864–10867, Apr. 2016, doi: 10.1039/c6cp00249h.

- [414] J. Li *et al.*, “Zeolitic imidazolate framework-8 with high efficiency in trace arsenate adsorption and removal from water,” *Journal of Physical Chemistry C*, vol. 118, no. 47, pp. 27382–27387, Nov. 2014, doi: 10.1021/jp508381m.
- [415] X. He *et al.*, “Exceptional adsorption of arsenic by zirconium metal-organic frameworks: Engineering exploration and mechanism insight,” *J Colloid Interface Sci*, vol. 539, pp. 223–234, Mar. 2019, doi: 10.1016/j.jcis.2018.12.065.
- [416] T. Zheng *et al.*, “Overcoming the crystallization and designability issues in the ultrastable zirconium phosphonate framework system,” *Nat Commun*, vol. 8, May 2017, doi: 10.1038/ncomms15369.
- [417] D. Sheng *et al.*, “Efficient and Selective Uptake of TcO₄⁻ by a Cationic Metal-Organic Framework Material with Open Ag⁺ Sites,” *Environ Sci Technol*, vol. 51, no. 6, pp. 3471–3479, Mar. 2017, doi: 10.1021/acs.est.7b00339.
- [418] Y. Hu, S. Wang, and L. Zhang, “Selective adsorption of Au (III) from aqueous solution by a Cu-based bisligand metal organic framework adsorbent,” *J Environ Chem Eng*, vol. 9, no. 5, Oct. 2021, doi: 10.1016/j.jece.2021.106260.
- [419] J. Wei, W. Zhang, W. Pan, C. Li, and W. Sun, “Experimental and theoretical investigations on Se(IV) and Se(VI) adsorption to UiO-66-based metal-organic frameworks,” *Environ Sci Nano*, vol. 5, no. 6, pp. 1441–1453, 2018, doi: 10.1039/c8en00180d.
- [420] I. K. Rind, N. Memon, M. Y. Khuhawar, and M. F. Lanjwani, “Thermally activated mango peels hydrochar for fixed-bed continuous flow decontamination of Pb(II) ions from aqueous solution,” *International Journal of Environmental Science and Technology*, vol. 19, no. 4, pp. 2835–2850, Apr. 2022, doi: 10.1007/s13762-021-03272-8.
- [421] E. T. Abdel Salam, K. M. Abou El-Nour, A. A. Awad, and A. S. Orabi, “Carbon nanotubes modified with 5,7-dinitro-8-quinolinol as potentially applicable tool for efficient removal of industrial wastewater pollutants,” *Arabian Journal of Chemistry*, vol. 13, no. 1, pp. 109–119, Jan. 2020, doi: 10.1016/j.arabjc.2017.02.005.
- [422] J. H. Park *et al.*, “Exploration of the potential capacity of fly ash and bottom ash derived from wood pellet-based thermal power plant for heavy metal removal,” *Science of the Total Environment*, vol. 740, Oct. 2020, doi: 10.1016/j.scitotenv.2020.140205.
- [423] W. Wei, X. Han, M. Zhang, Y. Zhang, and C. Zheng, “Macromolecular humic acid modified nano-hydroxyapatite for simultaneous removal of Cu(II) and methylene blue from aqueous solution: Experimental design and adsorption study,” *Int J Biol Macromol*, vol. 150, pp. 849–860, May 2020, doi: 10.1016/j.ijbiomac.2020.02.137.
- [424] Z. Derakhshan Nejad, M. C. Jung, and K. H. Kim, “Remediation of soils contaminated with heavy metals with an emphasis on immobilization technology,” Jun. 01, 2018, *Springer Netherlands*. doi: 10.1007/s10653-017-9964-z.
- [425] J. Lu, C. Wu, C. Tian, L. Wang, W. Li, and B. Liu, “A multifunctional fertilizer for long-term release and remediation of Cr(VI)-polluted soil: Dialdehyde CMC urea-formaldehyde grafted on nZVI@MOF(Mg)-74,” *Surfaces and Interfaces*, vol. 46, Mar. 2024, doi: 10.1016/j.surfin.2024.104039.
- [426] T. A. Martin and M. V. Ruby, “Review of in situ remediation technologies for lead, zinc, and cadmium in soil,” *Remediation*, vol. 14, no. 3, pp. 35–53, 2004, doi: 10.1002/rem.20011.

- [427] R. B. García-Guerra, S. Montesdeoca-Esponda, Z. Sosa-Ferrera, A. Kabir, K. G. Furton, and J. J. Santana-Rodríguez, “Rapid monitoring of residual UV-stabilizers in seawater samples from beaches using fabric phase sorptive extraction and UHPLC-MS/MS,” *Chemosphere*, vol. 164, pp. 201–207, Dec. 2016, doi: 10.1016/j.chemosphere.2016.08.102.
- [428] I. Bruheim, X. Liu, and J. Pawliszyn, “Thin-film microextraction,” *Anal Chem*, vol. 75, no. 4, pp. 1002–1010, Feb. 2003, doi: 10.1021/ac026162q.
- [429] S. L. Chong, D. Wang, J. D. Hayes, B. W. Wilhite, and A. Malik, “Sol-Gel Coating Technology for the Preparation of Solid-Phase Microextraction Fibers of Enhanced Thermal Stability,” 1997. [Online]. Available: <https://pubs.acs.org/sharingguidelines>
- [430] B. W. WRIGHT PAUL A PEADEN, M. L. Lee, and T. J. Stark, “FREE RADICAL CROSS-LINKING IN THE PREPARATION OF NON-EXTRACTABLE STATIONARY PHASES FOR CAPILLARY GAS CHROMA-TOGRAPHY*,” Ekevier !Scientic Publishing Company, 1982.
- [431] C. M. Graham, Y. Meng, T. Ho, and J. L. Anderson, “Sorbent coatings for solid-phase microextraction based on mixtures of polymeric ionic liquids,” *J Sep Sci*, vol. 34, no. 3, pp. 340–346, Feb. 2011, doi: 10.1002/jssc.201000367.
- [432] Y. Liu, Y. Shen, and M. L. Lee, “) Potter, D.; Pawliszyn,” 1994. [Online]. Available: <https://pubs.acs.org/sharingguidelines>
- [433] R. Kumar, Gaurav, Heena, A. K. Malik, A. Kabir, and K. G. Furton, “Efficient analysis of selected estrogens using fabric phase sorptive extraction and high performance liquid chromatography-fluorescence detection,” *J Chromatogr A*, vol. 1359, pp. 16–25, Sep. 2014, doi: 10.1016/j.chroma.2014.07.013.
- [434] N. Fontanals, F. Borrull, and R. M. Marcé, “Fabric phase sorptive extraction for environmental samples,” *Advances in Sample Preparation*, vol. 5, Feb. 2023, doi: 10.1016/j.sampre.2022.100050.
- [435] S. S. Saini, A. Kabir, A. L. J. Rao, A. K. Malik, and K. G. Furton, “A novel protocol to monitor trace levels of selected polycyclic aromatic hydrocarbons in environmental water using fabric phase sorptive extraction followed by high performance liquid chromatography-fluorescence detection,” *Separations*, vol. 4, no. 2, Jun. 2017, doi: 10.3390/separations4020022.
- [436] T. Sun *et al.*, “Fabric-phase sorptive extraction coupled with ion mobility spectrometry for on-site rapid detection of PAHs in aquatic environment,” *Talanta*, vol. 195, pp. 109–116, Apr. 2019, doi: 10.1016/j.talanta.2018.11.018.
- [437] S. Montesdeoca-Esponda, Z. Sosa-Ferrera, A. Kabir, K. G. Furton, and J. J. Santana-Rodríguez, “Fabric phase sorptive extraction followed by UHPLC-MS/MS for the analysis of benzotriazole UV stabilizers in sewage samples,” *Anal Bioanal Chem*, vol. 407, no. 26, Sep. 2015, doi: 10.1007/s00216-015-8990-x.
- [438] R. Kumar, Gaurav, A. Kabir, K. G. Furton, and A. K. Malik, “Development of a fabric phase sorptive extraction with high-performance liquid chromatography and ultraviolet detection method for the analysis of alkyl phenols in environmental samples,” *J Sep Sci*, vol. 38, no. 18, pp. 3228–3238, Sep. 2015, doi: 10.1002/jssc.201500464.
- [439] S. S. Lakade, F. Borrull, K. G. Furton, A. Kabir, N. Fontanals, and R. M. Marcé, “Comparative study of different fabric phase sorptive extraction sorbents to determine emerging contaminants from

- environmental water using liquid chromatography-tandem mass spectrometry,” *Talanta*, vol. 144, pp. 1342–1351, Nov. 2015, doi: 10.1016/j.talanta.2015.08.009.
- [440] R. Guedes-Alonso *et al.*, “Determination of androgens and progestogens in environmental and biological samples using fabric phase sorptive extraction coupled to ultra-high performance liquid chromatography tandem mass spectrometry,” *J Chromatogr A*, vol. 1437, pp. 116–126, Mar. 2016, doi: 10.1016/j.chroma.2016.01.077.
- [441] S. Santana-Viera, R. Guedes-Alonso, Z. Sosa-Ferrera, J. J. Santana-Rodríguez, A. Kabir, and K. G. Furton, “Optimization and application of fabric phase sorptive extraction coupled to ultra-high performance liquid chromatography tandem mass spectrometry for the determination of cytostatic drug residues in environmental waters,” *J Chromatogr A*, vol. 1529, pp. 39–49, Dec. 2017, doi: 10.1016/j.chroma.2017.10.070.
- [442] R. Kaur *et al.*, “Fabric phase sorptive extraction/GC-MS method for rapid determination of broad polarity spectrum multi-class emerging pollutants in various aqueous samples,” *J Sep Sci*, vol. 42, no. 14, pp. 2407–2417, Jul. 2019, doi: 10.1002/jssc.201900089.
- [443] H. İ. Ulusoy, K. Köseoğlu, A. Kabir, S. Ulusoy, and M. Locatelli, “Fabric phase sorptive extraction followed by HPLC-PDA detection for the monitoring of pirimicarb and fenitrothion pesticide residues,” *Microchimica Acta*, vol. 187, no. 6, Jun. 2020, doi: 10.1007/s00604-020-04306-7.
- [444] S. Santana-Viera *et al.*, “Fabric Phase Sorptive Extraction for the Determination of Anthracyclines in Sewage,” *Separations*, vol. 9, no. 3, Mar. 2022, doi: 10.3390/separations9030069.
- [445] M. Roldán-Pijuán, R. Lucena, S. Cárdenas, M. Valcárcel, A. Kabir, and K. G. Furton, “Stir fabric phase sorptive extraction for the determination of triazine herbicides in environmental waters by liquid chromatography,” *J Chromatogr A*, vol. 1376, pp. 35–45, Jan. 2015, doi: 10.1016/j.chroma.2014.12.027.
- [446] G. Huang, S. Dong, M. Zhang, H. Zhang, and T. Huang, “Fabric phase sorptive extraction: Two practical sample pretreatment techniques for brominated flame retardants in water,” *Water Res*, vol. 101, pp. 547–554, Sep. 2016, doi: 10.1016/j.watres.2016.06.007.
- [447] S. S. Lakade, F. Borrull, K. G. Furton, A. Kabir, R. M. Marcé, and N. Fontanals, “Dynamic fabric phase sorptive extraction for a group of pharmaceuticals and personal care products from environmental waters,” *J Chromatogr A*, vol. 1456, pp. 19–26, Jul. 2016, doi: 10.1016/j.chroma.2016.05.097.
- [448] N. Manousi *et al.*, “Magnet integrated fabric phase sorptive extraction as a stand-alone extraction device for the monitoring of benzoyl urea insecticides in water samples by HPLC-DAD,” *J Chromatogr A*, vol. 1672, Jun. 2022, doi: 10.1016/j.chroma.2022.463026.
- [449] G. Huang *et al.*, “Comparative Study of Hyper-crosslinked Polymer-Solid Phase Microextraction and Stir Bar Fabric Phase Sorptive Extraction for Simultaneous Determination of Fluoroquinolones in Water,” *Chromatographia*, vol. 85, no. 6, pp. 539–549, Jun. 2022, doi: 10.1007/s10337-022-04165-9.
- [450] A. Anthemidis, V. Kazantzi, V. Samanidou, A. Kabir, and K. G. Furton, “An automated flow injection system for metal determination by flame atomic absorption spectrometry involving on-line fabric disk sorptive extraction technique,” *Talanta*, vol. 156–157, pp. 64–70, 2016, doi: 10.1016/j.talanta.2016.05.012.

- [451] A. Kabir and K. G. Furton, “Fabric phase sorptive extraction: A new generation, green sample preparation approach,” in *Solid-Phase Extraction*, Elsevier, 2019, pp. 355–386. doi: 10.1016/B978-0-12-816906-3.00013-3.
- [452] E. Zilfidou, A. Kabir, K. Furton, and V. Samanidou, “Fabric Phase Sorptive Extraction: Current State of the Art and Future Perspectives,” *Separations*, vol. 5, no. 3, p. 40, Aug. 2018, doi: 10.3390/separations5030040.
- [453] A. Kabir, R. Mesa, J. Jurmain, and K. G. Furton, “Fabric Phase Sorptive Extraction Explained,” *Separations*, vol. 4, no. 2, p. 21, Jun. 2017, doi: 10.3390/separations4020021.
- [454] A. Kabir and V. Samanidou, “Fabric Phase Sorptive Extraction: A Paradigm Shift Approach in Analytical and Bioanalytical Sample Preparation,” *Molecules*, vol. 26, no. 4, p. 865, Feb. 2021, doi: 10.3390/molecules26040865.
- [455] V. Kazantzi and A. Anthemidis, “Fabric Sol–gel Phase Sorptive Extraction Technique: A Review,” *Separations*, vol. 4, no. 2, p. 20, May 2017, doi: 10.3390/separations4020020.
- [456] A. Kabir and V. Samanidou, “Fabric Phase Sorptive Extraction: A Paradigm Shift Approach in Analytical and Bioanalytical Sample Preparation,” *Molecules*, vol. 26, no. 4, p. 865, Feb. 2021, doi: 10.3390/molecules26040865.
- [457] A. Spietelun, M. Pilarczyk, A. Kloskowski, and J. Namieśnik, “Current trends in solid-phase microextraction (SPME) fibre coatings,” *Chem Soc Rev*, vol. 39, no. 11, p. 4524, 2010, doi: 10.1039/c003335a.
- [458] C. K. Hasan, A. Ghiasvand, T. W. Lewis, P. N. Nesterenko, and B. Paull, “Recent advances in stir-bar sorptive extraction: Coatings, technical improvements, and applications,” *Anal Chim Acta*, vol. 1139, pp. 222–240, Dec. 2020, doi: 10.1016/j.aca.2020.08.021.
- [459] V. Vázquez-Gomis, J. Grau, J. L. Benedé, D. L. Giokas, A. Chisvert, and A. Salvador, “Fundamentals and applications of stir bar sorptive dispersive microextraction: A tutorial review,” *Anal Chim Acta*, vol. 1153, p. 338271, Apr. 2021, doi: 10.1016/j.aca.2021.338271.
- [460] M. Bazargan, F. Ghaemi, A. Amiri, and M. Mirzaei, “Metal–organic framework-based sorbents in analytical sample preparation,” *Coord Chem Rev*, vol. 445, p. 214107, Oct. 2021, doi: 10.1016/j.ccr.2021.214107.
- [461] F. Maya, C. Palomino Cabello, R. M. Frizzarin, J. M. Estela, G. Turnes Palomino, and V. Cerdà, “Magnetic solid-phase extraction using metal-organic frameworks (MOFs) and their derived carbons,” *TrAC Trends in Analytical Chemistry*, vol. 90, pp. 142–152, May 2017, doi: 10.1016/j.trac.2017.03.004.
- [462] M. Bazargan, F. Ghaemi, A. Amiri, and M. Mirzaei, “Metal–organic framework-based sorbents in analytical sample preparation,” *Coord Chem Rev*, vol. 445, p. 214107, Oct. 2021, doi: 10.1016/j.ccr.2021.214107.
- [463] P. Rocío-Bautista and V. Termopoli, “Metal–Organic Frameworks in Solid-Phase Extraction Procedures for Environmental and Food Analyses,” *Chromatographia*, vol. 82, no. 8, pp. 1191–1205, Aug. 2019, doi: 10.1007/s10337-019-03706-z.

- [464] J. Xiong, A. Li, Y. Liu, L. Wang, X. Qin, and J. Yu, “Scalable and hierarchically designed MOF fabrics by netting MOFs into nanofiber networks for high-performance solar-driven water purification,” *J Mater Chem A Mater*, vol. 9, no. 37, pp. 21005–21012, 2021, doi: 10.1039/D1TA05589E.
- [465] A. Yao, X. Jiao, D. Chen, and C. Li, “Bio-Inspired Polydopamine-Mediated Zr-MOF Fabrics for Solar Photothermal-Driven Instantaneous Detoxification of Chemical Warfare Agent Simulants,” *ACS Appl Mater Interfaces*, vol. 12, no. 16, pp. 18437–18445, Apr. 2020, doi: 10.1021/acsami.9b22242.
- [466] M. Schelling, M. Kim, E. Ota, and J. Hinestroza, “Decoration of Cotton Fibers with a Water-Stable Metal–Organic Framework (UiO-66) for the Decomposition and Enhanced Adsorption of Micropollutants in Water,” *Bioengineering*, vol. 5, no. 1, p. 14, Feb. 2018, doi: 10.3390/bioengineering5010014.
- [467] W. Li, R. Wang, and Z. Chen, “Zr-based metal-organic framework-modified cotton for solid phase micro-extraction of non-steroidal anti-inflammatory drugs,” *J Chromatogr A*, vol. 1576, pp. 19–25, Nov. 2018, doi: 10.1016/j.chroma.2018.09.032.
- [468] Y. Gao, S. Wang, N. Zhang, X. Xu, and T. Bao, “Novel solid-phase extraction filter based on a zirconium meta-organic framework for determination of non-steroidal anti-inflammatory drugs residues,” *J Chromatogr A*, vol. 1652, p. 462349, Aug. 2021, doi: 10.1016/j.chroma.2021.462349.
- [469] P. González-Hernández *et al.*, “Application of a Pillared-Layer Zn-Triazolate Metal-Organic Framework in the Dispersive Miniaturized Solid-Phase Extraction of Personal Care Products from Wastewater Samples,” *Molecules*, vol. 24, no. 4, p. 690, Feb. 2019, doi: 10.3390/molecules24040690.
- [470] N. Morin, C. Miège, M. Coquery, and J. Randon, “Chemical calibration, performance, validation and applications of the polar organic chemical integrative sampler (POCIS) in aquatic environments,” Jun. 2012. doi: 10.1016/j.trac.2012.01.007.
- [471] J. Ou *et al.*, “Unexpected superhydrophobic polydopamine on cotton fabric,” *Prog Org Coat*, vol. 147, Oct. 2020, doi: 10.1016/j.porgcoat.2020.105777.
- [472] A. Yao, X. Jiao, D. Chen, and C. Li, “Bio-Inspired Polydopamine-Mediated Zr-MOF Fabrics for Solar Photothermal-Driven Instantaneous Detoxification of Chemical Warfare Agent Simulants,” *ACS Appl Mater Interfaces*, vol. 12, no. 16, pp. 18437–18445, Apr. 2020, doi: 10.1021/acsami.9b22242.
- [473] M. Schelling, M. Kim, E. Ota, and J. Hinestroza, “Decoration of cotton fibers with a water-stable metal–organic framework (UiO-66) for the decomposition and enhanced adsorption of micropollutants in water,” *Bioengineering*, vol. 5, no. 1, Mar. 2018, doi: 10.3390/bioengineering5010014.
- [474] R. M. Abdelhameed, M. Rehan, and H. E. Emam, “Figuration of Zr-based MOF@cotton fabric composite for potential kidney application,” *Carbohydr Polym*, vol. 195, pp. 460–467, Sep. 2018, doi: 10.1016/j.carbpol.2018.04.122.
- [475] D. DeSantis, J. A. Mason, B. D. James, C. Houchins, J. R. Long, and M. Veenstra, “Techno-economic Analysis of Metal-Organic Frameworks for Hydrogen and Natural Gas Storage,” *Energy and Fuels*, vol. 31, no. 2, pp. 2024–2032, Feb. 2017, doi: 10.1021/acs.energyfuels.6b02510.
- [476] A. Kabir, R. Mesa, J. Jurmain, and K. G. Furton, “Fabric phase sorptive extraction explained,” *Separations*, vol. 4, no. 2, Jun. 2017, doi: 10.3390/separations4020021.

- [477] K. I. Hadjiivanov *et al.*, “Power of Infrared and Raman Spectroscopies to Characterize Metal-Organic Frameworks and Investigate Their Interaction with Guest Molecules,” Feb. 10, 2021, *American Chemical Society*. doi: 10.1021/acs.chemrev.0c00487.
- [478] A. Yao, X. Jiao, D. Chen, and C. Li, “Photothermally Enhanced Detoxification of Chemical Warfare Agent Simulants Using Bioinspired Core-Shell Dopamine-Melanin@Metal-Organic Frameworks and Their Fabrics,” *ACS Appl Mater Interfaces*, vol. 11, no. 8, pp. 7927–7935, Feb. 2019, doi: 10.1021/acsami.8b19445.
- [479] B. Hashemi, P. Zohrabi, N. Raza, and K. H. Kim, “Metal-organic frameworks as advanced sorbents for the extraction and determination of pollutants from environmental, biological, and food media,” Dec. 01, 2017, *Elsevier B.V.* doi: 10.1016/j.trac.2017.08.015.
- [480] V. Kazantzi and A. Anthemidis, “Fabric sol–gel phase sorptive extraction technique: A review,” Jun. 01, 2017, *MDPI Multidisciplinary Digital Publishing Institute*. doi: 10.3390/separations4020020.
- [481] Izabela Narloch and Grażyna Wejnerowska, “An Overview of the Analytical Methods for the Determination of Organic Ultraviolet Filters in Cosmetic Products and Human Samples,” *Molecules*, vol. 26, no. 4780, Aug. 2021, doi: <https://doi.org/10.3390/molecules26164780>.
- [482] S. Kim *et al.*, “PubChem in 2021: New data content and improved web interfaces,” *Nucleic Acids Res*, vol. 49, no. D1, pp. D1388–D1395, Jan. 2021, doi: 10.1093/nar/gkaa971.
- [483] J. L. Benedé, A. Chisvert, D. L. Giokas, and A. Salvador, “Development of stir bar sorptive-dispersive microextraction mediated by magnetic nanoparticles and its analytical application to the determination of hydrophobic organic compounds in aqueous media,” *J Chromatogr A*, vol. 1362, pp. 25–33, Oct. 2014, doi: 10.1016/j.chroma.2014.08.024.
- [484] J. L. Benedé, A. Chisvert, C. Moyano, D. L. Giokas, and A. Salvador, “Expanding the application of stir bar sorptive-dispersive microextraction approach to solid matrices: Determination of ultraviolet filters in coastal sand samples,” *J Chromatogr A*, vol. 1564, pp. 25–33, Aug. 2018, doi: 10.1016/j.chroma.2018.06.003.
- [485] A. Voulgari *et al.*, “Solid ink-printed filter paper as a green adsorbent material for the solid-phase extraction of UV filters from water samples,” *Int J Environ Anal Chem*, vol. 97, no. 12, pp. 1163–1177, Sep. 2017, doi: 10.1080/03067319.2017.1390087.
- [486] V. Vállez-Gomis, J. Grau, J. L. Benedé, D. L. Giokas, A. Chisvert, and A. Salvador, “Fundamentals and applications of stir bar sorptive dispersive microextraction: A tutorial review,” *Anal Chim Acta*, vol. 1153, Apr. 2021, doi: 10.1016/j.aca.2021.338271.
- [487] R. Kaur, R. Kaur, S. Rani, A. K. Malik, A. Kabir, and K. G. Furton, “Application of fabric phase sorptive extraction with gas chromatography and mass spectrometry for the determination of organophosphorus pesticides in selected vegetable samples,” *J Sep Sci*, vol. 42, no. 4, pp. 862–870, Feb. 2019, doi: 10.1002/jssc.201800854.
- [488] G. Rigkos *et al.*, “An improved fabric-phase sorptive extraction protocol for the determination of seven parabens in human urine by HPLC–DAD,” *Biomedical Chromatography*, vol. 35, no. 2, Feb. 2021, doi: 10.1002/bmc.4974.

RERERENCES

- [489] A. Chisvert, D. Giokas, J. L. Benedé, and A. Salvador, “Environmental Monitoring of Cosmetic Ingredients,” in *Analysis of Cosmetic Products*, Elsevier, 2018, pp. 435–547. doi: 10.1016/B978-0-444-63508-2.00016-3.
- [490] J. Ouyang, B. Na, G. Xiong, L. Xu, and T. Jin, “Determination of Solubility and Thermodynamic Properties of Benzophenone in Different Pure Solvents,” *J Chem Eng Data*, vol. 63, no. 5, pp. 1833–1840, May 2018, doi: 10.1021/acs.jced.8b00196.
- [491] H. Li, P. A. Helm, and C. D. Metcalfe, “Sampling in the great lakes for pharmaceuticals, personal care products, and endocrine-disrupting substances using the passive polar organic chemical integrative sampler,” *Environ Toxicol Chem*, vol. 29, no. 4, pp. 751–762, 2010, doi: 10.1002/etc.104.
- [492] S. L. Macleod, E. L. McClure, and C. S. Wong, “LABORATORY CALIBRATION AND FIELD DEPLOYMENT OF THE POLAR ORGANIC CHEMICAL INTEGRATIVE SAMPLER FOR PHARMACEUTICALS AND PERSONAL CARE PRODUCTS IN WASTEWATER AND SURFACE WATER,” 2007. [Online]. Available: <http://www12.statcan.ca>
- [493] Y. Li *et al.*, “In situ calibration of polar organic chemical integrative samplers to monitor organophosphate flame retardants in river water using polyethersulfone membranes with performance reference compounds,” *Science of the Total Environment*, vol. 610–611, pp. 1356–1363, Jan. 2018, doi: 10.1016/j.scitotenv.2017.08.234.
- [494] Payá Pérez, A., Rodríguez E.N., “Status of local soil contamination in Europe : revision of the indicator ‘Progress in the management contaminated sites in Europe,’” 2018. doi: 10.2760/093804.
- [495] M. C. Tomei and A. J. Daugulis, “Ex Situ Bioremediation of Contaminated Soils: An Overview of Conventional and Innovative Technologies,” *Crit Rev Environ Sci Technol*, vol. 43, no. 20, pp. 2107–2139, Jan. 2013, doi: 10.1080/10643389.2012.672056.
- [496] S. Kuppusamy, T. Palanisami, M. Megharaj, K. Venkateswarlu, and R. Naidu, “In-Situ Remediation Approaches for the Management of Contaminated Sites: A Comprehensive Overview,” 2016, pp. 1–115. doi: 10.1007/978-3-319-20013-2_1.
- [497] S. Kuppusamy, T. Palanisami, M. Megharaj, K. Venkateswarlu, and R. Naidu, “Ex-Situ Remediation Technologies for Environmental Pollutants: A Critical Perspective,” 2016, pp. 117–192. doi: 10.1007/978-3-319-20013-2_2.
- [498] B. Koul and P. Taak, “In Situ Soil Remediation Strategies,” in *Biotechnological Strategies for Effective Remediation of Polluted Soils*, Singapore: Springer Singapore, 2018, pp. 59–75. doi: 10.1007/978-981-13-2420-8_3.
- [499] A. Hussain *et al.*, “In-situ, Ex-situ, and nano-remediation strategies to treat polluted soil, water, and air – A review,” *Chemosphere*, vol. 289, p. 133252, Feb. 2022, doi: 10.1016/j.chemosphere.2021.133252.
- [500] P. de Voogt, Ed., *Reviews of Environmental Contamination and Toxicology Volume 236*, vol. 236. in *Reviews of Environmental Contamination and Toxicology*, vol. 236. Cham: Springer International Publishing, 2016. doi: 10.1007/978-3-319-20013-2.
- [501] Payá Pérez, A., Rodríguez E.N., “Status of local soil contamination in Europe : revision of the indicator ‘Progress in the management contaminated sites in Europe,’” 2018. doi: 10.2760/093804.

- [502] M. Guo, W. Song, and J. Tian, “Biochar-Facilitated Soil Remediation: Mechanisms and Efficacy Variations,” *Front Environ Sci*, vol. 8, Oct. 2020, doi: 10.3389/fenvs.2020.521512.
- [503] Z. Derakhshan Nejad, M. C. Jung, and K.-H. Kim, “Remediation of soils contaminated with heavy metals with an emphasis on immobilization technology,” *Environ Geochem Health*, vol. 40, no. 3, pp. 927–953, Jun. 2018, doi: 10.1007/s10653-017-9964-z.
- [504] G. Murtaza *et al.*, “Biochar as a Green Sorbent for Remediation of Polluted Soils and Associated Toxicity Risks: A Critical Review,” *Separations*, vol. 10, no. 3, p. 197, Mar. 2023, doi: 10.3390/separations10030197.
- [505] J. Wang *et al.*, “Analysis of the long-term effectiveness of biochar immobilization remediation on heavy metal contaminated soil and the potential environmental factors weakening the remediation effect: A review,” *Ecotoxicol Environ Saf*, vol. 207, p. 111261, Jan. 2021, doi: 10.1016/j.ecoenv.2020.111261.
- [506] D. Kupryianchyk, E. P. Reichman, M. I. Rakowska, E. T. H. M. Peeters, J. T. C. Grotenhuis, and A. A. Koelmans, “Ecotoxicological Effects of Activated Carbon Amendments on Macroinvertebrates in Nonpolluted and Polluted Sediments,” *Environ Sci Technol*, vol. 45, no. 19, pp. 8567–8574, Oct. 2011, doi: 10.1021/es2014538.
- [507] Z. Chen, Z. Zhang, P. Wang, and T. Liu, “Pivotal roles of nanoscale zerovalent iron supported on metal-organic framework material in cadmium (II) migration and transformation in soil,” *Journal of Environmental Science and Health, Part B*, vol. 57, no. 5, pp. 430–440, May 2022, doi: 10.1080/03601234.2022.2071561.
- [508] L. Yuan, J. Wang, Z. Zhong, J. Li, and H. Deng, “Immobilization of antimony in soil and groundwater using ferro-magnesium bimetallic organic frameworks,” *Journal of Environmental Sciences*, vol. 125, pp. 194–204, Mar. 2023, doi: 10.1016/j.jes.2022.01.030.
- [509] G. Liu *et al.*, “Rapidly reducing cadmium from contaminated farmland soil by novel magnetic recyclable Fe₃O₄/mercapto-functionalized attapulgite beads,” *Environmental Pollution*, vol. 351, p. 124056, Jun. 2024, doi: 10.1016/j.envpol.2024.124056.
- [510] V. Gouma, C. Tziasiou, A. D. Pournara, and D. L. Giokas, “A novel approach to sorbent-based remediation of soil impacted by organic micropollutants and heavy metals using granular biochar amendment and magnetic separation,” *J Environ Chem Eng*, vol. 10, no. 2, p. 107316, Apr. 2022, doi: 10.1016/j.jece.2022.107316.
- [511] V. Gouma, A. D. Pournara, M. J. Manos, and D. L. Giokas, “Fabric phase sorptive extraction and passive sampling of ultraviolet filters from natural waters using a zirconium metal organic framework-cotton composite,” *J Chromatogr A*, vol. 1670, p. 462945, May 2022, doi: 10.1016/j.chroma.2022.462945.
- [512] V. Gouma, C. Tziasiou, A. D. Pournara, and D. L. Giokas, “A novel approach to sorbent-based remediation of soil impacted by organic micropollutants and heavy metals using granular biochar amendment and magnetic separation,” *J Environ Chem Eng*, vol. 10, no. 2, Apr. 2022, doi: 10.1016/j.jece.2022.107316.
- [513] V. Gouma, A. D. Pournara, M. J. Manos, and D. L. Giokas, “Fabric phase sorptive extraction and passive sampling of ultraviolet filters from natural waters using a zirconium metal organic framework-cotton composite,” *J Chromatogr A*, vol. 1670, p. 462945, May 2022, doi: 10.1016/j.chroma.2022.462945.

- [514] A. D. Pournara, E. Moisiadis, V. Gouma, M. J. Manos, and D. L. Giokas, "Cotton fabric decorated by a Zr^{4+} MOF for selective As(V) and Se(IV) removal from aqueous media," *J Environ Chem Eng*, vol. 10, no. 3, p. 107705, Jun. 2022, doi: 10.1016/j.jece.2022.107705.
- [515] E. Moisiadis, A. D. Pournara, M. J. Manos, and D. L. Giokas, "Development of a New Method to Estimate the Water Purification Efficiency of Bulk-Supported Nanosorbents under Realistic Conditions," *Separations*, vol. 10, no. 2, p. 140, Feb. 2023, doi: 10.3390/separations10020140.
- [516] A. Yao, X. Jiao, D. Chen, and C. Li, "Photothermally Enhanced Detoxification of Chemical Warfare Agent Simulants Using Bioinspired Core–Shell Dopamine–Melanin@Metal–Organic Frameworks and Their Fabrics," *ACS Appl Mater Interfaces*, vol. 11, no. 8, pp. 7927–7935, Feb. 2019, doi: 10.1021/acsami.8b19445.
- [517] T. R. Sahoo and B. Prelot, "Adsorption processes for the removal of contaminants from wastewater: The perspective role of nanomaterials and nanotechnology," in *Nanomaterials for the Detection and Removal of Wastewater Pollutants*, Elsevier, 2020, pp. 161–222. doi: 10.1016/B978-0-12-818489-9.00007-4.
- [518] A. N. Ebelegi, N. Ayawei, and D. Wankasi, "Interpretation of Adsorption Thermodynamics and Kinetics," *Open J Phys Chem*, vol. 10, no. 03, pp. 166–182, 2020, doi: 10.4236/ojpc.2020.103010.
- [519] Y. R. Ma *et al.*, "Polydopamine-coated magnetic nanoparticles for enrichment and direct detection of small molecule pollutants coupled with MALDI-TOF-MS," *ACS Appl Mater Interfaces*, vol. 5, no. 3, pp. 1024–1030, Feb. 2013, doi: 10.1021/am3027025.
- [520] X. Hu *et al.*, "Sensitive characterization of polyphenolic antioxidants in *Polygonatum odoratum* by selective solid phase extraction and high performance liquid chromatography-diode array detector-quadrupole time-of-flight tandem mass spectrometry," *J Pharm Biomed Anal*, vol. 112, pp. 15–22, Aug. 2015, doi: 10.1016/j.jpba.2015.04.018.
- [521] V. Gouma, A. D. Pournara, M. J. Manos, and D. L. Giokas, "Fabric phase sorptive extraction and passive sampling of ultraviolet filters from natural waters using a zirconium metal organic framework-cotton composite," *J Chromatogr A*, vol. 1670, May 2022, doi: 10.1016/j.chroma.2022.462945.
- [522] J. Chu *et al.*, "Facile and reversible digestion and regeneration of zirconium-based metal-organic frameworks," *Commun Chem*, vol. 3, no. 1, Dec. 2020, doi: 10.1038/s42004-019-0248-7.
- [523] M. Bundschuh *et al.*, "Nanoparticles in the environment: where do we come from, where do we go to?," *Environ Sci Eur*, vol. 30, no. 1, p. 6, Dec. 2018, doi: 10.1186/s12302-018-0132-6.
- [524] S. Smita, S. K. Gupta, A. Bartonova, M. Dusinska, A. C. Gutleb, and Q. Rahman, "Nanoparticles in the environment: assessment using the causal diagram approach," *Environmental Health*, vol. 11, no. S1, p. S13, Jun. 2012, doi: 10.1186/1476-069X-11-S1-S13.
- [525] F. Gottschalk, T. Sonderer, R. W. Scholz, and B. Nowack, "Modeled Environmental Concentrations of Engineered Nanomaterials (TiO₂, ZnO, Ag, CNT, Fullerenes) for Different Regions," *Environ Sci Technol*, vol. 43, no. 24, pp. 9216–9222, Dec. 2009, doi: 10.1021/es9015553.
- [526] N. C. Mueller and B. Nowack, "Exposure Modeling of Engineered Nanoparticles in the Environment," *Environ Sci Technol*, vol. 42, no. 12, pp. 4447–4453, Jun. 2008, doi: 10.1021/es7029637.

- [527] A. A. Keller, Y. Zheng, A. Praetorius, J. T. K. Quik, and B. Nowack, "Predicting environmental concentrations of nanomaterials for exposure assessment - a review," *NanoImpact*, vol. 33, p. 100496, Jan. 2024, doi: 10.1016/j.impact.2024.100496.
- [528] M. A. Kiser, P. Westerhoff, T. Benn, Y. Wang, J. Pérez-Rivera, and K. Hristovski, "Titanium Nanomaterial Removal and Release from Wastewater Treatment Plants," *Environ Sci Technol*, vol. 43, no. 17, pp. 6757–6763, Sep. 2009, doi: 10.1021/es901102n.
- [529] L. Li, G. Hartmann, M. Döblinger, and M. Schuster, "Quantification of Nanoscale Silver Particles Removal and Release from Municipal Wastewater Treatment Plants in Germany," *Environ Sci Technol*, vol. 47, no. 13, pp. 7317–7323, Jul. 2013, doi: 10.1021/es3041658.
- [530] R. J. B. Peters *et al.*, "Detection of nanoparticles in Dutch surface waters," *Science of The Total Environment*, vol. 621, pp. 210–218, Apr. 2018, doi: 10.1016/j.scitotenv.2017.11.238.
- [531] A. K. Venkatesan *et al.*, "Using single-particle ICP-MS for monitoring metal-containing particles in tap water," *Environ Sci (Camb)*, vol. 4, no. 12, pp. 1923–1932, 2018, doi: 10.1039/C8EW00478A.
- [532] L. Xu, Z. Wang, J. Zhao, M. Lin, and B. Xing, "Accumulation of metal-based nanoparticles in marine bivalve mollusks from offshore aquaculture as detected by single particle ICP-MS," *Environmental Pollution*, vol. 260, p. 114043, May 2020, doi: 10.1016/j.envpol.2020.114043.
- [533] G. Z. Tsogas, D. L. Giokas, and A. G. Vlessidis, "Ultratrace Determination of Silver, Gold, and Iron Oxide Nanoparticles by Micelle Mediated Preconcentration/Selective Back-Extraction Coupled with Flow Injection Chemiluminescence Detection," *Anal Chem*, vol. 86, no. 7, pp. 3484–3492, Apr. 2014, doi: 10.1021/ac404071v.
- [534] F. Salim and T. Górecki, "Theory and modelling approaches to passive sampling," *Environ Sci Process Impacts*, vol. 21, no. 10, pp. 1618–1641, 2019, doi: 10.1039/C9EM00215D.
- [535] K. Godlewska, P. Stepnowski, and M. Paszkiewicz, "Pollutant analysis using passive samplers: principles, sorbents, calibration and applications. A review," *Environ Chem Lett*, vol. 19, no. 1, pp. 465–520, Feb. 2021, doi: 10.1007/s10311-020-01079-6.
- [536] B. Vrana *et al.*, "Passive sampling techniques for monitoring pollutants in water," *TrAC Trends in Analytical Chemistry*, vol. 24, no. 10, pp. 845–868, Nov. 2005, doi: 10.1016/j.trac.2005.06.006.
- [537] M. Senila, "Metal and metalloid monitoring in water by passive sampling – A review," *Rev Anal Chem*, vol. 42, no. 1, Dec. 2023, doi: 10.1515/revac-2023-0065.
- [538] P. Kumar, A. Pournara, K.-H. Kim, V. Bansal, S. Rapti, and M. J. Manos, "Metal-organic frameworks: Challenges and opportunities for ion-exchange/sorption applications," *Prog Mater Sci*, vol. 86, pp. 25–74, May 2017, doi: 10.1016/j.pmatsci.2017.01.002.
- [539] F. Formalik, K. Shi, F. Joodaki, X. Wang, and R. Q. Snurr, "Exploring the Structural, Dynamic, and Functional Properties of Metal-Organic Frameworks through Molecular Modeling," *Adv Funct Mater*, Oct. 2023, doi: 10.1002/adfm.202308130.
- [540] C. Tziasiou, A. D. Pournara, M. J. Manos, and D. L. Giokas, "Dispersive solid phase extraction of noble metal nanoparticles from environmental samples on a thiol-functionalized Zirconium(IV) metal organic framework and determination with atomic absorption spectrometry," *Microchemical Journal*, vol. 195, p. 109387, Dec. 2023, doi: 10.1016/j.microc.2023.109387.

- [541] Y. Shao *et al.*, “Adsorption of Ag/Au nanoparticles by ordered macro-microporous ZIF-67, and their synergistic catalysis application,” *J Clean Prod*, vol. 346, p. 131032, Apr. 2022, doi: 10.1016/j.jclepro.2022.131032.
- [542] E. E. Michaelides, “Nanoparticle diffusivity in narrow cylindrical pores,” *Int J Heat Mass Transf*, vol. 114, pp. 607–612, Nov. 2017, doi: 10.1016/j.ijheatmasstransfer.2017.06.098.
- [543] J. E. Conde-González, E. M. Peña-Méndez, S. Rybáková, J. Pasán, C. Ruiz-Pérez, and J. Havel, “Adsorption of silver nanoparticles from aqueous solution on copper-based metal organic frameworks (HKUST-1),” *Chemosphere*, vol. 150, pp. 659–666, May 2016, doi: 10.1016/j.chemosphere.2016.02.005.
- [544] P. Wagener, A. Schwenke, and S. Barcikowski, “How Citrate Ligands Affect Nanoparticle Adsorption to Microparticle Supports,” *Langmuir*, vol. 28, no. 14, pp. 6132–6140, Apr. 2012, doi: 10.1021/la204839m.
- [545] A. Kabir, R. Mesa, J. Jurmain, and K. Furton, “Fabric Phase Sorptive Extraction Explained,” *Separations*, vol. 4, no. 2, p. 21, Jun. 2017, doi: 10.3390/separations4020021.
- [546] G. Vecchio *et al.*, “Concentration-dependent, size-independent toxicity of citrate capped AuNPs in drosophila melanogaster,” *PLoS One*, vol. 7, no. 1, Jan. 2012, doi: 10.1371/journal.pone.0029980.
- [547] N. I. Kapakoglou, D. L. Giokas, G. Z. Tsogas, A. K. Ladavos, and A. G. Vlessidis, “Development of a chromium speciation probe based on morphology-dependent aggregation of polymerized vesicle-functionalized gold nanoparticles,” *Analyst*, vol. 134, no. 12, pp. 2475–2483, 2009, doi: 10.1039/b909619a.
- [548] Xiaohua Huang, “Gold Nanoparticles Used in Cancer Cell Diagnostics, Selective Photothermal Therapy and Catalysis of NADH Oxidation Reaction,” Georgia Institute of Technology, Atlanta, USA, 2006. Accessed: Dec. 07, 2023. [Online]. Available: <https://smartech.gatech.edu/handle/1853/10565>
- [549] G. Hartmann, T. Baumgartner, and M. Schuster, “Influence of particle coating and matrix constituents on the cloud point extraction efficiency of silver nanoparticles (Ag-NPs) and application for monitoring the formation of Ag-NPs from Ag+,” *Anal Chem*, vol. 86, no. 1, pp. 790–796, Jan. 2014, doi: 10.1021/ac403289d.
- [550] S. P. Mandyla, G. Z. Tsogas, A. G. Vlessidis, and D. L. Giokas, “Determination of gold nanoparticles in environmental water samples by second-order optical scattering using dithiotreitol-functionalized CdS quantum dots after cloud point extraction,” *J Hazard Mater*, vol. 323, pp. 67–74, Feb. 2017, doi: 10.1016/j.jhazmat.2016.03.039.
- [551] N. I. Kapakoglou, D. L. Giokas, G. Z. Tsogas, A. K. Ladavos, and A. G. Vlessidis, “Development of a chromium speciation probe based on morphology-dependent aggregation of polymerized vesicle-functionalized gold nanoparticles,” *Analyst*, vol. 134, no. 12, p. 2475, 2009, doi: 10.1039/b909619a.
- [552] W. Haiss, N. T. K. Thanh, J. Aveyard, and D. G. Fernig, “Determination of Size and Concentration of Gold Nanoparticles from UV–Vis Spectra,” *Anal Chem*, vol. 79, no. 11, pp. 4215–4221, Jun. 2007, doi: 10.1021/ac0702084.
- [553] N. Morin, C. Miège, M. Coquery, and J. Randon, “Chemical calibration, performance, validation and applications of the polar organic chemical integrative sampler (POCIS) in aquatic environments,” *TrAC Trends in Analytical Chemistry*, vol. 36, pp. 144–175, Jun. 2012, doi: 10.1016/j.trac.2012.01.007.

- [554] H. T. Ong, D. D. Suppiah, and N. Muhd Julkapli, "Fatty acid coated iron oxide nanoparticle: Effect on stability, particle size and magnetic properties," *Colloids Surf A Physicochem Eng Asp*, vol. 606, Dec. 2020, doi: 10.1016/j.colsurfa.2020.125371.
- [555] J. L. Brédas, G. B. Street, B. Thémans, and J. M. André, "Organic polymers based on aromatic rings (polyparaphenylene, polypyrrole, polythiophene): Evolution of the electronic properties as a function of the torsion angle between adjacent rings," *J Chem Phys*, vol. 83, no. 3, pp. 1323–1329, 1985, doi: 10.1063/1.449450.
- [556] C. Rous and M. Leclerc, "Rod-to-Coil Transition in Alkoxy-Substituted Polythiophenes," 1992.
- [557] K. Fai and M. Leclerc, "Responsive Supramolecular Polythiophene Assemblies," 1998.
- [558] T. Klingstedt *et al.*, "Distinct spacing between anionic groups: An essential chemical determinant for achieving thiophene-based ligands to distinguish β -amyloid or tau polymorphic aggregates," *Chemistry - A European Journal*, vol. 21, no. 25, pp. 9072–9082, Jun. 2015, doi: 10.1002/chem.201500556.
- [559] C. S. Inagaki, M. M. Oliveira, and A. J. G. Zarbin, "Direct and one-step synthesis of polythiophene/gold nanoparticles thin films through liquid/liquid interfacial polymerization," *J Colloid Interface Sci*, vol. 516, pp. 498–510, Apr. 2018, doi: 10.1016/j.jcis.2018.01.076.
- [560] Y. J. Jung *et al.*, "Luminescent gold-poly(thiophene) nanoaggregates prepared by one-step oxidative polymerization," *J Mater Chem*, vol. 20, no. 43, pp. 9770–9774, Nov. 2010, doi: 10.1039/c0jm01793k.
- [561] C. Xiong, S. Wang, L. Zhang, Y. Li, Y. Zhou, and J. Peng, "Preparation of 2-aminothiazole-functionalized poly(glycidyl methacrylate) microspheres and their excellent gold ion adsorption properties," *Polymers (Basel)*, vol. 10, no. 2, Feb. 2018, doi: 10.3390/polym10020159.
- [562] Y. Keren, M. Borisover, and N. Bukhanovsky, "Sorption interactions of organic compounds with soils affected by agricultural olive mill wastewater," *Chemosphere*, vol. 138, pp. 462–468, Nov. 2015, doi: 10.1016/j.chemosphere.2015.06.085.
- [563] M. C. Alcudia-León, R. Lucena, S. Cárdenas, and M. Valcárcel, "Stir membrane extraction: A useful approach for liquid sample pretreatment," *Anal Chem*, vol. 81, no. 21, pp. 8957–8961, Nov. 2009, doi: 10.1021/ac9016192.
- [564] Q. Abbas *et al.*, "Transformation pathways and fate of engineered nanoparticles (ENPs) in distinct interactive environmental compartments: A review," May 01, 2020, *Elsevier Ltd*. doi: 10.1016/j.envint.2020.105646.
- [565] Z. P. Li, Y. C. Wang, C. H. Liu, and Y. K. Li, "Development of chemiluminescence detection of gold nanoparticles in biological conjugates for immunoassay," *Anal Chim Acta*, vol. 551, no. 1–2, pp. 85–91, Oct. 2005, doi: 10.1016/j.aca.2005.07.014.
- [566] Y. Wang *et al.*, "Simultaneous measurements of eight oxyanions using high-capacity diffusive gradients in thin films (Zr-Oxide DGT) with a high-efficiency elution procedure," *Environ Sci Technol*, vol. 50, no. 14, pp. 7572–7580, Jul. 2016, doi: 10.1021/acs.est.6b00206.
- [567] A. K. Venkatesan *et al.*, "Using single-particle ICP-MS for monitoring metal-containing particles in tap water," *Environ Sci (Camb)*, vol. 4, no. 12, pp. 1923–1932, Dec. 2018, doi: 10.1039/c8ew00478a.
- [568] R. J. B. Peters *et al.*, "Detection of nanoparticles in Dutch surface waters," *Science of the Total Environment*, vol. 621, pp. 210–218, Apr. 2018, doi: 10.1016/j.scitotenv.2017.11.238.

- [569] L. Li, G. Hartmann, M. Döblinger, and M. Schuster, “Quantification of nanoscale silver particles removal and release from municipal wastewater treatment plants in Germany,” *Environ Sci Technol*, vol. 47, no. 13, pp. 7317–7323, Jul. 2013, doi: 10.1021/es3041658.
- [570] F. Gottschalk, T. Sonderer, R. W. Scholz, and B. Nowack, “Modeled environmental concentrations of engineered nanomaterials (TiO₂, ZnO, Ag, CNT, fullerenes) for different regions,” *Environ Sci Technol*, vol. 43, no. 24, pp. 9216–9222, Dec. 2009, doi: 10.1021/es9015553.
- [571] N. C. Mueller and B. Nowack, “Exposure modeling of engineered nanoparticles in the environment,” *Environ Sci Technol*, vol. 42, no. 12, pp. 4447–4453, Jun. 2008, doi: 10.1021/es7029637.
- [572] R. Aguilar-Martínez, M. M. Gómez-Gómez, and M. A. Palacios-Corvillo, “Mercury and organotin compounds monitoring in fresh and marine waters across Europe by Chemcatcher passive sampler,” *Int J Environ Anal Chem*, vol. 91, no. 11, pp. 1100–1116, Sep. 2011, doi: 10.1080/03067310903199534.
- [573] J. Petersen, D. Pröfrock, A. Paschke, J. A. C. Broekaert, and A. Prange, “Laboratory calibration and field testing of the Chemcatcher-Metal for trace levels of rare earth elements in estuarine waters,” *Environmental Science and Pollution Research*, vol. 22, no. 20, pp. 16051–16059, Oct. 2015, doi: 10.1007/s11356-015-4823-x.
- [574] J. Knutsson, P. Knutsson, S. Rauch, T. J. R. Pettersson, and G. M. Morrison, “Evaluation of a passive sampler for the speciation of metals in urban runoff water,” *Environmental Sciences: Processes and Impacts*, vol. 15, no. 12, pp. 2233–2239, 2013, doi: 10.1039/c3em00247k.
- [575] I. J. Allan, J. Knutsson, N. Guigues, G. A. Mills, A. M. Fouillac, and R. Greenwood, “Chemcatcher® and DGT passive sampling devices for regulatory monitoring of trace metals in surface water,” *Journal of Environmental Monitoring*, vol. 10, no. 7, pp. 821–829, 2008, doi: 10.1039/b802581a.
- [576] S. Su, B. Chen, M. He, Z. Xiao, and B. Hu, “A novel strategy for sequential analysis of gold nanoparticles and gold ions in water samples by combining magnetic solid phase extraction with inductively coupled plasma mass spectrometry,” *J Anal At Spectrom*, vol. 29, no. 3, pp. 444–453, Mar. 2014, doi: 10.1039/c3ja50342a.
- [577] S. M. Majedi, B. C. Kelly, and H. K. Lee, “Efficient hydrophobization and solvent microextraction for determination of trace nano-sized silver and titanium dioxide in natural waters,” *Anal Chim Acta*, vol. 789, pp. 47–57, Jul. 2013, doi: 10.1016/j.aca.2013.06.011.
- [578] C. Tziasiou, A. D. Pournara, M. J. Manos, and D. L. Giokas, “Dispersive solid phase extraction of noble metal nanoparticles from environmental samples on a thiol-functionalized Zirconium(IV) metal organic framework and determination with atomic absorption spectrometry,” *Microchemical Journal*, vol. 195, Dec. 2023, doi: 10.1016/j.microc.2023.109387.
- [579] F. Van Koetsem *et al.*, “Use of filtration techniques to study environmental fate of engineered metallic nanoparticles: Factors affecting filter performance,” *J Hazard Mater*, vol. 322, pp. 105–117, Jan. 2017, doi: 10.1016/j.jhazmat.2016.05.098.
- [580] M. Hitrik, Y. Pisman, G. Wittstock, and D. Mandler, “Speciation of nanoscale objects by nanoparticle imprinted matrices,” *Nanoscale*, vol. 8, no. 29, pp. 13934–13943, Aug. 2016, doi: 10.1039/c6nr01106c.
- [581] I. Hagarová, L. Nemček, M. Šebesta, O. Zvěřina, P. Kasak, and M. Urík, “Preconcentration and Separation of Gold Nanoparticles from Environmental Waters Using Extraction Techniques Followed by Spectrometric Quantification,” Oct. 01, 2022, *MDPI*. doi: 10.3390/ijms231911465.

REFERENCES

- [582] K. Leopold, A. Philippe, K. Wörle, and G. E. Schaumann, “Analytical strategies to the determination of metal-containing nanoparticles in environmental waters,” Nov. 01, 2016, *Elsevier B.V.* doi: 10.1016/j.trac.2016.03.026.
- [583] I. Taverniers, M. De Loose, and E. Van Bockstaele, “Trends in quality in the analytical laboratory. II. Analytical method validation and quality assurance,” *TrAC - Trends in Analytical Chemistry*, vol. 23, no. 8, pp. 535–552, 2004, doi: 10.1016/j.trac.2004.04.001.

RERERENCES